République Algérienne Démocratique et Populaire
Ministère de l'Enseignement Supérieur et de la Recherche Scientifique

UNIVERSITÉ YAHIA FARÈS DE MÉDÉA

Département de Génie Mécanique
Laboratoire de Biomatériaux et Phénomènes de Transport (LBMPT)

THÈSE DE DOCTORAT

Présentée par :

SELLOUM Ahmed

En vue de l'obtention du diplôme de Doctorat LMD en Génie Climatique

THÈME

Modélisation et étude des performances d'un système de réfrigération hybride fonctionnant à l'énergie solaire

Soutenue publiquement le **25/05/2024** devant le jury composé de :

BOUAZIZ Mohamed Nadjib	Professeur	Université de Médéa	Président
ZIRARI Mounir	Professeur	Université de Médéa	Examinateur
MALKI Maamar	MCA	ENST d'Alger	Examinateur
TRIKI Zakaria	Professeur	Université de Médéa	Directeur de thèse
CHIBA Younes	Professeur	Université de Médéa	Co-directeur de thèse

République Algérienne Démocratique et Populaire
Ministère de l'Enseignement Supérieur et de la Recherche Scientifique

UNIVERSITÉ YAHIA FARÈS DE MÉDÉA

Département de Génie Mécanique
Laboratoire de Biomatériaux et Phénomènes de Transport (LBMPT)

THÈSE DE DOCTORAT

Présentée par :

SELLOUM Ahmed

En vue de l'obtention du diplôme de Doctorat LMD en Génie Climatique

THÈME

Modeling and Performance Study of a Hybrid Refrigeration System Powered by Solar Energy

Soutenue publiquement le **25/05/2024** devant le jury composé de :

BOUAZIZ Mohamed Nadjib	Professeur	Université de Médéa	Président
ZIRARI Mounir	Professeur	Université de Médéa	Examinateur
MALKI Maamar	MCA	ENST d'Alger	Examinateur
TRIKI Zakaria	Professeur	Université de Médéa	Directeur de thèse
CHIBA Younes	Professeur	Université de Médéa	Co-directeur de thèse

« True science is an ignorance that is known »

Michel de Montaigne

To my dear **father**.

To my loving **mother** who always helped me with her presence, her advice and her prayers.

To my dear **wife** for her generosity, her daily sacrifice and her support and encouragement.

To my little angels **IBRHIM,** and **YOUCEF** who have become my reason for existing.

To my dear in-laws for their kindness and infinite availability whenever I needed them.

To my dear brothers and sisters **ABDERHMANE**, **HAMZA**, **MERIEM** and **AMINA**.

To my brothers-in-law and sisters-in-law **HSSEN, NADJIB**, **ANISSA**, **FAHIMA**, **NORA**, **RIMA**, **AMIRA** and **MAISSA**.

To all my friends and colleagues…

AKNOWLEDGMENTS

First of all, I would like to thank **God Almighty** for all the wonders he does in my life and for giving me the courage, strength and patience to complete this modest work.

I extend my sincere thanks and all my gratitude to my thesis director, Professor **Triki Zakaria**, for having agreed to direct this work and for the trust he showed in me by giving me great freedom in my research. In addition to his scientific rigor and his interest in the subject, he gave me considerable moral support.

I also extend my greatest thanks to Professor **Chiba Younes**, thesis co-director for his constant help throughout of this study, and for the rigor of spirit that he communicated to me.

I thank Professor **Bouaziz Mohamed Nadjib** for doing me the honor of examining this work and chairing the jury for my thesis.

I also thank Professor **Zirari Mounir**, and Doctor **Malki Maamar** the honor they gave me by agreeing to be part of the thesis jury.

Finally, I will end by thanking all those who participated directly or indirectly in carrying out this research work.

TABLE OF CONTENTS

AKNOWLEDGMENTS

TABLE OF CONTENTS

PREAMBLE

ABSTRACT

LIST OF FIGURES

LIST OF TABLES

NOMENCLATURE

INTRODUCTION……...**1**

PART I BIBLIOGRAPHICAL RESEARCH

1. **LITERATURE REVIEW** ……..**7**

1.1. Vapor compression refrigeration systems…….……7
1.1.1. Historical development and principles of VCR systems …….7
1.1.2. Types and characteristics of refrigerants used in VCR systems…….….9
1.2. Solar energy applications…….…….9
1.2.1. Principles of photovoltaic solar energy…….……11
1.2.2. Integration of solar energy in refrigeration systems……..52
1.3. Hybrid refrigeration systems……...74
1.3.1. Concept and advantages of hybrid systems combining solar energy with conventional refrigeration……..…..74
1.3.2. Review of existing hybrid refrigeration systems (PV + VCR) and their performance……..76
1.4. Conclusion……**.**111

PART II TECHNICAL STUDY

2. **METHODOLOGY**…….**112**

2.1. Introduction……...…112
2.2. System description……...…112
2.3. Choice and description of the site studied…….……..114
2.3.1. Climate data of Ghardaia……**....**114
2.4. Description of the refrigerants (R134a and R1234ze) and their properties……...115
2.4.1. Refrigerants development and environmental assessment……...115
2.4.2. Properties of the refrigerants studied (R1234ze and R134a)……121
2.4.3. Properties and state equations for the refrigerant R1234ze…….**.....**125
2.2.4. Properties and state equations for the refrigerant R134a.....131

2.5. Development of the numerical model……...134
2.5.1. Software used (MATLAB)……134
. 2.5.2. Heat and mass transfer equations……..…..136
2.6. Definition of different operating conditions…….……137

3. **THERMODYNAMIC PERFORMANCE ANALYSIS**……..**139**

3.1. Coefficient of performance (COP).....139
3.2. Thermodynamic efficiency……...…139
3.3. Solar PV panel……..139
3.4. Results and discussion…….……140
3.5. Conclusion……...……150

4. **EXERGETIC PERFORMANCE ANALYSIS**……**152**

4.1. Introduction……152
4.2. Definition of exergy……..……152
4.3. Exergy analisys……....156
4.3.1. Exergy analisys of photovoltaic panels…….…..156
4.3.2. Exergy analysis of vapor compression refrigeration system VCR……..157
4.3.3. Exergy analysis of global system (PV+ vapor compression refrigeration cycle VCR)…….……..159
4.4. Results and discussion……..160
4.4.1. Exergy analysis of the PV system……..160
4.4.2. Exergy analysis of the VCR system……..163
4.4.3. Exergy analysis of the global solar refrigeration system (PV + VCR)……...170
4.5. Industrial implication, recommendations for improvement……..……177
4.6. Conclusion……...……178

CONCLUSION AND RECOMMENDATIONS…….……..**181**

REFERENCES……..……184

APPENDICES

PREAMBLE

In the last years, the growing demand for refrigeration and air conditioning has caused a significant increase in demand for primary energy resources. Solar-powered cooling is one of the technologies which allows to obtain, by using the renewable solar source, an important energy saving compared to traditional refrigeration and air conditioning installations.

On the other hand, the production of electrical energy to operate these systems has a bad impact on the environment, so using solar energy reduces this impact.

Finally, the use of CFC, HCFC, or HFC refrigerants in the event of a leak into the atmosphere, influences the ozone layer, and contributes to global warming through the greenhouse effect.

Therefore, the use of new refrigerants such as HFO, which have a low GWP and ODP, considerably reduces this nuisance.

In conclusion, to save electrical energy and preserve the environment as much as possible, it is preferable to use solar thermal or photovoltaic energy, and also refrigerants with low environmental impact in refrigeration and air conditioning installations.

RÉSUMÉ

Ce travail de recherche consiste à étudier et analyser les performances thermodynamiques et exergétiques d'un système de réfrigération à compression de vapeur (VCR) fonctionnant à l'énergie solaire pour une possible implantation dans un site isolé. Pour accomplir cet objectif, un modèle numérique a été développé sous l'environnement MATLAB à partir des equations de transfert de chaleur et de masse. L'étude mis en évidence la comparaison entre deux fluides frigorigènes : le R134a (HFC), et le R1234ze (HFO) à faible GWP. Ainsi, l'effet des différents paramètres de fonctionnement, et de conception sur les performances du système a été étudié pour les deux fluides frigorigènes choisis. Les résultats de l'analyse thermodynamique ont montré que le coefficient de performance (COP) et l'efficacité thermodynamique du système solaire VCR a augmenté avec la diminution de la température ambiante en raison de la diminution de la consommation électrique du compresseur. Le COP au 21ème jour du mois de juillet est obtenu dans la plage de 4,37 à 5,77 pour le réfrigérant R1234ze qui sont proches et à plus de 90 % de la valeur COP maximale, alors qu'elle est comprise entre 2,56 et 3,17 pour le fluide R134a. Les valeurs du COP les plus basse se trouvent de midi à 15h00. Par ailleurs, les résultats de l'analyse exergétique ont révélé que, pour les deux réfrigérants, le compresseur se distingue comme le composant avec la destruction exergétique la plus élevée, suivi du condenseur, du détendeur et de l'évaporateur. Cependant, l'irréversibilité du système utilisant le réfrigérant R1234ze(E) s'avère inférieure à celle utilisant le fluide R134a, renforçant l'adéquation du R1234ze(E) en tant qu'alternative prometteuse dans les applications de refroidissement et de réfrigération.

Mots clés : Réfrigération à compression mécanique, Energie solaire photovoltaïque, R134a, R1234ze(E), Analyse thermodynamique, Analyse exergétique, Comparaison.

ABSTRACT

This research work involves studying and analyzing the thermodynamic and exergetic performance of a vapor compression refrigeration (VCR) system operating on solar energy for potential implementation in an isolated site. To achieve this objective, a numerical model was developed in the MATLAB environment based on heat and mass transfer equations. The study highlighted the comparison between two refrigerants: R134a (HFC) and R1234ze (HFO) with low GWP. Thus, the effect of different operating and design parameters on the system's performance was studied for the two chosen refrigerants. The results of the thermodynamic analysis showed that the coefficient of performance (COP) and the thermodynamic efficiency of the solar VCR system increased with the decrease in ambient temperature due to the reduction in the compressor's electrical consumption. The COP on the 21st day of July is obtained in the range of 4.37 to 5.77 for the R1234ze refrigerant, which are close to and over 90% of the maximum COP value, while it ranges between 2.56 and 3.17 for the R134a refrigerant. The lowest COP values are found from noon to 3 PM. Furthermore, the results of the exergetic analysis revealed that, for both refrigerants, the compressor stands out as the component with the highest exergy destruction, followed by the condenser, the expansion valve, and the evaporator. However, the irreversibility of the system using the R1234ze(E) refrigerant is found to be lower than that using the R134a refrigerant, reinforcing the suitability of R1234ze(E) as a promising alternative in cooling and refrigeration applications.

Keywords: Mechanical vapor compression refrigeration, Photovoltaic solar energy, R134a, R1234ze(E), Thermodynamic analysis, Exergetic analysis, Comparison.

ملخص:

يتناول هذا البحث دراسة وتحليل الأداءات الديناميكية الحرارية والإجزرجية لنظام تبريد بالضغط البخاري (VCR) يعمل بالطاقة الشمسية لإمكانية تنفيذه في موقع معزول. لتحقيق هذا الهدف، تم تطوير نموذج رقمي في بيئة MATLABبناءً على معادلات نقل الحرارة والكتلة. أبرزت الدراسة مقارنة بين مبردين: R134a (HFC) ، و 1234ze (HFO)ذو تأثير احتراري منخفض. كما تم دراسة تأثير مختلف المعايير التشغيلية والتصميمية على أداء النظام للمبردين المختارين. أظهرت نتائج التحليل الديناميكي الحراري أن معامل الأداء والكفاءة الديناميكية الحرارية للنظام الشمسي VCR زادا مع انخفاض درجة الحرارة المحيطة بسبب انخفاض استهلاك الكهرباء من قبل الضاغط. تم الحصول على معامل الأداء في اليوم الواحد والعشرين من شهر يوليو في نطاق من 4.37 إلى 5.77 للمبرد R1234ze، وهي قريبة وأكثر من 90% من القيمة القصوى لـ معامل الأداء، بينما تراوحت بين 2.56 و3.17 للمبرد .R134a كانت قيم معامل الأداء الأدنى بين الساعة الثانية عشرة ظهرًا والثالثة مساءً. علاوة على ذلك، كشفت نتائج التحليل الإجزرجتي أن الضاغط يعتبر العنصر الأكثر تدميرًا للإجزرجيا للمبردين، يليه المكثف، ثم الصمام الخانق والمبخر. ومع ذلك، تبين أن اللاإنعكاسية للنظام الذي يستخدم المبرد R1234ze(E) أقل من تلك التي تستخدم المبردR134a ، مما يعزز ملاءمة R1234ze(E) كبديل واعد في تطبيقات التبريد والتجميد.

الكلمات المفتاحية: تبريد بالضغط الميكانيكي، الطاقة الشمسية الكهروضوئية، R134a، R1234ze(E)، تحليل ديناميكي حراري، تحليل إجزرجتي، مقارنة.

LIST OF FIGURES

Figure 1.1 : Principles of VCR systems 9
Figure 1.2 : Comparison of non-hydro renewable energy capacities between countries 12
Figure 1.3 : Annual average solar irradiance distribution over the surface of the Earth 15
Figure 1.4 : Classification of the present solar energy technologies 15
Figure 1.5 : Mono - Crystalline cell and module 19
Figure 1.6 : Poly - Crystalline cell and module 20
Figure 1.7 : Amorphous solar cells 21
Figure 1.8 : Illustrating a typical III-V triple junction solar 23
Figure 1.9 : The J -V curves of the three junctions 24
Figure 1.10 : Single junction circuit 24
Figure 1.11 : Multi-junction circuit 25
Figure 1.12 : Copper-indium-selenide (CIS) cells 26
Figure 1.13 : Schematic of PV concentrator Fresnel lens 26
Figure 1.14 : Representative CPV system 29
Figure 1.15 : Organic PV construction 31
Figure 1.16 : Organic PV sample 31
Figure 1.17 : Black silicon solar Cell 32
Figure 1.18 : A diagram showing the photovoltaic effect 33
Figure 1.19 : Off-grid diagram with DC load 40
Figure 1.20 : Off-grid diagram with AC load 41
Figure 1.21 : String inverter 42
Figure 1.22 : Micro inverter 43
Figure 1.23 : Hybrid solar inverter 43
Figure 1.24 : Power inverter 44
Figure 1.25 : Solar cell I-V characteristic curve 44
Figure 1.26 : Solar panel I-V characteristic curves 46
Figure 1.27 : Equivalent number of hours 48
Figure 1.28 : Modeling of a DC cable 50

Figure 1.29 : Example of a solar absorption refrigeration system 54
Figure 1.30 : Test plant of 5 kW solar thermally driven absorption chiller 54
Figure 1.31 : Adsorption cycle 56
Figure 1.32 : Principle of solar adsorption refrigeration cycle 56
Figure 1.33 : Ejector parts 58
Figure 1.34 : Ejector layout and pressure-Mach number profiles 59
Figure 1.35 : Layout (top) and T-s diagram (bottom) of a generic ejector cooling cycle 66
Figure 1.36 : Solar assisted desiccant cooling system 64
Figure 1.37 : Water/air heat exchanger 65
Figure 1.38 : The schematic of solar powered liquid desiccant cooling system 66
Figure 1.39 : Schematic of a solar liquid desiccant system 66
Figure 1.40 : The yearly rate of publication on solar cooling technologies 68
Figure 1.41 : General classification of the main solar cooling technologies 70
Figure 1.42 : The main components of a PTC-driven absorption cooling cycle 71
Figure 1.43 : Main components in the CPC-driven absorption cooling module 71
Figure 1.44 : A schematic diagram of the adsorption cooling layout powered by CPC field 72
Figure 1.45 : The examined parabolic dish collector in HEnergia research center for domestic cooling and heating 73
Figure 1.46 : LFR, ice storages, cold store room, and absorption chiller, a pilot plant in Germany 73
Figure 1.47 : Experimental setup for AC and DC refrigerators performance analysis 78
Figure 1.48 : Components of the solar electric-vapor compression refrigeration (SE-VCR) system 78
Figure 1.49 : Schematic diagram of PV direct-driven refrigerators with different control systems 79
Figure 1.50 : Schematic diagram of directly coupled refrigeration system 79
Figure 1.51 : Vapour compression solar refrigerator unit: (a) pictorial view and (b) schematic diagram 79
Figure 1.52 : Schematic diagram of the solar PV-powered vapor compression refrigeration system 80

Figure 1.53 : A hut for accommodating the solar refrigeration system 81
Figure 1.54 : The solar hybrid system proposed 81
Figure 1.55 : Schematic diagram for the solar-powered mechanical subcooling refrigeration system 82
Figure 1.56 : Schematic representation of solar refrigeration: 83
Figure 1.57 : System Configuration of Solar Refrigerator 84
Figure 1.58 : The integrated solar PV refrigerator and heat pump (ISPVRHP) assembled for testing 85
Figure 1.59 : The components of the solar PV refrigerator and heat pump (ISPVRHP) 85
Figure 1.60 : The layout of the evaporator and the condenser 86
Figure 1.61 : Bellville campus scientific weather station 86
Figure 1.62 : Design of experimental rig and solar control panel 87
Figure 1.63 : Experimental set up 88
Figure 1.64 : Solar assisted refrigeration system 89
Figure 1.65 : Concept model 89
Figure 1.66 : Set-up of solar assisted refrigeration system 89
Figure 1.67 : Battery 90
Figure 1.68 : Charge controller 90
Figure 1.69 : Solar panel 90
Figure 1.70 : Experimental set-up of the PV powered refrigerator 91
Figure 1.71 : Scheme of the horizontal solar vapour compression refrigerator with internal heat exchanger 92
Figure 1.72 : Solar powered air conditioning system 93
Figure 1.73 : Block diagram of PV system and air conditioning system 94
Figure 1.74 : Diagrams of the operating principle of the Solar VCR system 94
Figure 1.75 : Front of the refrigerator 95
Figure 1.76 : Back view of the refrigerator 95
Figure 1.77 : 3D view of the proposed refrigerator 96
Figure 1.78 : Installed photovoltaic system used for the experiment 96
Figure 1.79 : Battery bank and UPS system (uninterruptible power supply) 96
Figure 1.80 : No load test picture 96

Figure 1.81 : Full load test picture 97
Figure 1.82 : Schematic of the miniature photovoltaic refrigeration system 97
Figure 1.83 : System layout of solar driven refrigeration system 98
Figure 1.84 : (a) Solar refrigeration system set-up, (b) evaporator tank 98
Figure 1.85 : Schematic diagram for solar PV powered vapour compression cooling system for potato storage 99
Figure 1.86 : Curing of potato tubers using evaporatively cooled (EC) chamber 99
Figure 1.87 : Schematic of the PV refrigeration system 100
Figure 1.88 : Layout of vapor compression refrigeration cycle powered by solar energy 102
Figure 1.89 : The experimental test rig 102
Figure 1.90 : Backup transformer to support the rig on cloudy days 103
Figure 1.91 : Programmable logic control (PLC) used in the test rig 103
Figure 1.92 : Standard, conventional pressure and temperature measuring backup set 103
Figure 1.93 : The housing structure of the test rig 103
Figure 1.94 : Sample of the monitor view while working on CodeSys software 104
Figure 1.95 : Energy flow of PV integrated cooling truck 104
Figure 1.96 : The components in domestic refrigeration with the PV 105
Figure 1.97 : A DC refrigeration powered by PV 105
Figure 1.98 : Hybrid PVT connected to ejector-compression refrigeration 106
Figure 1.99 : Experimental set-up of SPV powered refrigerator 106
Figure 1.100 : Experimental setup 107
Figure 1.101 : Block diagram of the solar assisted refrigerator 107
Figure 1.102 : Top side view of the refrigerator 108
Figure 1.103 : Themometer probes placed at various points inside the refrigerator chamber 108
Figure 1.104 : Different components of the banana cold storage facility in Mardan city based on conventional VCRS 109
Figure 1.105 : Solar electric vapor compression refrigeration system 109

Figure 1.106 : Operational modes of the PV integrated refrigeration system for cold storage facility 110
Figure 2.1 : Schematic diagram of the solar PV assisted cooling system 113
Figure 2.2 : Pressure-enthalpy diagram of a vapor compression refrigeration cycle 114
Figure 2.3 : Monthly solar irradiation and monthly average daily ambient temperature for the year 2018 115
Figure 2.4 : Comparison between R1234ze(E) and R134a at different temperatures 123
Figure 3.1 : Hourly mean variation of solar radiation and ambient temperature (Ghardaïa site) 141
Figure 3.2 : Hourly variation of mass flow rate (Ghardaïa site) 142
Figure 3.3 : Hourly variation of cooling capacity (Ghardaïa site) 143
Figure 3.4 : Hourly variation of coefficient of performance (Ghardaia region) 144
Figure 3.5 : Hourly variation of thermodynamic efficiency (Ghardaia region) 144
Figure 3.6 : Hourly variation of overall solar efficiency (Ghardaia region) 146
Figure 3.7 : Hourly variation of PV power production (Ghardaia region) 146
Figure 3.8 : Hourly variation of compressor power (Ghardaia region) 147
Figure 3.9 : Hourly variation of PV required area (Ghardaia region) 148
Figure 3.10 : Comparison of the compressor power consumption and PV power production for R1234ze (Ghardaia region) 149
Figure 3.11 : Comparison of the cumulative compressor power consumption and cumulative PV power production for R1234ze (Ghardaia region) 150
Figure 4.1 : Hourly variation of solar radiation intensity and input exergy 160
Figure 4.2 : Hourly variation of input solar exergy and electrical exergy 161
Figure 4.3 : Hourly variation of input solar exergy and exergy efficiency 161
Figure 4.4 : Hourly variation of destroyed exergy, solar input exergy, electrical exergy and thermal exergy 162
Figure 4.5 : Hourly variation of energy and exergy efficiencies 163
Figure 4.6 : Variation of exergy efficiency of the VCR cycle with ambient temperature (Tev = 0°C) 164

Figure 4.7 : Hourly variation of exergy efficiency of the vapor compression refrigeration cycle (Tev = 0°C) 165
Figure 4.8 : Variation of exergy efficiency of the VCR cycle with evaporating temperature 165
Figure 4.9 : Variation of total exergy destruction of the VCR cycle with evaporating temperature 166
Figure 4.10 : Hourly variation of total exergy destruction of the vapor compression refrigeration cycle (Tev = 0°C) 167
Figure 4.11 : Exergy destruction in each component of the VCR cycle 167
Figure 4.12 : The ration of exergy destruction in each component of the vapor compression refrigeration cycle at Tev = 0°C and t = 12:00 PM (refrigerant R1234ze) 168
Figure 4.13 : The ration of exergy destruction in each component of the vapor compression refrigeration cycle at Tev = 0°C and t = 12:00 PM (refrigerant R134a) 169
Figure 4.14 : Relatives irreversibilities for different components 169
Figure 4.15 : Variation of exergy efficiency of VCR sys, Sol sys, and VCRS sys depending on the evaporating temperature, at t = 12:00 PM 171
Figure 4.16 : Variation of total exergy destruction of VCR sys, Sol sys, and VCRS sys depending on the evaporating temperature, at t = 12:00 PM 171
Figure 4.17 : Hourly variation of exergy efficiency of VCR sys, Sol sys and VCRS sys, at Tev = 0°C 173
Figure 4.18 : Hourly variation of total exergy destruction of VCR sys, Sol sys, and VCRS sys, at Tev = 0°C 173

LIST OF TABLES

Table 1.1 : Refrigerants used in vapor compression refrigeration systems 9

Table 1.2 : Comparison of the global power capacity between different renewable energy sectors 16

Table 1.3 : The 2015 global ranking for solar power generation capacity 17

Table 1.4 : Efficiency recent for research of PV and CPV 25

Table 1.5 : Two most common types of batteries for PV system storage 35

Table 1.6 : Recommended voltages for photovoltaic systems based on their powers 49

Table 1.7 : General comparison of two cooling systems: absorption and adsorption systems 57

Table 1.8 : The comparison between desiccant system and conventional systems 63

Table 2.1 : Refrigerant types and status 120

Table 2.2 : Main refrigerant properties of R1234ze(E) and R134a 124

Table 2.3 : Basic properties of the R1234ze(E) refrigerant 125

Table 2.4 : Coefficients of polynomials describing the temperature, specific enthalpy, specific entropy, and specific heat of the R1234ze(E) refrigerant in the saturated liquid state 126

Table 2.5 : Coefficients of polynomials describing the density, specific volume, and heat transfer coefficient of the R1234ze(E) refrigerant in the saturated liquid state 126

Table 2.6 : Coefficients of polynomials describing the dynamic viscosity coefficient, Prandtl number, and surface tension of the R1234ze(E) refrigerant in the saturated liquid state 126

Table 2.7 : Coefficients of polynomials describing the specific enthalpy, specific entropy, specific heat, and density of the R1234ze(E) refrigerant in the saturated vapour state 127

Table 2.8 : Coefficients of polynomials describing the specific volume, heat transfer coefficient, dynamic viscosity coefficient, and Prandtl number of the R1234ze(E) refrigerant in the saturated vapour state 128

Table 2.9 : Coefficients of polynomials describing the properties of the R1234ze(E) refrigerant in the superheated vapour state (h = f(p,t), h = f(p,s), s = f(p,t)) 128

Table 2.10 : Coefficients of polynomials describing the properties of the R1234ze(E) refrigerant in the superheated vapour state (T = f(p,h), σ = f(p,h)) 129
Table 2.11 : Coefficients of polynomials describing the properties of the R1234ze(E) refrigerant in the subcooled liquid state (h = f(p,t), s = f(p,t), T = f(p,h)) 130
Table 2.12 : The scope of equations describing the properties of the R1234ze(E) refrigerant and the amount of data used for analysis 130
Table 2.13 : Field of use of the proposed mathematical models 131
Table 2.14 : Coefficients ai of equations 133
Table 2.15 : Operating parameters 137
Table 2.16 : Solar PV module (Vertex 580 W+ Trina Solar, TSM-580 DE19R) parameters 138
Table 4.1 : Differences between exergy and energy 153

NOMENCLATURE

Symbols:

Bd : daily electricity consumption	(Wh/d)
Pi : nominal power of the load	(W)
Ti : number of hours of daily use	(h/d)
Esol : daily solar energy	(kWh/m².d)
Neq : equivalent number of hours of sunshine in STC conditions	(h/d)
Ppv,tot : power of the photovoltaic field	(W)
Cp : loss coefficient	(—)
Npv : number of photovoltaic panels	(—)
Ppv,u : unit PV power	(W)
Cbat,tot : storage battery capacity	(Ah)
Nda : number of days of autonomy	(d)
Pdd : depth of discharge of the battery	(—)
ηbat : energy efficiency of batteries	(—)
Ubat : operating voltage of the battery	(V)
Cbat,u : unit battery capacity	(Ah)
Nbat : number of batteries	(—)
VA : voltage at point A	(V)
VB : voltage at point B	(V)
U : electric potential difference	(V)
overall heat loss coefficient	($W/m^2.°K$)
R : cable resistance	(Ohm)
I : current intensity	(A)
solar radiation	(kW/m^2)
L : cable length	(m)
me : mass flow rate of the secondary	(kg/s)
mg : mass flow rate of the primary	(kg/s)
rp : pressure ratio	(—)

Pc : ejector discharge flow pressure (bar)

condenser pressure (bar)

Pe : secondary flow pressure (bar)

evaporator pressure (bar)

h1 : specific enthalpies at state (1) (kJ/kg)

h4 : specific enthalpies at state (4) (kJ/kg)

Qe : cooling capacity (kW)

h2 : specific enthalpies at state (2) (kJ/kg)

W : compressor power consumption (kW)

ηe : electric motor efficiency (—)

ηb : belt transmission efficiency (—)

ηm : compressor mechanic efficiency (—)

m : refrigerant's mass flow rate (kg/s)

T2 : discharge temperature (°K)

T1 : temperature at state 1 (°K)

Cp : specific heat at constant pressure (kJ/kg.°K)

Cv : specific heat at constant volume (kJ/kg.°K)

Qc : heat transfer in the condenser (kJ)

h3 : specific enthalpies at state (3) (kJ/kg)

COP : coefficient of the performance (—)

ηth : thermodynamic efficiency (—)

COPmax : theoretical maximum COP (—)

Te : evaporating temperature (°K)

Tc : condensation temperature (°K)

temperature at critical point (R134a) (°C)

Wpv : PV power production (kW)

ηpv : solar electric panel's efficiency (—)

Qs : solar radiation input (kW)

A : solar cell or panel surface area (m^2)

ηs : overall efficiency (—)

WT : daily cumulative power consumption of the compressor (kW)

(WPV)T : daily cumulative power production of the PV panels	(kW)
Wi : hourly power consumption of the compressor	(kW)
IT : daily total solar radiation	(kWh/m^2/day)
Q : heat transfer	(kW)
heat emitted to the surrounding	(W)
EXtransfer : exergy transfer	(kW)
Ψin : exergy per unit mass in	(kJ/kg)
Ψout : exergy per unit mass out	(kJ/kg)
V : voltage	(V)
Voc : open-circuit voltage	(V)
Isc : short-circuit current	(A)
Vmp : voltage at maximum power point	(V)
Imp : current at maximum power point	(A)
FF : fill factor	(—)
G : global irradiance	(W/m^2)
Pel : electrical power	(W)
Pmax : maximum power	(W)
Exin : input exergy	(W)
Exloss : exergy loss	(W)
Exout : output exergy	(W)
Exthermal : thermal exergy	(W)
Exelectrical : electrical exergy	(W)
Ta : ambient temperature	(°K)
Ts : surface temperature of the sun	(°K)
Tm : module temperature	(°K)
Tsky : sky temperature	(°K)
hconv : convective heat transfer coefficient	(W/m^2.°K)
hrad : radiative heat transfer coefficient	(W/m^2.°K)
Vw : wind velocity	(m/s)
NOCT : nominal operating cell temperature	(°C)
Ppvu : peak power of the unit photovoltaic field	(W)

CoeffTPmax : PMAX temperature coefficient (%/°K)

Ėx : exergy in any state (W)

m r : the refrigerant's mass flow rate (kg/s)

h0 : enthalpy values of the refrigerant at dead state (kJ/kg)

T0 : dead state temperature (ambient temperature) (°K)

S : entropy of the refrigerant (kJ/kg.°K)

entropy (J/kg·°k)

cable section (m^2)

S0 : entropy values of the refrigerant at dead state (kJ/kg.°K)

ED : rate of exergy destruction (W)

ED in : total exergy transferred by heat, work and mass inlet (W)

ED out : total exergy transferred by heat, work and mass outlet (W)

(Ė D) evp : exergy destruction in evaporator (W)

Ė X4 : exergy in state 4 (W)

Q̇e : net refrigeration effect produced (W)

Tb : constant boundary temperature (room temperature) (°K)

Ė X1 : exergy in state 1 (W)

(Ė D) comp : exergy destruction in compressor (W)

Ẇcomp : work of the compressor (W)

Ė X2 : exergy in state 2 (W)

Ė X3 : exergy in state 3 (W)

(Ė D) exp : exergy in expansion valve (W)

Σ(Ė D) : total exergy destruction (W)

ηex : exergetic efficiency (%)

Σ(Eout) : total exergy recovered (W)

Σ(Ė in) : total exergy supplied (W)

ηex sys : exergetic efficiency of global system (%)

Σ(Ė D) sys : total exergy destruction of the global system (W)

Tev : evaporating temperature (°C)

t : time	(hour)
temperature	(°C)
Exd : total exergy destruction	(kW)
T : temperature	(°K)
temperature	(°C)
temperature at which the heat transfer occurs	(°K)
P : pressure	(bar)
pressure	(kPa)
h' : specific enthalpy	(kJ/kg)
s' : specific entropy	(kJ/kg.°K)
cp' : specific heat	(kJ/kg.°K)
V' : specific volume	(m^3/kg)
Pr' : Prandtl number	(—)
h'' : specific enthalpy	(kJ/kg)
s'' : specific entropy	(kJ/kg.°K)
cp'' : specific heat	(kJ/kg.°K)
V'' : specific volume	(m^3/kg)
Pr'' : Prandtl number	(—)
h : specific enthalpy	(kJ/kg)
specific enthalpy	(J/kg)
enthalpy of the refrigerant	(kJ/kg)
t' : saturated liquid temperature	(°C)
t'' : saturated vapour temperature	(°C)
d : density	(kg/m^3)
ΔT : superheating temperature	(°C)
X : variable defined by equation 27	(—)
k : hour of the day	(hour)

Greek letters:

ε : voltage drop in the DC part (%)

emissivity of the module (—)

ρ : linear resistivity of the conductor constituting the cable (Ohm.m)

density (kg/m^3)

$\underset{\sim}{w}$: entrainment ratio (—)

γ : polytropic exponent (—)

Ψ : exergy per unit mass (kJ/kg)

σ : Stefan Boltzmann's constant ($W/m^2.°K^4$)

surface tension (N/m)

ρ' : density (kg/m^3)

$\boldsymbol{\lambda}'$: heat transfer coefficient (W/m.°K)

μ' : dynamic viscosity coefficient (kg/m.s)

$\boldsymbol{\lambda}''$: heat transfer coefficient (W/m.°K)

μ'' : dynamic viscosity coefficient (kg/m.s)

Indices:

n : index of the coefficients of the properties equations (R1234ze)

is : the isentropic compression

liq : liquid

Sat : saturated

Vap : superheated steam vapor

vsat : saturated steam

0 : reference state

1 : on the suction side

2 : on the discharge side

ai : coefficients of the properties equations (R134a)

Abbreviations:

VCR sys : vapor compression refrigeration system

Sol sys : photovoltaic solar panels

VCRS sys : solar vapor compression refrigeration system

INTRODUCTION

INTRODUCTION

Increasing average global temperatures due to climate change, economic growth and urbanization are widely expected to lead to a greater demand for cooling.

Any efforts to limit access to cooling would likely create major productivity losses as well as adverse impacts on the provision of quality health care, nutritious food, and education, thereby undermining the efforts and opportunities for dozens of countries to realize the UN Sustainable Development Goals, such as ending poverty, hunger and disease [1].

RAC (refrigeration and air conditioning) equipment and systems are already widely used throughout the economy, from small domestic equipment (e.g. refrigerators and room air-conditioners) to very large commercial and industrial systems (e.g. large building air-conditioning and food processing refrigeration).

According to current estimates, RAC equipment represents between 25% and 30% of the global consumption of electricity [2].

Global RAC related energy consumption is expected to surge as much as 33-fold by 2100 versus current levels to more than 10,000 TWh [3]. The lion's share of this growth will be in emerging economies / developing countries.

In addition to the major trends already mentioned – climate change, economic growth and urbanization – several additional factors are driving this growth : Assessments made by the International Energy Agency forecast that the number of air conditioners in use globally will increase from 1.5 billion to 5.5 billion units between 2015 and 2050 [4].Meanwhile, the number of domestic refrigerators would double to more than 2 billion [5].

Greater use of RAC equipment is already creating significant stresses on power systems and increasing peak electricity demand, especially in high ambient temperature countries. As cooling demand grows further, countries will need to consider the need for significant investment in power generation equipment and in electricity transmission and distribution systems.In high ambient temperature countries, peak electrical demand occurs when the demand for air‑conditioning is particularly high.

RAC equipment generates two distinct types of GHG (greenhouse gas) emissions :

1-Direct emissions created by leakage of refrigerants, during operation, maintenance and at end-of-life.

2-Indirect emissions generated at the power station supplying the electricity used by the RAC equipment (if the power is generated from fossil fuels).

The majority of GHG emissions related to RAC equipment are indirect emissions.

According to the Green Cooling Initiative [6], over 70% of GHG emissions from refrigeration systems are due to indirect emissions from electricity generation.

Algeria ranks 38 th in the world in the production of electrical energy, with a total global electricity capacity in 2022 which is equal to 25.9 GW. Which represents a significant environmental impact, especially when we know that the main source for the production of electricity in Algeria, is the natural gas with 99%, according to the Algerian ministry of energy.

In today's rapidly evolving energy landscape, the importance of renewable energy sources cannot be overstated. As the world grapples with the challenges of climate change, dwindling natural resources, and increasing energy demands, renewable energy emerges as the beacon of hope for a sustainable future.

we can site the advantages of renewable energies and its importance in the years to come as follow:

-Environmental benefits:

-Economic growth : in its contribution to job creation and industry growth.)

-Energy independence: by investing in renewable energy in the future, countries can ensure a more stable, reliable and independent energy supply, thereby preserving their energy security.

Inexhaustible energy: while fossil fuels are finite and depleting, the sun, wind, and water are endless sources of energy.

-Technological advancements: as research in this sector intensifies, we're witnessing innovations that make renewable energy more efficient and accessible.

-Reduction in energy costs: as technology advances and becomes more widespread, the costs associated with renewable energy are decreasing.

-Health Benefits: transitioning to renewable energy can mitigate the health risks.

-Diversification of energy sources: solely relying on one energy source is risky.

Supporting local communities: stimulate local economies by creating jobs

-Addressing climate change.

Among the oldest, most widely used and most efficient refrigeration systems in the world we find:

The Vapor Compression Refrigeration Cycle VCR that has nearly 200 years old, but it does not seem ready to leave the scene any time soon. While some people have viewed this method as environmentally harmful and energy-intensive, the cycle is still applicable in the industrial sphere. Natural gas plants, petroleum refineries, and petrochemical plants and most of the food and beverage processes are some of the industrial plants that utilize vapor compression refrigeration systems.

Other industries soon saw the benefits of artificial cooling (VCR). In metalworking, tools could be tempered. With less moisture in the air, iron production could increase. Even textile mills found a use for refrigeration during the bleaching and dyeing processes. Floral seasons were extended and human bodies could be better preserved for study. Refrigeration found a use in almost all industries from oil refineries to paper manufacturers to fur warehouses, and other applications such as storage of perishable foods, air conditioning, and preservation of vaccines and medicines…

By reducing carbon emissions and promoting sustainable energy solutions, we can combat the adverse effects of climate change, ensuring a safer planet for future generations.

Reduced greenhouse gas pollution, reduced running costs, and energy freedom are just a few advantages of solar-powered fridge and air conditioning systems.

While expanding access to refrigeration and cooling in places without dependable power supply, these systems have the potential to significantly help mitigate the impacts of climate change.

The extensive use of solar-powered refrigeration and air conditioning faces a number of obstacles, such as expensive initial costs, storage space constraints, and the requirement for efficient upkeep and repair services. In addition, problems with grid integration, energy storage, and funding require technological and policy answers.

In general, it is critical to investigate and engage in sustainable and energy-efficient options, such as solar-powered air conditioning and refrigeration, as the demand for cooling keeps rising.

We can build a more sustainable and fair future for everyone by tackling the issues and taking advantage of the advantages.

At present, isolated electric systems largely depend on fossil fuels [7]. Until recently, only diesel generator groups were able to ensure a secure and reliable supply in exchange for very high prices in the transport of fuel and in the operation of the system.

New energy models pursue two main objectives: replacing conventional generation with renewable sources and improving overall system efficiency.

Even in the industrialized countries an important number of small communities (or isolated sites) have the problem of the lack of electrical energy.

To extend electrical networks by interconnection quickly is very costly where villages are far apart, population density is low, or consumption is limited. In addition, the absence of adequate road systems makes the transport of fuel to these sites very difficult and therefore, the installation of a local fuel powered system is not a suitable alternative.

For countries with important mean daily total (direct and diffuse) solar radiation, solar cells could provide electrical energy for thousands of small villages before the end of this century. Photovoltaic technology is in a unique position to fill the resulting electricity gap. Although the cost is still quite high, photovoltaic systems are often the most reliable, least expensive option for small, remote applications.[8].

Our work exposes and proposes solutions to the following problems :

-To cope with the high consumption of electrical energy by refrigeration and air conditioning installations, photovoltaic solar energy can be used as a source of renewable energy, and free especially for areas with high solar radiation, either by using this energy totally, or partially with the use of electrical energy from the electrical network of non-isolated areas connected to the electrical network.

-To reduce the negative impact of refrigeration and air conditioning installations on the environment, we can on the one hand use the electrical energy produced by photovoltaic solar panels, and on the other hand use refrigerants with very low impact on the environment. such as new refrigerants, in this case the fluid studied in this thesis, the HFO R1234ze fluid which has a zero ODP, and a very low GWP (7).

-To power refrigeration and air conditioning installations on isolated sites not connected to electrical networks, solar electrical energy produced by photovoltaic solar panels with storage battery can be used. to supply VCR vapor compression refrigeration installations, giving as result a hybrid system combining high performance of the VCR system, and a PV photovoltaic solar panel system producing sustainable electrical energy, and without negative impact on the environment. The energy from the batteries can be used, during the period of the day when solar radiation is low, and is not sufficient to power the refrigeration, or air conditioning system.

In another way this research work falls within the framework of sustainable development for isolated sites, in terms of refrigeration and air conditioning, to resolve the problems of :

-The excessive demand for electrical energy from refrigeration systems in general.

-The negative impact of the production of this electrical energy on the environment.

-The absence of this energy in isolated sites not connected to electrical networks.

-The use of conventional refrigerants, which contribute to the destruction of the ozone layer, and to global warming in the event of release or leakage to the outside.

To this end, we have considered a solution to all these problems, we propose to study and simulate the operation of a vapor compression refrigeration system powered by electrical energy, but produced by photovoltaic solar panels, in an isolated region in southern Algeria with very significant solar energy potential, which is Ghardaia.

The performance study and simulation was carried out using a MATLAB computer program, based on equations, formulas and mathematical relationships available in the literature.

To our knowledge, the particularity of this program consists of the use of analytical equations drawn from recent articles for the determination of the thermodynamic properties of the refrigerant, and not from software.

The proposed system operates with the new generation HFO refrigerant R1234ze with low global warming potential, greenhouse effect GWP. and zero potential for destruction of the ozone layer ODP.

The influence of the different operating parameters on the performance of the system is thus studied, with a thermodynamic and exergy analysis of the system.

The entire study is carried out by comparing the performance of the system using the HFO R1234ze fluid, and using the HFC R134a fluid, to prove and confirm that the first fluid represents a significant replacement potential for the latter.

This work is accomplished by presenting the obvious environmental benefit that this alternative offers, particularly for isolated sites.

This thesis is composed of two parts and four chapters. So after presenting the problem of the research theme in the “introduction”.

The first part, consisting of a chapter : “literature review” , which is reserved for the presentation of the fundamental notions of photovoltaic solar energy, and for bibliographic research concerning the different technologies of solar refrigeration systems as well as most of the work relating to the solar vapor compression refrigeration technique using photovoltaic PV solar energy and the state of the art of these systems.

The second part is composed of three chapters including the second chapter of the thesis : “methodology” which is reserved for the presentation of the proposed system, and the development of the numerical model in “MATLAB” based on the laws, equations and mathematical approaches available in the literature.

A thermodynamic analysis of the system is treated in the 3rd chapter :“thermodynamic performance analysis”.

In the 4th chapter : “ exergetic performance analysis” an exergy analysis of the proposed system will be carried out.

The simulation results will be discussed in chapters 3 and 4.

Finally, the : “conclusions and recommendations” section will summarize the main results of the thesis, and present some perspectives of this work.

PART I

BIBLIOGRAPHICAL RESEARCH

CHAPTER 1

LITERATURE REVIEW

CHAPTER 1

Literature review

1.1 Vapor compression refrigeration systems

1.1.1 Historical development and principles of VCR systems

Refrigeration in the broadest sense of the world refers to any process that lowers and maintains a temperature below the temperature of the surrounding ambient. The concept of refrigeration and cooling objects has been around a long time. Evidence of ice houses go back to Mesopotamia in 1780 BC and evaporative cooling Yakhchals have existed since 400 BC in Persian deserts. Needless to say, humans have long recognized the importance and the power of refrigeration.

The first instance of using mechanical refrigeration, however, was not until 1755. Scottish professor William Cullen drafted a machine that used a pump to create a vacuum in a container of diethyl ether. The vacuum lowered the boiling point of the ether and allowed the ether to absorb more heat from the surrounding air when boiled. Though hailed as a useful advancement, no practical application resulted.

Fifty years later the American Oliver Evans expanded on this principle with his invention of the closed vapor-compression cycle. He used Cullen's understanding of a lowered boiling point in a vacuum and demonstrated how the vapor could be used to cool. However a working model was not created until 1835 by Jacob Perkins. Another 7 years were needed before John Gorrie created a commercially successful one! Gorrie was able to use the vapor-compression cycle to cool hot air in rooms. Unfortunately, his unit required too much ice to provide lasting, practical cooling.

Finally, in 1851 British journalist James Harrison used the technology to artificially create ice. By using ether, alcohol, or ammonia as opposed to simple air, Harrison's invention allowed both the reuse of cooling agent and for temperatures to be brought well below the freezing point of water. Harrison used a compressor to force the refrigeration gas through a condenser where it cooled and liquefied. The cooled gas than circulated through coils and vaporized, cooling the surrounding process. His refrigeration cycle essentially matches the existing cycle today.

In the early 20th century, the mechanical refrigerator underwent several changes & improvements. Eventually, the Frigidaire Company purchased the compressor-variant refrigerant in 1918. With a solid design & large company capital, the mass production of refrigerators for the home began.

Other companies soon joined in and by the middle of the 20th century, the icebox was virtually gone from the American home. In its place stood the reliable home refrigerator.

The Vapor Compression Refrigeration Cycle involves four components: compressor, condenser, expansion valve/throttle valve and evaporator. It is a compression process, whose aim is to raise the refrigerant pressure, as it flows from an evaporator. The high-pressure refrigerant flows through a condenser/heat exchanger before attaining the initial low pressure and going back to the evaporator.

Step 1: Compression

The refrigerant (for example R-717) enters the compressor at low temperature and low pressure. It is in a gaseous state. Here, compression takes place to raise the temperature and refrigerant pressure. The refrigerant leaves the compressor and enters to the condenser. Since this process requires work, an electric motor may be used. Compressors themselves can be scroll, screw, centrifugal or reciprocating types.

Step 2: Condensation

The condenser is essentially a heat exchanger. Heat is transferred from the refrigerant to a flow of water. This water goes to a cooling tower for cooling in the case of water-cooled condensation. Note that seawater and air-cooling methods may also play this role. As the refrigerant flows through the condenser, it is in a constant pressure.

Step 3: Throttling and expansion

When the refrigerant enters the throttling valve, it expands and releases pressure. Consequently, the temperature drops at this stage. Because of these changes, the refrigerant leaves the throttle valve as a liquid vapor mixture, typically in proportions of around 75 % and 25 % respectively. Throttling valves play two crucial roles in the vapor compression cycle. First, they maintain a pressure differential between low- and high-pressure sides. Second, they control the amount of liquid refrigerant entering the evaporator.

Step 4: Evaporation

At this stage of the Vapor Compression Refrigeration Cycle, the refrigerant is at a lower temperature than its surroundings. Therefore, it evaporates and absorbs latent heat of vaporization. Heat extraction from the refrigerant happens at low pressure and temperature. Compressor suction effect helps maintain the low pressure.

There are different evaporator versions in the market, but the major classifications are liquid cooling and air cooling, depending whether they cool liquid or air respectively.

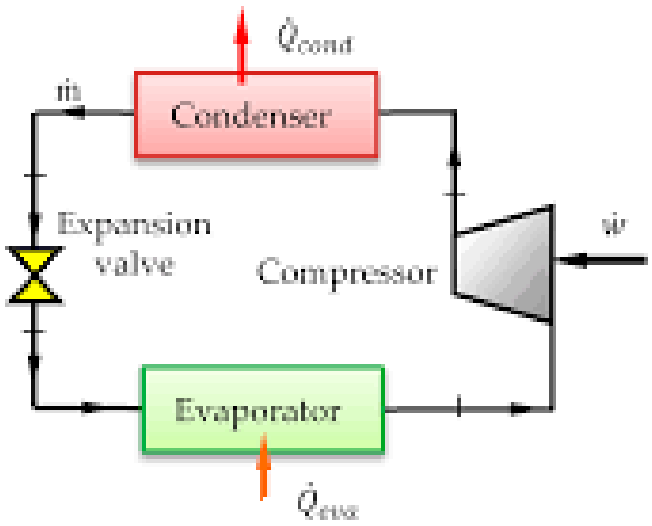


Figure 1.1: principles of VCR systems

1.1.2 Types and characteristics of refrigerants used in VCR systems

The table 1.1 shows the refrigerants used in vapor compression refrigeration systems

Table 1.1 : refrigerants used in vapor compression refrigeration systems [9]

Period	Refrigerants
1800–1900	Ethyl alcohol, methyl amine, ethyl amine, methyl chloride, ethyl chloride, sulphur dioxide, carbon dioxide, ammonia
1900–1930	Ethyl bromide, carbon tetrachloride, water, propane, isobutene, gasoline, methylene chloride
1931–1990	Chlorofluorocarbons, hydrochlorofluorocarbons, ammonia, water
1990–2010	Hydrofluorocarbons, ammonia, isobutene, propane, carbon dioxide, water
Immediate future	Hydrofluorooelifins, hydrofluorocarbons, hydrocarbons, carbon dioxide, water

The basic environmental properties of the main fluids used as refrigerants in vapor compression refrigeration and air conditioning equipment are :

-Chloroflurocarbons (CFC)

These are fully halogenated fluids that have high ODP and were found to be the most responsible for the creation of ozone hole.

Use of formerly popular CFCs such as R12 and R11 in new equipment was banned by the Montreal Protocol. While R12 recovered from old systems may still be available, new lots of CFCs are no longer being produced.

-Hydrochlorofluorocarbons (HCFC)

Unlike fully-halogenated CFCs, which contain only carbon and halogen atoms, in the case of partially-halogenated HCFCs, not all hydrogen atoms are replaced by halogen atoms. The remaining hydrogen atoms facilitate partial breakdown of the compounds in the troposphere. For this reason these compounds are less harmful to the stratospheric ozone layer, though they still have the some potential to damage the ozone layer. However, since they are known to cause global warming, HCFCs are no longer used in the industrialized countries of the West. Phase-out of HCFCs is being accelerated.

-Hydrofluorocarbons (HFC)

Hydrofluorocarbons contain fluorine but no chlorine or bromine in the molecule, so that their ODP is zero. Some examples of HFCs areR23, R32, R125, 134a, 143a and 152a. A problemwith HFCs is that they are chemically stable and can accumulate in the atmosphere contributing to the global warming. Hence, HFCs need to be eventually replaced.

-Hydrofluorooelifins (HFO)

These also belong to a class of HFCs, but are derived from unsaturated hydrocarbon molecules such as propylene. HFOs are relatively unstable, have a small atmospheric lifetime and therefore a small GWP. R1234yf and R1234ze are two HFO refrigerants invented recently.

-Fluoroiodocarbons (FIC)

These are a group of chemicals containing fluorine, iodine and carbon such as, trifluoromethyl iodide (CF3I), perfluoroethyl iodide (C2F5I) and perfluoropropyl iodide (C3F7I). The FICs are reported to have zero ODP and negligible GWP due to their very short life periods. These can also be used in blends. A blend of CF3I andHFC 152a (51/49mole percent)was run in a refrigerator without oil change for over 1,500 hours without apparent ill effects. Measurements showed that the energy efficiency and capacity were equal to or slightly better than CFC 12. [9]

1.2 Solar energy applications

1.2.1 Principles of photovoltaic solar energy

1.2.1.1 Solar energy

The sun is a major source of inexhaustible free energy (i.e., solar energy) for the planet Earth. Currently, new technologies are being employed to generate electricity from harvested solar energy. These approaches have already been proven and are widely practiced throughout the world as renewable alternatives to conventional nonhydro technologies. Fig.1.1 shows a comparison of the non-hydro renewable energy capacities between countries for 2012.

Theoretically, solar energy possesses the potential to adequately fulfill the energy demands of the entire world if technologies for its harvesting and supplying were readily available [10]. Nearly four million exajoules (1EJ = 1018J) of solar energy reaches the earth annually, ca. 5 × 104 EJ of which is claimed to be easily harvestable [11]. Despite this huge potential and increase in awareness, the contribution of solar energy to the global energy supply is still negligible [12].

Another major prospect with regard to solar research is associated with the current drive toward reducing global carbon emissions, which has been a major global environmental, social, and economic issue in recent years [12]. For example, 696,544 metric tons of CO_2 emissions have been reduced or avoided via the installation of 113533 household

solar systems in California, USA [13]. Therefore, the adoption of solar technologies would significantly mitigate and alleviate issues associated with energy security, climate change, unemployment, etc.

It is also anticipated that its use will play an important role within the transportation sector in the future as it does not require any fuel transportation.

Policies, investment, and supports (such as research funding) from various governmental and non-governmental organizations for solar technologies have helped build up a solid foundation for the exploitation of this renewable energy system.

While incentives and rebates can be effective motives for the development of these markets, there are also growing efforts to reduce the fiscal burden of these policy incentives.

However, solar power subsidies have already faced sharp cuts in many countries, which may retard growth within the industry.

To revert this potential decline, policies are changing to support the deployment of solar power systems for large-scale power generation.

Furthermore, greater subsidies should be provided for residential solar generators over utility- scale generators.

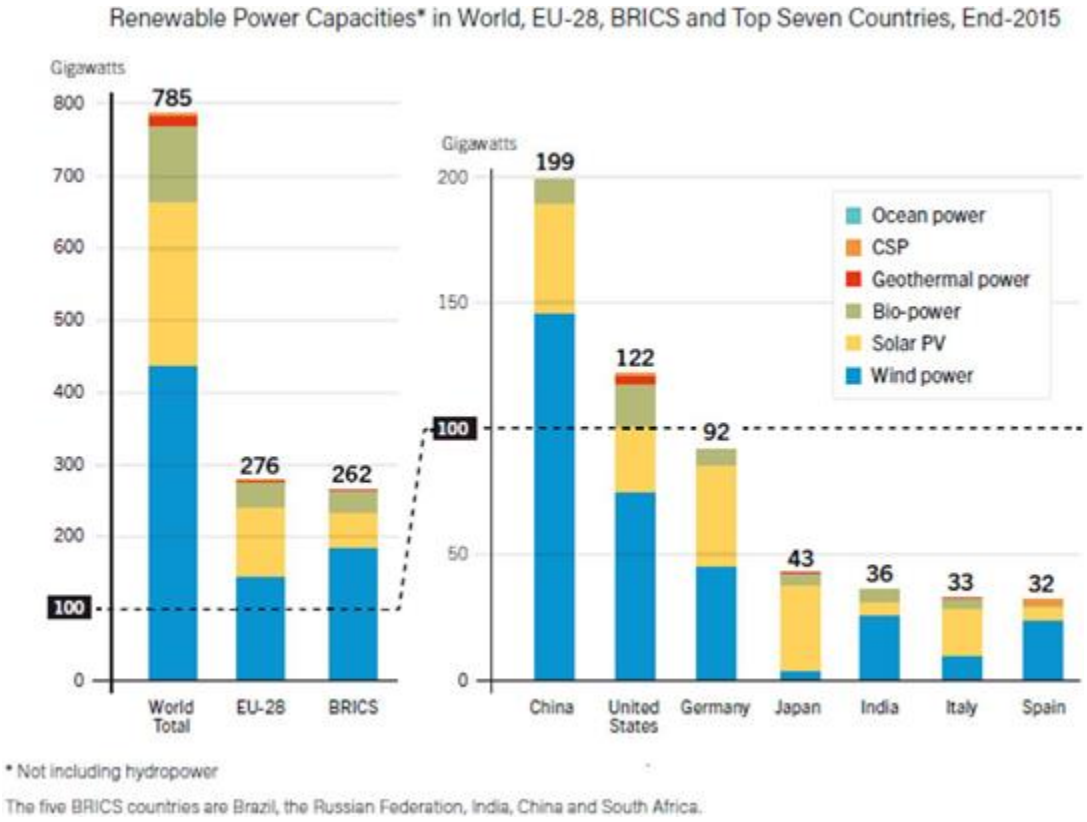


Figure I.2 : Comparison of non-hydro renewable energy capacities between countries [14]

1.2.1.2 Potential of solar energy technologies and comparisons between locations

Only three renewable energy sources (i.e., biomass, geothermal, and solar) can be utilized to yield sufficient heat energy for power generation.

Of these three, solar energy exhibits the highest global potential since geothermal sources are limited to a few locations and the supply of biomass is not ubiquitous in nature [15,16].

A number of factors (e.g., latitude, diurnal variation, climate, and geographic variation) are largely responsible for determining the intensity of the solar influx that passes through Earth's atmosphere [17]. The average amount of solar energy received at Earth's atmosphere is around 342 W m^{-2}, of which ca. 30% is scattered or reflected back to space, leaving ca. 70% (239 W m^{-2}) available for harvesting and capture [18]. The annual effective solar irradiance varies from 60 to 250 W m^{-2} worldwide [19].

Fig. 1.3 depicts the annual average intensity of solar radiation over the surface of the earth.

Research has shown that “black dot” areas could provide more than the entire world's total primary energy demand, assuming that a conversion efficiency as low as 8% is achieved [20]. In comparison, the sunniest places of the planet are found on the continent of Africa.

As theoretically estimated, the potential concentrated solar power (CSP) and PV energy in Africa is around 470 and 660 petawatt hours (PWh), respectively [21]. However, in the regions other than Africa (like south-western United States, Central and South America, North and Southern Africa, Middle East, the desert plains of India, Pakistan, Australia, etc.), such potential is only limited to generate 125 gigawatt hours (GWh) from a 1 km^2 land area [22]. Hang et al. [23] estimated that around 6300 km^2 of the wasteland located in the northern and western regions of China (where solar radiation is among the highest in the country) has around 1300 GW electricity generation capacity.

In contrast, the National Renewable Energy Laboratory (NREL) in the United States has estimated that the solar energy potential within the USA is capable enough to provide 400 zettawatt-hours annually (ZWh) [24], hugely exceeding the current electrical generation capacity (22,813 terawatt-hours (TWh) [25]).

Morocco, a northern African country that enjoys about 3000 h of sunshine per year has recently launched one of the world's largest solar energy projects (including both PV and CSP technologies), targeting the generation of 2000 MW (MW) by the year 2020 [26].

Such a plan is ideal due to their suitable atmospheric conditions (such as high altitudes, low fugitive dust, high transparency, and low humidity).

Similarly, the Tibetan plateau in Northern China has been reported to receive a very high solar radiation of ca. 195 kCal cm^{-2} y^{-1} [27].

In a similar environment, the yearly duration of sunshine in Lhasa was reported to be 3021 h, while those in Chengdu and Shanghai were 1186 and 1932 h, respectively [27].

Australia has the highest solar radiation per square meter of all continents and is estimated to have the best solar energy resource in the world.

On the Australian continent, a relatively high daily solar irradiance of 4–6 $kWhm^{-2}$ has been reported [28].

Comparable levels of solar radiation were also observed in the desert areas of northern and southern Africa, the southwestern United States, adjacent areas of Mexico, and regions of the Pacific coast off South America [22].

The whole solar energy concept is regarded as the harvesting and utilization of light and/or heat energy generated by the Sun and technologies (passive and active) involved in achieving such goals [29].

A classification of present solar energy technologies is shown in Fig.1.4.

By definition, passive technology involves the accumulation of solar energy without transforming thermal or light energy into any other form (for power generation, for instance) [30]. Solar energy collection, storage, and distribution in the form of heat for the heating of homes (especially during the winter season) exemplifies a form of passive solar technology.

On the other hand, active solar system collects solar radiation and uses mechanical and electrical equipment (e.g., pumps or fans) for the conversion of solar energy to heat and electric power.

The most well known application of this system is the solar water heater system.

In general, active solar energy technology can be further grouped into two categories: (i) photovoltaic technology and (ii) solar thermal technology [31].

In recent years, photovoltaic technology involving the use of semiconductors to convert sunlight directly into electrical energy has become a highly desirable option [32].

The intense research efforts of energy scientists with regard to solar options have helped to yield an improved efficiency of photovoltaic technology; in case of hybrid perovskite solar cells ((CH3NH3)PbI3), a promising achievement (e.g., an efficiency increase of ca. 18%) has been reported [33,34].

Currently, photovoltaic technology involving wafer-based cells (traditional crystalline silicon or gallium arsenide), commercial thin-film cells (cadmium telluride, amorphous silicon, copper indium gallium diselenide), and new thin-film technologies (perovskites, organic materials,quantum dots) are progressing with the advent of intense R & D efforts [35]. In solar thermal technology, solar energy is harnessed into thermal energy for domestic and/or commercial applications such as drying, heating, cooling, cooking, etc. [36,37]. However, on the industrial scale, concentrated solar thermal (CST) technologies are being used to fulfill such heating requirements while concentrated solar power (CSP) technologies are being employed to generate electricity.

The latter involves the use of high-magnification mirrors to concentrate solar energy prior to converting it into heat energy to power a steam turbine [38].

Four types of CSP technologies are currently available on the open market: (i) paraboli troughs (these concentrate sunlight onto a receiver tube containing a working liquid); (ii) Fresnel mirrors (use multiple flat mirrors to concentrate solar sunlight onto a receiver tube);
(iii) power towers (an array of thousands of sun-tracking reflecting mirrors positioned in a field to concentrate solar radiation to a single point), and (iv) solar dish collectors (concentrate power by focusing ST energy onto a single point situated above a reflector dish) [39].

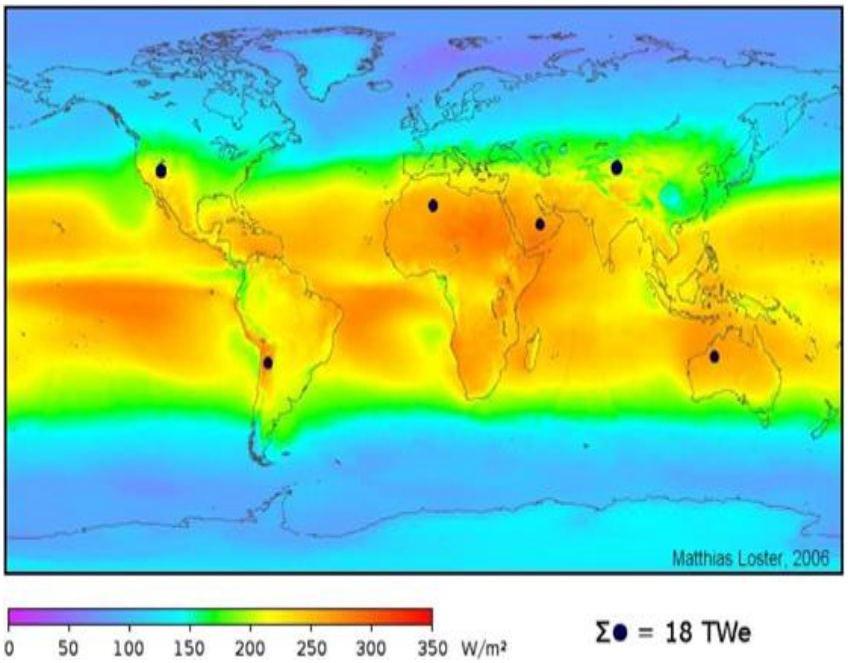


Figure 1.3 : Annual average solar irradiance distribution over the surface of the Earth [20]

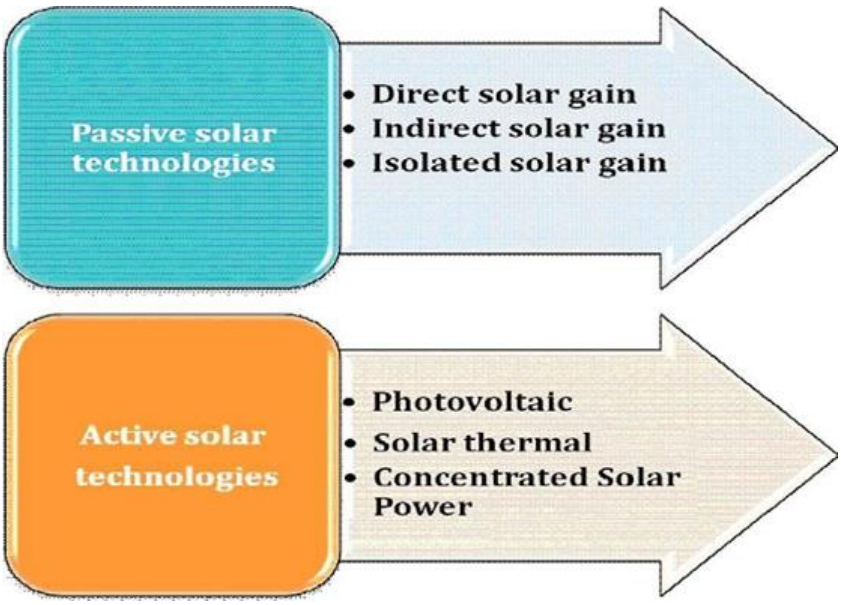


Figure 1.4 : Classification of the present solar energy technologies [29]

1.2.1.3 Current global status for solar energy

The availability of most renewable energy sources (i.e., wind, solar, tidal wave, hydro, etc.) tends to vary widely throughout the course of a day, season, year, even from one geographical location to another [40].

A comparison of the global power capacities between different renewable energy sectors is listed in Table 1.2. In many countries, the use of renewable energy has been pursued competitively along with conventional energy sources, thereby making a significant contribution to the national generation of power [41]. For example, solar PV contributes an estimated 7.9%, 7.6%, and 7.0% of the electricity demand in Italy, Greece, and Germany, respectively [42]. Solar PV capacities have grown at phenomenal rates, from ca. 3.7 in 2004 – 225 GW in 2015 [43].

In 2015, with a total of $161 bn investment and additional 59 GW (a 34% increase over 2014's total) on solar energy led to cumulative installations of total solar capacity 256 GW worldwide at the end of the year [44]. However, with nearly 100 GW of installed capacity, Europe is still the most solarized continent. In 2015, the solar capacity for Europe increased by 8 GW, while the United Kingdom, Germany, and France achieved an increase of only 5.3 GW (75%) [45].

However, China has excelled with a total installed solar power capacity of ca. 43 GW as of December 2015, thereby replacing long-time table topper Germany in the global rankings [44].Moreover, China also has plans to increase its solar power capacity to 150 GW by 2020.

Table 1.2: Comparison of the global power capacity between different renewable energy sectors (Unit: GW) [14]

Order	Power capacity	Year		
		2013	2014	2015
1	Total Renewable power	1578	1712	1849
2	Hydropower	1018	1055	1064
3	Bio-power	88	93	106
4	Geothermal	12.1	12.8	13.2
5	Solar PV	138	177	227
6	Concentrating solar thermal	3.4	4.4	4.8
7	Wind power capacity	319	370	433

According to the American Solar Energy Industries Association, the total solar PV capacity of the USA could reach 45 GW by 2017 [46].

In Australia, solar power has become the foremost source of new power, producing 913 MW against 774 MW derived from wind power in 2015 [47].

Interestingly, 1300 MW of coal power was decommissioned in Australia at the same year [47].

This was applauded as a huge drive towards replacing conventional coal-based power generation and achieving a greener earth.

In India, the installed solar power grid reached a capacity of 3743 (March 2015), 6762 (March 2016), and 8062 MW (July 2016) [48].

With such developments, India is currently planning to increase its solar power capacity to a staggering 100,000 MW by 2022 [48].

Similarly on the European front, France plans to construct a 1,000-kilometer-long solar roadway, with each kilometer capable of providing enough clean energy to power 5000 homes [49].

To recap, Table 1.3 lists the present solar power generation capacities and world rankings at the end of 2015.

Table 1.3: The 2015 global ranking for solar power generation capacity [14]

World Ranking	Country Name	Total Capacity (MW) at 2015	Installed (MW) in 2015
1	China	43,180	15,130
2	Germany	39,553	1418
3	Japan	33,300	10,000
4	USA	27,400	7260
5	Italy	19,160	700
6	UK	8437	3109
7	Spain	6967	6946
8	France	6680	1020
9	Australia	5049	913
10	India	4680	2048

1.2.1.4 Photovoltaic solar energy

1.2.1.4.1 History of photovoltaic solar energy

Photovoltaic, also called solar cells, are electronic devices that convert sunlight directly into electricity. Photovoltaic power were first discovered by a French scientist Edmond Becquerel in 1839. The first working solar cell was successfully made by Charles fritts in 1882. It was made of thin sheets of selenium and coated with gold. The use of solar panels for generating electricity and heat seems relatively like new development, it has actually been widely used to generate power since early 1900‟s. In 1954 Bell laboratory mass produced the first crystal silicon solar cell. The bell PV converted 4% of the sun's energy into electricity a rate that was considered the cutting edge in energy technology. heir scientists Daryl M. Chapin et al made a silicon-based solar cell with an efficiency of about 6% reported in [50]. Scientists continued to reinvent and enhanced on the design of the original solar cell and were able to produce a solar cell that was capable of putting 20% return electricity rate. In the late 1900‟s as awareness grew in the science community about the effects of global warming and the need for renewable energy sources, scientists continued to refine the silicon PV and by early 2000 they were able to make a solar cell with 24% electricity return. In just seven years scientists were again able to increase the electricity return of silicon solar cell using space age materials. By 2007, modern silicon PV Solar cells were operating with 28% electricity return. There are a wide range of PV cell technologies on the market today and more applications.

1.2.1.4.2 Photovoltaic generation

PV cell technologies are usually classified into three generations, depending on the basic material used [51].

1.Crystalline Silicon

2.Thin Film

3.Concentrated photovoltaic (CPV) and Organic Material

a/ First-generation: crystalline silicon

Silicon is a semiconductor material illustrated in suitable for PV applications, with energy band gap of 1.1 eV. Crystalline silicon is the material commonly used in the PV industry, wafer-based C-Si PV cells and modules dominate the current market. Crystalline silicon cells are classified into three types as : mono-crystalline (Mono c-Si) - poly-crystalline (Poly c-Si),or multi-crystalline (mc-Si) - ribbon silicon.

Commercial production of C-Si modules began in 1963 when sharp Corporation of Japan started producing commercial PV modules and installed a 242 W PV module on a light house, the world's largest commercial PV installation at that time [52]. Crystalline silicon technologies accounted for about 87% of global PV sales in 2010 [53]. The efficiency of crystalline silicon modules ranges from 14% to 19%. While a mature technology continued cost reductions through improvements in materials and manufacturing processes. if the market continues to grow, enable a number of high-volume manufacturers to emerge [54].

Mono-crystalline silicon

Mono – crystalline silicon cells as shown in Fig.1.5 have the highest degree of efficiency of the three most common technologies up to 20%.

Production: is a type of photovoltaic cell material manufactured from a single crystal silicon structure high purity silicon rods (ingots) are extracted from a cast then cutted into thin slices (wafers), which are then processed into PV cells. Expected lifespan of these cells is typically 25 - 30 years [55].

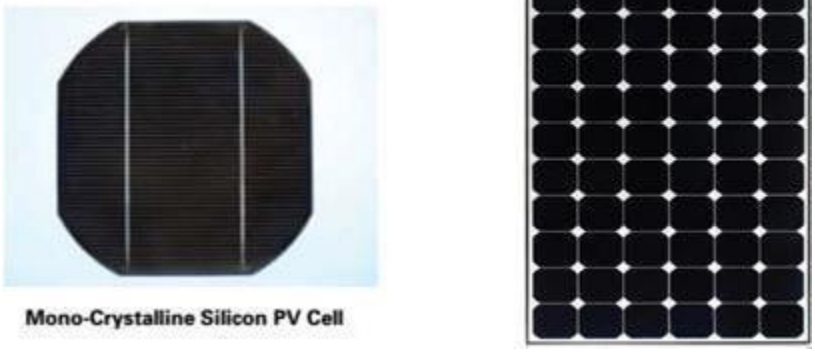


Figure 1.5 : Mono - Crystalline cell and module [56]

Poly-crystalline silicon

The silicon molecular structure consists of several smaller groups or grains of crystals, which introduce boundaries between them as Shown in Fig.1.6.

Production: The production of these cells is more economically and more efficient compared to mono - crystalline.

Making the solar cell to have a lower efficiency. unlike mono-crystalline silicon, the silicon is cast in blocks. When it hardens, it results in crystal structures of different sizes on whose border defects occur. These defects reduce the degree of efficiency [55], Lab efficiency: 18% to 23% , and Production range: 14% to 17%.

Advantages:

· Well established and tested technology

· Stable efficiency

· less expensive than single crystal silicon

· square cells allow efficient packing density

Disadvantages:

· Uses expensive material

· Waste in slicing wafers

· Slightly less efficient than single crystal

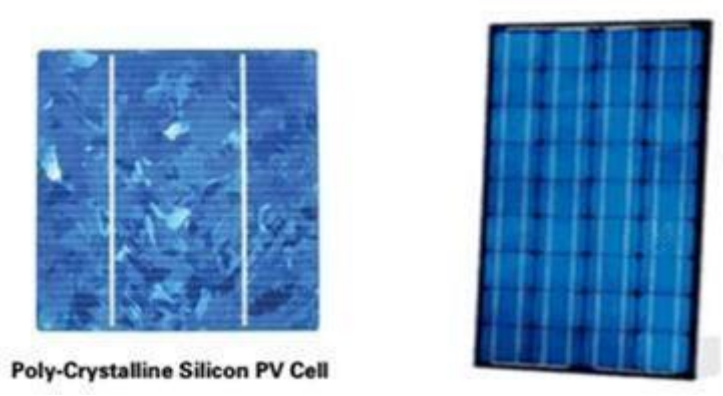


Figure 1.6 : Poly - Crystalline cell and module [56]

Ribbon silicon

String Ribbon Si wafers are grown by a vertical sheet growth technique that is currently in multi-megawatt Production at Evergreen Solar [57]. This technique produces low cost Si due to the high utilization of the Si feed stock. The high quality of the processed String Ribbon wafers has been previously demonstrated through high minority carrier lifetimes following cell processing. Recent research on processing String Ribbon cells has focused on industrial type processing.

The using of screen printing for metallization and the relatively deep junctions necessary for firing the screen printable inks. A few years ago, it has been recorded as high with a percentage of 16.2% efficiency cell.

However, recent cells made with screen-printing are now approaching the 16% level.

b/Second-generation: thin-film

Thin - film solar cells are beginning to be deployed in significant quantities. Thin - film solar cells could potentially provide lower cost electricity than c-Si wafer based solar cells [58].

Thin - film solar cells are comprised of successive thin layers, just 1 to 4 μm thick, of solar cells deposited into a large inexpensive substrate such as glass, polymer, or metal and Cadmium is a by product of zinc. A potential problem is that tellurium is produced in far lower quantities than cadmium and availability in the long term may depend on whether the copper industry can optimize extraction, refining and recycling yields.

Cadmium also has issues around its toxicity that may limit its use. As a consequence, they require a less semiconductor material to manufacture in order to absorb the same amount of sunlight (up to 99% less material than crystalline solar cells). In addition, thin films can be packaged into flexible and light weight structures, which can be easily integrated into building Components building integrated Photovoltaic (BIPV). The three primary types of thin-film solar cells that have been commercially developed are : Amorphous silicon (A-Si and A- Si/μc-Si), Cadmium -Telluride (CdTe),Copper-Indium-Selenide (CIS) and Copper-Indium- Gallium-Diselenide (CIGS).

Amorphous silicon solar cells

Along with CdTe PV cells are the most developed and widely known thin - film solar cells. Amorphous silicon can be deposited on cheap and very large substrates (up to 5.7 m^2 of glass) based on continuous deposition techniques, thus considerably reducing manufacturing costs. A Companies are also developing light, flexible A-Si modules perfectly suitable for flat and curved surfaces, amorphous silicon module efficiencies are in the range 4% to 8%. Very small cells at laboratory level may reach efficiencies of 12.2% [59],[60]. see cell in Fig 1.7.



Figure 1.7 : Amorphous solar cells

The main disadvantage of amorphous silicon solar cells is that they suffer from a significant reduction in power output over time (15% to 35%). As the sun degrades their performance. Even thinner layers could increase the electric field strength across the material and provide stability and less reduction in power output, but this reduces light absorption and hence cell efficiency.

A notable variant of amorphous silicon solar cells is the multi-junction thin-film silicon (a - Si/μc Si) Which consists of A-Si cell with additional layers of A -Si and micro crystalline silicon (μc - Si) applied onto the Substrate.

The advantage of the μc - Si layer is that it absorbs more light from the red and near infrared part of the light spectrum, thus increasing the efficiency by up to 10%. The thickness of the μc - Si layer is in the order of 3 μm and makes the cells thicker and more stable.

The current deposition techniques enable the production of multi-junction thin-films up to 1.4 m^2.

Cadmium telluride and concept of multi-junction

The abbreviation CdTe stands for the combination of tellurium and cadmium, which are combined to produce cadmium telluride (CdTe) [55]. The material is cheaper than silicon but also less efficient. As it contains the heavy metal cadmium, the take back of the modules after reinstallations is guaranteed. At present, a maximum degree of efficiency of 16 % is achieved.

Concept of multi- junction

PV devices can reach very high efficiencies because they are often based on the multi - junction concept, which means that more than one band gap is used. The maximum theoretical efficiency of single-junction cells is described by the Shockley-Queisser limit. A large fraction of the energy of the energetic photons are lost as heat, while photons with energies below the band gap are lost as they are not absorbed., e.g, if we use a low band gap material, a large fraction of the energy carried by the photons will be not used.

However, if we use more band gaps, the same amount of photons can be used but less energy is wasted as heat. Thus, large parts of the solar spectrum and largest part of the energy in the solar spectrum can be utilized at the same time, if more than one p-n junctions are used in Fig 1.8 a typical III - V triple junction cell is illustrated. As substrate, a germanium (Ge) wafer is used. From this wafer, the bottom cell is created. Germanium has a band gap of 0.67 eV.

The middle cell is based on GaAs and has a band gap of about 1.4 eV. The top cell is based on GaInP with a band gap in the order of 1.86 eV. Let us take a closer look on how a multijunction solar cell works.

Light will enter the device from the top. As the spectral part with the most energetic photons (like blue light) has the smallest penetration depth in materials, the junction with the highest band gap always acts as the top cell.

On the other hand, as the near infrared light outside the visible spectrum has the longest penetration depth, the bottom cell is the lowest band gap.Fig 1.9 shows the J-V curve of the three single p-n junctions.

We observe p-n junction one has the highest open circuit voltage and the lowest short circuit current density, which means that this p-n junction has the highest band gap. In contrast, p-n junction three has a low open circuit voltage and a high current density, consequently it has the lowest band gap. p-n junction two has a band gap in between.

Hence, if we are designing a triple junction cell out of these three junctions, junction one will act as the top cell, junction two will act as the middle cell and junction three will act as the bottom cell.

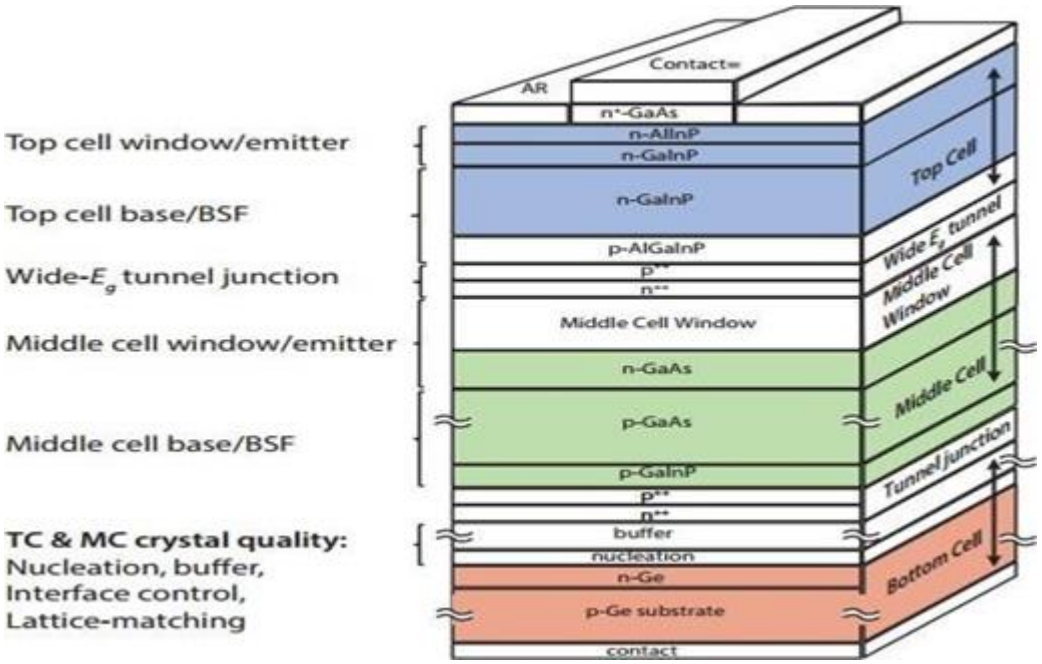


Figure 1.8 : Illustrating a typical III-V triple junction solar [61]

For understanding how the J - V curve of the triple junction looks like, we take a look at the equivalent circuit.

Every p-n junction in the multi-junction cell can be represented by the circuit of a single – junction cell Fig 1.10. As the three junctions are stacked onto each other, they are connected to each other in series, as illustrated in Fig 1.11. In a series connection, the voltages of the individual cell add up in the triple junction cell.

Further, the current density in a series connection is equal over the entire solar cell. hence the current density is determined by the p- n junction generating the lowest current. The resulting J -V curve is also in Fig 1.9 We see that the voltages add up and the current is determined by the cell delivering the lowest current [61].The development of efficiency in multi-junction as follow from with concentration method will discuss in the Table 1.4

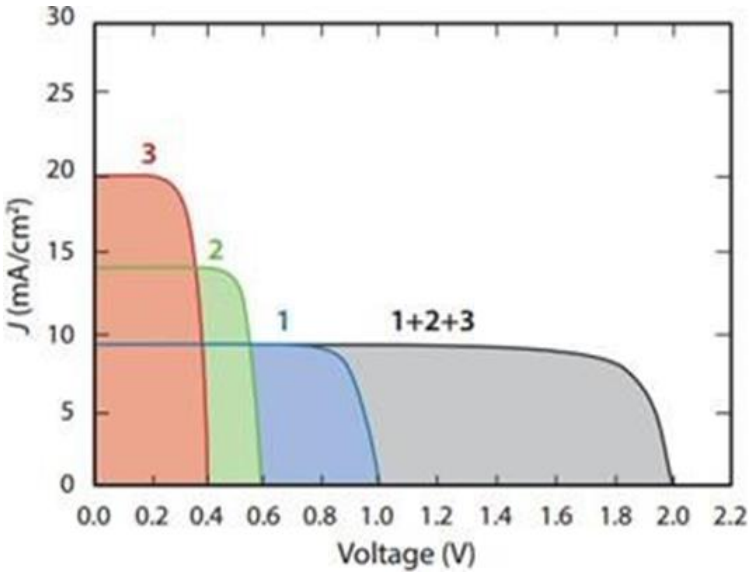


Figure 1.9 : The J -V curves of the three junctions [61]

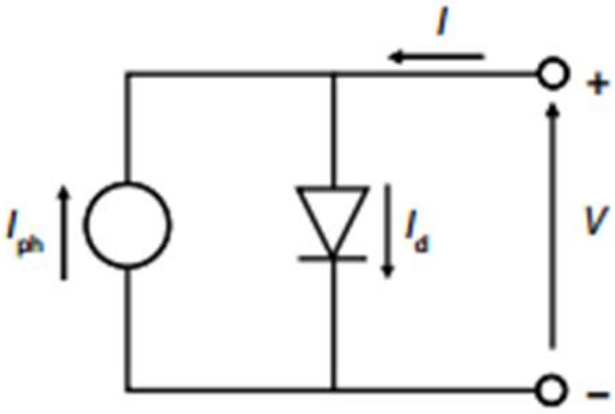


Figure 1.10 : Single junction circuit [61]

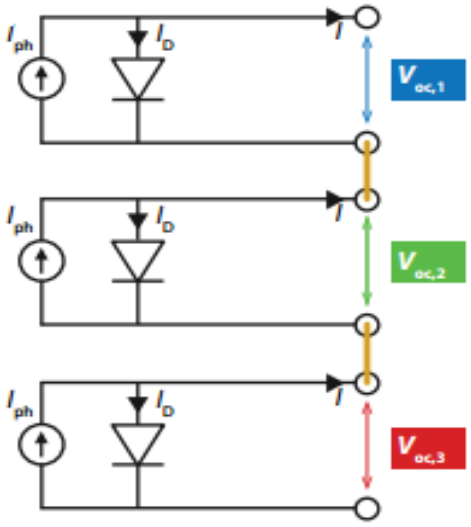


Figure 1.11 : Multi-junction circuit [61]

Table 1.4: Efficiency recent for research of PV and CPV [62]

Type	Effeciency
Single-Junction (non concentrator)	25%
Single-Junction (concentrator)	27.6%
Double-Junction (non concentrator)	31.1%
Double-Junction (concentrator)	32.6%
Triple-Junction (non concentrator)	37.7%
Triple-Junction (concentrator)	44%
Four-junction (non concentrator)	37.8%

Copper-indium-selenide (CIS) and copper-indium gallium-diselenide (CIGS)

(CIGS) PV cells offer the highest efficiencies of all thin-film PV technologies. CIS solar cell production has been successfully commercialized by many firms as shown in Fig 1.12. Current module efficiencies are in the range of 7% to 16%, but efficiencies of up to 20.3% have been achieved in the laboratory, close to that of C-Si cells [63]. The race is now on to Increase the efficiency of commercial modules. CIGS producer Solar Frontier has reached an annual Production capacity of 1 GW (Bank Sarasin, 2010). on the one hand, the CIGS module has the advantage of a low static load thanks to its light cells, while it also has the ability to absorb direct and indirect sunlight and is therefore suitable for use on flat roofs and in winter.

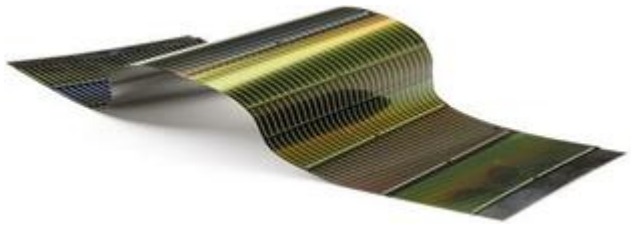


Figure 1.12 : Copper-indium-selenide (CIS) cells

c/ Third-generation PV technology

Third - generation PV technologies are at the pre-commercial stage and vary from technologies under Demonstration (Multi - junction concentrating PV) to novel concepts still in need of (quantum-structured PV cells). Some third - generation PV technologies are beginning to be commercialized, but it remains to be seen how successful they will be in taking market share from existing technologies. There are four types of third-generation PV technologies: Concentrating PV (CPV), Cooling of concentrating PV system, Organic solar cells and Dye-sensitized solar cells (DSSC).Responsible for the charge separation (photocurrent).

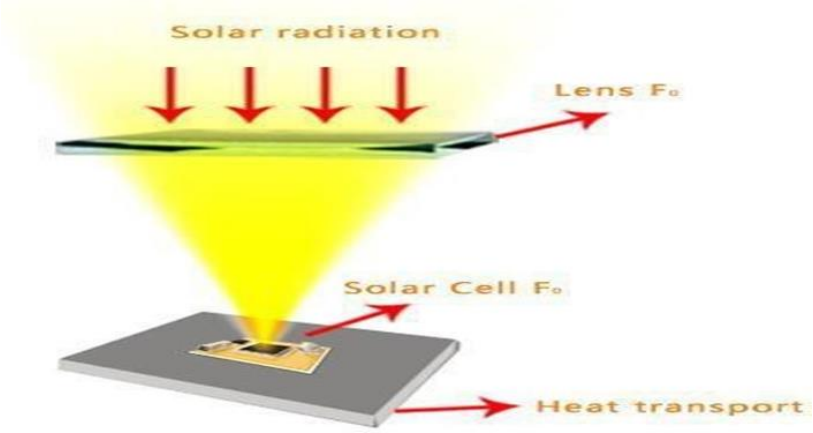


Figure 1.13 : Schematic of PV concentrator Fresnel lens

Concentrating photovoltaic technology

The concentrator is an important component for concentrating PV systems. It is classified according to optical principle, concentrator types, and geometric concentration ratio. The line focus solar concentrator includes the lens, parabolic trough, and line focusing parabolic collector. The point focusing concentrator is called the axial concentrator. The concentrator lens or reflectors of this type of concentrator are on the same optical axis of the solar cell [64]. According to the geometric concentration ratio, the concentrator can be divided into a low- concentration system and a high concentration system with a solar tracking.

Although the concentration ratio of the low-concentration system is not high, the scattered radiation can be used without a solar tracking and be applied in the area with inadequate direct radiation. Generally, if the concentration ratio is more than 10, the system can only use direct sunlight. As a result, the tracking system must be adopted. Since the mid - 1970s, with a concentration ratio of 50 and efficiency of 12.7%, the first concentrating PV system was developed in Sandia National Laboratories in US. This technology has rapidly developed. In its earlier stage, the Fresnel lens was superior in property to other light concentrating devices. The passive cooling was also feasible with the highconcentration ratio, and the application of the diamond plate and copper heat sink promoted the development of the technology.

The schematic diagram of the PV concentrator Fresnel lens is shown in Fig 1.13. The solar PV power generation has benefited from the improvement of the Fresnel lens. For instance, the 20 kW point focusing Fresnel lens array was developed by A monix and Sun Power after 15 years of continuous research designed the modularized and micro faceted Fresnel lens with a moderate concentration ratio, bringing about efficient superposition and finally uniform distribution of incident solar flux [65],[66].

They also formulated a mathematical model to solve the distribution of the energy flux on PV panel and the collecting efficiency. The calculation indicates that the non - uniformity of energy distribution remains within 20%. Under the condition of the lower-middle concentration ratios (50 times), the radiation transmittance is more than 70% designed the full glass high concentration ratio PV modular with second concentration lens of small aperture between the Fresnel lens and cells [67], which further improve the light concentration. The concentrating ratio of the concentrator system reaches 1000, and the size of PV is only 1.2 mm. It is convenient to scale up the module and improve its weathering resistance. [68] designed a line focused PV system with Fresnel lens.

It was found that heat conduction between solar cells and heat absorber is crucial to the energy efficiency of the whole system.Recently, [69] conducted extensive indoor experimental investigation on the heat loss from a point focus Fresnel lens PV concentrator with concentration ratio of 100 times under a range of simulated solar radiation intensities between 200 and 1000 W/m at different ambient air temperatures, and natural and forced convection.

It was found that the solar cell temperature increased proportionally with the increase in simulated solar radiation for all experimental tests, indicating that conductive and convective heat transfer were significantly larger than the long wave radiative heat transfer within and from the system.

The reflecting concentrator can overcome this weakness.

The point focused rotating parabolic concentrators and the line focused trough-type concentrators PV systems are mostly employed in the reflective PV concentrator.

A representative 10 m trough concentrator PV with geometric concentration ratio of 30.8 is shown in Fig 1.14 (a) [70].

The trough-type PV system caused the solar cell to be between the sun and the reflecting surface. The solar cell is always below the reflective parabolic focal line where the rays are inevitably sheltered, thus leading to optical non - uniform flux distribution.

In recent years, the butterfly – shaped PV concentrator has been developed.

A row of plane mirrors is installed at its bottom. A solar cell module is fixed on its top, reducing the shelter of sunlight by the PV devices to a certain extent [71] developed a butterfly - shaped PV concentrator, as shown by the Fig 1.14 (b).

The sunlight reflected through the mirror plane uniformly reaches the solar cell array of the corresponding side, with its concentrations varying between 2 and 12 times.

A multidisc parabolic concentrator PV with adual-axis tracking system was developed by NREL of US.

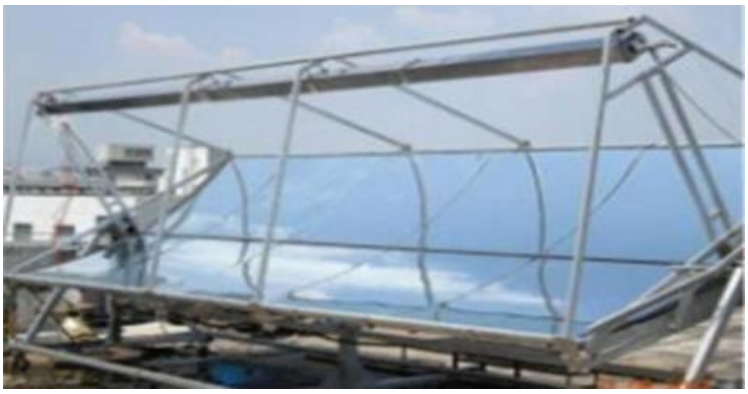
This disc type concentrator system includes 16 reflecting surfaces, with each surface containing 76 reflecting blocks.

The mirror area of the system covers 113 m with a highly precise tracking system and a concentration ratio of 250 [72].

The well - known Spanish solar energy research institution PSA developed a multidisc PV concentrator demonstration system with a concentration ratio of 2000.

It includes the heliostat, optical grating, multidisc concentrator, and PV board and can simultaneously test the PV response to the direct solar radiation and thermal flux distribution [73].

In terms of the low concentration PV system, [74] integrated the mono-crystalline silicon solar cell into the V-type reflection trough made of aluminum foil.



(a)



(b)

Figure 1.14 : Representative CPV system [75]

a)Trough CPV system

b)Butterfly-shaped Cooling of concentrating PV system

Cooling of concentrating PV system

For different types of concentration PV at a fixed temperature, the general tendency of the change in the solar cell efficiency corresponds to the change in the concentration ratio. The cell efficiency increases with the increase in the concentration ratio at the low concentration ratio and decreases with the increase in the concentration ratio at the high-concentration ratio. Under the condition of the given output power, the tandem-type cell may increase the voltage output and reduce the ohmic loss. However, the non - uniformity of light intensity distribution and the poor heat dissipation leads to overheat of the cell panel, affecting the current output of the whole cell array. This is called "the current matching problem.

" The effective PV cell cooling or the appropriate design of the concentrator may lessen the consumption of the parasitic power [76].

J.Wennerberg, J.Kessler at el [77] demonstrated that the distribution of light intensity produced by the parabolic trough concentrator is similar to a Gaussian curve. Compared to uniform illumination, both the open - circuit voltage and efficiency of the concentrator PV cell would decrease. The decrease could be aggravated when the peak intensity of light distribution is increased. This decrease may lead to a serious non-uniform flux distribution. Currently, tandem type module was adopted by most polycrystalline silicon solar cells and the current output of each cell module is equal in this case. For such type of module, the low light intensity in some areas (corresponding to the smaller light current) greatly limits the general current output of the whole PV system. Therefore, in case one or more cells are shaded, module performance will be limited by the output of these cells [78].

Organic solar cells

Organic solar cells are composed of organic or polymer materials as shown in Fig 1.15. They are inexpensive, but not very efficient. Organic PV module efficiencies are now in the range 4% to 5% for commercial systems and 6% to 8% in the laboratory [79]. In addition to the low efficiency, Suppliers of organic solar cells are moving towards full commercialization and have announced plans to increase production to more than 1 GW [80].Organic cell production uses high speed and low temperature roll-to-roll manufacturing processes and standard printing technologies. As a result, organic solar cells may be able to compete with other PV technologies in some applications, because manufacturing costs are continuing to decline and are expected to reach $ 0.50/W by 2020 [81].Organic cells can be applied to plastic sheets in a manner similar to the printing and coating industries, meaning that organic solar cells are light weight and flexible as shown in Fig 1.16, making them ideal for mobile applications and for fitting to a variety of uneven surfaces.

This makes them particularly useful for portable applications, Potential uses include battery chargers for mobile phones, laptops, radios, Flash lights, toys and almost any hand held device that uses a battery.They can also be rolled up or folded for storage when not In use. These properties will make organic PV modules attractive for building-integrated applications as it will expand the range of shapes and forms where PV systems can be applied.

Another advantage is that the technology uses abundant, non-toxic materials and is based on a very scalable production process with high productivity.

Novel and emerging solar cell concepts in addition to the above mentioned third-generation technologies that relay on using quantum dots/wires, quantum wells, or super lattice technologies [82].

These technologies are likely to be used in concentrating PV technologies where they could achieve very high efficiencies by overcoming the thermodynamic limitations of conventional (crystalline) cells. The novel concepts, often incorporating enabling technologies such as nanotechnology, which aim to modify the active layer to better match the solar spectrum [83].

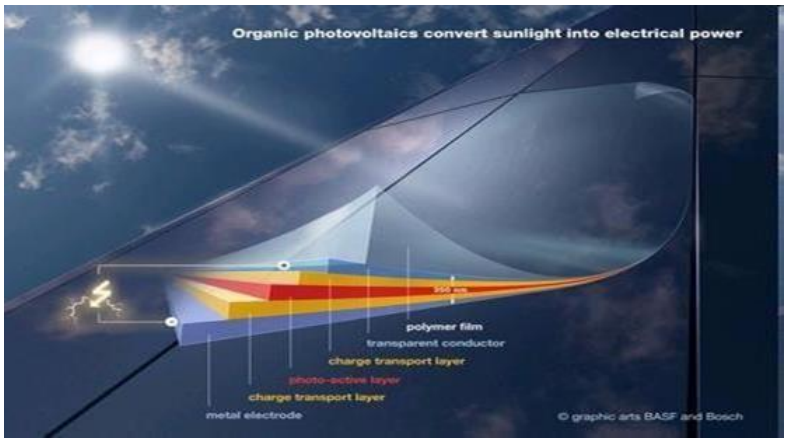


Figure 1.15 : Organic PV construction [84]

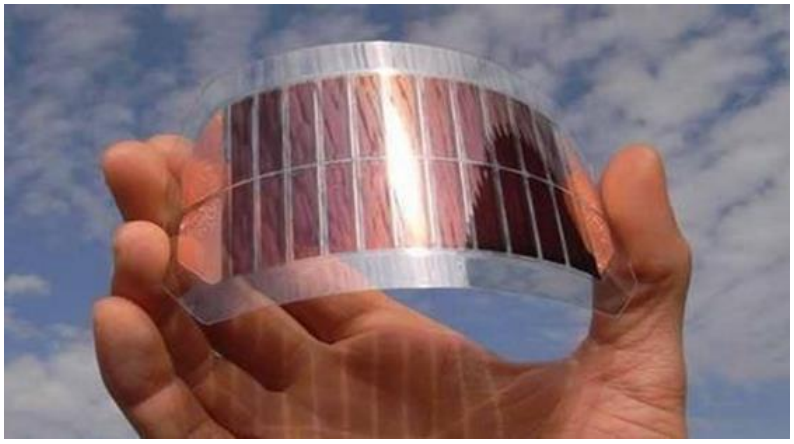


Figure 1.16 : Organic PV sample [84]

Dye-sensitized solar cells (DSSC)

Solar cells use photo-electrochemical solar cells, which are based on semiconductor structures formed between a photo - sensitized anode and an electrolyte. In a typical DSSC, the semiconductor nano crystals serve as antenna that harvest the sunlight (photons). the dye molecule is responsible for the charge separation (photocurrent).

It is unique in that it mimics natural photosynthesis [85]. These cells are attractive because they use low cost materials and are simple to manufacture, e.g, titanium dioxide covered by a light absorbing pigment. However, their performance can degrade over time with exposure to UV light and the use of a liquid electrolyte can be problematic when there is a risk of freezing.

1.2.1.4.3 Black silicon solar cell

New nanostructured silicon solar cells coated with a passivating film as shown in Fig 1.17, The nanostructuring of silicon surfaces is a promising approach to eliminate front-surface reflection in photovoltaic devices without the need for a conventional antireflection coating. This might lead to both an increase in efficiency and a reduction in the manufacturing costs of solar cells. However, all previous attempts to integrate black silicon into solar cells have resulted in cell efficiencies well below 20% due to the increased charge carrier recombination at the nanostructured surface. Here, we show that a conformal alumina film can solve the issue of surface recombination in black silicon solar cells by providing excellent chemical and electrical passivation.

We demonstrate that efficiencies above 22% can be reached, even in thick interdigitated back-contacted cells, where carrier transport is very sensitive to front surface passivation.

This means that the surface recombination issue has truly been solved and black silicon solar cells have real potential for industrial production. Furthermore, we show that the use of black silicon can result in a 3% increase in daily energy production when compared with a reference cell with the same efficiency, due to its better angular acceptance [86].

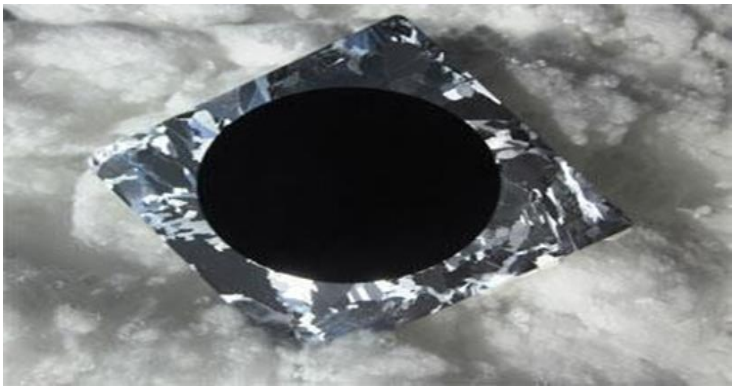


Figure 1.17 : Black silicon solar Cell

1.2.1.5 How PV power is created

Photovoltaic energy is created via these steps :

-The semiconductor absorbs light and transfers that energy to negatively charged particles, called electrons.

-The electrons flow through the semiconductor as electrical current – other cell layers extract the current from the semiconductor.

-The current flows through metal contacts – the grid-like lines on a solar cell – before it travels to an inverter.

-The inverter converts the direct current (DC) to an alternating current (AC).

-The AC travels into the electric grid or, depending on the system, connects to the circuit of the system to be powered.

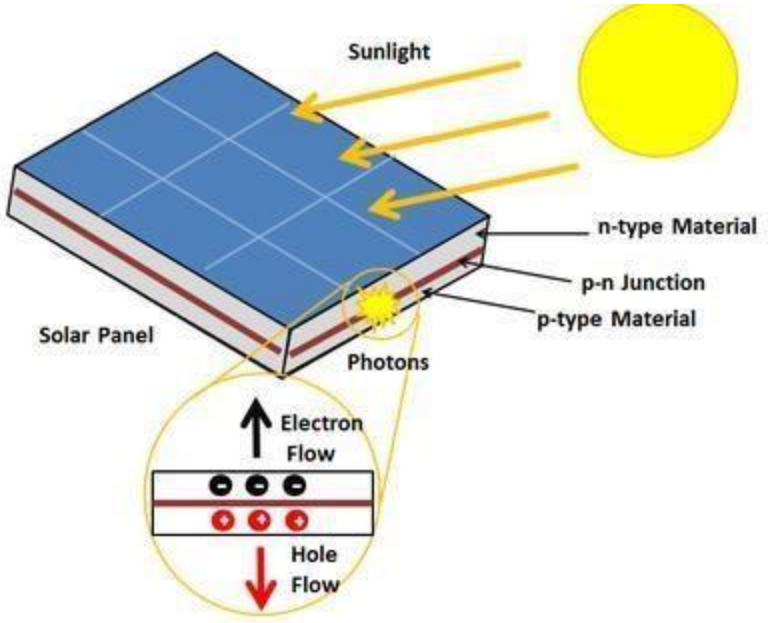


Figure 1.18 : A diagram showing the photovoltaic effect

1.2.1.6 The photovoltaic effect

The photovoltaic effect is a process that generates voltage or electric current in a photovoltaic cell when it is exposed to sunlight. These solar cells are composed of two different types of semiconductors a p-type and an n-type that are joined together to create a p-n junction. By joining these two types of semiconductors, an electric field is formed in the region of the junction as electrons move to the positive p-side and holes move to the negative n-side.

This field causes negatively charged particles to move in one direction and positively charged particles in the other direction.Light is composed of photons, which are simply small bundles of electromagnetic radiation or energy.

When light of a suitable wavelength is incident on these cells, energy from the photon is transferred to an electron of the semiconducting material, causing it to jump to a higher energy state known as the conduction band. In their excited state in the conduction band, these electrons are free to move through the material, and it is this motion of the electron that creates an electric current in the cell.

1.2.1.7 Battery energy storage for the PV system

Batteries store and produce energy as needed. In PV systems, they capture surplus energy generated by your PV system to allow you to store energy for use later in the day. Like technologies such as fuel cells, a battery converts chemical energy to electrical energy. Rechargeable batteries also convert electrical energy into chemical energy. Depending upon your particular PV system, batteries may help you to use more of the energy collected by your PV system. Batteries can provide power when electrical loads require more power than the PV panels are generating. This can be due to the generation of less electricity due to adverse weather conditions, greater than normal power usage, or other anomalies with the PV power collection. Batteries also help establish the DC operating voltage for the required auxiliary components in the PV system. However, they can be expensive, and each system needs to be designed extremely well so that they are worth the added expense. During the day:

· The PV system generates solar energy

· The system PV will check to see if all of the energy generation can be used to power your system

· Any surplus energy will be used to charge the battery

· If the battery is already charged, excess energy will be exported to the grid At night or when there

At night or when there is low power generation:

· The PV system generates little to no solar energy

· Energy is obtained from the battery system

· After the battery is discharged, electricity can be obtained from the grid

Solar PV systems that do not have a method of energy storage will transport surplus energy to the local energy grid, and when the PV panels are not generating enough energy for your needs, electricity needs to be supplied by the grid.

PV systems that have battery backup cost significantly more to install because there is a lot of other equipment required, such as inverters, batteries and charge controllers. The design and installation of these systems involve conducting a load analysis and specific wiring in specific subpanels. Battery sizing is based upon the average daily electrical load and the number of days of battery storage.

1.2.1.7.1 Battery types

There are many types of batteries that can be used in PV systems. The lead-acid type of the most common, but lithium-ion batteries are becoming more popular. Table 1.5 compares these two most common battery types. A motive power (traction battery) is a lead-acid battery designed for use in deep discharge applications, such as electric vehicles. Traction batteries are used in stand-alone PV systems and differ from deep discharge batteries because they use heavier, thicker plates and strong intercell connections to withstand the mechanical stresses from deep discharges.

Table 1.5: Two most common types of batteries for PV system storage

Lithium-ion batteries	Lead-acid batteries
Becoming more common in domestic grid-connected solar PV storage systems • More expensive • Lighter and smaller • Requires integrated controller to manage charging and discharging • More efficient • Can discharge more stored energy • Longer expected lifetime	• Used for off-grid storage systems where additional storage is required • Less expensive • Heavier and larger • Requires good charging and discharging process to maintain battery health • Less efficient • Shorter expected lifetime

Flooded batteries have a liquid electrolyte solution. Vented lead-acid batteries release hydrogen and oxygen gases; therefore, adequate ventilation must be provided for both vented and sealed battery systems. It is usually advisable to provide adequate ventilation requirements similar to a combustion water heater. There are no specific ventilation requirements, vented cells should incorporate a flame arrestor to help prevent explosions from external ignition sources, and sealed batteries must have pressure relief vents. Valve-regulated lead-acid (VRLA) batteries have a gel-based electrolyte and do not have the same maintenance requirements as vented lead-acid batteries. However, they are less tolerant of overcharging and higher temperatures as well as being more expensive.

1.2.1.7.2 Battery capacity

Battery storage systems often have power ratings in kiloWatts (kW) and are typically between 1 – 7 kW. The power rating is the capability of the battery to provide power. The measurement for battery storage capacity is in ampere-hours (Ah) or kilowatt-hours (kWh). A 12-volt battery rated at 480 Ah stores 2.25 kWh of energy.

This is usually larger than the batteries actual capacity because :

•Batteries lose some energy during charging and discharging

•Batteries cannot be fully discharged

The battery power output is affected by the battery design and chemistry -- so the number of plates, plate dimensions, and electrolyte specific gravity affects the power output. The actual battery capacity is always less than the rated battery capacity. The battery capacity over time affect the usable battery capacity, i.e., the battery age, operating temperature, and discharge rate. The "depth of discharge" for typical lead-acid battery systems is approximately 50%, and it is 75% for lithium-ion batteries.

The charge or discharge rate is expressed as a ratio of the battery capacity (C) to the charge or discharge time period in hours. A 50 ampere-hour battery discharged at 5 amps for 10 hours is rated C/10 or a 10-hour discharge rate. Electrical capacity can alternatively be given in Amp- hours (Ah); where Ah x Voltage = kWh. The percent of available battery capacity is called the state-of-charge. The depth-of-discharge is the percent of capacity that has been removed. These two are related by the following:

State of charge + depth of discharge = 100%

The allowable depth-of-discharge is approximately 75 – 80% for deep cycle batteries. In very cold climates, batteries must be protected from freezing because the electrolyte density decreases with increasing temperature.

A battery's lifetime depends upon the battery chemistry and the number of cycles (complete battery charge and discharge cycles) that they undergo. The battery life expectancy is usually given in years or charge-discharge cycles. An example would be a specification of 10 years or 10000 cycles. Often the battery performance will be monitored via the PV system so that you will know when the batteries need replacing.

When looking at battery specifications, there are many factors to consider:

•Capacity

•Voltage

•Charge/discharge rates

•Lifecycle

•Size

•Weight

•Flooded or VRLA

•Safety

•Environmental conditions

•Storage requirements

•Warranty

•Costs

PV systems require a charge controller to protect batteries from overcharge. A general rule of thumb is if the max charge rate from the PV modules multiplied by one hour is equal to 3% of the battery nominal amp-hour capacity or greater, a charge controller is required. A battery that is overcharged can create a hazardous condition and greatly reduces the battery life. Therefore, may charge controllers have overcharge protection built-in.

The requirements of battery installations limit the voltage of lead-acid batteries to no more than 48 volts. This implies 24 2 volt lead-acid cells connected in series or 40 1.2 volt alkali type nickel-cadmium cells in series. Battery installations must include adequate working spaces, clearances, and ventilation. If the batteries connected together produce more than 48 V, then the batteries should be separated or connected in a way to only allow a maximum of 48 volts.

1.2.1.7.3 Battery system mounting

Racks and trays for mounting battery systems are usually made from metal, fiberglass or other non-conductive materials. Metal racks should be painted or covered with insulation to provide protection from electrolyte leakage from the batteries. Conductive racks should not be located within 150 mm from the tops of the battery cases. Any conductive racks should be properly grounded, and current-limiting overcurrent devices must be installed.

When installing battery systems, special safety precautions are necessary.

Batteries present hazards such as caustic electrolyte, high short-circuit currents, arc flash hazards and hydrogen and oxygen gas. High voltage systems may have arc flash hazards. Batteries are also very heavy and sometimes may need to be moved using the appropriate methods supported by the manufacturer.

1.2.1.7.4 Autonomy

The number of days that a fully charged battery can meet the system load without recharging is called autonomy. Autonomy can be calculated using the average daily load, nominal battery capacity, and the maximum allowable depth of discharge. The basics for selecting the appropriately sized battery is to:

•Calculate the system load

•Select the number of days that the battery needs to deliver autonomy in the system

•Use the appropriate depth of discharge to calculate the usable amp-hours

If the system load is 75 Ah per day and a 300 Ah battery is selected with an allowable depth-of-discharge of 75%, then there would be 225 Ah usable.

The battery design would then deliver 225 Ah/ (75 Ah/day) = 3 days.

Certain loads may need more than 3 days of autonomy, and if there is another backup source such as a generator, then less autonomy may be required.

1.2.1.8 Solar charge controller

An essential part of nearly all battery-based renewable energy systems, charge controllers serve as a current and/or voltage regulator to protect batteries from overcharging. Their purpose is to keep your deep cycle batteries properly fed and safe for the long term.

Solar charge controllers are a necessity for the safe and efficient charging of solar batteries. Think of the charge controller as a strict regulator between your solar panels and solar battery. Without a charge controller, solar panels can continue to deliver power to a battery past the point of a full charge, resulting in damage to the battery and a potentially dangerous situation. The basic functions of a controller are quite simple. Charge controllers block reverse current and prevent battery overcharge. Some controllers also prevent battery over-discharge, protect from electrical overload, and/or display battery status and the flow of power.

Modern solar charge controllers work by detecting and monitoring the battery's voltage level and closely regulating the flow of current from the panels to the battery.

Battery charging is best done in three stages: maximizing the current to charge the battery up to approximately 80% as quickly as possible (the "bulk charging" stage), then reducing the current as the battery approaches a full charge (the "absorb" stage), and finally maintaining a "float" or "trickle" charge to keep the battery topped off and ready for use.

1.2.1.8.1 Types of solar charge controllers

When you begin searching for solar charge controllers, you'll quickly realize that there are many different options. You can find a broad range of brands, sizes, price points, and features to choose from, which gives you the benefit of having great options but it can also be overwhelming.

Generally, the three primary charge controller types are 1 or 2 stage solar charge controllers, 3 stage and/or PWM solar charge controllers, and maximum power point tracking (MPPT). You'll also find charge controllers for electric vehicles and golf carts. The most commonly used charge controllers range from 4 to 60 amps of charging current, but there are newer MPPT controllers that can achieve upwards of 80 amps.

a/Simple 1 or 2 stage controllers

These charge controllers use shunt transistors or relays to control voltage in either one or two steps (hence the names 1 stage or 2 stage controller). These are the oldest types and are extremely basic and sometimes inefficient in their components.

However, their reliability and affordability do still attract some people.

b/3 Stage and/or PWM controllers

Manufactured by well-known brands such as Xantrex, Morningstar, Steca, and Blue Sky, PWM charge controllers are inexpensive and reliable. Their drawback is that they should only be used when the nominal voltage of the solar panels matches the battery voltage and even then, they have inefficiencies in larger systems.

c/Maximum power point tracking (MPPT) controllers

MPPT charge controllers are the highest-quality, most advanced option available, but they come with the high prices to match. Produced by brands like Victron Energy, OutBack Power, MidNite Solar, and others, MPPT controllers provide an impressive 94-98% efficiency level, delivering about 10-30% more power to the solar battery than other types. Unless your solar system is small (cabin-sized or smaller) and its battery voltage is no more than 24V, an MPPT controller is usually worth the extra initial investment. With larger, more advanced systems and 48V battery banks becoming much more common over the years, MPPT charge controllers are the new standard.

Maximum power point tracking (MPPT) is a technique that allows the maximum available energy to be transferred from a transducer.

Energy transducers, such as solar panels, have nonlinear characteristic power curves; the optimal load for maximum power output depends on the operating point for given conditions This technique requires monitoring the incoming energy, determining the optimal operation point, and adapting the load .The optimal load can be determined using a number of different techniques [87].

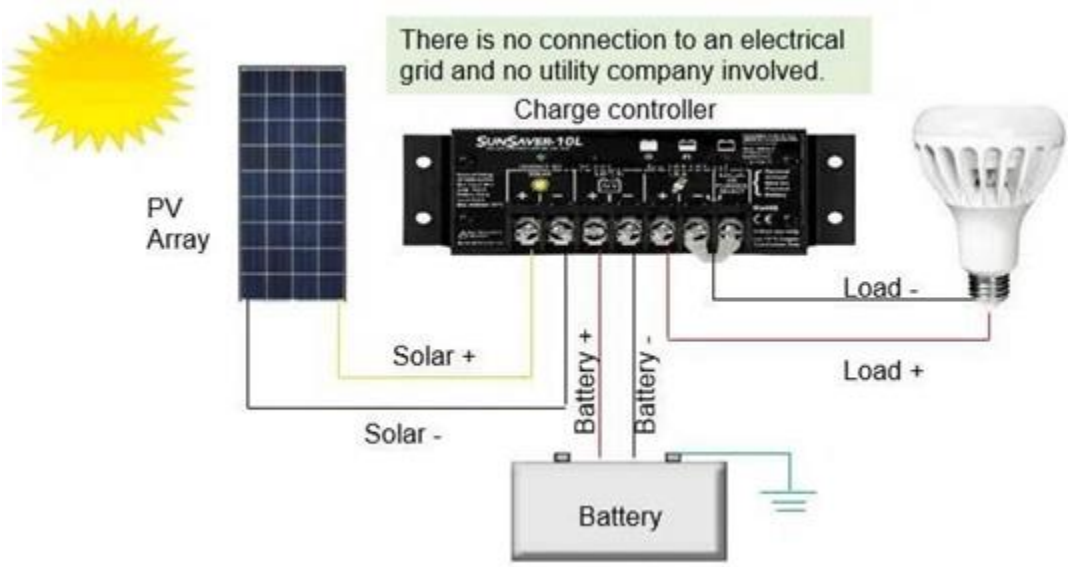


Figure 1.19 : Off-grid diagram with DC load

When installing a solar charge controller, it is recommended that you connect and disconnect in the following order:

1-Battery to the controller first 2-PV array to the controller 3-electrical load to the controller. When disconnecting, you reverse that order. The battery provides power to the controller so always make sure that solar and loads are disconnected before connecting or disconnecting the battery from the controller. Connections between the battery, load, PV array, and the controller should have disconnect switches to enhance safety and facilitate ease of installation and breakdown. In the wire diagram schematic above with DC load Fig 1.19, sunlight contacts the solar modules, which convert solar into DC electrical power that it delivers to a charge controller. The charge controller regulates the amperage and voltage that is delivered to the loads and any excess power is delivered to the battery system so the batteries maintain their state of charge without getting overcharged. During the evening when there is no sunlight, battery power is used to run the load.

The diagram of Fig 1.20 depicts the components and connections to power an AC load. This diagram with an AC load looks similar to the previous example with a DC load, except that in this example, we have added an inverter to the system.

The purpose of the inverter is to convert the DC power from the battery to AC power that can be used to run an AC load like the TV you see in the schematic.It's important to note that the inverter is connected and powered from the battery, not the controller's load terminals like we did in the DC load example. That's because the inverter can have a high energy surge upon startup, and this high current surge might be higher than the rated capacity of the charge controller, whereas the batteries will be able to meet the high energy surge requirement.

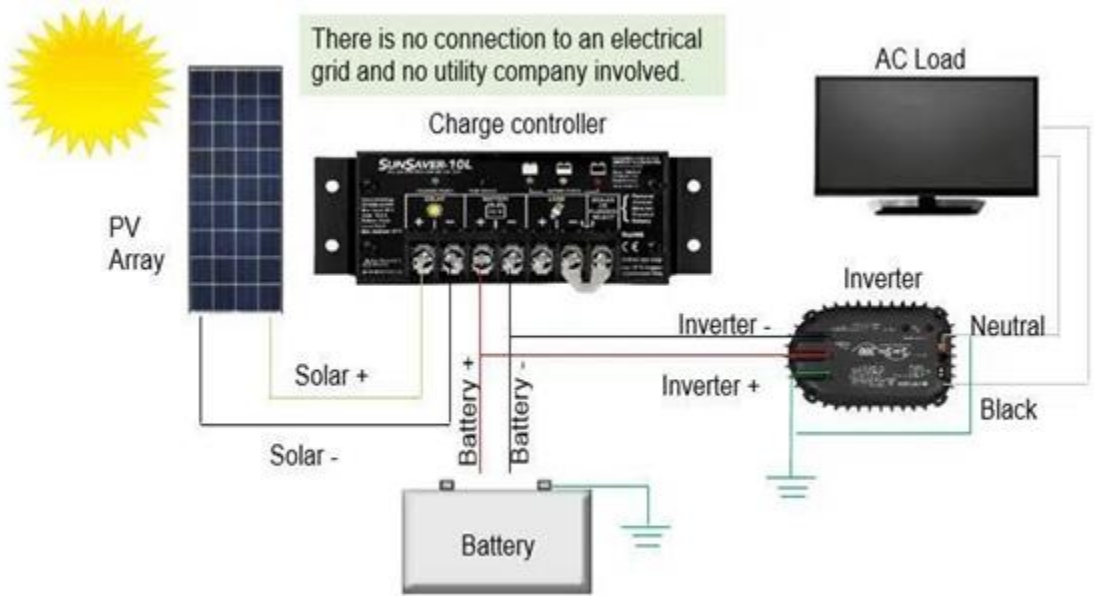


Figure 1.20 : Off-grid diagram with AC load

1.2.1.9 Solar inverter

A solar inverter is the component in your solar panel system which changes the direct current (DC) electricity captured by the solar panels, into alternating current (AC). AC current is the standard flow of electricity required to power your home appliances and connect to the National Grid. It is usually equal to either 120 volts or 240 volts depending on the country. Simply without a solar inverter in your system, you would be unable to power your home safely from your solar energy.As a solar panel system is only as efficient as its weakest part, a high quality inverter is an essential part of your panel set up. Capable of maximising the available energy being generated by your Solar Panels. PV inverters are considered the brains of any Solar PV system.

Their essential features include:

-The ability to convert direct current to alternating current.

-Maximising power output.

-Communicating with the National Grid.

-Giving feedback information about power production.

-Ensuring that your solar PV system is operating safely.

1.2.1.9.1 The different types of solar inverters

There are four main types of solar inverters. String inverters, micro-inverters, hybrid inverters and power optimisers.

a/String inverters

A ‘string’ is a chain of solar panels that are arranged into groups or rows, connected in series. In order for a string inverter to work efficiently all the panels in a string must be at the same pitch and orientation. Multiple strings can be connected to a single inverter, in fact many string inverters have 2 or even 3 MPPTs (Maximum Power Point Tracking). This means that you can have a different string of solar panels on each MPPT. This is ideal for an east/west set up, where the two strings of panels will have an unmatched solar generation.



Figure 1.21 : String inverter

b/Micro inverters

Micro inverters are a relatively new technology, becoming a popular choice amongst home solar PV systems. Whereas as solar panel system on a string inverter is impacted by a fault or shading on a single panel, a micro inverter system solves this problem. This is because in a micro inverter system each individual solar panel has an inverter to itself, therefore isolating any issues. As a result, micro inverters are often considered as the way to install more solar panels onto a roof. As shaded areas are no longer a no go or the need for mixing orientations no longer becomes an issue.

Despite being generally more expensive than your classic string inverter, a micro inverter system is set to increase your solar energy generation and therefore return on investment.



Figure 1.22 : Micro inverter

c/Hybrid solar inverters

If you are installing a new Solar PV system with storage, then a hybrid inverter is well worth considering. As solar panels generate DC electricity, we know that an inverter must convert the energy into AC electricity in order to power your home's appliances. However, solar batteries store electricity in DC form. A hybrid solar inverter is capable of converting the incoming DC into AC, while also sending any surplus DC power to store in a solar battery, or to be sold to the grid. When your stored energy is in demand, the electricity can then be inverted to AC to be used in your household. Brands which manufacturer hybrid solar inverters, include GivEnergy, Solis, Growatt and Fox-Ess.



Figure 1.23 : Hybrid solar inverter

d/Power inverters

Offering many of the same benefits as micro-inverters, power inverters are also located on each individual panel. Also known as DC power optimisers, power inverters offer panel-level optimisation and performance monitoring. Unlike a micro-inverter system, instead of directly converting DC to AC at roof level, the optimiser moves the DC power through to a string inverter.

Which is likely fitted next to your battery storage system. As they are at module- level they are often a cheaper alternative to micro-inverters.



Figure 1.24 : Power inverter

1.2.1.10 Solar cell I-V characteristic and the solar cell I-V curve

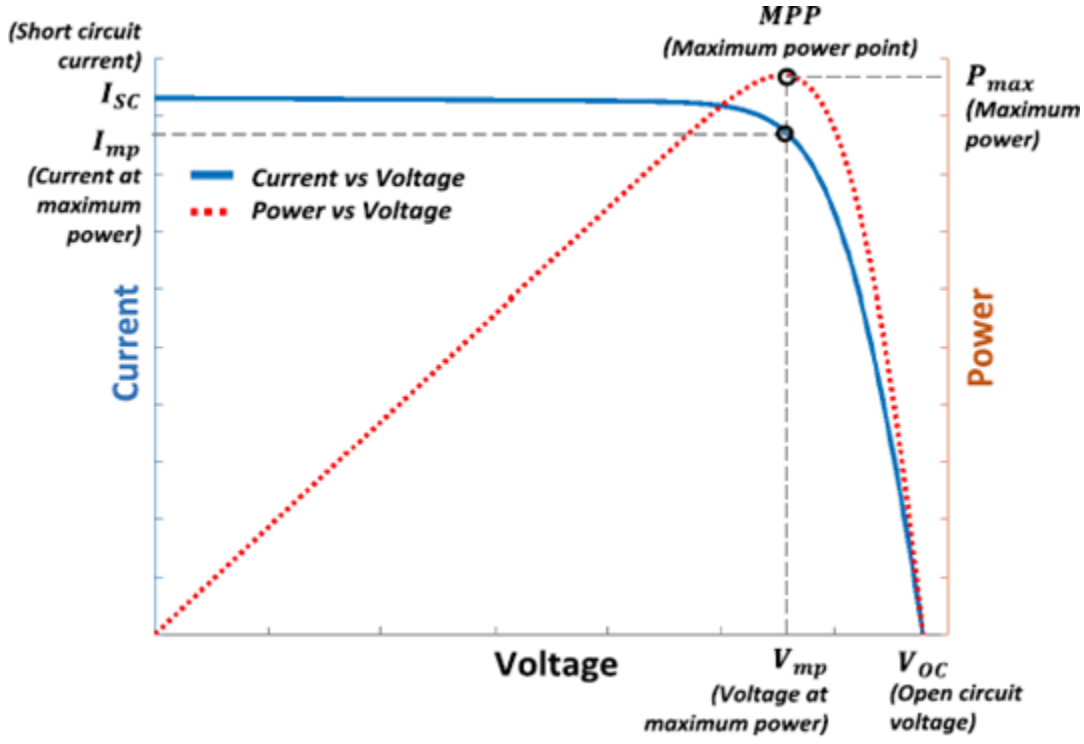


Figure 1.25 : Solar cell I-V characteristic curve [88]

The solar cell I-V characteristic curves shows the current and voltage (I-V) characteristics of a particular photovoltaic (PV) cell, module or array. It gives a detailed description of its solar energy conversion ability and efficiency. Knowing the electrical I-V characteristics (more importantly Pmax) of a solar cell, or panel is critical in determining the device's output performance and solar efficiency.

The main electrical characteristics of a PV cell or module are summarized in the relationship between the current and voltage produced on a typical solar cell I-V characteristics curve. The intensity of the solar radiation (insolation) that hits the cell controls the current (I), while the increases in the temperature of the solar cell reduces its voltage (V).

Solar cells produce direct current (DC) electricity and current times voltage equals power, so we can create solar cell I-V curves representing the current versus the voltage for a photovoltaic device. Solar cell I-V characteristics curves are basically a graphical representation of the operation of a solar cell or module summarising the relationship between the current and voltage at the existing conditions of irradiance and temperature. I-V curves provide the information required to configure a solar system so that it can operate as close to its optimal peak power point (MPP) as possible.

The graph of Figure 1.25 shows the current-voltage (I-V) characteristics of a typical silicon PV cell operating under normal conditions. The power delivered by a single solar cell or panel is the product of its output current and voltage (I x V). If the multiplication is done, point for point, for all voltages from short-circuit to open-circuit conditions, the power curve above is obtained for a given radiation level.

With the solar cell open-circuited, that is not connected to any load, the current will be at its minimum (zero) and the voltage across the cell is at its maximum, known as the solar cells open circuit voltage, or Voc. At the other extreme, when the solar cell is short circuited, that is the positive and negative leads connected together, the voltage across the cell is at its minimum (zero) but the current flowing out of the cell reaches its maximum, known as the solar cells short circuit current, or Isc.

Then the span of the solar cell I-V characteristics curve ranges from the short circuit current (Isc) at zero output volts, to zero current at the full open circuit voltage (Voc).

In other words, the maximum voltage available from a cell is at open circuit, and the maximum current at closed circuit. Of course, neither of these two conditions generates any electrical power, but there must be a point somewhere in between were the solar cell generates maximum power.

However, there is one particular combination of current and voltage for which the power reaches its maximum value, at Imp and Vmp. In other words, the point at which the cell generates maximum electrical power. This is the “maximum power point” or MPP. Therefore the ideal operation of a photovoltaic cell (or panel) is defined to be at the maximum power point.

1.2.1.10.1 Solar panel I-V characteristic curves

Photovoltaic panels can be wired or connected together in either series or parallel combinations, or both to increase the voltage or current capacity of the solar array. If the array panels are connected together in a series combination, then the voltage increases and if connected together in parallel then the current increases.

The electrical power in Watts, generated by these different photovoltaic combinations will still be the product of the voltage times the current, (P = V x I). However the solar panels are connected together, the upper right hand corner will always be the maximum power point (MPP) of the array.

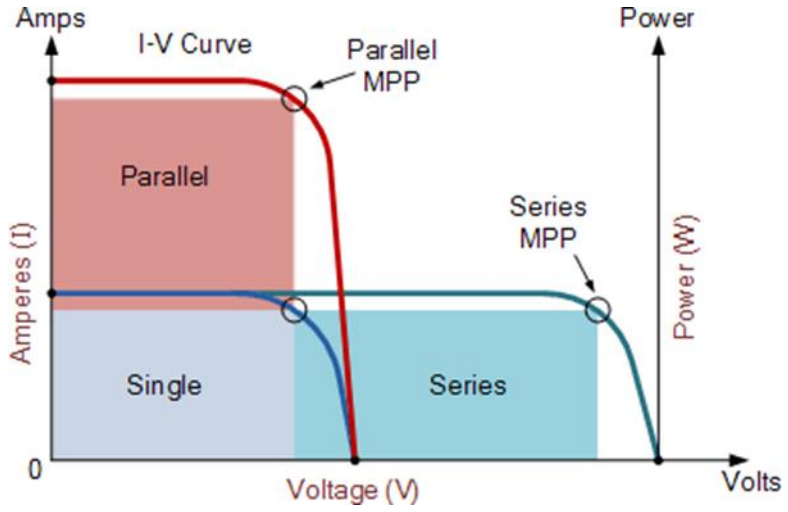


Figure 1.26 : Solar panel I-V characteristic curves

1.2.1.10.2 The electrical characteristics of a photovoltaic array

The electrical characteristics of a photovoltaic array are summarised in the relationship between the output current and voltage. The amount and intensity of solar insolation (solar irradiance) controls the amount of output current (I), and the operating temperature of the solar cells affects the output voltage (V) of the PV array. Solar cell I-V characteristic curves that summarise the relationship between the current and voltage are generally provided by the panels manufacturer and are given as :

Solar array parameters

VOC = open-circuit voltage : this is the maximum voltage that the array provides when the terminals are not connected to any load (an open circuit condition). This value is much higher than Vmp which relates to the operation of the PV array which is fixed by the load. This value depends upon the number of PV panels connected together in series.

ISC = short-circuit current : the maximum current provided by the PV array when the output connectors are shorted together (a short circuit condition). This value is much higher than Imp which relates to the normal operating circuit current.

MPP = maximum power point : this relates to the point where the power supplied by the array that is connected to the load (batteries, inverters) is at its maximum value, where MPP = Imp x Vmp. The maximum power point of a photovoltaic array is measured in Watts (W) or peak Watts (Wp).

FF = fill factor : the fill factor is the relationship between the maximum power that the array can actually provide under normal operating conditions and the product of the open-circuit voltage multiplied by the short-circuit current, (VOC x ISC) This fill factor value gives an idea of the quality of the array and the closer the fill factor is to 1 (unity), the more power the array can provide. Typical values are between 0.7 and 0.8.

% eff = percent efficiency : the efficiency of a photovoltaic array is the ratio between the maximum electrical power that the array can produce compared to the amount of solar irradiance hitting the array. The efficiency of a typical solar array is normally low at around 10-12%, depending on the photovoltaic type (monocrystalline, polycrystalline, amorphous or thin film) of cell being used.

Solar cell I-V characteristic curves are graphs of output voltage versus current for different levels of insolation and temperature and can tell you a lot about a PV cell or panel's ability to convert sunlight into electricity. The most important values for calculating a particular panels power rating are the voltage and current at maximum power.

Some solar panels are rated at slightly higher or lower voltages than others of the same wattage value, and this affects the amount of current available and therefore the panels MPP. Other parameters also important are the open circuit voltage and short circuit current ratings from a safety point of view, especially the voltage rating.

An array of six panels in series, while having a nominal 72 volt (6 x 12) rating, could potentially produce an open-circuit voltage of over 120 volts DC, which is more than enough to be dangerous.

Photovoltaic I-V characteristics curves provide the information needed for us to configure a solar power array so that it can operate as close as possible to its maximum peak power point.

The peak power point is measured as the PV module produces its maximum amount of power when exposed to solar radiation equivalent to 1000 watts per square metre, 1000 W/m^2 or 1kW/m^2.

1.2.1.11 Sizing a photovoltaic system with battery

The efficiency of any electrical installation fundamentally depends on the rigor of its sizing and use because it directly influences the cost and performance of an installation. The aim of the sizing is to determine the power of the photovoltaic generator and the capacity of the battery, based on the site's sunshine data on the one hand and the user's electrical needs on the other. The following steps allow you to size a photovoltaic system.

1.2.1.11.1 Estimated electricity needs (Wh/d)

The daily electricity consumption (or daily need (Bd) in (Wh/d)) is given by the product of the nominal power of the load (W) and the number of hours of daily use (h/d).

$$Bd = \sum_{i=1}^{n} Pi\ Ti \qquad (1.1)$$

1.2.1.11.2 Estimated sunshine

Sunshine is always chosen during the least sunny time of year.

To calculate daily solar energy, we assimilate the energy produced during a day of sunshine to the product of instantaneous radiation **1000W/m²** by a certain number of hours called number of equivalent hours. Daily solar energy is expressed in (kWh/m².d) or in hours of full sunshine. (hours/d X 1000W/m^2).

$$\boldsymbol{Esol = Neq\ X\ 1000}$$

Neq: equivalent number of hours of sunshine in STC conditions [h/d].

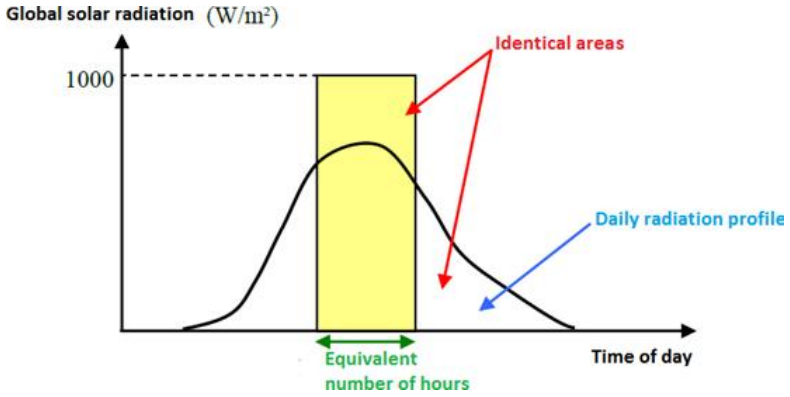


Figure 1.27 : Equivalent number of hours [89]

Note:

It should be noted that good orientation of the PV panels is required.

The ideal orientation of a photovoltaic module obeys the rule towards the equator. What gives an orientation towards the south in the northern hemisphere and a north orientation in the southern hemisphere.

1.2.1.11.3 Calculation of the power of the photovoltaic field

The power of the photovoltaic field is given by the following equation:

$$Ppv,tot = \frac{Bd}{(Neq.Cp)} \quad (1.2)$$

Where:

Neq: Number of hours per day of exposure to STC conditions.

Cp: Loss coefficient which is due to losses due to dirt on the photovoltaic panel (snow, sand), losses at the regulator and wiring levels as well as efficiency energy of batteries.

As a general rule we find losses of 5 to 1% (Cp = 0.9 to 0.95).

The number of photovoltaic panels is calculated by the ratio of the power Total PV and unit PV power (Ppv,u), and we take the entire ratio by excess:

$$Npv = Ent\left[\frac{Ppv,tot}{Ppv,u}\right] \quad (1.3)$$

Operating voltage

The voltage of the photovoltaic field depends on the type of application, the power photovoltaic system and availability of equipment (modules and receivers).

The following table indicates the voltage suitable for the PV generator.

Table 1.6: Recommended voltages for photovoltaic systems based on their powers [89]

Field power photovoltaic	**0 -500 Wc**	**500-2K Wc**	**2-10 K Wc**	**>10K Wc**
Tension recommended	**12V DC**	**24V DC**	**24V DC**	**> 48V DC**

1.2.1.11.4 Calculation of storage battery capacity

The sizing of batteries requires particular attention in order to reduce the overall cost of the system.

The required storage capacity is calculated as follows:

$$Cbat,tot = \frac{(Bd.Nda)}{(Pdd.nbat.Ubat)} \quad (1.4)$$

Where :

Nda: the number of days of autonomy.[d]

Pdd: the depth of discharge of the battery.

ηbat: the energy efficiency of batteries

Ubat: The operating voltage of the battery. [V]

The number of batteries is calculated by the ratio of the total capacity of the batteries and of the unit battery capacity (Cbat,u), and we take the entire ratio by excess:

$$Nbat = Ent\left[\frac{Cbat,tot}{Cbat,u}\right] \quad (1.5)$$

1.2.1.11.5 DC cable sizing

It is necessary to limit the length of the connections between the photovoltaic field and the receptors. To limit line losses in thermal form due to the Joule effect which will cause voltage drops. The UTE C15-712 guide relating to installations photovoltaic systems indicate that the voltage drop in the DC part must be less than 3%, ideally 1%. That means :

$$\varepsilon = \left[\frac{VA-VB}{VA}\right] < 0.03 \quad (1.6)$$

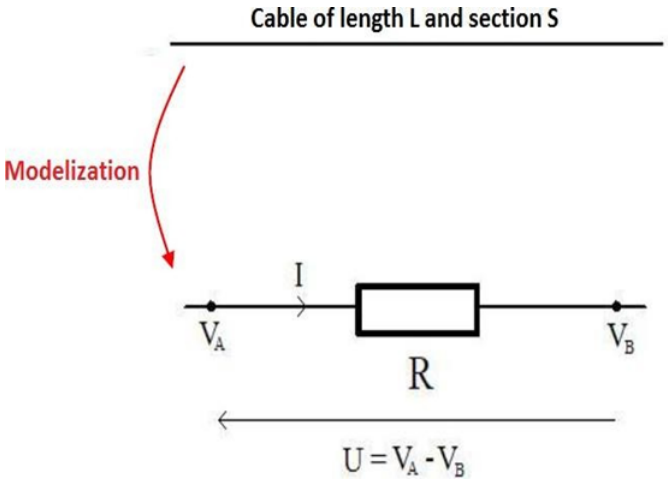


Figure 1.28 : Modeling of a DC cable [89]

So

$$\varepsilon = \left[\frac{U}{VA}\right] = \left[\frac{R.I}{VA}\right] = \left[\frac{\rho.L.I}{S.VA}\right] \quad (1.7)$$

In practice, the length of the cables is known. We then calculate the section of these under the constraint of a maximum voltage drop of 3%.

Thus, the cable section is calculated by the following formula:

$$S = \left[\frac{\rho.L.I}{\varepsilon.VA}\right] \quad (1.8)$$

Where :

R: cable resistance (Ohm)

ε: voltage drop

ρ : linear resistivity of the conductor constituting the cable (Ohm.m)

I : current intensity (Ampere)

S : cable section (m^2)

L : cable length (m)

1.2.1.12 Sizing a photovoltaic system without battery

The sizing of this type of system differs from that of a system with battery.

The size of the photovoltaic field is determined by the need to match power supply with energy demand.

Furthermore, there is no need to worry about the battery. The design steps are as follows:

-Define site conditions.

-Estimate the load.

-Size the field and the energy conditioning devices without taking takes into account battery performance.

As there is no battery, the field must be sized to satisfy to the load for the weakest sunlight conditions.

The utilization factor nominal will be equal to the maximum number of hours of sunshine during the month of operation where the sunshine is the weakest [89].

1.2.2 Integration of solar energy in refrigeration systems

The energy demand for cooling and air conditioning systems is increasing worldwide, especially in regions with high solar radiation intensity. One of the reasons for this is the increase of comfort demands worldwide. The most cooling and air conditioning systems are the conventional electrically driven one type such as compression refrigeration machines and air conditioning systems.

Through the huge electricity consumption for cooling and air conditioning, the environmental problems get bigger and bigger, because of carbon dioxide (CO_2) and other pollutant emissions.

One of the possibilities to reduce the primary energy consumption is through the use of solar energy for driving the thermal driven absorption or adsorption refrigeration systems, or desiccant cooling. Another possibility is using solar energy to produce electrical energy and this can be used to drive the conventional refrigeration systems.

Many research and developmental efforts in the last years have been done to enforce the spreading of solar driven cooling systems.

1.2.2.1 Different technologies of solar refrigeration systems

1.2.2.1.1 Sorption refrigeration technology

Sorption refrigeration technology can be divided in two groups :

closed and open cycle systems. Closed-cycle systems consist of several types as absorption cooling, adsorption cooling, ejector, and solar assisted heat pump systems. Open-cycle frameworks give a direct treatment of air, for example, desiccant cooling [90].

a/Closed sorption cycle

Based on the sorption material, closed sorption cycles are divided mainly into liquid sorption and solid sorption.

The liquid sorption refers to the absorption, while the solid sorption refers to the adsorption.

Absorption involves a liquid or solid sorbent that absorbs refrigerant molecules into its inside and changes chemically and/or physically in the process.

The most widely used working pairs in the absorption processes are water-lithium chloride (H2O–LiCl), ammonia-water and water –lithium bromide (H2O–LiBr).

There are some research works about using of a new working pair Acetone- Zink bromide [91–92]. This working pair is especially suitable for the use in solar thermal driven absorption Refrigeration machines by low driving temperatures as flat plate solar collectors.

Adsorption, on the other hand, refers to a solid sorption process where a solid sorbent attracts refrigerant molecules into its surface by chemical or physical force and without changing its form in the process.

The adsorption refrigeration process is achieved using a combination of adsorbate and adsorbent. Ammonia-activated, methanol-activated carbon, ethanol-activated carbon, water–silica gel and water-zeolite are the most widely used working pairs in the adsorption processes [93].

Absorption systems

The absorption chiller is popular worldwide in the solar cooling market due to its higher coefficient of performance (COP) values compared to other solar cooling technologies, which are in the range from 0.6 to 0.8 for single stage chillers, and achieve a higher COP of 0.9–1.3 for two stage machines by utilizing the rejected heat from the first stage as the input for the second stage [90,94].

The common heat supply temperature required 80 to 95 °C for a single stage and 130–160 °C for double stages, which requires a more expensive solar collector as evacuated tubes, parabolic troughs or concentrating collectors [90,94]. Typical solution pairs were used in absorption chiller are ammonia as a refrigerant and water as a sorbent or water as the refrigerant and lithium bromide as a sorbent.

For ammonia and water pairs, the evaporator temperature can be below 0 °C, and heat rejection temperatures of 50 °C. Consequently, they can be utilized for freezing purposes by the use of dry air-cooled condensers for heat rejection. For water and lithium bromide pairs, the evaporator temperature is restricted to 4 °C and the condenser temperature is beneath 35 °C.

The condenser temperature implies that an expensive and high water expending wet cooling tower is regularly required [95]. In the last years, various numbers of absorption frameworks have been exploited and developed for small capacity underneath 100 kW and specifically beneath 20 kW down to 4.5 kW.

Most of these mall capacity systems operated by a single effect of various kinds, utilized essentially for domestic buildings and small commercial applications.

While the medium and large absorption chiller with cooling capacity existed for a long while. In general, the absorption chiller is available with the cooling capacity in the range 10.5 to 500 kW [96].

These chillers were mainly manufactured in Japan, China, South Korea, India, Europe and the United States. Many research works have been undertaken to investigate and improve performance of absorption air conditioning.

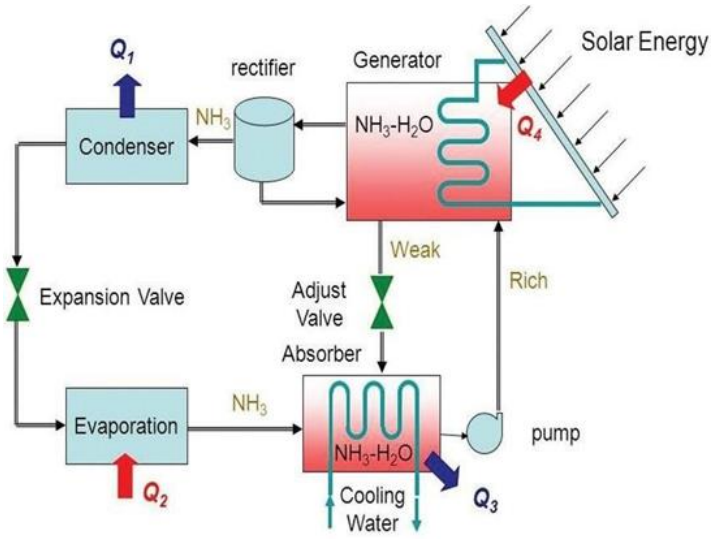


Figure 1.29 : Example of a solar absorption refrigeration system [97]



Figure 1.30 : Test plant of 5 kW solar thermally driven absorption chiller [98]

Figure 1.29 shows a schematic diagram of a solar absorption refrigeration system. This system is different from a conventional vapor compression refrigeration system. Basic components of such refrigeration system are absorber, generator, solar panel, condenser, expansion valve, evaporator, DC battery and fan.

The compressor in the vapor compression system is replaced by a generator, absorber and a pump. Refrigerant (NH3) in the evaporator absorbs the heat from the refrigerated space and gets evaporated.It is then passed to absorber where it is dissolved with absorbent (H_2O) and pumped to generator [97].

Adsorption system

The adsorption cooling system can be a suitable selection in most industrial countries. About 25% of the total industrial energy demand is needed for thermal process heat applications in the range up to 300 °C. More than half (57%) of this energy is used to produce heat below 150 °C [58]. Therefore, this technique allows us to utilize renewable energy or low temperature gains from solar energy, waste heat and cogeneration to drive the cooling cycle. It can also save a global energy and it is environmentally sound since it reduces chlorofluorocarbons (CFCs) and CO_2 emissions.

Besides, adsorption systems can be operated with no rotating parts, no corrosion problem, and are less sensitive to shocks and the installation position.

They also do not require a solution pump and rectifier. Table 1.7 displays a comprehensive comparison between two solar cooling systems in terms of absorption and adsorption systems [99–100].

In addition, the solar powered adsorption chillers are very promising in the widespread, but due to their low COP value and higher product cost, they are not feasible for commercialization.

In general, the adsorption chiller is available with the cooling capacity in the range of 8 to 370 kW [95]. Many research works have been undertaken to investigate and improve the performance of adsorption air conditioning systems by employing a heat recovery, mass recovery, multi-bed and multi-stage technologies.

Adsorption cycle is shown in Figure 1.31 works with the interaction of gases and solids.

With adsorption chilling, molecular interaction between solids and gases allows gases to be adsorbed into the solids.

The adsorption chamber of the chiller is filled with solid material, silica gel, eliminating the need for moving parts and eliminating noises associated with those moving parts.

The silica gel creates an extremely low humidity condition that causes water refrigerant to evaporate at low temperatures.

As water evaporates in the evaporator, it cools chilled water.

The adsorption chiller has four chambers; an evaporator, a condenser and two adsorption chambers. All four chambers are operated at nearly a full vacuum.

These systems can use a variety of energy sources, typically process waste heat, biomass heat, solar collectors, tri-generation (CHP) generators, or traditional power plants [101,102].

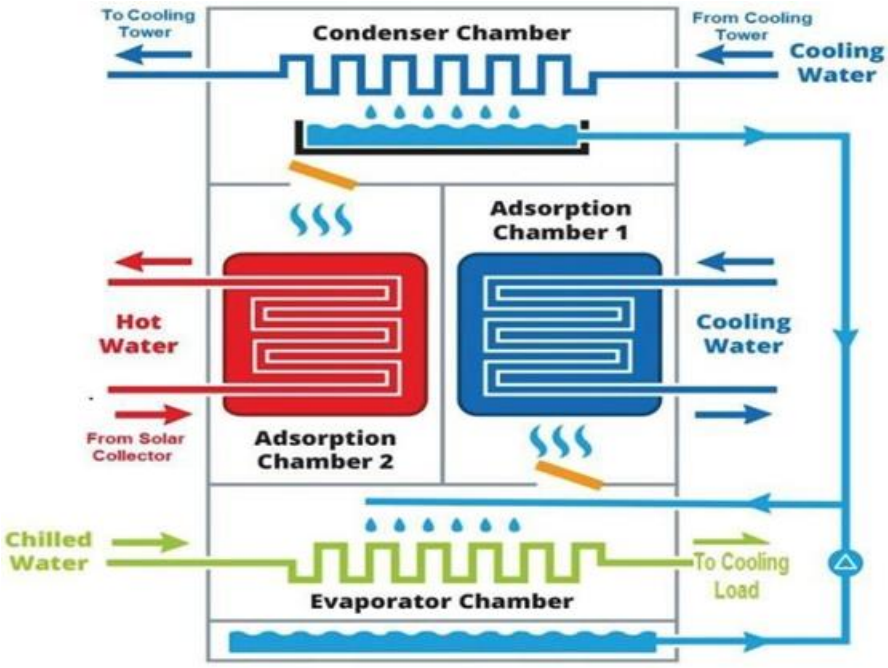


Figure 1.31 : Adsorption cycle [103]

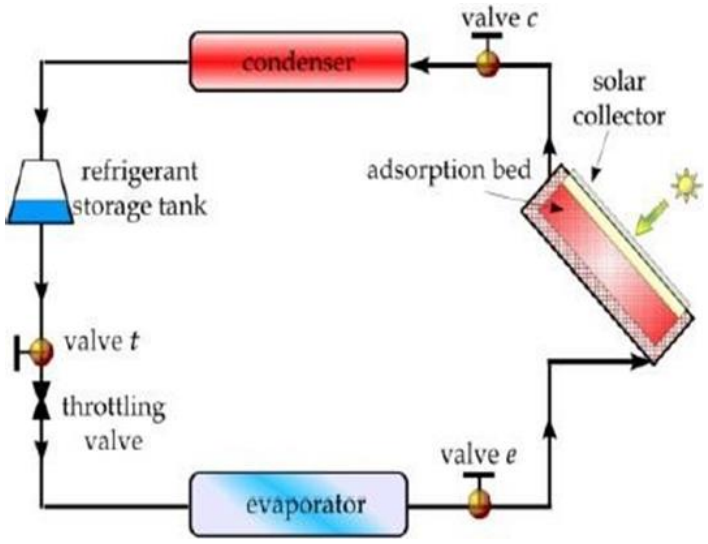


Figure 1.32 : Principle of solar adsorption refrigeration cycle [104]

Table 1.7 : General comparison of two cooling systems: absorption and adsorption systems [99–100]

Comparison criteria	Adsorption system	Absorption system
Initial cost	Higher	Lower
Phenomenon	It is a surface phenomenon	It is a bulk phenomenon
Heat exchange	Exothermic process	Endothermic process
Temperature	It is favoured by low temperature	It is not affected by temperature
Rate of reaction	It steadily increases and reach to equilibrium	It occurs at a uniform rate
Concentration	Concentration on the surface of adsorbent is different from that in the bulk	It is same throughout the material
Example	- Water vapors adsorbed by silica gel - NH_3 is adsorbed by charcoal	- Water vapours absorbed by LiBr - NH_3 is absorbed in water
Continuous operating	More than 8000 h per year	Require two times yearly shutdown for dilution of lithium bromide solution.
Life span	The silica gel up to 30 years	20 years with continuously maintenance
Maintenance	Replacement vacuum pump every 5 years, annual cleaning of condenser tubes	Require more preventative maintenance for pumps, heat exchanger. Replacement, controls, and air leakage
Refrigerant	Water, methanol	Water or ammonia.
Adsorbent/absorbent	Silica Gel, zeolite or activated carbon	Lithium bromide or water
COP	Water/silica gel Single stage 0.3–0.7 Two Stages0.35–0.8	Water-LiBr Single stage 0.5–0.75 Two stages 0.8–1.2 NH_3-Water Single stage 0.5–0.6 Two stages 1.2–1.3
Corrosion	None	Lithium bromide is corrosive in nature.
Crystallization	None	Yes, can occur in low temperature cooling water by H_2O/LiBr-System
Frequent Replacement Adsorbent/ absorbent	Not necessary	Every 5 years
Required hot water temperature	Variable 50–100 °C	Variable 80–120 °C, Back-up heat is required if the temperature below 80 °C to prevent crystallization
Typical Cooling Capacity (kW Cold)	8–370 kW	5 kW–5 MW
Cooling water requirement	30–40 °C, lower temperature increases system capacity	It should be between 20 and 40 °C
Chilled water output	3–9 °C	Higher than 4 °C for H_2O/LiBr, and unlimited by NH_3/H_2O until till −50 °C
Solar collector	Vacuum tube, Flat plate collectors	Vacuum tube + flat plate collectors by small cooling capacities
Refrigeration cycle	Closed Refrigerant Cycle	Closed Refrigerant Cycle
Evaporator temperature	Water- Silica gel or zeolite 6–20 °C	Water-LiBr 6–20 °C NH_3-Water −30 to +20 °C
Heating temperature	Water-Silica gel or zeolite 50–95 °C	LiBr-Water 60–95 °CWater-NH_3 65–150 °C
Heat rejection temperature	Water-Silica gel or zeolite 25–35 °C	Water-LiBr 25–35 °C NH_3-Water 25–50 °C
Cooling capacity range (per unit)	Water-Silica gel or zeolite 5–430 kWr	Water-LiBr 10–20,500 kWr NH_3-Water 19–1000 kWr

Ejection system

The ejector device

Ejectors are flow devices with two inlet and one outlet ports. A high-pressure stream (primary flow, also known as motive or driving flow) enters through the first inlet port and is mixed with a low-pressure stream (secondary flow, also known as entrained flow) that enters from the low- pressure inlet port.The mixed stream (mixed flow) is subsequently discharged at an intermediate pressure, called backpressure, through the outlet port. The goal of the above process is to increase the pressure of a low-pressure stream by entraining it by a high pressure, accelerating stream. The main parts of an ejector, also shown in Figure 1.33, are the following:

-Converging-diverging nozzle (CDN)

-Suction chamber

-Mixing chamber or constant area section (CAS)

-Diffuser

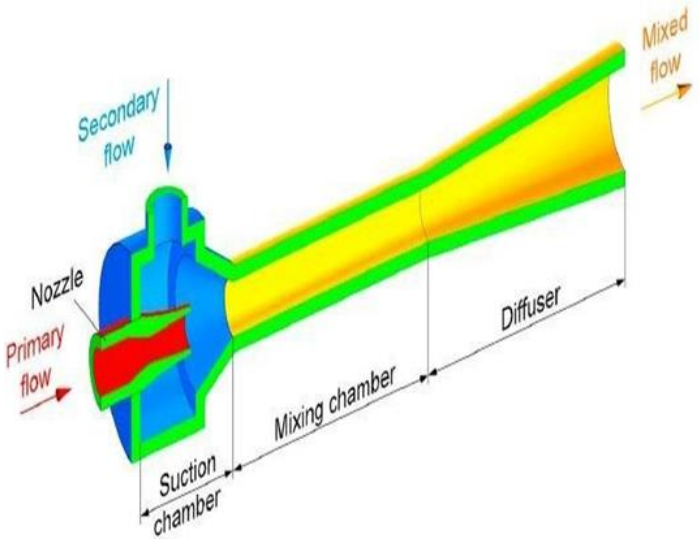


Figure 1.33 : Ejector parts [105]

A detailed schematic of an ejector is shown in Fig 1.34 (top).

At the bottom, the pressure and Mach number profiles of the ejector flows along different positions of the device are plotted.

The primary flow enters the ejector (g) at the CDN at subsonic speed (M < 1).

Within the converging CDN section, it is accelerated, reaching sonic speed (M = 1) at the throat (t). After the throat, it is accelerated at supersonic velocity (M > 1) in the diverging CDN section until its exit (1). Throughout the entire process, the pressure of the primary flow drops from **pg** to **pt** and eventually to **p1**.

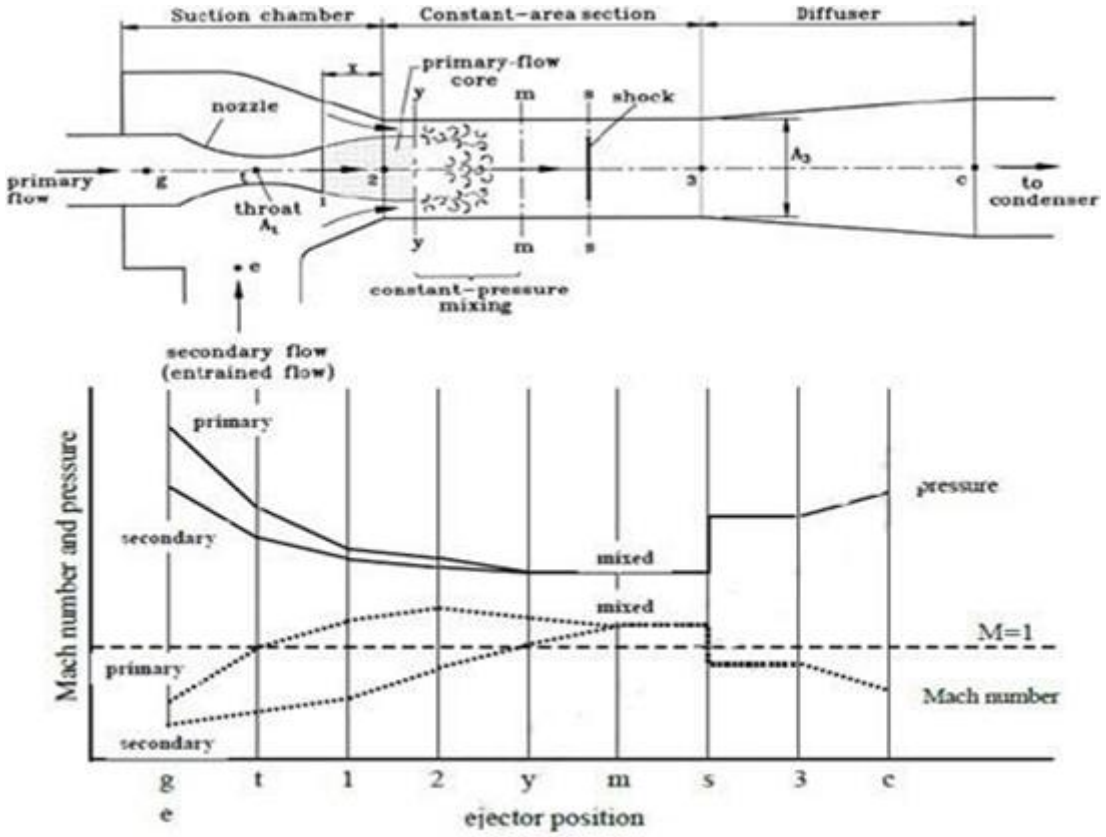


Figure 1.34 : Ejector layout and pressure-Mach number profiles [106]

The secondary flow enters the ejector at the suction chamber (e), also at subsonic speed.The entrainment and mixing of the two flows start at the CDN exit (1) and continue along the converging section of the suction chamber (points 1 to 2) and the CAS (points 2 to 3). This process is in reality complex, and several models have been proposed to simplify it by breaking it down into simpler sub-processes. A very common assumption, originally introduced by Keenan et al. [107], is that the mixing of the primary and secondary flows does not initiate at the CDN exit and that the two streams initially flow independently before being mixed.

Most 1-D models assume that the secondary flow passes through a gradually decreasing annular crossflow area formed by the ejector walls and the primary flow core (which expands at a specific angle) and accelerates while its pressure drops until it acquires sonic velocity. While Keenan et al. [107] considered that the pressures of the primary and secondary flows are equal at the CDN exit and that their mixing begins at the CAS inlet, subsequent models, firstly proposed by Munday and Bagster [105, 108] and built upon by Huang et al. [106], introduced the concept of the hypothetical throat (y-y), typically located within the CAS, at which the primary and secondary flow pressures are equalized and their mixing begins, being completed at cross-section m-m.The mixed flow undergoes a shock at cross-section s-s, which leads to its steep pressure increase and velocity decrease. After the shock, the flow enters the diffuser (point 3) in which its velocity gradually declines and its pressure is further increased, eventually exiting the ejector (c) at a pressure equal to pc. There are two indexes for evaluating the performance of ejector devices. The first is the entrainment ratio (ω), which is the ratio of the mass flow rates of the secondary and the primary flows, according to the following equation:

$$\omega = \dot{m}_e / \dot{m}_g \tag{1.9}$$

The second is the pressure ratio (rp), which is the ratio of the ejector discharge and the secondary flow pressures, according to the following equation:

$$r_p = Pc/Pe \tag{1.10}$$

Higher entrainment and pressure ratios are in principle desirable, as they indicate that higher amounts of low-pressure flow can be increased at higher pressures per mass unit of high- pressure flow.

The solar ejector cooling cycle (SECC)

Ejectors can replace compressors of vapor compression cycles, turning them into ejector cooling cycles (ECCs). Solar-driven ECCs (SECCs) consist of two parts: the solar circuit (which includes the solar collectors and the storage tank) and the ejector cooling cycle itself. Solar collectors capture solar radiation and convert it to heat, which is typically delivered via a heat transfer fluid (HTF) to the working fluid of the cooling cycle. A simple schematic of a generic SECC and its thermodynamic processes in a temperature-entropy (T-s) diagram is shown in Figure 1.35. One part of the liquid refrigerant exiting the condenser (6) is pressurized and then conveyed to the generator, in which it evaporates and is converted to high-pressure vapor (2).

The remaining part is throttled to low-pressure (3) and driven to the evaporator, in which cooling is produced via its evaporation. The high-pressure stream exiting the generator enters the ejector, in which it entrains the low-pressure stream exiting the evaporator (4). .
The mixed flow exiting the ejector at an intermediate pressure (5) enters the condenser, in which it is cooled down and condenses until it becomes saturated or sub-cooled liquid [109].

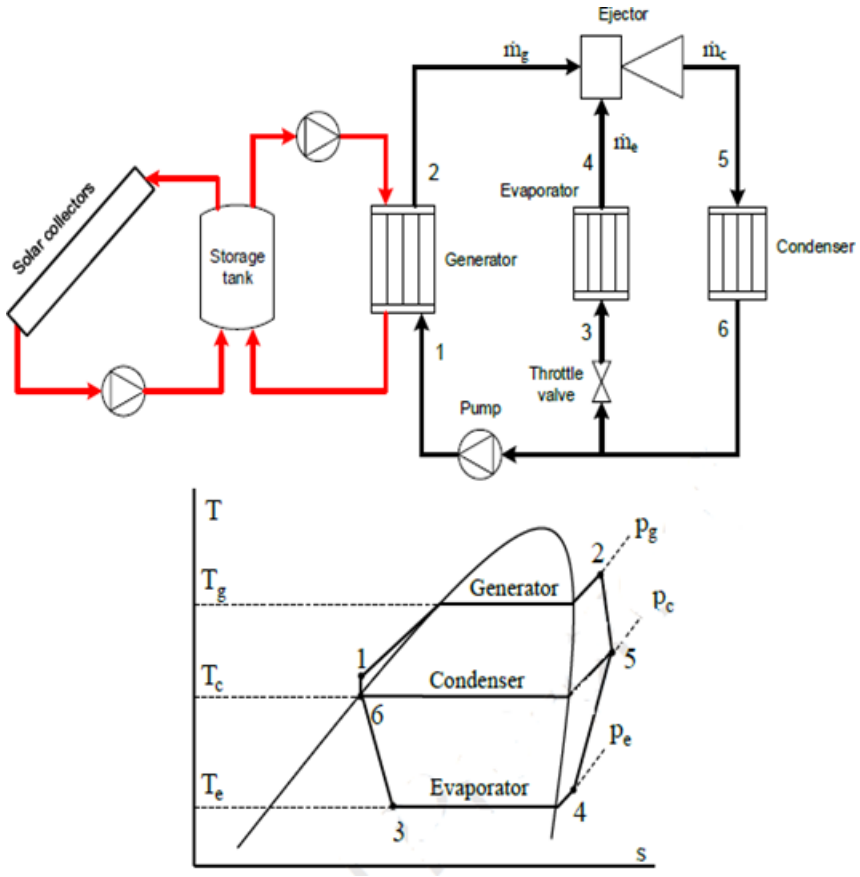


Figure 1.35 : Layout (top) and T-s diagram (bottom) of a generic ejector cooling cycle [109]

b/Open orption cycle

The open sorption cycle is classified as liquid or solid desiccant systems that are used foreither humidification or dehumidification.Basically, there are two processes to transfer moisture from one air stream to another in the desiccant systems: desorption or regeneration process and sorption process. Liquid or solid desiccants behave similarly because their water vapor pressure is a function of moisture content and temperature [110].

The liquid desiccant system mostly uses liquid desiccant materials to absorb moisture through physical or chemical processes. Lithium bromide (H2O–LiBr), lithium chloride, and calcium chloride are the most popular materials typically in liquid desiccant systems. However, the solid desiccant system is mostly used solid desiccant materials to adsorb the moisture without chemical reaction, such as silica gel, or zeolite, which means there is just a physical process in solid desiccant systems [111].

Desiccant system

The desiccant cooling system can be a suitable selection for thermal comfort, especially in climates with high humidity. Moreover, this technique allows us to utilize renewable energy or low-temperature gains from solar energy, waste heat and cogeneration to drive the cooling cycle. It can also save global energy and its environmental issues through avoid CFCs and CO_2 emissions.

The desiccant air conditioning system utilizes the capability of desiccant materials in removing the air moisture content by the sorption process by the use of the vapor pressure differences between the air and the desiccant surface to attract and release moisture [112].

A wheel desiccant dehumidifier rotates two separate air streams, the process airstream and the regeneration or reactivation airstream. When the wheel rotates, the outside humid air enters the rotating wheel through the desiccant, which absorbs the moisture of airstream to leave as warm and dry. At the same time, in a regenerative section, a waste heat from the combustion process or solar energy is used to heat the desiccant and, consequently, dries the desiccant [113]. The main advantages of using solid desiccant can be summarized in the following points [114–115]: (i) high drying capability compared to liquid desiccant; (ii) more efficient when the latent heat load is larger than the sensible load; which leads to air dehumidification for 40–60% of the cooling load for air conditioning in hot and humid weather [116]; (iii) utilizing different energy sources especially low grade energy; (iv) clean technology, which operates without the use of harmful refrigerants; (v) control of humidity is better than conventional cooling system; (vi) cost of energy to regenerate the desiccant is less than the cost of energy to dehumidify the air by cooling it below its dew point; (vii) improves indoor air quality; (viii) capable of removing airborne pollutants and finally (ix) compact construction, resistance to corrosion, and ability to work continuously. The main disadvantages it requires a higher regeneration temperature of more than 70°C and a high pressure drop in the air stream, also requires a high energy system.

The comparison between the desiccant system and conventional systems is listed in Table 1.8.There are many required properties of an desiccant materials selected in open-cycle cooling based on [117,118]: (i) mechanical and chemical stability; (ii) large moisture capacity per unit weight; (iii) low heat of adsorption/absorption to regenerate; (iv) sorption rate; (v) large adsorption/ absorption capacity at low water vapor pressures; (vi) cheap cost; (vii) sorption at low relative humidity; and finally (viii) ideal isotherm shape. The performance of wheel desiccant depends on key design and operating parameters such as [119,120]: process air moisture, process air temperature, process air velocity through the desiccant, air volume flow rates, desiccant rotor thickness, regeneration temperature, regeneration air velocity through the desiccant, sector angle of regeneration section, regeneration air moisture, rotational speed, amount of desiccant presented to the reactivation and process airstreams, and finally desiccant sorption–desorption characteristics.

Table 1.8 : The comparison between desiccant system and conventional systems [99,121,122]

Parameter	Conventional system	Desiccant system
Operation cost	High	Low
Performance	High	Low
Energy source	Mainly electricity	Low grade energy
Environmental safety	less	High
System care	less	High
Control over humidity	Average	Accurate
Indoor air quality	Less	more
System installation	Simple	More Complicate
Energy storage capacity	Mainly not applicable	Applicable
Installation cost	High	Low
System Control	Average	Complicate

Desiccant cooling systems are basically open cycle systems, using water as refrigerant in direct contact with air.

The thermally driven cooling cycle is a combination of evaporative cooling with air dehumidification by a desiccant material.

For this purpose, liquid or solid materials can be used. The term ‘open’ is used to indicate that the refrigerant is discarded from the system after providing the cooling effect and new refrigerant is supplied in its place in an open-ended loop. Therefore only water is possible as refrigerant with direct contact to the surrounding air.

The common technology applied today uses rotating desiccant wheels, equipped either with silica gel or lithium-chloride as an absorption material.

Solid desiccant cooling

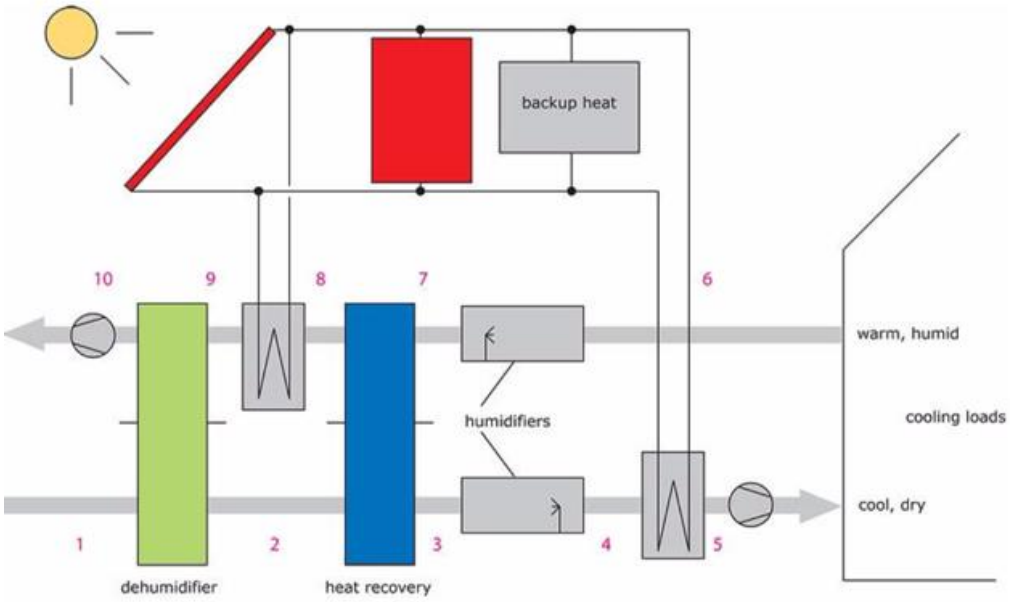


Figure 1.36 : Solar assisted desiccant cooling system

The main components of a solar assisted desiccant cooling system are shown in the figure 1.36. The basic process in providing conditioned air may be described as follows. Warm and humid air enters the slowly rotating desiccant wheel and is dehumidified by adsorption of water (1-2). Since the air is heated up by the adsorption heat, a heat recovery wheel is passed (2-3), resulting in a significant pre-cooling of the supply air stream.

Subsequently, the air is humidified and thus further cooled by a controlled humidifier (3-4) according to the set-values of supply air temperature and humidity.

The exhaust air stream of the rooms is humidified (6-7) close to the saturation point to exploit the full cooling potential in order to allow an effective heat recovery (7-8). Finally, the sorption wheel has to be regenerated (9-10) by applying heat in a comparatively low temperature range from 50°C – 75°C and to allow a continuous operation of the dehumidification process.

Solid desiccant systems can also be used to provide heating for periods with low heating demand. The solar system may consist of XCPC collectors (external concentrating parabolic collector) using water as fluid and a water storage tank, which will increase the use of the solar system.

This configuration however requires an additional water/air heat exchanger, to connect the solar system to the air system as seen in the Figure 1.37. The Desiccant wheel is absorbing moisture on the supply side (process air stream) and the solar heated coil is drying desiccant material on the return side (regeneration air stream).

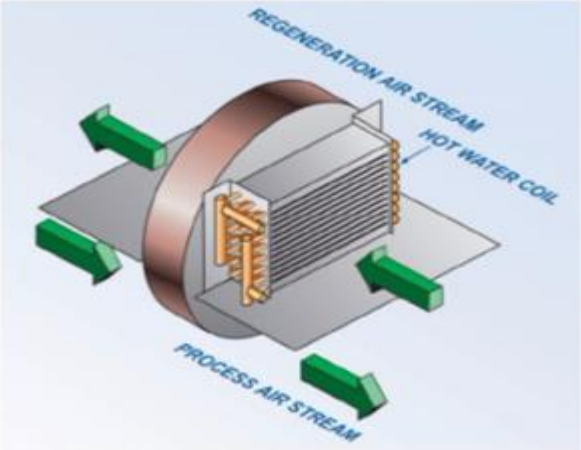


Figure 1.37 : Water/air heat exchanger

Special design of the desiccant cycle is needed in case of extreme outdoor conditions such as coastal areas of the United States and the Caribbean region. Due to the high humidity of ambient air, a standard configuration of the desiccant cooling cycle is not able to reduce the humidity down to a level that is low enough to employ direct evaporative cooling. In many cases the dryer air in a building is easier to cool and reduces air-conditioning costs. In some cases the ambient air temperatures would be considered comfortable if the humidity levels were lowered.

In most cases the supply air humidification may be avoided in moderate climates. Since the absorption material in the supply side of the heat exchanger will be saturated after some time, a periodic operation with two heat exchangers of which one is regenerated, is required.

Liquid desiccant cooling

A new technology, close to market introduction, are desiccant cooling systems using a liquid water-lithium chloride solution as sorption material. This type of systems shows several advantages like higher air dehumidification at the same driving temperature range of solid desiccant cooling systems, and the possibility of high energy storage by storing the concentrated solution.

This technology is a promising option for a further increase in exploitation of solar thermal systems for air conditioning. Currently, a few systems of this type are installed in Germany in pilot and demonstration applications, driven either with solar thermal heat or from other heat sources.

-Example of a solar-powered liquid desiccant cooling system for greenhouses in hot climates

A solar regenerator was applied to provide the required latent heat to remove the water from the liquid desiccant and restore the dehumidifying ability (Figure 1.38). The results showed that the desiccant system of magnesium chloride liquid decrease the temperature of the greenhouse by 5.5-7.5 ºC comparing with the standard evaporative cooling. Furthermore, at periods of year when the liquid desiccant system provides lower temperatures than desired, it could run in evaporative cooling mode only [123].

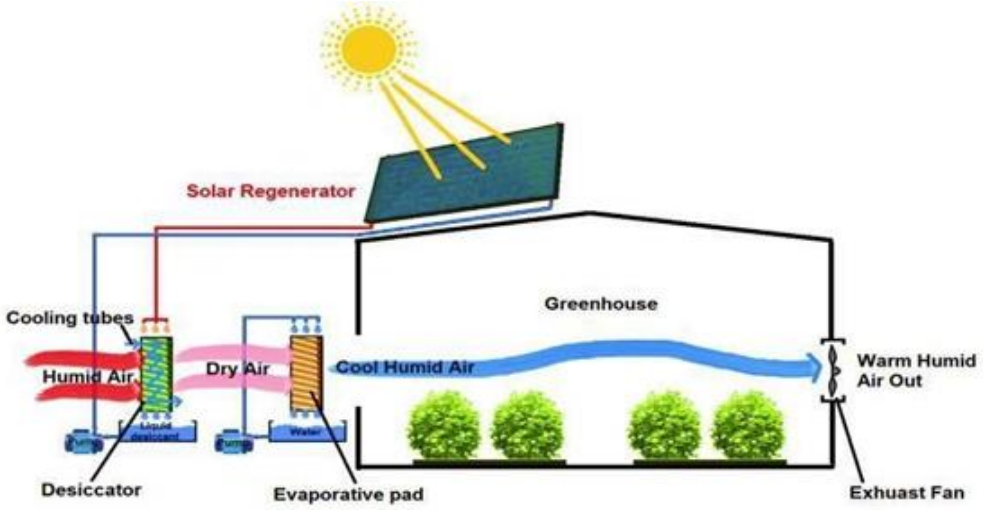


Figure 1.38 : The schematic of solar powered liquid desiccant cooling system [123]

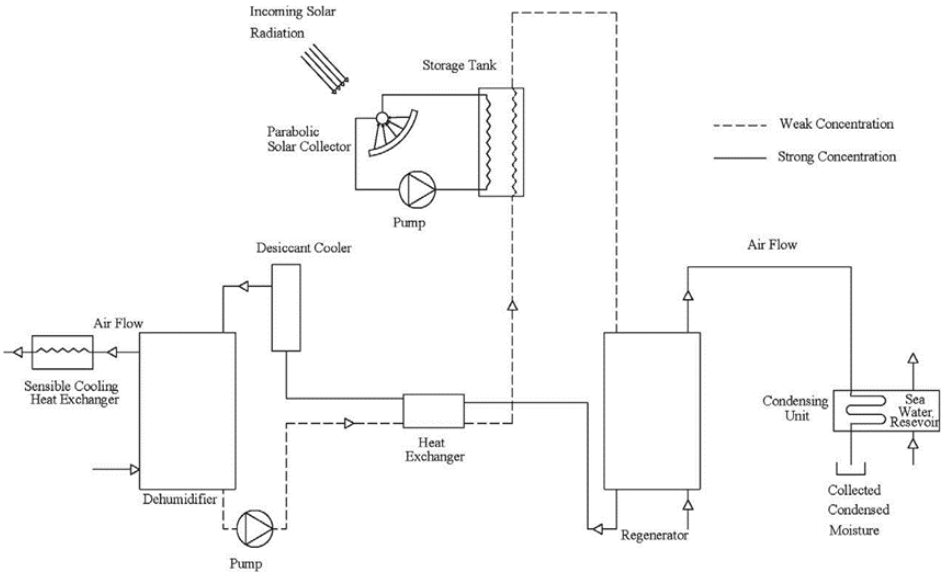


Figure 1.39 : Schematic of a solar liquid desiccant system [124]

-Example of solar powered liquid desiccation cooling system to provide water and comfort

Fig 1.39 depicts the solar-powered liquid desiccant system (LDS) and condensing unit. The system is composed of a dehumidifier, regenerator, parabolic solar collectors, heat exchangers, and desiccant cooler. The input variables of the dehumidifier are the ambient air temperature and humidity ratio, the flowr ate of the desiccant calcium chloride solution and the air flow rate. The entering humid air moisture is absorbed by the desiccant. The air leaving the desiccant bed is used for household air conditioning. The liquid desiccant leaving the dehumidifier enters a heat exchanger where it is warmed up. It is further heated before entering the regenerator by another exchanger in the water storage tank heated indirectly by solar energy transmitted from the concentrators' closed fluid circuit. The hot lo concentration liquid desiccant enters the regenerator where counter flow ambient air absorbs the water accumulated from the desiccant.

The regenerator exit humidified air is directed to a cooling coil submerged in cold sea water (temperature varying between 16 °C and 20 °C depending on depth from which it is withdrawn) where condensation occurs and distilled water is collected.

Several researchers have concluded that the separation of the evaporation and condensing parts of the solar still into two distinct parts will lead to a reduction in thermal inefficiencies and improved overall performance [125–126].

This separation into evaporation (humidification) and condensation (dehumidification) components is the underlying principle for the humidification – dehumidification technology which is currently receiving a great deal of attention in the literature as it may yet prove to be the technology of choice for inexpensive decentralized small scale desalination plants. The desiccant that leaves the regenerator re-enters the dehumidifier after it is cooled down and the loop is closed.

1.2.2.2 Concentrating solar collectors for solar thermal cooling systems

From 2004, the economic and technological developments and growing market of solar thermal technologies, led to a steep growth in the rate of research works on solar thermal cooling technologies. Fig 1.40 illustrates the rate of publications in the fields of different solar cooling technologies.

As it is obvious from Fig 1.40, among all solar thermal cooling technologies, the solar absorption chilling has had a higher rate of growth [127].

Consequently, the solar-driven absorption chilling systems could represent the most interesting candidate among all solar cooling technologies.

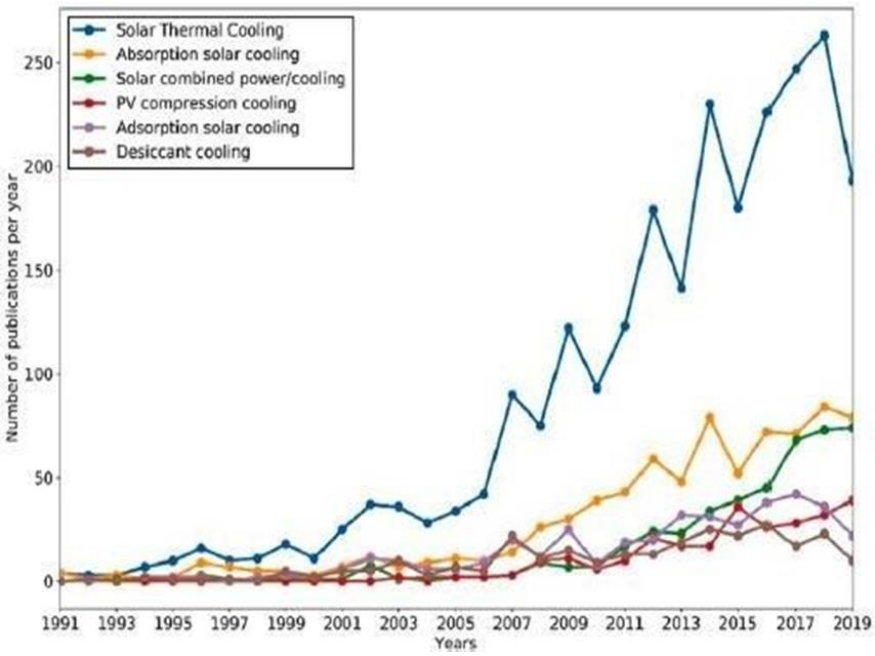


Figure 1.40 : The yearly rate of publication on solar cooling technologies [127]

Fig 1.41 depicts the classification of solar technologies, which are commonly used for cooling applications.

Among solar thermal-driven cooling technologies, the solar absorption cooling techniques have received a considerable interest, in all over the world [128]. Specifically, in the regions with high solar energy potential and high need for cooling load, solar cooling have become a favorable item [129]. Adsorption cooling technology has been applied in a variety of ways. The difference between the adsorption and absorption processes is that, adsorption is a surface phenomenon, while absorption is a volumetric phenomenon [130].

In terms of the number of the absorbing effects, solar absorption chiller (ACH) could be categorized into three types of absorption cycle as the single-effect, double-effect, and multi-effect. For single-effect absorption chillers, if the generator temperature is ranged from 80 ◦C to 100 ◦C, the coefficient of performance (COP) would reach 0.7. Meanwhile, in the double-effect absorption cooling, the maximum COP of 1.4 could be obtained with the source temperature between 100 and 150 ◦C.

Eventually, the highest COP, as high as 1.8, is belonged to the tripleeffect absorption cycle, driving with the temperature of 180–240 ◦C [131].

As it is obvious, moving towards more number of effects of absorption needs higher driving temperature, resulting in higher COP [132].

On the other side, adsorption chillers have a lower COP, in comparison with the absorption ones. Actually, the adsorption chillers could operate at lower generator temperatures, ranging from 45 °C to 65 °C [133].

Besides, solar concentrating collectors have the potential to provide higher drivin temperature, in comparison to the other simple flat collectors [134].

In general, solar collectors are divided into concentrating collectors and non-concentrating collectors.

The concentrating collectors typically have a concentrating reflecting surface to focus the solar irradiations toward a small receiver.

This type of solar collector mainly operates at a higher temperature, compared to the non-concentrating collectors.

The concentrating collectors are classified as the parabolic trough collectors (PTC), compound parabolic collectors (CPC), parabolic dish collectors (PDC), linear Fresnel collectors (LFR), and central receivers.

A comprehensive description of various solar collectors and their advancements was presented by Suman et al. [135].

There are a lot of influential parameters in the performance of concentrated collectors, which were reviewed by Rajendran et al. [136].

They discussed the impacts of the geometry design, materials, and heat transfer fluids on the performance of concentrated solar collectors.

Another option, which gives the possibility of enhancing the performance of a solar collector, is the usage of nanofluids.The application of this technology, in order to amplify the solar collector performance, was reviewed by Kasaeian et al. [137]. Regarding the importance of nanoparticles in the field of energy storage, energy conversion, and heat transfer, Zhao et al.

[138] emphasized the role of different forms of graphene products in energy transfer and storage development.They concluded that nano graphene and graphene coating could provide the possibility of miniaturization of energy storage units, providing the portable TES tanks.

It is important to highlight that, any enhancement in the heat transfer and energy conversion could positively affect the solar technology‘s efficiencies, as Zhao et al. [139] proved this in their study. They introduced the Field synergy principle as a profitable theory to improve the heat transfer capability and reduce the design errors of solar receiver devices.

Furthermore, owing to enhancing the heat transfer capability, the theory of Field synergy principle has been widely used in the fields of the flow process, heat dissipation, solar energy technologies, and micro combustion [140].

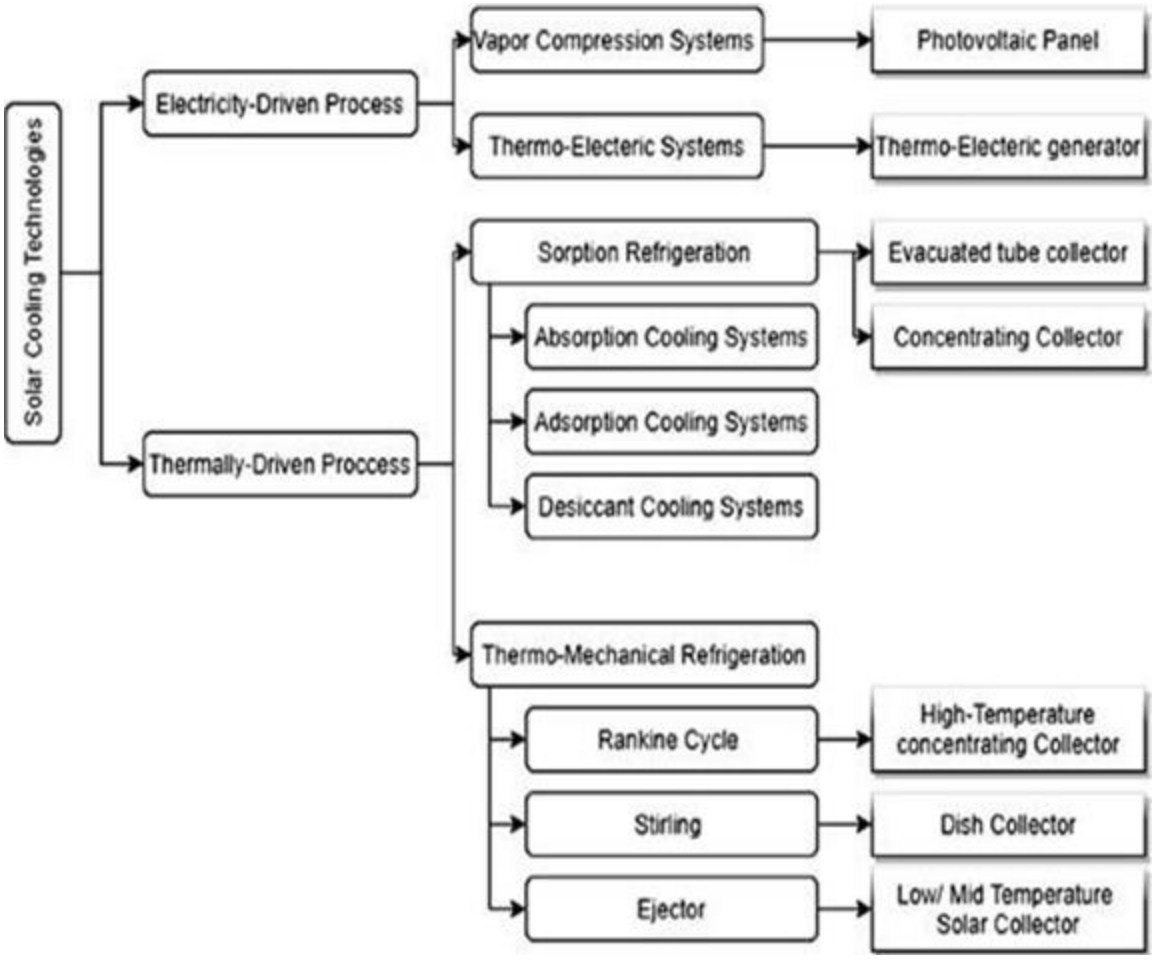


Figure 1.41 : General classification of the main solar cooling technologies [141]

1.2.2.2.1 Parabolic trough collectors in refrigeration

A parabolic trough collector composes of a parabolic reflector, a concentric transparent cover, and a working fluid tube (absorber tube), equipped with sun trackers [142]. This type of solar collector has found as an efficient thermal collector for double-effect chillers, due to its high operation temperature, around 400 ◦C [143].Fig 1.42 shows the main components included in the examined solar absorption cooling. The average COP of the whole refrigeration cycle of 0.11–0.27 was found, when the maximum hot water temperature was 90 ◦C. The authors stated that the reason of this relatively low COP could be attributed to the low temperature hot water.

1.2.2.2.2 Compound parabolic collectors in refrigeration

The CPC is a non-imaging concentrator, capable of reflecting all the solar radiation to the absorber [144].



Figure 1.42 : The main components of a PTC-driven absorption cooling cycle [145]



Figure 1.43 : Main components in the CPC-driven absorption cooling module [146]

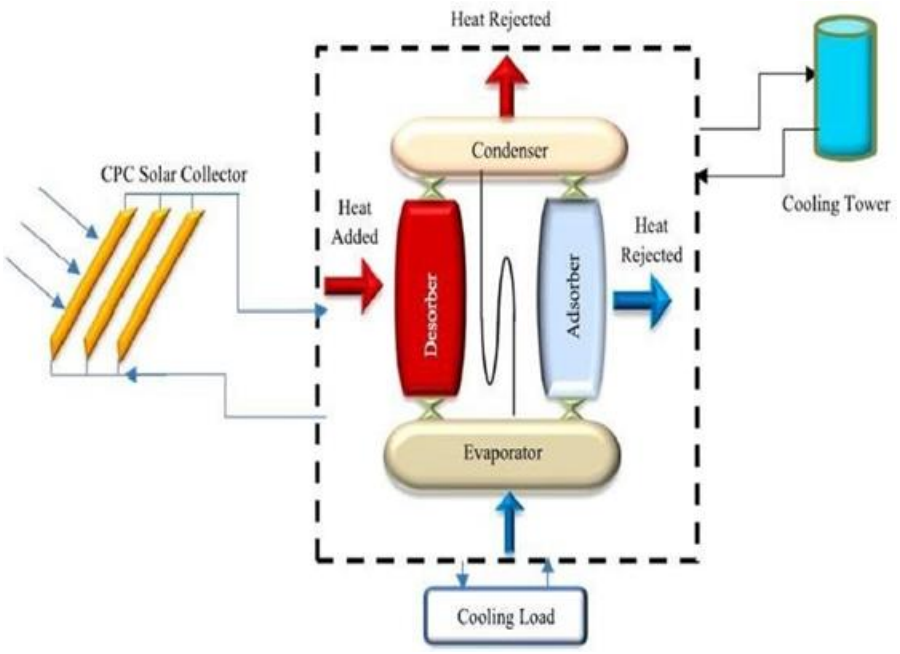


Figure 1.44 : A schematic diagram of the adsorption cooling layout powered by CPC field [147]

1.2.2.2.3 Dish collectors in refrigeration

A parabolic dish collector is a point-focus collector which concentrates the solar beams onto a receiver installed in the focal point of the dish [148].

The dish collector's capability is producing heat at variety temperature ranges.

Consequently, it can be effectively used in combination with other devices for driving multi-generation units [134].

A series of studies have been conducted to enhance the dish collector performance.

As a sample, Jiaqiang et al. [149] presented a harmonic response analysis of a dish collector with wind-induced vibration.

They considered the effects of pitch angle, wind velocity, and azimuth angle on the amplitude and frequency of the wind-induced vibration.

As another sample, in a numerical study, the drag coefficient and lift coefficient of a dish collector under various height angles and wind attack angles was investigated by Zuo et al. [150].

Such studies could be considered as a key step toward solar technology advancement.



Figure 1.45 : The examined parabolic dish collector in HEnergia research center for domestic cooling and heating [151]

1.2.2.2.4 Fresnel collectors in refrigeration

Linear Fresnel lens, as a linear concentrating solar device, could operate in the medium and high temperatures. This collector comprises a primary mirror and a linear non-movable receiver [152]. The LFR can be used not only for power generation, but also for solar cooling applications [134].

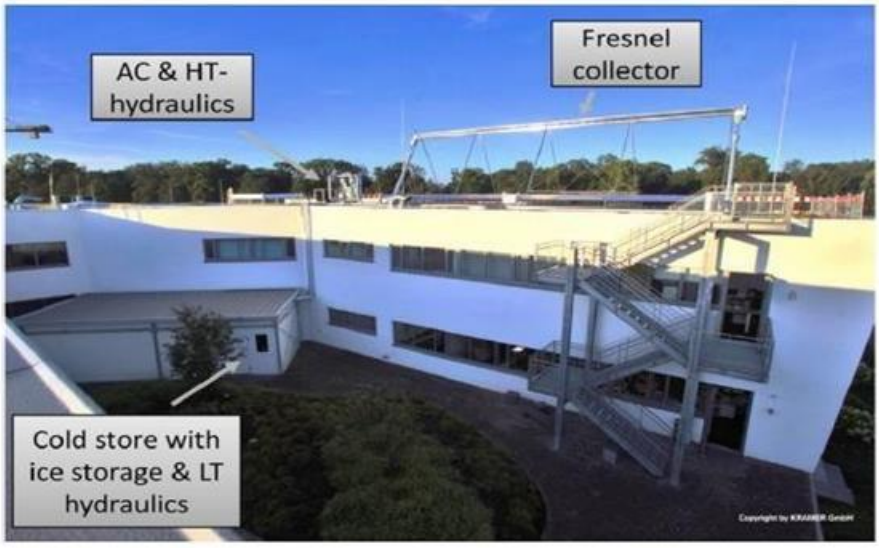


Figure 1.46 : LFR, ice storages, cold store room, and absorption chiller, a pilot plant in Germany [153]

1.3 Hybrid refrigeration systems

1.3.1 Concept and advantages of hybrid systems combining solar energy with conventional refrigeration

1.3.1.1 Concept of hybrid systems combining solar energy with conventional refrigeration

Hybrid systems combining solar energy with conventional refrigeration is a type of refrigeration system that uses both solar energy and grid electricity to operate. Unlike conventional systems that run entirely on grid power, hybrid solar refrigeration systems use solar panels to generate electricity, store it in batteries or feed it back into the grid. This reduces the amount of grid power needed to run the system, leading to lower electricity bills and carbon emissions.

There are two main types of hybrid solar systems: direct and indirect.

Direct hybrid solar systems : use solar thermal collectors to heat a refrigerant, which then cools the air via a heat exchanger.

Indirect hybrid solar systems : use photovoltaic (PV) panels to produce electricity, which then powers the compressor.

Both types of hybrid solar systems have a backup system that switches to grid power when solar power is insufficient or unavailable.

Direct hybrid solar system : it consists of four main components: a solar thermal collector, a thermal compressor, a condenser and an evaporator.

The solar thermal collector collects solar energy and transfers it to the thermal compressor.

The thermal compressor compresses the refrigerant, increasing its temperature and pressure.

The refrigerant flows to the condenser, where it condenses and releases heat to the outside air.

The refrigerant flows to the evaporator, where it evaporates and absorbs heat from the indoor air, thereby cooling it.

The refrigerant returns to the compressor, completing the cycle.

Direct hybrid solar system can also use grid power or gas as a backup heat source for the compressor when solar power is insufficient or unavailable.

Indirect hybrid solar system : it consists of four main components: a photovoltaic (PV) panel, a battery, an inverter and a conventional refrigeration unit.

The photovoltaic panel collects solar energy and converts it into DC electricity.

DC electricity is stored in the battery or fed back into the grid, depending on demand and supply.

The inverter converts DC electricity into AC electricity which can power the refrigeration unit.

The unit cools the air using the conventional refrigeration cycle.

The indirect hybrid solar system can also use grid power as a backup source for the unit when solar power is insufficient or unavailable.

1.3.1.2 Advantages of hybrid systems combining solar energy with conventional refrigeration

Reduced electricity bills:

The solar hybrid system can reduce the electricity consumption of the refrigeration unit by using solar energy, which is free and abundant. This can save you money on your electricity bills and make your cooling system more cost-effective in the long run.

Reduced carbon footprint:

The hybrid solar system can reduce the carbon emissions of the refrigeration unit by using renewable, clean and green energy. This can help you reduce your environmental impact and contribute to the fight against climate change.

Higher efficiency:

The hybrid solar system can increase the efficiency of the refrigeration unit by using solar power, which is more stable and consistent than grid power. This can improve the performance and reliability of your cooling system and extend its lifespan.

Increased flexibility:

The hybrid solar system can give you more flexibility and control over your cooling system by allowing you to switch between solar power and grid power, depending on availability and cost. This can help you optimize your energy consumption and savings.

1.3.2 Review of existing hybrid refrigeration systems (PV+ VCR) and their performance

Solar cooling systems can be broadly categorized into two primary types: solar thermal cooling systems and photovoltaic (PV) cooling systems. Solar thermal systems directly utilize solar radiation to expose the refrigerant, eliminating the need for electrical power. Conversely, PV cooling systems harness electricity generated by PV modules to drive their operations. Within the realm of thermal cooling systems, there exist four distinct categories: solar adsorp-tion, absorption, ejector, and desiccant systems.

On the other hand, PV-based solar cooling systems can be classified as either thermoe-lectric refrigeration systems or PV compression refrigeration systems. Among these, PV solar vapor compression refrigeration (VCR) systems prevail as the most commonly utilized and commercially accessible options. Notably, they have found practical applications in cold storage and the preservation of vaccines in rural areas [154-155].

1.3.2.1 State of the art of solar photovoltaic vapor compression refrigeration systems

Numerous experiments have been conducted to evaluate the effectiveness of vapor compression solar cooling systems, encompassing both alternating current (AC) and direct current (DC) variants [156-157]. In addition, various researchers have undertaken theoretical investiga-tions into solar cooling systems using PV technology [158-159]. One particular focus in recent years has been on low global warming potential (GWP) refrigerants, with studies exploring the utilization of refrigerant mixtures with low GWP values to enhance the performance of vapor refrigeration systems. Hydro-Fluoro-Olefin (HFO) refrigerants like R1234yf and R1234ze have emerged as promising alternatives to Hydro-Fluoro-Carbon (HFC) refrigerants due to their reduced GWP values.

Mota Babiloni et al. [160] compiled relevant research on R1234ze, encompassing investigations into its thermophysical and compatibility properties, heat transfer and pressure drop characteristics, and the performance of vapor compression systems incorporating this refrigerant.

Other studies have assessed the viability of R1234ze and HFO1234yf as alternatives to HFC- 134a, analyzed vapor compression refrigeration (VCR) systems employing different evaporators, and compared the performance of various vapor compression configurations uti- lizing low GWP refrigerants.

In a study by Ben Jemaa et al. [161], an exergy analysis was conducted on an air-cooled vapor compression chilled water system utilizing R1234ze, with findings indicating no significant differences in energy and exergy efficiencies when compared to R134a.

Rajendran Prabakaran et al. [162] conducted a comprehensive examination of the thermodynamic performance of an automobile air conditioning (AAC) system at three distinct vehicle speed conditions, employing R134a, R1234yf, and a 50/50 mixture of R1234yf and R134a. Their findings indicated that the performance of the R1234yf/R134a mixture closely resembled that of R134a within the AAC unit. However, they proposed utilizing a 90/10 R1234yf/R134a mixture to adhere to environmental protocols (GWP <150) without necessitating component modifications.

Toualbi et al. [163] investigated the energy performance of a vapor compression refrigeration cycle employing low GWP fluids (R1234yf and R1234ze) and compared it to high GWP fluids. The study revealed that R1234ze exhibited a superior coefficient of performance (COP) of 3.14, which closely approached that of R134a (3.17).

More recently, Shamkar Prased et al. [164] carried out both experimental and simulation investigations to explore various refrigerants and blends as potential replacements for R134a in vapor compression refrigeration systems. The researchers analyzed heat transfer parameters and predicted the performance of low-GWP refrigerants across the HFO and HFC categories through energy and exergy analyses, considering commercial refrigerants such as R134a.

As shown in Figure 1.50, Elias M. Salilih et al [165] proposed a method for analyzing and simulating solar energy-driven vapor compression refrigeration system with variable speed compressor in real weather conditions using technical data sheets (from PV panel and compressor) available from manufacturers.The research study includes a non-tracking photovoltaic power source directly coupled to a variable speed DC compressor.

Somjet Pattarapanitchai et al [166] studied the experimental performance and autoregressive modeling with exogenous variable (ARX) of a vapor compression refrigeration system operated by solar photovoltaic (PV) energy. The system is composed of a conventional refrigerator and photovoltaic modules (Fig 1.51 , Fig 1.52 , Fig 1.53).

The performance of the system was evaluated in terms of its cooling effect suitable for the storage of food and agricultural products.

The performance analysis clearly shows that a DC electric motor operated by solar PV with storage of electrical energy in batteries can be used for domestic applications using an environment-friendly renewable resource of solar energy.

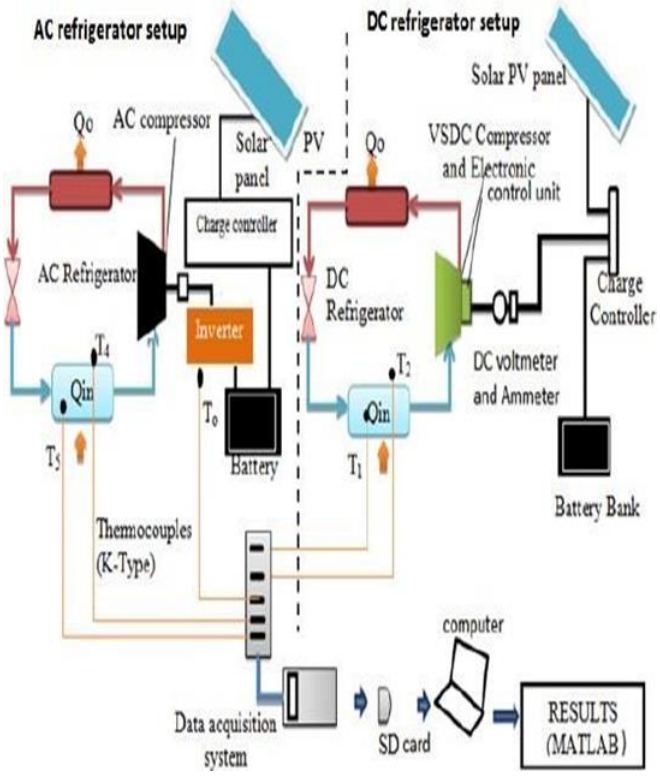


Figure 1.47 : Experimental setup for AC and DC refrigerators performance analysis [157]

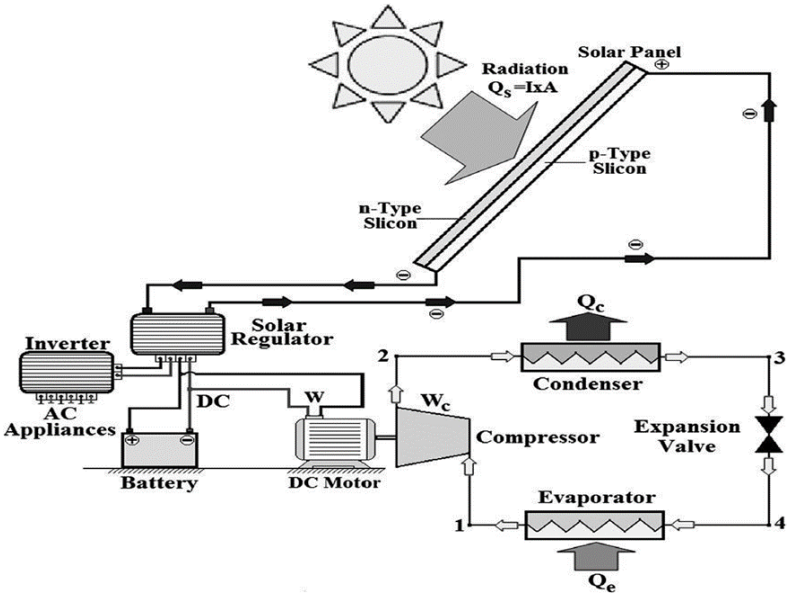


Figure 1.48 : Components of the solar electric-vapor compression refrigeration (SE-VCR) system [158]

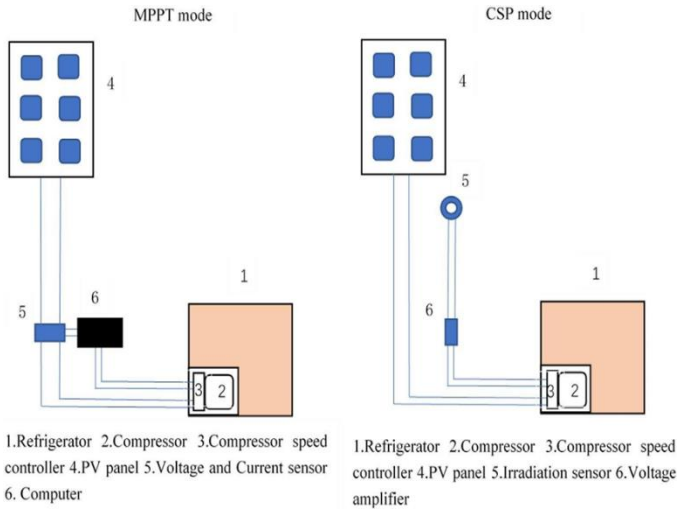


Figure 1.49 : Schematic diagram of PV direct-driven refrigerators with different control systems [159]

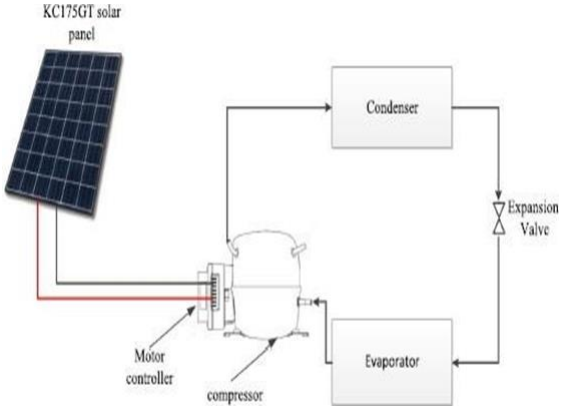


Figure 1.50 : Schematic diagram of directly coupled refrigeration system [165]

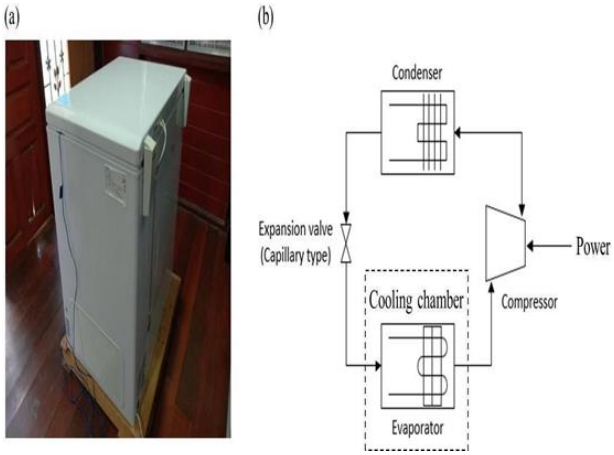


Figure 1.51 : Vapour compression solar refrigerator unit: (a) pictorial view and(b) schematic diagram [166]

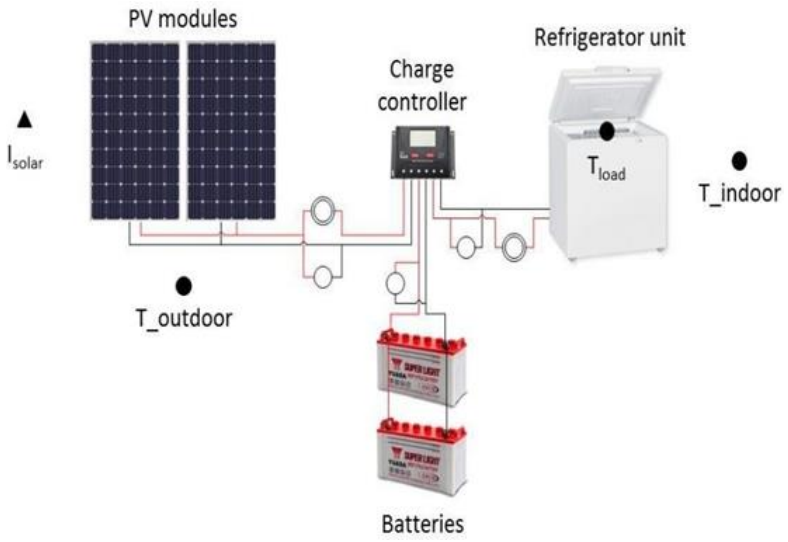


Figure 1.52 : Schematic diagram of the solar PV-powered vapor compression refrigeration system with the measurement points (• is position of temperature measurement, Δ is position of solar radiation measurement, O position of current measurement and © position of voltage measurement.) [166]

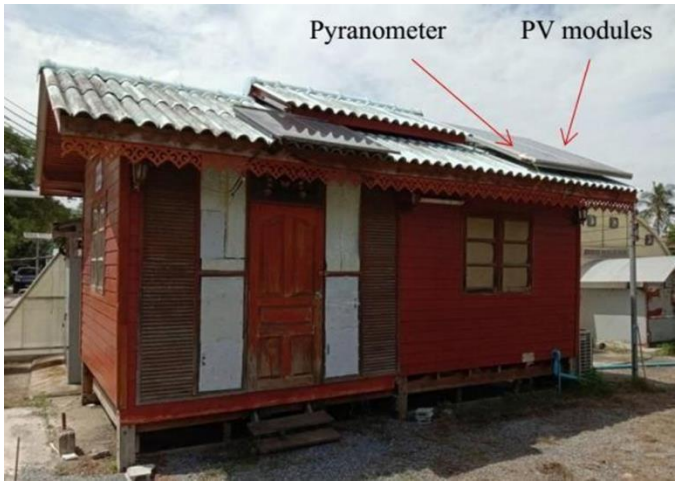


Figure 1.53 : A hut for accommodating the solar refrigeration system [166]

As shown in Figure 1.54, Valeria Palomba et al [167] describes a model of a solar hybrid adsorption-compression system, realised in Modelica language using the commercial software Dymola. The models of the main components of the sorption and vapour compression unit are described in details and their validation presented. In addition, the integrated model is used for proving the feasibility of the system under dynamic realistic conditions and an example of the technical sizing that the model is able to accomplish is given.

-If solar energy is not available, cold energy is produced directly from the vapour compression chiller, that can be directly connected to the dry cooler.

-If there is a mismatch between the solar availability and user demand, in order to exploit the renewable source, cold energy can be produced using the cascade system and stored in a sensible or latent cold storage.

-During winter, the heating demand of the building can be satisfied by direct connection to the solar collectors (if solar energy is available) or by the heat pump.

-Domestic hot water can be supplied by the solar collectors, coupled to a small water buffer or a back-up system (i.e., existing gas boiler in case of retrofitting).

To further enhance the share of renewables, electricity needed to drive the compression chiller can be supplied by PV panels when solar energy is available.

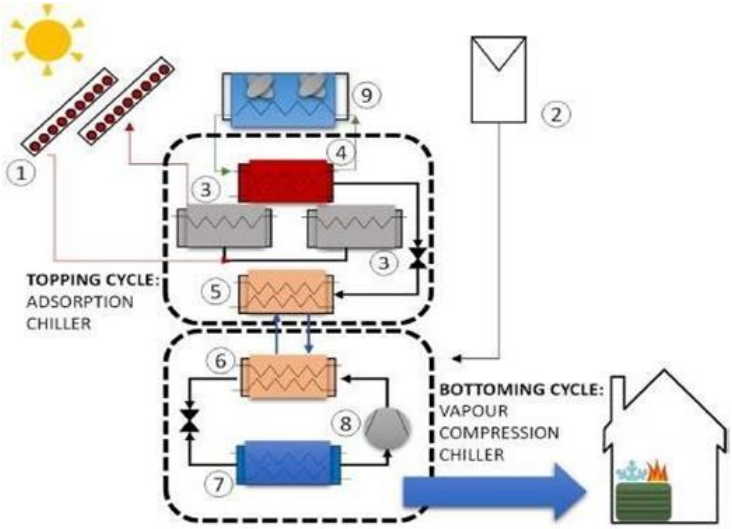


Figure 1.54 : The solar hybrid system proposed [167]

1) Solar thermal collectors field **2) Photovoltaic panels**

3) Adsorbers of the adsorption chiller **4) Adsorption chiller condenser**

5) Adsorption chiller evaporator **6) Vapour compression chiller condenser**

7) Vapour compression chiller evaporator **8) Compressor**

9) Dry cooler for heat rejection to the ambient

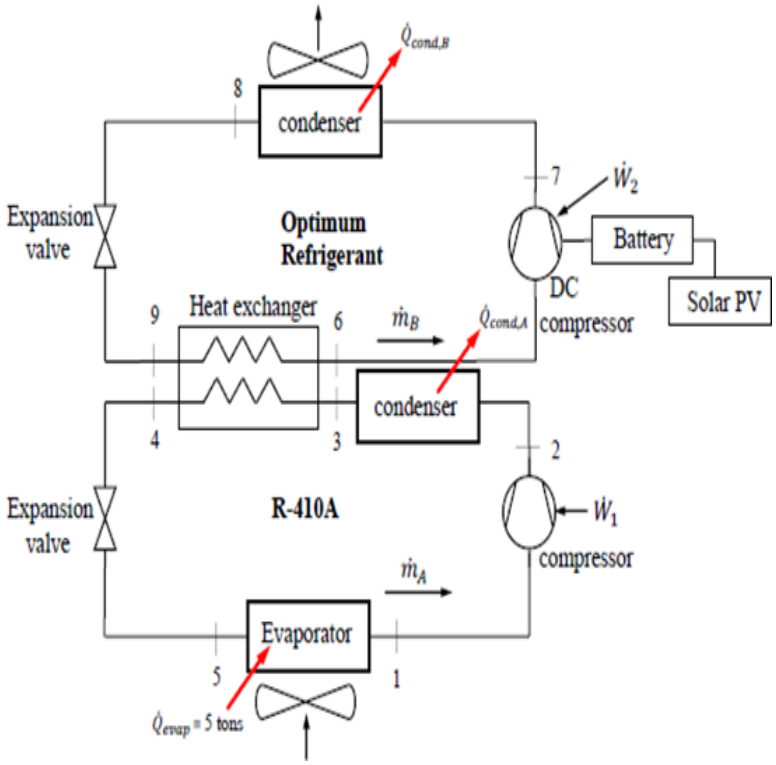


Figure 1.55 : Schematic diagram for the solar-powered mechanical subcooling refrigeration system [168]

Sara Baraghash et al [168] have studied the performance of a solar-powered mechanical subcooling cycle to improve the performance of a refrigeration system in hot climates as shown in Figure 1.55. The mechanical subcooling cycle helped the main refrigeration cycle by further subcool the refrigerant and improve the cooling capacity.

The mechanical subcooling cycle used the energy generated by the solar photovoltaics to run its own compressor. The system was evaluated under Kuwait's weather condition for a typical residential air conditioning (AC) unit of 5 tons of refrigeration (17.6 kW), where different refrigerants were examined in the mechanical subcooling cycle. The refrigerants considered in this study were R-410A, R-32, R-290, R-600, R-600a, R-1234yf, and R-1234ze(E). Parametric studies were performed using an equation solver software to understand the effect of the subcooling temperature and solar panel area on the overall performance of the refrigeration system. The results were compared with a baseline conventional refrigeration cycle using R-410A. The results show that the optimum subcooling temperature for the summer days in Kuwait ranges from 10°C to 20°C, while the best refrigerant that maximizes the overall performance of the system is R-600.

In addition, the dedicated mechanical subcooling system improved the overall system COP between 5% up to 16% compared to the conventional system during the typical day of July which is the hottest month in Kuwait. The results also concluded that the solar panel area required to produce sufficient solar power to run the dedicated mechanical subcooling cycle is 3.9 m^2 using a single-axis solar tracking system, which saves utility power during the summer months between 17-20%.

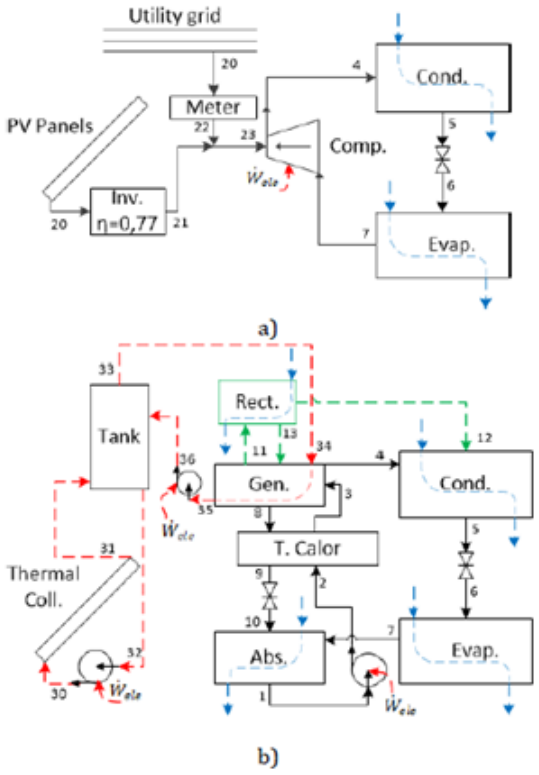


Figure 1.56 : Schematic representation of solar refrigeration:
a) VCRC (vapor compression refrigeration cycles) coupled with PV solar energy , and b) ARC (absorption refrigeration cycles) driven by ST energy [169]

Beethoven Narváez-Romo et al [169] have studied the technical-economic feasibility of photovoltaic energy to drive the vapor compression refrigeration system, and solar thermal energy for the ammonia-water and water-lithium bromide absorption cycles (Figure 1.56.) It developed thermodynamic models of both vapor compression and absorption cycles using the mass and energy conservation equations under steady-state regime. The systems of linear equations were solved by using the Engineering Equation Solver - EES.

One obtained the air conditioning thermal load profile and the characteristics of the thermal collectors and photovoltaic panels from EnergyPlus, from São Paulo-Brazil solar irradiation. Results showed that the monthly energy consumption is reduced from 626 kWh to 196 kWh, achieving a 44% reduction in the value of the electric energy bill for the photovoltaic solar cooling proposed when compared to the conventional one. A 7-years payback time is achieved. For the absorption cycle, the use of a flat thermal collector is unfeasible due to the need for natural gas as a complementary source of energy. It is concluded that solar cooling with photovoltaic has advantages compared to thermal activation, as the overall efficiency has a performance 30% higher than solar cooling by the thermal collector. Results showed that PREUPV (Primary Renewable Energy Usage PV) is always higher than PREUST (Primary Renewable Energy Usage ST).

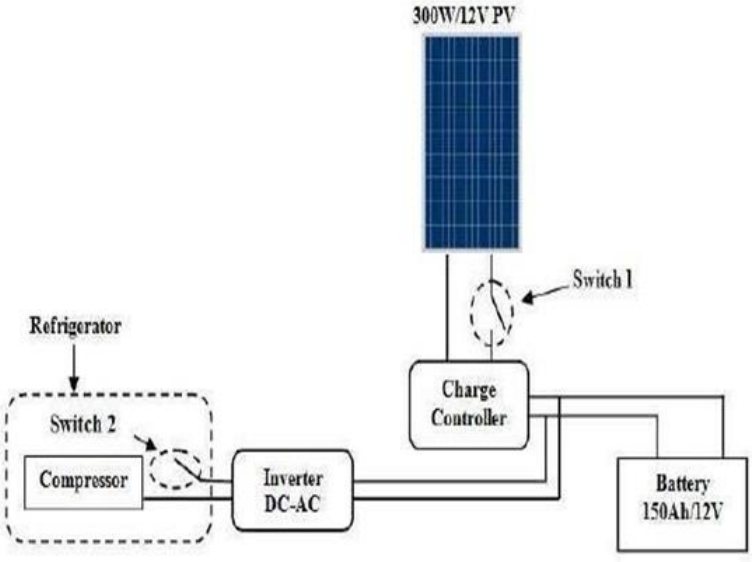


Figure 1.57 : System Configuration of Solar Refrigerator [170]

Cho Lin Han et al [170] studied and analysed a solar powered vapour compression refrigeration system to keep vaccine placed at rural area in the temperature range between 2 to 8 °C without grid (Figure 1.57).

The cooling load to be met by the photovoltaic generator depends on ambient air temperature, the special condition of refrigerator to preserve vaccine at this temperature range and size of the cooling space and matching condition between the photovoltaic module and compressor's power. They also calculated the heat gain through the refrigerator wall and heat absorbed by the vaccine bottle based on ambient air temperature of the hottest months (March, April, and May).

The performance analysis of refrigeration system is represented by using experimental result data. The photovoltaic generator and vapour compression refrigerator are matched by DC inverter. The relationship of outside temperature of surrounding and power of photovoltaic module are deal by MATLAB software.

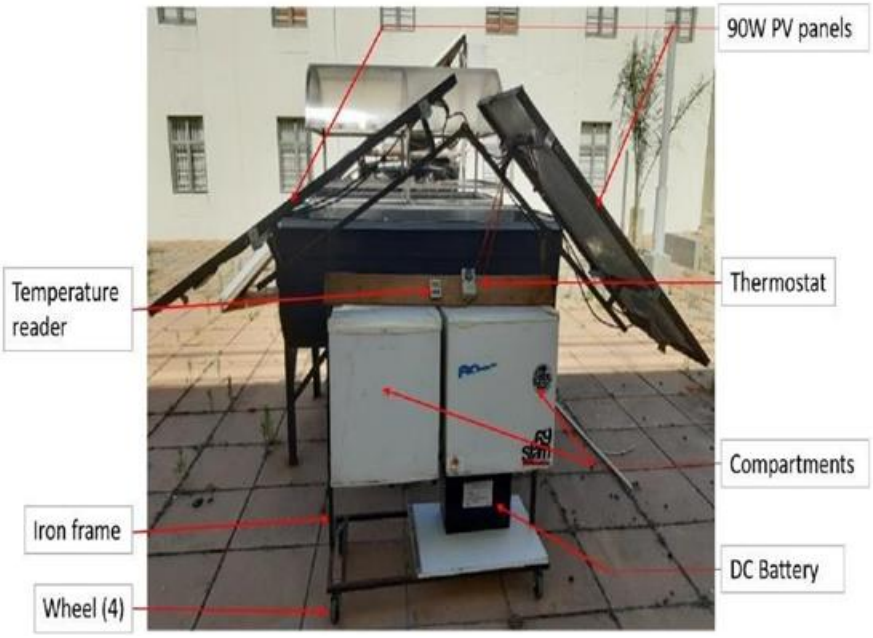


Figure 1.58 : The integrated solar PV refrigerator and heat pump (ISPVRHP) assembled for testing [171]



Figure 1.59 : The components of the solar PV refrigerator and heat pump (ISPVRHP) [171]

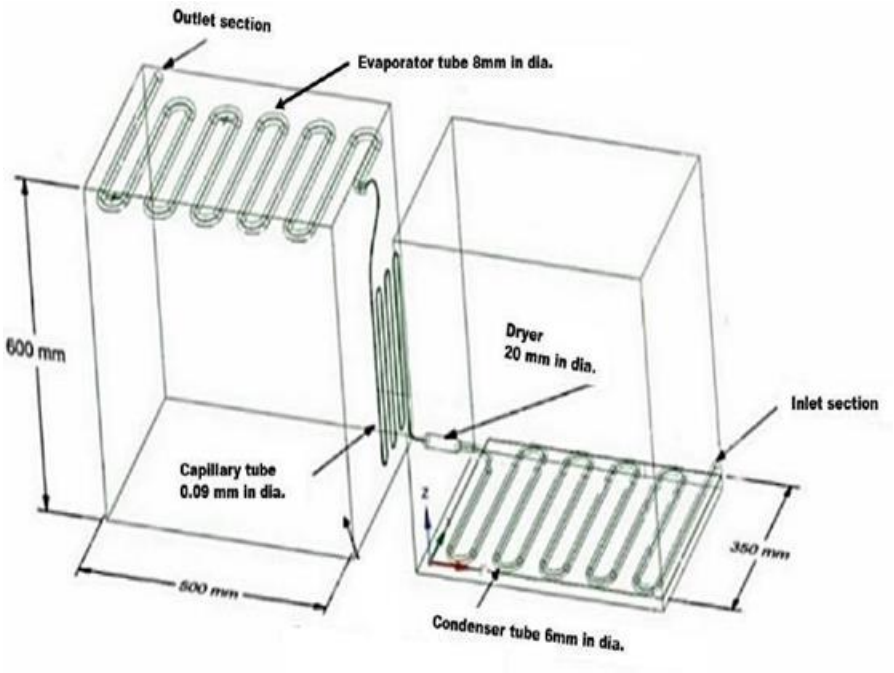


Figure 1.60 : The layout of the evaporator and the condenser [171]

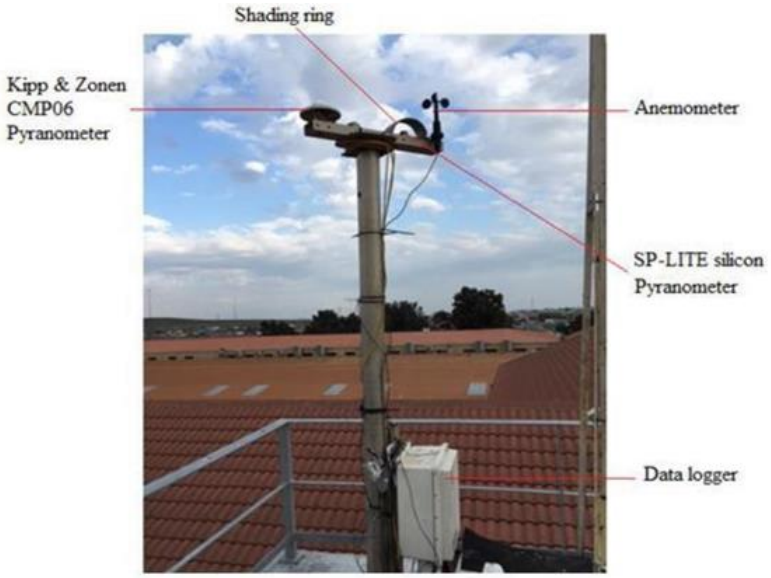


Figure 1.61 : Bellville campus scientific weather station [171]

Gracia Wa Mwamba Musifu et al [171] proposed an integrated solar PV refrigerator and heat pump (ISPVRHP) (Figure 1.58) for Sub-Saharan African food vendors , the refrigerant used is R134a ; the warm chamber would keep prepared food warm until the food is sold, while the cold chamber would minimise food spoilage. The ISPVRHP proposed can cool water or other beverages and be capable of utilising the heat rejected to the atmosphere by the condenser for warming food. The ISPVRHP was modelled using ANSYS software, and the results were validated experimentally.

The results show that both systems work well at peak hours, especially under more intense sun rays. The study found that the variation of incident solar radiation and ambient temperature has significant effects on the performance of the ISPVRHP; the wind speed, however, has only a minor impact on the total heat load of the system. In addition, the systems (cooling and heating) reached the desired temperatures and maintained them for long periods. The capacity of the refrigeration system can be increased by increasing the component sizes, including the PV system size. The ISPVRHP performance dropped substantially when the doors remained open for extended periods due to loss of energy through mass transfer.

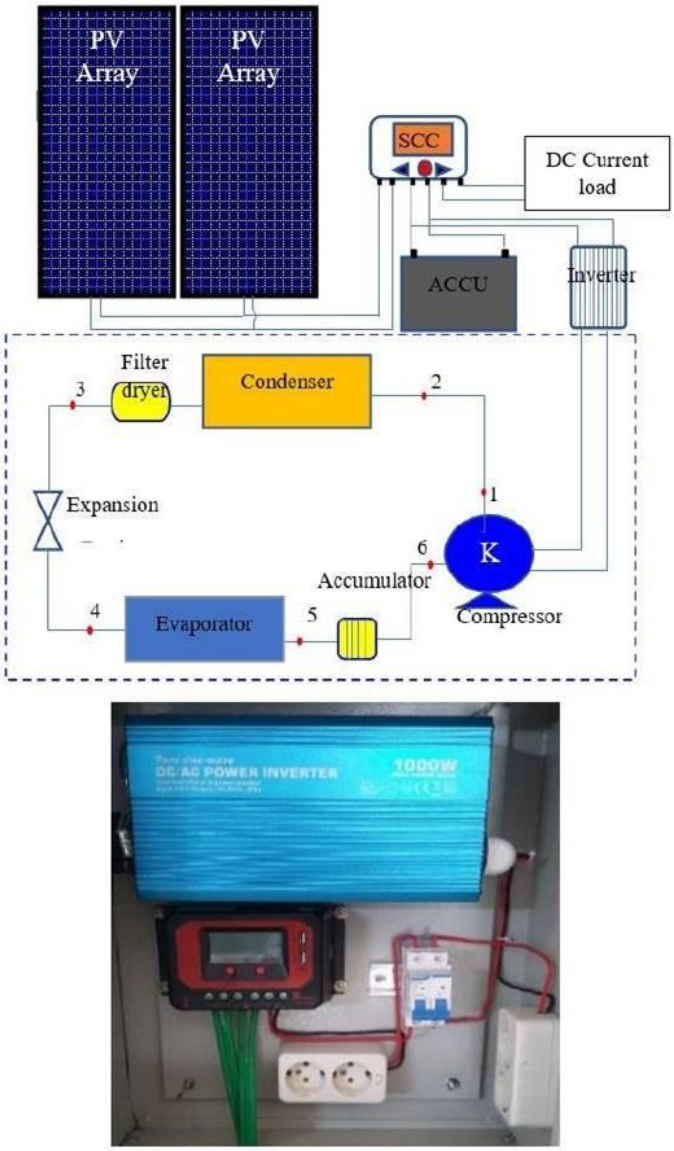


Figure 1.62 : Design of experimental rig and solar control panel [172]

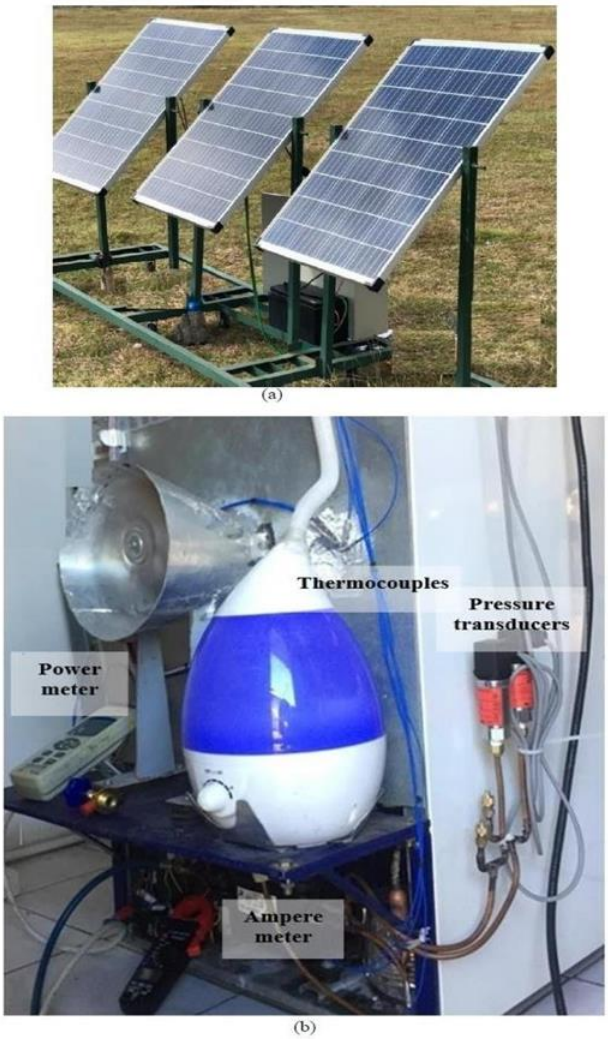


Figure 1.63 : Experimental set up: (a) photovoltaic array, (b) measurement position of the refrigerator prototype [172]

I. D. M. Cipta Santosa et al [172] proposed an experimental research consisting of a refrigerator prototype operating with R600A refrigerant and a photovoltaic array (Figure 1.62). Measurements and data acquisition were using data logger system. The refrigerator prototype measurements consist of temperature, pressure, power supply and mass flow rate. For solar power array system, measurement consist of current and voltage output. Ther study is a preliminary study with the focus on carried out on the calculation and analysis of coefficient of performance (COP) of the refrigerator. The results obtained are the photovoltaic arrays can provide energy continuously during high solar intensity (during the day). The performance of the refrigerator is quite good, with an average COP of 3.2.



Figure 1.64 : Solar assisted refrigeration system [173]

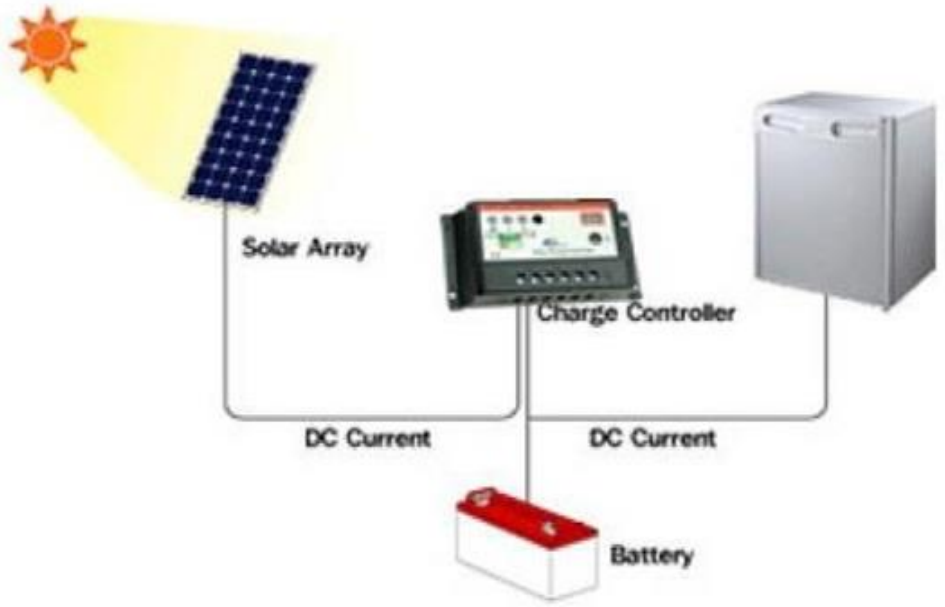


Figure 1.65 : Concept model [173]



Figure 1.66 : Set-up of solar assisted refrigeration system [173]

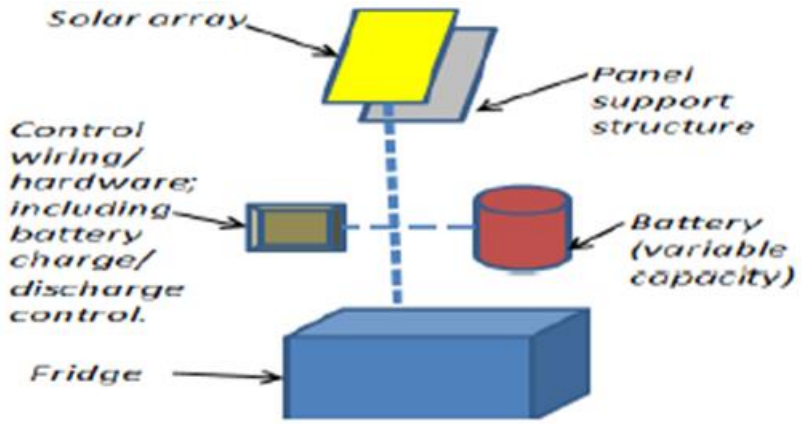


Figure 1.67 : Battery [173]



Figure 1.68 : Charge controller [173]

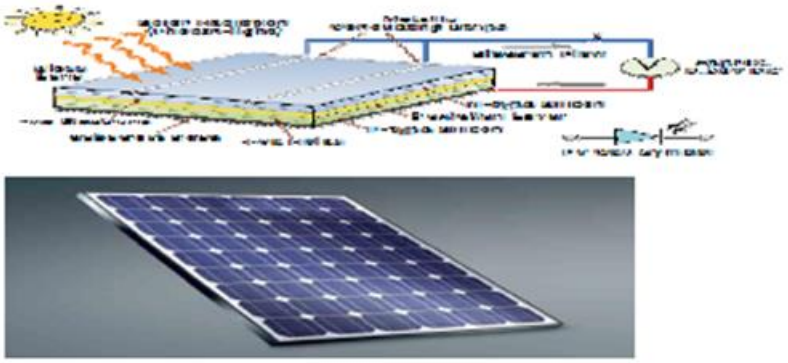


Figure 1.69 : Solar panel [173]

S. V. GANORKAR et al [173] proposed an experimental research which consists of the installation of a prototype refrigerator powered by photovoltaic solar energy (Figure 1.64), they showed that the system has more advantages than disadvantages.

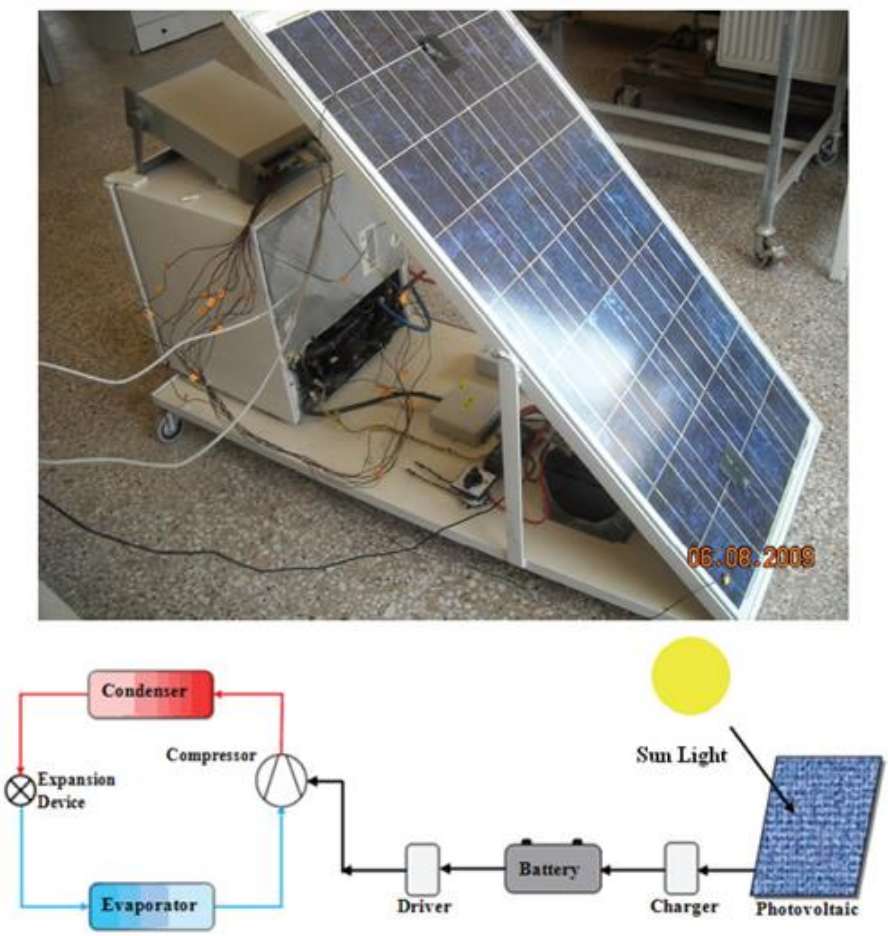


Figure 1.70 : Experimental set-up of the PV powered refrigerator [174]

O. Ekren et al [174] carried out an exergy analysis of a domestic refrigerator,powered by a photovoltaic system (Figure 1.70) . Ozone-friendly R134a is used as a refrigerant. In their study. they demonstrated that a small domestic refrigerator equipped with a DC compressor can run on photovoltaic energy without any inverter. These reduce the initial cost of the system since the inverter represents a significant cost for solar powered systems. Experiments under different conditions were carried out. According to the energy analysis, the highest COP (0.670) is observed without storage. In addition, the electrical consumption of the compressor is low for this operation. However, the highest exergy performance coefficient is

0.068 under low load conditions. At low load, the overall exergy efficiency of the refrigeration system is 0.859%. The overall exergy efficiency of the system is also very low since energy conversion efficiency (about 12%) and exergy efficiency (about 11%) of the PV is low. It is also clearly seen from exergy destruction values. For all cases, exergy is destroyed highly in the PVs.

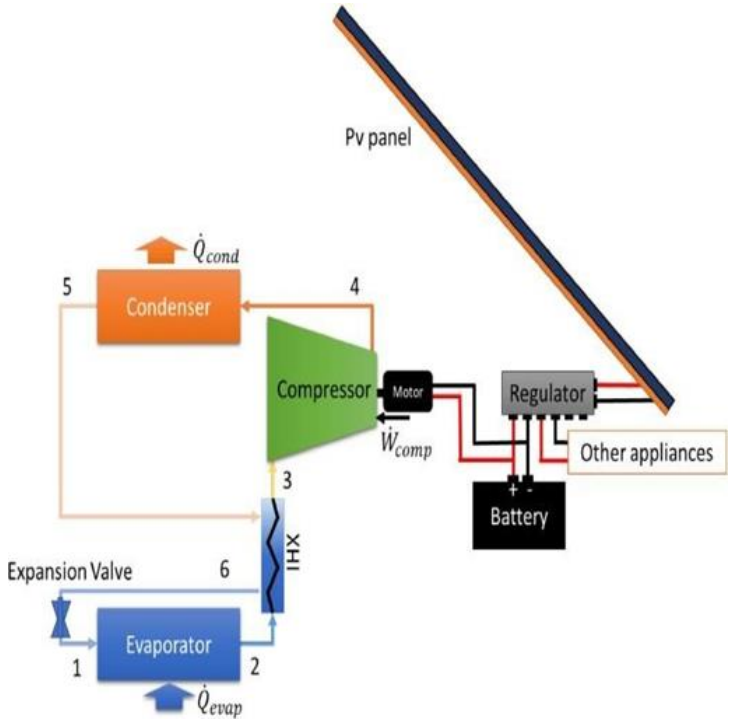


Figure 1.71 : Scheme of the horizontal solar vapour compression refrigerator with internal heat exchanger [175]

In a recent study (last year) Carlos Amaris et al [175] studied a small capacity DC refrigerator with internal heat exchange using R600a, R290, R717 and R134a as shown in Figure 1.71. A thermodynamic model was developed to assess a 200 W refrigerator performance at evaporation temperatures of -32/-10 °C, condensation temperatures of 35/46 °C, and different internal heat exchanger effectiveness values while considering the environmental conditions in the city of Barranquilla whose metropolitan and urban area presents a great potential for solar refrigeration. Results showed that the R290 system coefficient of performance was up to 2.6% higher than that of the R134a. The R600a system coefficient of performance was up to 2.7% higher than that of the R134a, but only under the most favourable conditions. The R717 system surpassed the compressor discharge temperature limits so it was found unsuitable for this application. Moreover, the internal heat exchanger was found beneficial to reduce the exergy destruction in the compressor and expansion valve but increased that in the condenser for R134a, R600a, and R290. The internal heat exchanger recommended effectiveness should be around 0.4 for R600a or 0.3 for R290 at an evaporation temperature of -32 °C. For an evaporation temperature of -10 °C, the IHX effectiveness can be up to 0.5 for both R600a and R290.

Finally, the maximum power consumption of the solar R290 refrigeration system was estimated around 4.08 kWh and 2.28 kWh at evaporation temperatures of -32 °C and -10 °C, respectively, which could be covered by a solar panel area of 3.76 m^2 and 2.10 m^2, respectively, while similar values were obtained for the solar R600a refrigeration system.



Figure 1.72 : Solar powered air conditioning system [176]

Khaled S. Al Qdah [176] studied the design and performance of solar powered air conditioning system integrated into the photovoltaic (PV) system composed of photovoltaic, solar panels charger, inverter and batteries (Figure 1.72). This air conditioning system can be used in non-electrified areas near Al Medina where the cost of electricity for this area is very high. The first step of his project was the calculation of the cooling load for the selected space that will be cooled and it was found to be approximately 1 ton of refrigeration (3.52 kW). Based on this cooling load, the photovoltaic (PV) system was increased and built with the necessary connections. A data recording system was used to measure temperatures at the main cycle components such as the compressor inlet and outlet as well as evaporator and condenser. The system input powers as well as the coefficient of performance (COP) for the climate system in Al Medina conditions were measured throughout the day. The coefficient of performance ranges from 2.16 to 4.22 for the system and these results compared with the performance of the conventional system with good agreement.

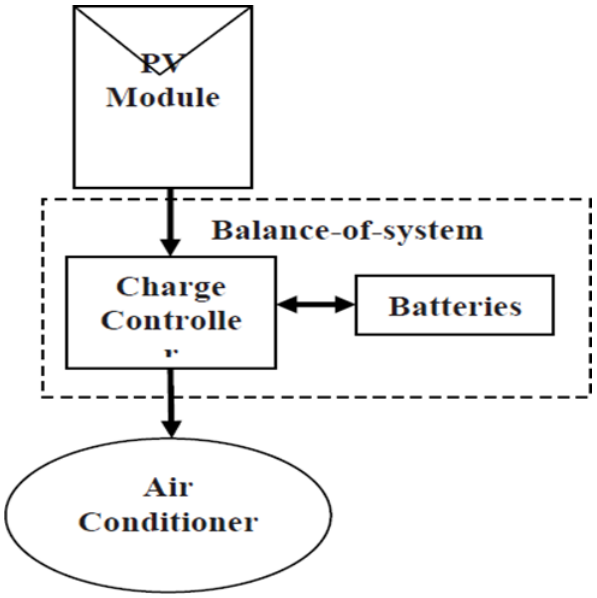


Figure 1.73 : Block diagram of PV system and air conditioning system [177]

I.Dauta et al [177] proposed the design and construction of a direct current (DC) air conditioning system integrated with photovoltaic (PV) system consisting of photovoltaic panels, solar charger and inverter and batteries (Figure 1.73).The air conditioning system can run on solar energy and can be used in non-electrified areas.

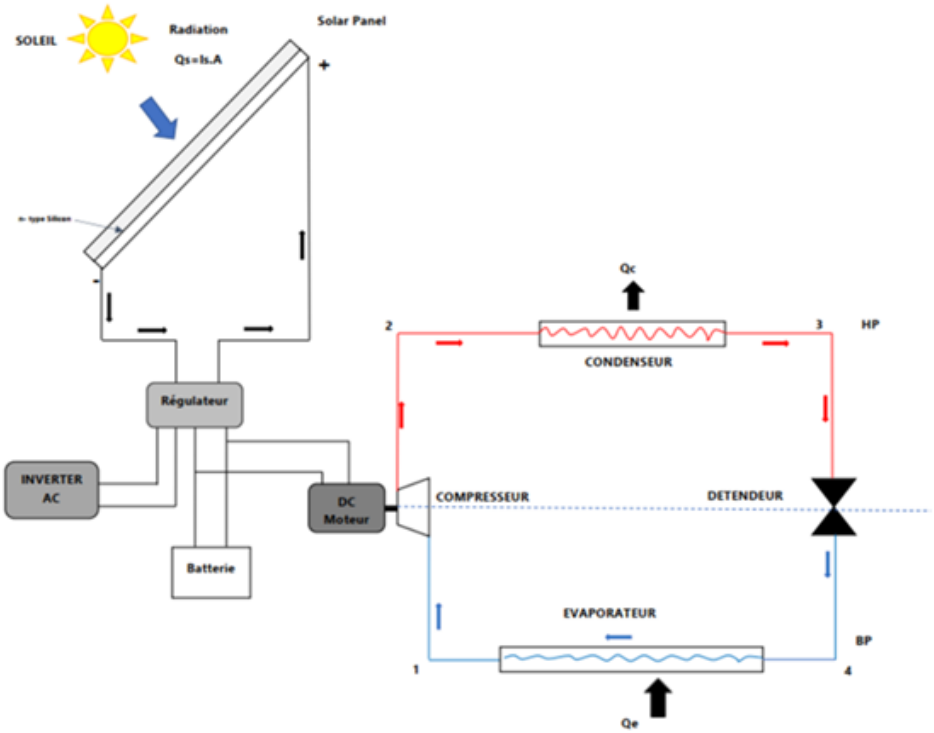


Figure 1.74 : Diagrams of the operating principle of the Solar VCR system [178]

Rakotondrazano Yvon et al [178] proposed a study to evaluate the performance of an electric vapor compression solar refrigeration system coupled with solar energies for the different climatic zones in Madagascar (Figure 1.74) . The refrigerant used for the vapor compression refrigeration cycle is R717 refrigerant or NH3 ammonia. For the 5 selected cities, a building of the same constructive design was used. Hourly building heat loads were estimated from the heat balance method using meteorological data from selected cities such as hourly average solar radiation and atmospheric temperatures. Then, the hourly evaluation of various parameters such as the coefficient of performance, the capacity of the condenser, the electrical consumption of the compressor and the power of the photovoltaic generators as well as its surface for different evaporation temperatures were determined. It was determined that the SE-VCR system could be used successfully for the province of Mahajanga, Antsiranana, Toliara and Tamatave while for the city of Antananarivo was not very interesting.

For these 4 cities, the coefficient of performance varies from around 3.3 to 4.43 for an evaporation temperature Te = 0 ° C. And the power of the compressor varies from 5.66 to 7.5 kW with a peak power of the solar panels varying from 21.16 to 25.23 kWp with a respective surface of 104.93 to 125.12 m². The overall efficiency of the installation varies from 0.483 to 0.521.



Figure 1.75 : Front of the refrigerator [179]



Figure 1.76 : Back view of the refrigerator [179]



Figure 1.77 : 3D view of the proposed refrigerator [179]



Figure 1.78 : Installed photovoltaic system used for the experiment [179]

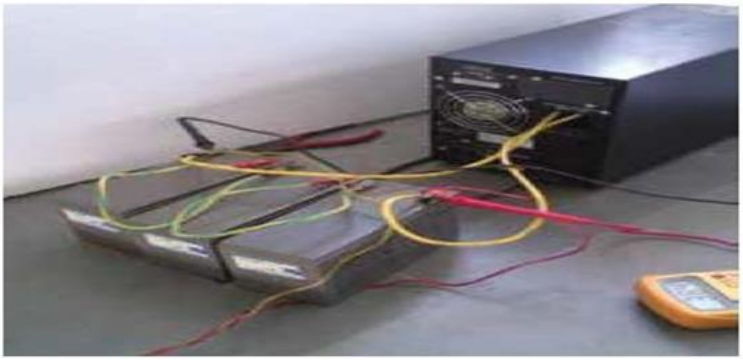


Figure 1.79 : Battery bank and UPS system (uninterruptible power supply) [179]



Figure 1.80 : No load test picture [179]



Figure 1.81 : Full load test picture [179]

KAPIL K. SAMAR et al [179] described the thermodynamic and economic results of the development of photovoltaic solar panels operating with a 20 liter refrigerator system (Figure 1.75). The system operates with R134a refrigerant.

In the study carried out by Lei Hayan et al [180], a micro-refrigeration experimental system driven by photovoltaic power generation and operates with R134a refrigerant was established (Figure 1.82). A study of the cooling capacity, load power, and system efficiency changes over time under sunny and cloudy weather conditions was carried out. The results show that the appendant battery makes the system run more stably, and the weather has no obvious effect on the operation of the indoor refrigeration system. The system exergy analysis indicates that the exergy loss of the compression process is the largest, accounting for more than 80% of the total in the refrigeration system.

The exergy efficiency of the refrigeration system can reach about 28% under both weather conditions.

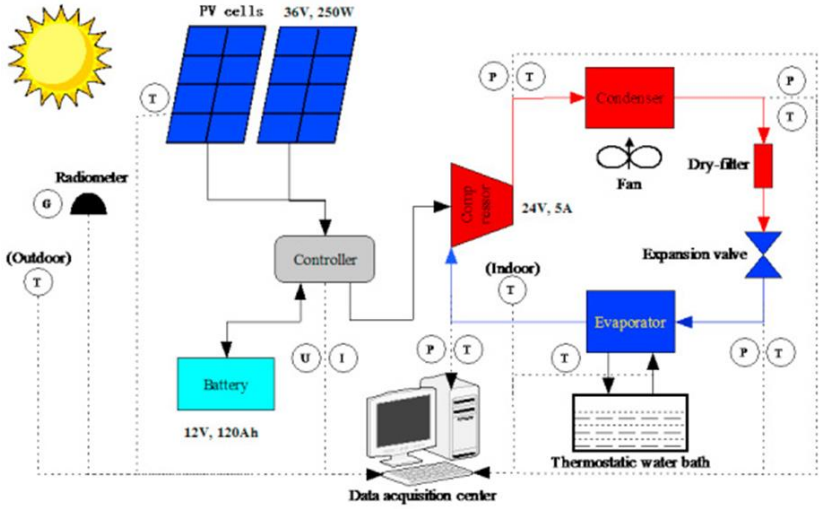


Figure 1.82 : Schematic of the miniature photovoltaic refrigeration system [180]

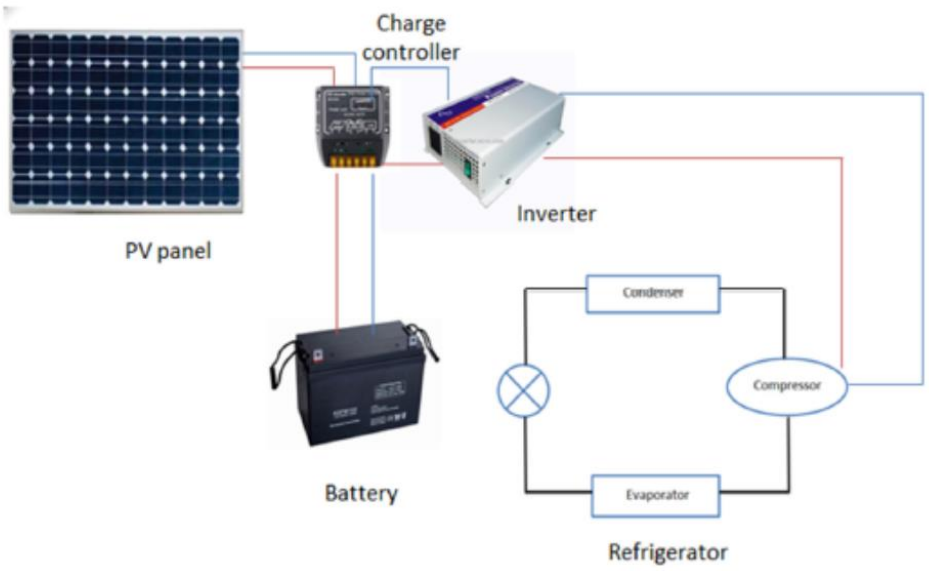


Figure 1.83 : System layout of solar driven refrigeration system [181]



Figure 1.84 : (a) Solar refrigeration system set-up, (b) evaporator tank [181]

In their work, Mohd Syahmiyadiy Jamaluddin et al [181] developed a small-scale solar driven refrigeration system (Figure 1.83) by combining several components such as a solar panel, a charge controller, a compressor, an inverter, an evaporator-tank, a condenser and a few connection wiring. They operated the system for several days to check its functionality and performance. During operation, they measured solar panel's current and voltage with a 5- minute interval to calculate power that has been supplied as an input to the compressor.

The evaporator coils pass through the water tank to cool down water to a desired temperature (i.e. 4 ºC). The temperature of the evaporator and condenser was also recorded for calculating the cooling effect created by the refrigerant R-134a. They calculated coefficient of performance (COP) of the system for both actual cooling load of water and cooling effect created by the refrigerant. The refrigeration system successfully operates with an actual COP of 0.95. Despite the COP is low, the solar driven refrigeration system, which does not require any fuel, is a promising option in regard to both environment and economic aspect.

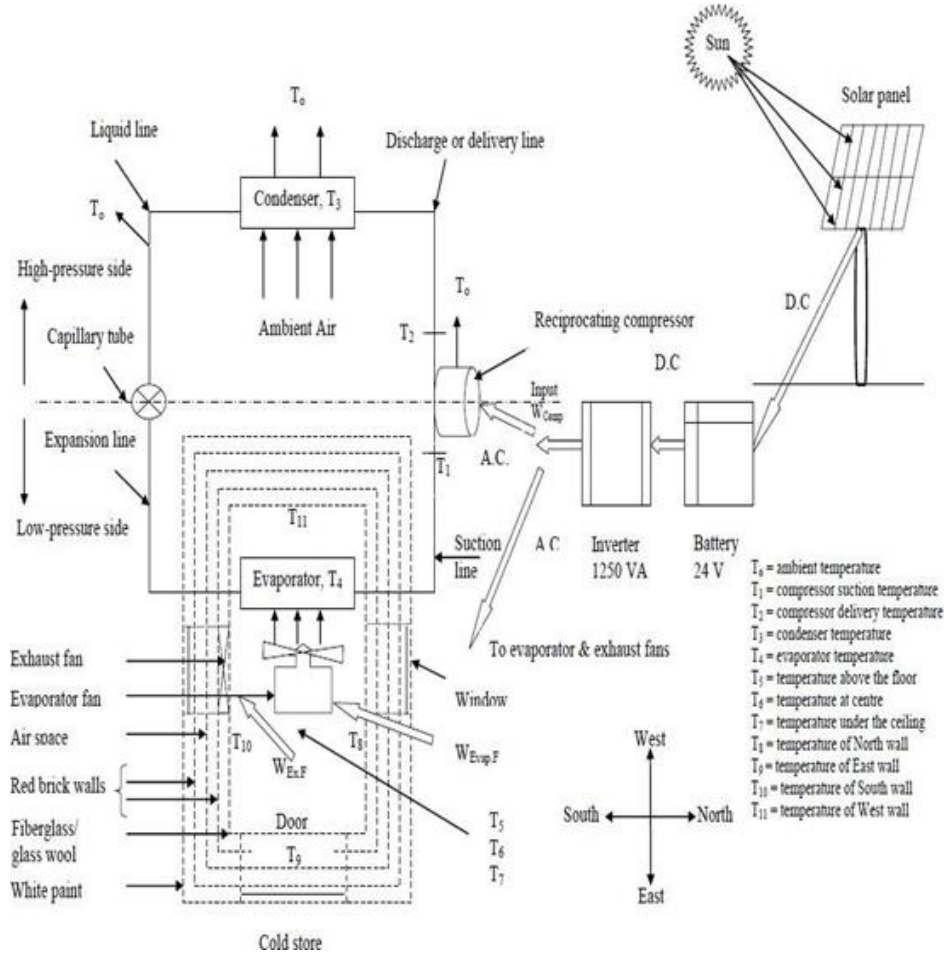


Figure 1.85 : Schematic diagram for solar PV powered vapour compression cooling system for potato storage [182]



Figure 1.86 : Curing of potato tubers using evaporatively cooled (EC) chamber [182]

Mohamed A. Eltawil et al [182] carried out a study to design and fabricate a solar PV powered vapour compression refrigeration system (Figure 1.85) to attain favourable conditions for potato storage, and to evaluate its shelf life under different operating conditions. The system is designed and fabricated in the division of Agril. Engineering at IARI, New Delhi. It consisted of PV panel, lead-acid battery, inverter and the vapour compression refrigeration system consists of a drier-cum-filter besides the main components: compressor, condenser, expansion device, evaporator, exhaust and evaporator fans. The 2.50 m^3 cold storage structure was constructed and insulated with proper materials. An evaporatively cooled storage structure (1.0 m^3) was used for curing process. The cured potato cultivar (Kufri Chandermukhi) were stored for 5 months. The stored tubers were divided into two lots, one used as control (free sprouting) and the second was manually desprouted. Measuring of moisture loss, dry matter, sprouting, rotting, sugars content, starch and chipping quality reflected the shelf life of potato. The average daily solar photovoltaic (SPV) energy output and energy consumption by the load were 5.65 and 4.115 kWh, respectively, under full load. The obtained results indicated that, the average daily actual COP for loaded and air circulated cold storage structure was 3.25.The average temperature and relative humidity maintained inside the loaded and air circulated storage structure were 283.13 K and 86 %, respectively. Solar panel can serve as an alternative source of energy for powering cooling system.

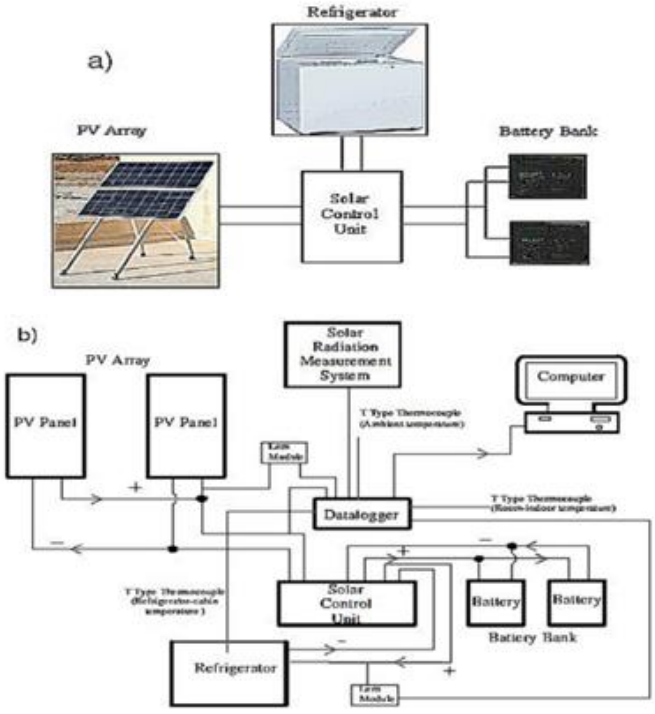


Figure 1.87 : Schematic of the PV refrigeration system [183]

Mehmet Azmi Aktacir [183], had studied a multipurpose PV refrigeration, he has built standalone PV refrigeration system as per Figure 1.87. In this study, a PV powered multipurpose refrigerator system has been established to investigate experimentally its daily and seasonal operating performance. The PV refrigerator system is independent of the local electricity available network area. Operation of this system under Sanliurfa climate conditions is continuously observed. During the daily operation of the refrigerator system, the parameters affecting the system capacity and performance were determined experimentally. The following findings were obtained from experimental study

1.Low temperature of -10.6°C can be reached in the refrigerator while average indoor and outdoor temperature are 26.3 and 24.9°C respectively.

2.During the daily period the highest energy amount produced by PV panels is recorded between 11:00 and 14:00.

3.Under Sanliurfa local conditions for a typical hot day in May 2009, energy consumption amount of refrigerator was determined to be 347.7 Wh/day. The amount of energy stored in the battery bank is 78.2 Wh/day while the amount of electric energy produced by photovoltaic panel is 425.9Wh/day.

4.The energy required for refrigerator is provided by photovoltaic power, clean energy source. There is no negative impact of the electrical energy generated by PV panel on the environment.

It has been seen from this study that the use of PV refrigerator system is suitable for applications in different sector fields, required the low and medium cooling capacity. Such small scale standalone system can suitably be used in many rural regions where electricity is unreliable or non-existent but refrigeration is continuously critical.

In the work of Soorkeu A. Atrooshi [184] the characterization and the performance assessment of a solar powered direct current variable speed twin compressor, vapor compression refrigeration cycle (Figure 1.88) has been presented for investigation in an insulated cooling chamber; 50 X 40 X 40 cm. The required DC power supply is provided by solar panels and backed up by DC transformers. Exergetic (available work potential) analyses are used to run a parametric study of the performance of this system operating with the R134a refrigerant.

The analyses focused on coefficient of performance, exergy destruction,exergetic efficiency and the efficiency defect.

When changing condenser input temperature the coefficient of performance responded inversely, exergetic efficiency peaked at 28.24% for condenser input temperature of 43.5 °C and the efficiency defect acted proportionally. Variation of evaporator load led to an increase in the cycle coefficient of performance and showed that the highest exergy destruction is done in the system compressor, followed by the condenser, expansion valve and finally the evaporator. The highest coefficient of performance (4.7) was achieved when running at 2500 RPM. Based on the achieved performance (energy analysis) figures and the marked weaknesses (exergy analysis) of the system it is recommended that similar solar powered D.C. installations can be integrated to actively participate in cooling partitioned spaces on large-scale basis.

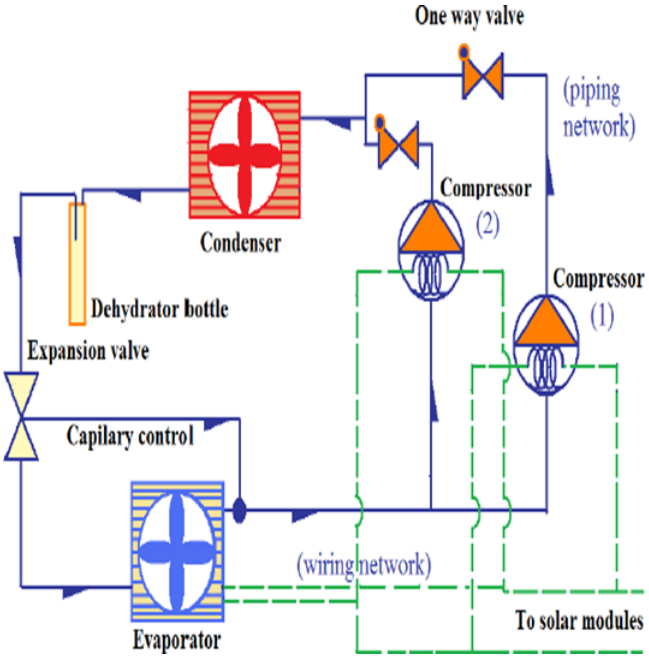


Figure 1.88 : Layout of vapor compression refrigeration cycle powered by solar energy [184]



Figure 1.89 : The experimental test rig [184]



Figure 1.90 : Backup transformer to support the rig on cloudy days [184]

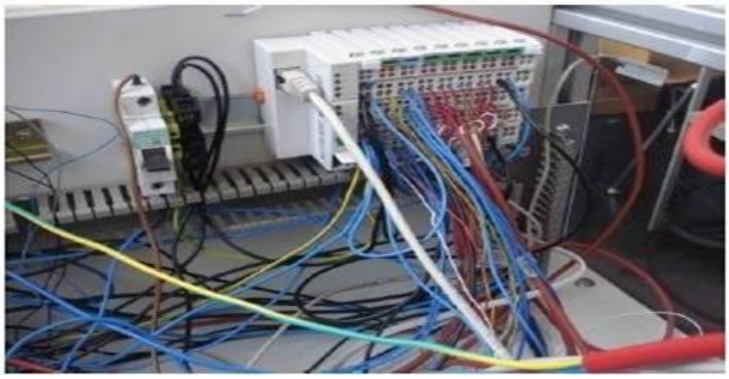


Figure 1.91 : Programmable logic control (PLC) used in the test rig [184]



Figure 1.92 : Standard, conventional pressure and temperature measuring backup set [184]

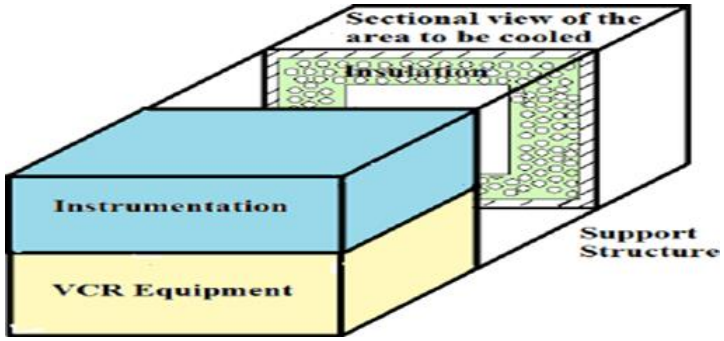


Figure 1.93 : The housing structure of the test rig [184]

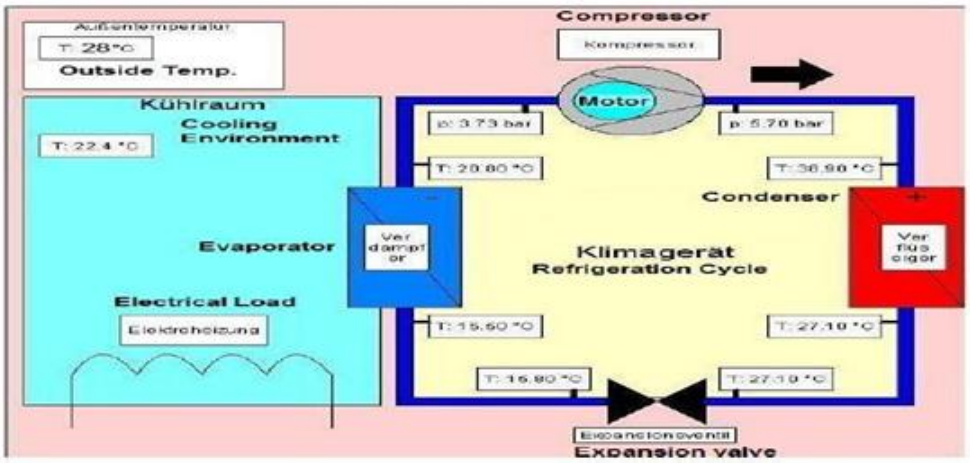


Figure 1.94 : Sample of the monitor view while working on CodeSys software [184]

Another application of photovoltaics refrigeration belonged to a food storage truck. So, as a result of the PV-integrated deliveries, it has been shown in the work of Meneghetti, A. et al [185] that refrigerated transports may embrace both the economic and environmental aspects of sustainability, making it an effective tool for food distribution.

The difficulties associated with refrigeration truck deliveries are determined by the many climate regions through which the vehicle traveled. As a result, optimization of the setup to get the desired output should be addressed. Figure 1.95 illustrates the energy flows of a refrigeration truck equipped with solar panels during a time interval of k. From this, the dependent parameter for improving the design approach should be determined.

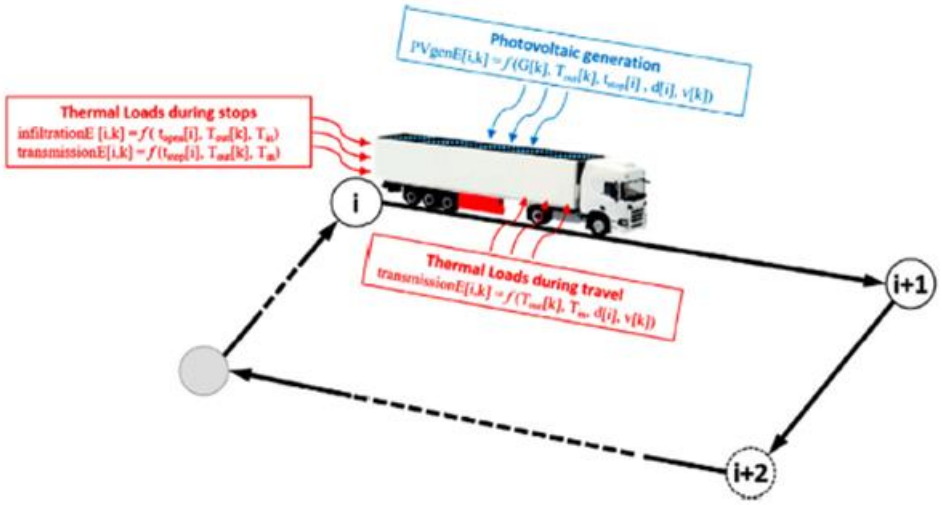


Figure 1.95 : Energy flow of PV integrated cooling truck (d: travel distance, G: solar irradiance, Tout: outdoor temperature, Tin: internal vehicle temperature, topen: door opening time, tstop: stop time at a client, v: travel speed) [186]

Gupta, B.et al [187] carried out a parameter study to find out the best combination of the PV panel wattage, battery capacity and insulation level to operate the refrigerator stand-alone on solar power (Figure 1.96). The transient simulation software (TRNSYS) is used to simulate the PV based refrigeration system. The system consists of a refrigerator with 50 l capacity, 24 V battery bank, 1 kVA inverter, and PV panels with charge controller.

The simulation model has been validated with experimental data. The parameters used are: wattage of PV panels in PV array, capacity of the battery bank and variation of insulation in refrigerator. The results conclude that it is feasible to operate a refrigerator (25 mm insulation thickness) on SPV without grid power with 320 Wpanel arrays with 50 Ah battery capacity. As the thickness of insulation is increased to 50 mm then 200W panel capacity is sufficient to drive the refrigerator.

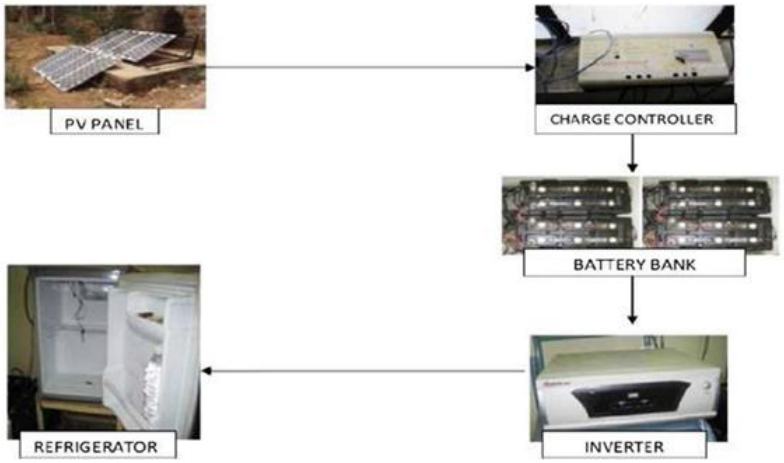


Figure 1.96 : The components in domestic refrigeration with the PV [187]

In 2018, Daffallah [188] analyzed a solar PV DC refrigerator (Figure 1.97) by changing the voltage from 12 to 24 Volts. The results showed that the 12 V had better outcomes than 24 V, particularly at the higher ambient temperatures.

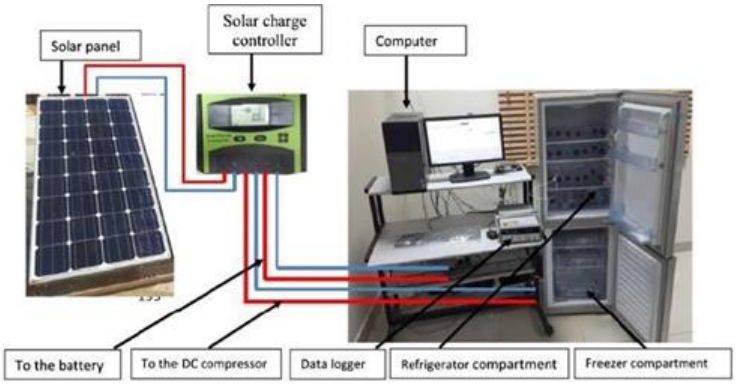


Figure 1.97 : A DC refrigeration powered by PV [188]

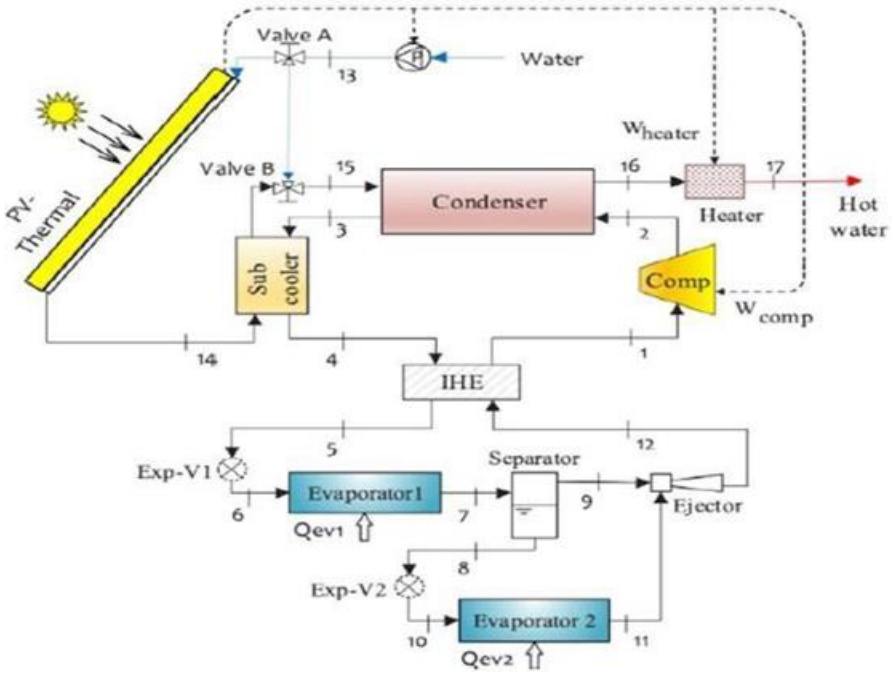


Figure 1.98 : Hybrid PVT connected to ejector-compression refrigeration [189]

Zarei et al. [189] simulated a PVT for combined heating and cooling by the EES software. The refrigeration cyclewas an ejector-compression cycle, and the used refrigerants were R600a and R290. They concluded that R290 could obtain a higher COP than the R600a and R134a. Figure 1.98 shows the schematic of the hybrid system thatwas used in their research work.



Figure 1.99 : Experimental set-up of SPV powered refrigerator [190]

A. J. Dhondge et al [190] undertook a comparative analysis of the energy and exergy performances of a refrigerator powered by photovoltaic solar energy for the storage of vaccines using the refrigerant R-134a and the nano-refrigerant (R-134a + 0.5% Al2O3) as refrigerants (Figure 1.99). Exergy destruction or losses, exergy efficiency and coefficient of performance (COP) were studied. They found that at higher evaporation temperatures, exergy losses are minimal. The maximum exergy loss occurred in the evaporator and compressor and the values were between 36% and 37% of the total system losses.

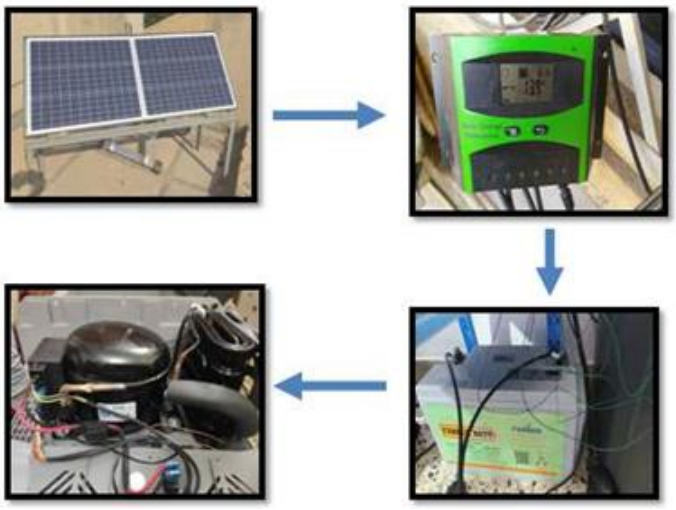


Figure 1.100 : Experimental setup [191]

Dalya Amjed Omer et al [191], carried out an experimental energetic and exergetic analysis for a small dc refrigerator driven by a solar photovoltaic (PV) panel (Figure 1.100) along the time of the day under the climate of Baghdad city. The experimental test has been carried out with load refrigerator (5 liters of water), they concluded, that the average exergy losses optimum value in evaporated temperature (-6 °C) is 24.63%.

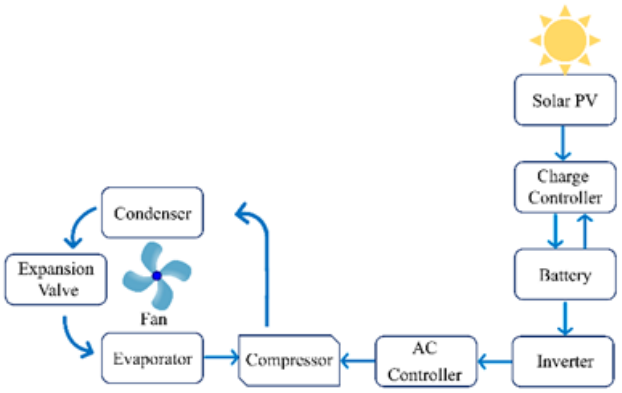


Figure 1.101 : Block diagram of the solar assisted refrigerator [192]

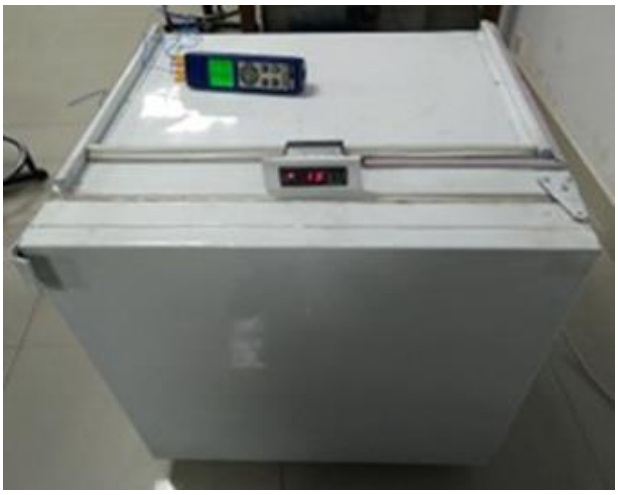


Figure 1.102 : Top side view of the refrigerator [192]

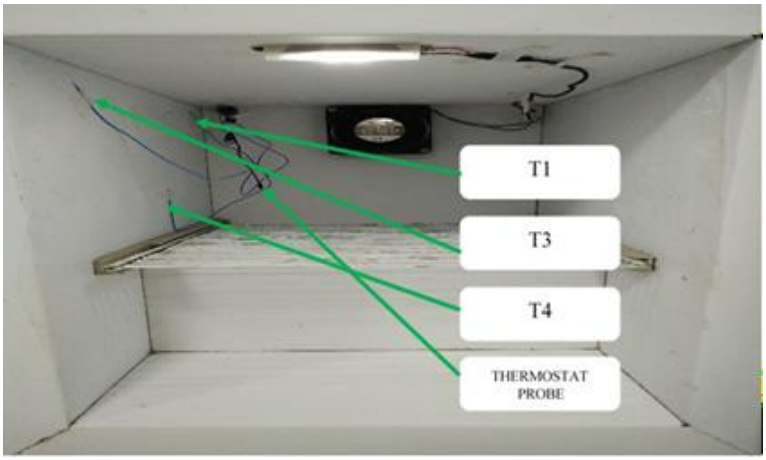


Figure 1.103 : Themometer probes placed at various points inside the refrigerator chamber [192]

Akbar Hossain et al [192] gived the evidence to the concept of using solar energy to preserve emergency lifesaving medicines and vaccines at low temperature. The target storage temperature range was between -15°C and 30°C. The model refrigerator (Figure 1.101) was designed and constructed totally by using local technology and placed in outdoor conditions to observe the effect of different weather conditions. By monitoring the temperature variation and compressor current after every one-hour, power consumption and the coefficient of performance (COP) were determined. The overall coefficient of performance (COP) was calculated 4.89 for the refrigerant "Iso-Butane (R600a)". The temperature and pressure profile have been observed using a highly accurate digital thermocouple thermometer and accurate pressure gauge to find out the heat transfer rate, suction and discharge pressure. Total power consumption per day was also calculated by observing the temperature and pressure profile.

It proved that the SAR (solar assisted refrigerator) can be implemented in rural areas and the areas where grid-connected electricity is not available to preserve emergency lifesaving medicines and vaccines at low temperature. This could be a means to save millions of people's lives in the disastrous regions and at the refugee camps.



Figure 1.104 : Different components of the banana cold storage facility in Mardan city based on conventional VCRS [193]

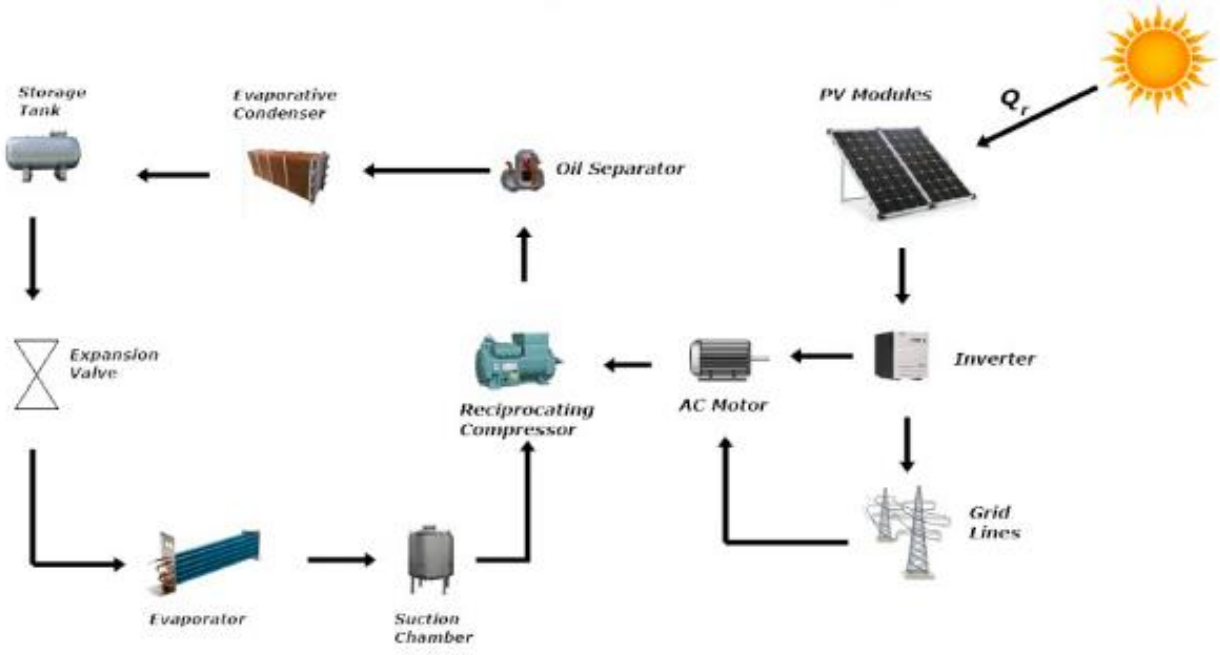


Figure 1.105 : Solar electric vapor compression refrigeration system [193]

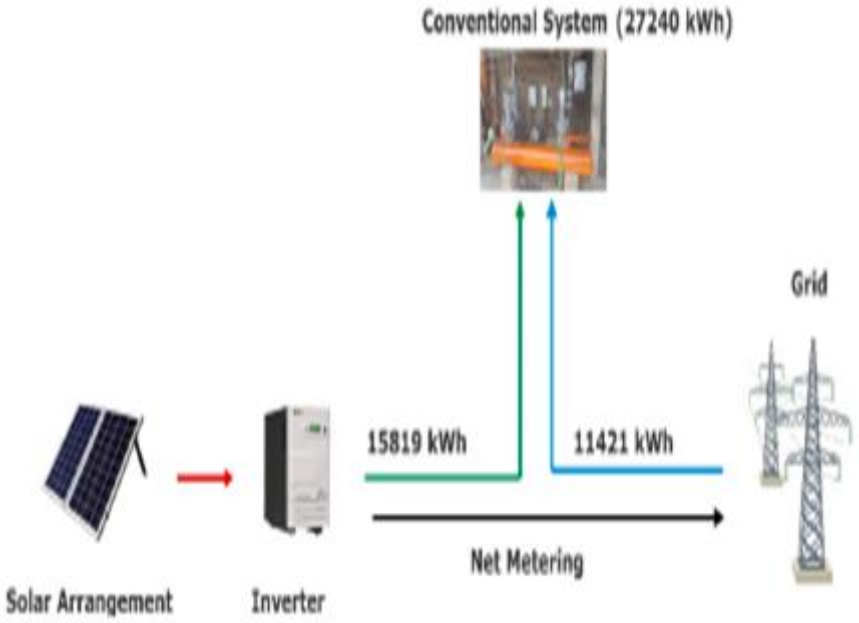


Figure 1.106 : Operational modes of the PV integrated refrigeration system for cold storage facility [193]

Hamid Ikram et al [193] presented a conceptual study of a solar PV integrated refrigeration system for a cold storage facility based on the conventional vapor compression system using refrigerant anhydrous ammonia (R-717) for banana fruit (Figure 1.104) . In the first stage, the conventional system has been thoroughly analyzed. Mathematical modelling has shown that the condenser is oversized, while the evaporator was undersized. Furthermore, the air- conditioning compressor was also found to be oversized by approximately 12 kW after an evaluation at no-load and full-load conditions. In the second stage, the optimized system with reduced consumption was integrated to a solar PV field (Figure 1.105) . The solar field sizing, and performance optimization of the proposed PV hybrid refrigeration system was accomplished in PV*SOL tool. The simulations demonstrated that with a 170 m^2 solar field, an optimized PV hybrid refrigeration system can achieve 58.1% solar fraction at a performance ratio of 59.2%, under given climatic conditions. With net metering, the hybrid system shows a high economic feasibility with the payback period of 5.2 years. The comprehensive methodology and all-inclusive results are valuable to generate explicit recommendations for repowering along with renewable integration of cold storage facilities operating in the region of Pakistan.

1.4 Conclusion

From what we saw in this chapter and to our knowledge despite the various studies found in the literature, there seems to be a lack of comprehensive thermodynamic and exergetic analysis for solar-driven vapor compression refrigeration system using R1234ze fluid as an alternative of R134a refrigerant for cooling applications. The mentioned gaps in the existing literature have been addressed by the presented study. In addition, the use of solar energy to power refrigeration systems is an emerging area of research and innovation, especially in regions with abundant sunlight.

The aim of this work is to evaluate the thermodynamic and exergetic performance of a solar- driven VCR system in the Ghardaïa region (southern Algeria) located in in the Sahara desert with hot and arid climate zone, which makes it an ideal location for the use of solar energy for cooling applications.

The traditional method of cooling in this region is through the use of evaporative coolers, which are not very efficient and consume a significant amount of water. The use of a solar- driven VCR systems can provide a more energy efficient and environmentally friendly cooling solution for this region. Two working fluids are studied and compared, the HFC high GWP going to be phased out, R134a and the low GWP, HFO refrigerant recently introduced R1234ze.

PART II

TECHNICAL STUDY

CHAPTER 2

METHODOLOGY

CHAPTER 2
Methodology

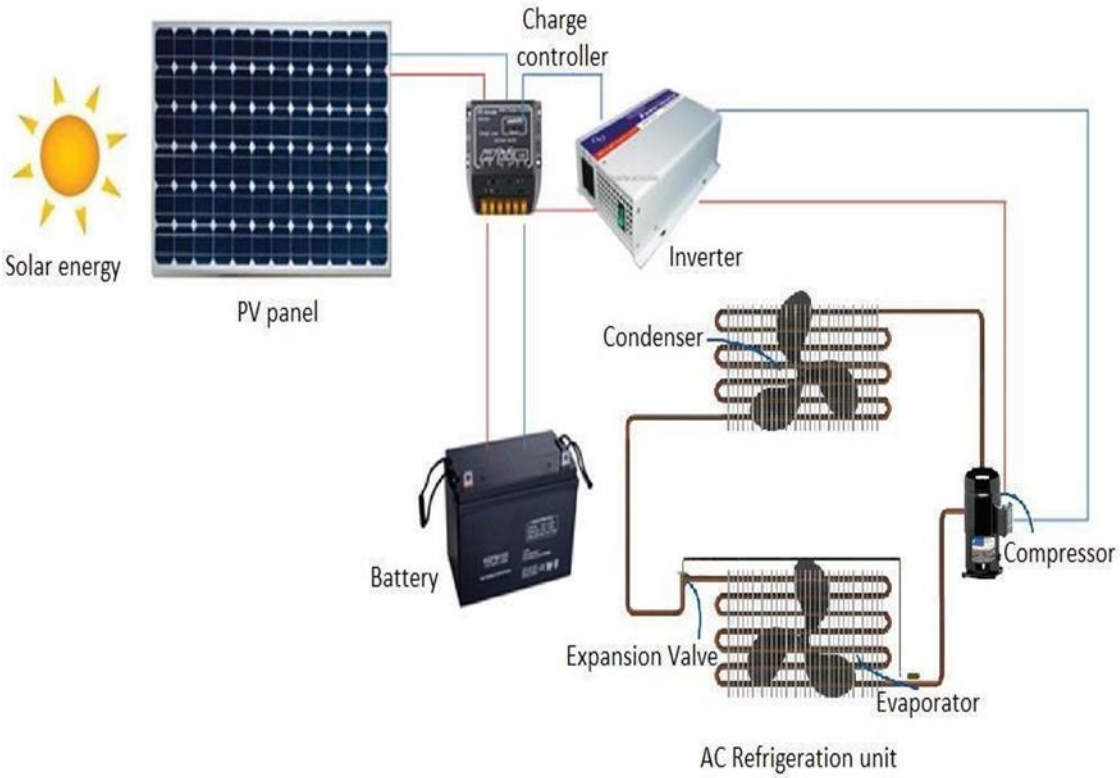
2.1 Introduction

This chapter presents a thermodynamic analysis of a photovoltaic solar-driven vapor compression refrigeration (VCR) system designed for use in the region of Ghardaïa (Southern Algeria) which is located in a desert with a semi-arid climate where the demand for cooling is high, and the solar radiation is abundant. Two working fluids are tested and compared, the HFC high GWP going to phased out, R134a and the low GWP, HFO refrigerant recently introduced R1234ze. The performance of the solar VCR system was evaluated using a numerical model developed in MATLAB software, based on thermodynamic properties of R1234ze and R134a refrigerants.

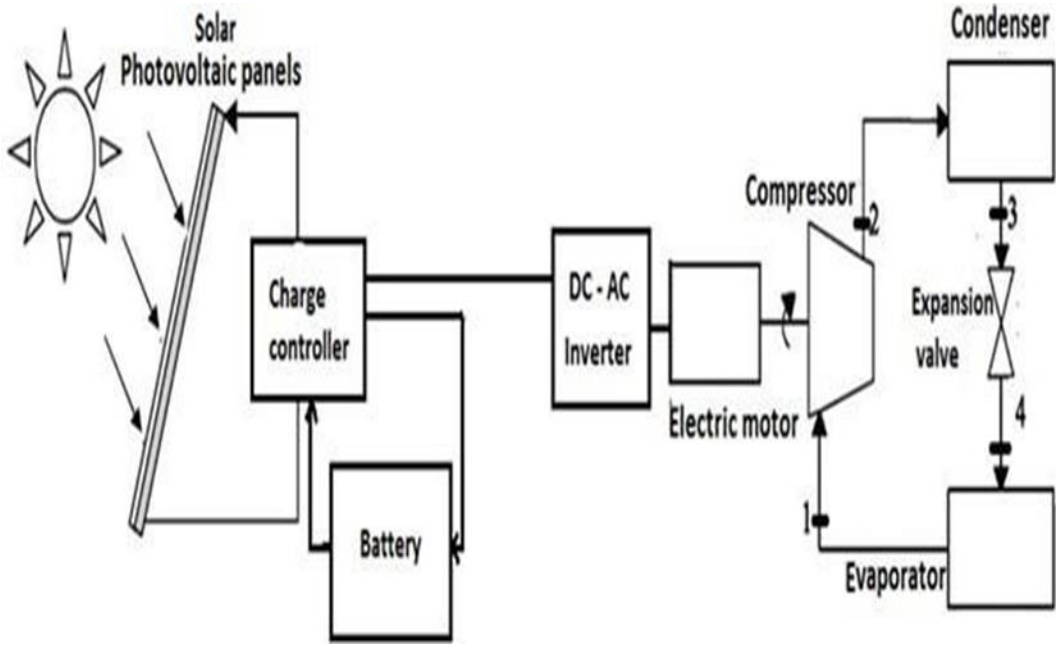
2.2 System description

The diagram in Figure 2.1 illustrates the key components of the solar VCR system under investigation. The system consists mainly of an AC refrigeration unit, a charge controller that prevents the battery from being over charged or deep-discharged, a DC-AC inverter which converts direct current from the solar PV panel or the battery into alternating current that can be fed to a conventional AC compressor, a battery to store and supply energy when the sun is not available and a PV generator which supplies power to the refrigeration unit and charges the battery with excess energy The compressor plays a crucial role in compressing the refrigerant gas (1) to form a high-pressure and high temperature gas. This high-pressure gas

(2) is then directed to the condenser, where it dissipates heat and undergoes condensation, transforming into a high-pressure and high-temperature-liquid. Subsequently, the high- pressure and high-temperature liquid (3) proceeds through a throttling mechanism, such as an expansion valve, experiencing a reduction in pressure and transforming into a low-pressure and low-temperature liquid. This low-pressure and low-temperature liquid (4) is then introduced into the evaporator, where it absorbs heat from its surroundings and transitions into a low-pressure and low-temperature gas. The resulting low-pressure and low-temperature gas is subsequently routed back to the compressor, initiating the cycle anew. A pressure- enthalpy diagram depicting the vapor compression cycle is provided in Figure 2.2.



(a)



(b)

Figure 2.1 : Schematic diagram of the solar PV assisted cooling system [194]

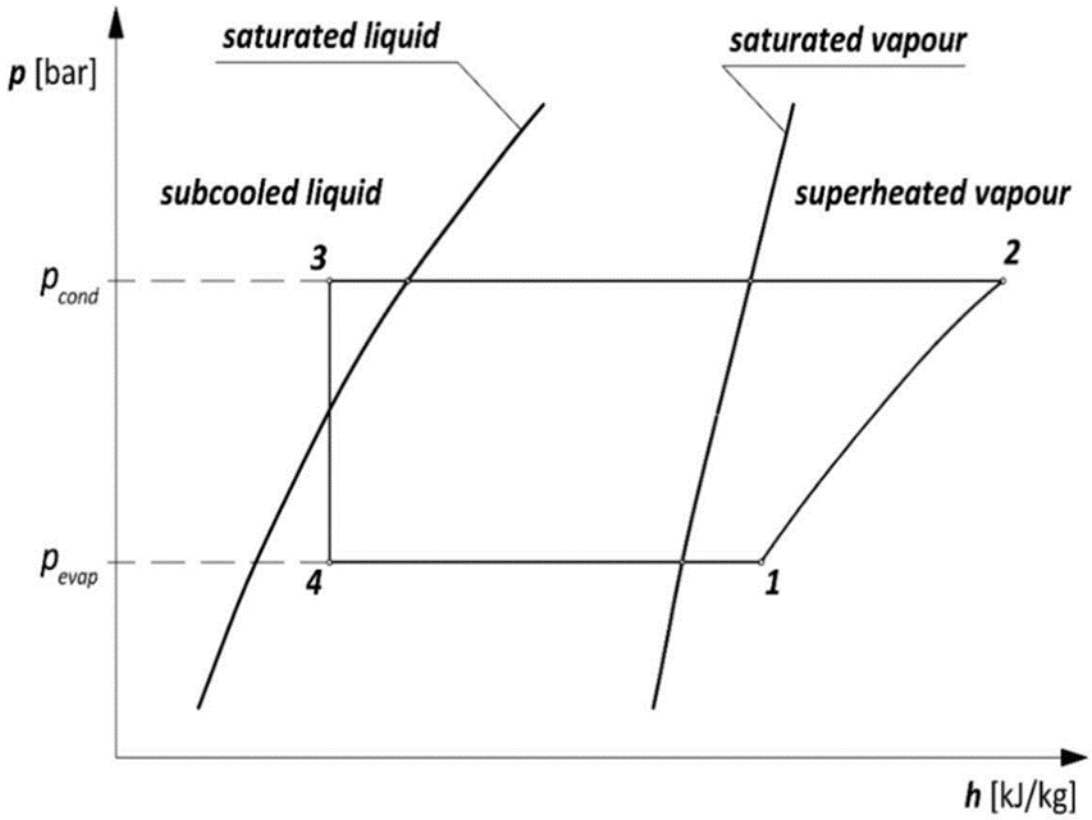


Figure 2.2 : Pressure-enthalpy diagram of a vapor compression refrigeration cycle [194]

2.3 Choice and description of the site studied

The system studied is located in the Ghardaia area. We chose this area because solar radiation is abundant, and we have a climatic database for this area.

The Ghardaia city is located in a south part of Algeria (latitude 32.26 N°, and longitude 03.46 E°).The climate of Ghardaia is called a desert. Throughout the year, there is virtually no rainfall. The average temperature is 21.0°C.

January is the coldest month of the year, the average temperature is 10.1°C. The warmest month of the year is July, with an average temperature of 33.4°C.

All climate data used in this research are provided by the Renewable Energy Applied Research Unit UREAR, Ghardaia [195].

2.3.1 Climate data of Ghardaia

Figure 2.3 shows the monthly ambient temperature and the monthly inclined global radiation in the year 2018.

As we can observe, the irradiance and temperatures vary depending on the season. We then notice that the radiation and temperature are high in the summer month.

The annual average ambient temperature is around 25°C and the monthly inclined radiation has reached 225 kWh/m^2/month. [195].

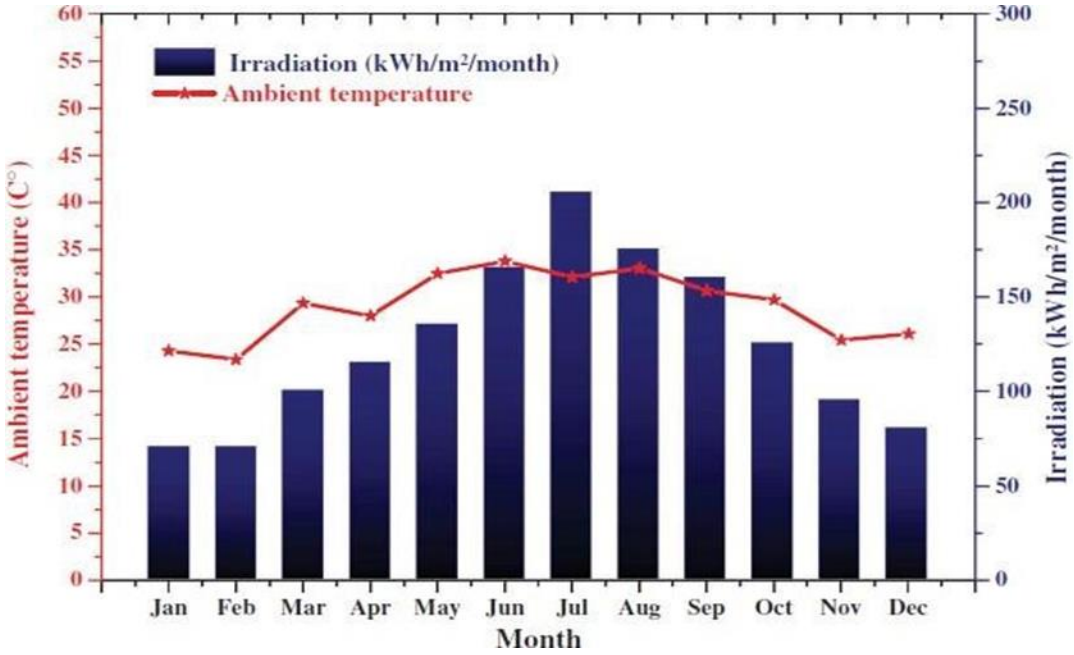


Figure 2.3: Monthly solar irradiation and monthly average daily ambient temperature for the year 2018 [195]

2.4 Description of the refrigerants (R134a and R1234ze) and their properties

2.4.1 Refrigerants development and environmental assessment

Refrigerants are used to absorb and transfer heat between space and the surrounding environment, mainly through vapor compression-based equipment. Most of these refrigerants are volatile and contain gases that affect the environment through their heat-trapping capacity or their global warming potential (GWP). Moreover, many of these refrigerants impact the ozone layer (ODP) [196].

The refrigerants used in most current systems, such as R134a and R410, have either no or a very low ODP. However, they still have a high GWP, which could last for 100 years for some refrigerants. Hence, they are expected to be phased out of the market in the next decade. The HVAC industry has undergone three main stages based on the refrigerant selection criteria.

The initial stage started with the invention of VCC systems and lasted until the late 1920s, when mainly natural materials such as ammonia, carbon dioxide, hydrocarbons, sulphur dioxide, chloroethene, air, ether, and methyl chloride were used as refrigerants.

Then, with the invention of freon in 1930, the market shifted toward the vast adoption of halogenated compounds known as chlorofluorocarbons (CFCs). These provided solutions for toxicity, flammability, and odour compared to the previous refrigerants, and they were marketed at that time as a safer and more efficient option before the subsequent discovery that CFCs represent a severe threat to human life through their direct relation to the depletion of the ozone layer. The environmental impact of CFCs was discovered 50 years after introducing them, leading to an international decision to phase out CFCs in the Montreal Protocol of 1987 [197]. In 2017, the Montreal Protocol issued the EDGE Document; this document set out a compulsory phase-out timeline for CFCs. According to this agreement, the timeline must be reviewed regularly to expedite the phase-out process. This collaborative work introduced hydrofluorocarbons (HFCs) as a replacement for CFCs [198].

In order to reduce the environmental impact of refrigerants, some restrictions on the use of HCFCs, also known as freons, were suggested due to their GWP. Furthermore, the Paris Agreement of 2015 set a framework through which to limit global warming and keep it below 2°C. The Kigali amendment of the Montreal Protocol was agreed upon in 2016; this agreed to phase out HFCs with a high GWP and called for an 85% reduction in GWP-weighted products in developed countries by 2036, with later phase-down dates for other countries.

FICs (Fluoroiodocarbons) were introduced in the nineties as a replacement option for CFCs; these refrigerants are not available in nature but are produced in special manufacturing facilities via a chemical reaction. One example of an FIC is CF3I. Generally, FICs decay photolytically in the visible light spectrum, resulting in a limited atmospheric lifetime, which is estimated to be 1.15 days. The ODP of these refrigerants is very low and is estimated to be around 0.009 based on a 5% leakage allowance [198].

The most promising replacement for the current refrigerants are the hydroflouroolefins (HFOs). These refrigerants have global warming potential but have a very short atmospheric lifetime compared to HFCs. Some of these refrigerants are toxic, and others are flammable, but HFO-1234yf is difficult to ignite and has an unstable flame.

Thus, it is widely used in automotive air-conditioning systems and is expected to replace the R-134a refrigerant soon for this particular application [199]. HFO-1234ze(E) and HFO- 1336mzz(Z) are non-flammable, have a low toxicity, and are more suitable for chiller applications. Development is also ongoing for some other HFOs, such as HFO-1132a, which has a relatively low boiling temperature of -83 °C, and HFO-1123, which one manufacturer has proposed as a replacement for R-410a. However, the use of this refrigerant is not always appropriate at a high pressure and temperature, and the company claims that risks could be mitigated by blending it with R-32 [200]. Hydrochlorofluoroolefins (HCFOs) are a new refrigerants group that contains fluorine and chlorine; this group has a relatively low GWP and a negligible ODP. HCFOs have been promoted as chiller-suitable refrigerants with a very short atmospheric lifetime.

A good example is HCFO-1233zd(E), which has an ODP < 0.0004. Another refrigerant from the same group still under investigation is HCFO-1224yz(Z) [201]. The Table III.3 shows the refrigerant types and their current technological status.

Some researchers have tried to investigate HFO/HFC blends. Yu et al. [202] theoretically investigated the air-conditioning and heat pump cycle performance of some HFC/HFO mixtures. The tested blends had medium flammability (A2L) with a GWP value below 150.

The blends used that were based on mass fraction were R-1123/R-161/R-13I1 (65/5/30), R-1123/R-152a/R-13I1 (65/5/30) and R-1123/R-1234ze(E)/R-13I1 (65/5/30). All of these blends achieved a GWP that was lower than 10. However, none of them achieved a high COP compared to the R-410a baseline.

For any substance to be used as a refrigerant, it must satisfy a set of thermodynamic, thermophysical, chemical, and environmental requirements. Thermodynamic and thermophysical properties, such as the thermal capacity, normal boiling temperature, density, thermal conductivity, and viscosity, dictate the efficiency of the refrigeration cycle. The main thermodynamic property that influences the selection of any refrigerant is its normal boiling temperature, as this is directly related to the system's operating pressure and the critical temperature of the refrigerant, which dictates the system's operating temperature.

These properties influence the system COP and volumetric efficiency, since refrigerants with high critical temperatures commonly have a higher COP but a lower volumetric efficiency [203]. In addition, the refrigerant's thermal capacity and latent heat of vaporisation affect the system efficiency.

The efficiency of the system's heat exchangers is highly related to the refrigerant's thermophysical properties, as they affect the system's energy intensity and account for the system's irreversibility losses [204].

Another aspect that has to be considered in refrigerant selection is the refrigerant's chemical properties, which directly relate to the system's operating safety.

These properties include its interaction with the system components and lubrication oil. Furthermore, other critical refrigerant properties include their flammability, explosivity, and breakdown temperature-decomposition temperature. A refrigerant with a higher decomposition temperature than the maximum system operation temperature should be selected [205].

The refrigerant's interaction with the environment and its physiological properties are essential aspects driving the industry nowadays, as refrigerants are one of the leading causes of ozone depletion; thus, they need to be selected with a comprehensive environmental assessment [206].

Previous studies have revealed that some systems, such as mobile air conditioners and large refrigeration systems, could leak up to 30% of their refrigerant capacity yearly.

Thus, they need to be as least environmentally harmful as possible.

In addition to global warming potential, the TEWI (Total Equivalent Warming Impact) is another index that combines both the GWP of the refrigerant and the estimated amount of CO2 released from the power plant in order to supply these systems with power throughout their lifetime [207].

The LCCP, or life-cycle climate performance, is similar to the TEWI with more accuracy, and is more complicated.

However, it indicates the refrigerant's direct and indirect impacts on global warming over the lifetime of the refrigeration system, including expected refrigerant leaks [208].

Refrigerant flammability is an important aspect that influences the refrigerant suitability of any system and identifies the practical refrigerant limits of operation.

The classifications used in the industry for refrigerant flammability are the lower flammability limit (LFL), the burning velocity and the heat of combustion (HOC).

The last environmental consideration is refrigerant toxicity, which is standardised in the industry as a 400 ppm occupational exposure limit; this is a defining point between low and hightoxicity refrigerants.

McLinden et al. [209] carried out a study to find new refrigerants via a systematic approach. The study mainly focuses on assessing the candidate refrigerants' thermodynamic properties and environmental impact.

The study concluded that low GWP options were limited, and most were slightly flammable. Hence, compromises must be considered when selecting the next generation of refrigerants.

Table 2.1: Refrigerant types and status [210]

Refrigerant Group	Description	Examples	Current Status	Availability	Environmental Impact
CFCs	Chlorofluorocarbons are very harmful to the environment due to their ODP, GWP, and long atmospheric life	R11, R12	Phased out in Jan 1996, in accordance with the Montreal protocol.	CFCs are usually produced by halogen exchange initiated by chlorinated ethane and methane.	ODP: High, GWP: Medium, Lifetime: 20-100 Years
HCFCs	Hydrochlorofluorocarbons have a relatively low ODP, GWP, and atmospheric life	R22, R123	Phased out in 2020, in accordance with the Montreal protocol.	Derived from propane, ethane, and methane as a volatile component.	ODP: Medium, GWP: Medium, Lifetime: <20 years
HFCs	Hydrofluorocarbons have zero ODP but a relatively high GWP	R-134a, R-245fa, R-125, R-32	Targeted for a phase-down in 2030.	Derived from propane, ethane, and methane as a volatile component.	ODP: Very Low, GWP: Low, Lifetime: <300 years
FICs	Fluoroiodocarbons have a ODP close to zero and a low GWP	Ikon-22A, Ikon-12C	New refrigerants.	Produced in the lab or special manufacturing facilities via chemical reactions.	ODP: Very low, GWP: Low Lifetime: Very short (estimated in days)
HFOs	Hydrofluoroolefins are stable, with a short atmospheric life, zero ODP and a very low GWP. However, they have relatively low efficiency	R1234yf, R1234ze, R-1233zd	The industry needs to evaluate the environmental benefits against the efficiency of these refrigerants.	Consist of hydrogen, carbon and fluorine atoms, but should have a minimum of one double bond between the carbon atoms.	ODP: Zero, GWP: Very Low Lifetime: <20 years
Natural refrigerants	Naturally available with a negligible effect on the environment	R717, R718, R290, R600, R744	Used currently for various applications. However, they have not been widely adopted due to unfavourable properties.	Available in nature.	ODP: Zero, GWP: Negligible Lifetime: <20 years

2.4.2 Properties of the refrigerants studied (R1234ze and R134a)

Although R1234ze(E) has been developed recently, many studies have been conducted to characterize the properties and therefore, the thermal and energetic behaviors of this fluid. Accurate thermophysical properties are necessary to design and build efficient refrigeration and air conditioning components (and systems). These studies can report individual properties measured in specific test rigs or they can analyze the accuracy of different equations of state (EOS) (or even modify them to improve their precision). Qiu et al. [211] presented a density measurement system at pressures of up to 100 MPa and temperature from 283 to 363 K, using a vibrating tube densimeter. The maximum expanded uncertainty for R1234ze(E) is 0.23%. Meng et al. [212] reported viscosity measurements at temperatures between 243 and 373 Kand saturated pressures up to 30 MPa, using a vibrating-wire viscometer. The AAD (average absolute deviation) of the experimental results for R1234ze(E) is 0.59%. Di Nicola et al. [213] measured R1234ze(E) triple point value and obtained results very close that present in open literature. An EOS is a thermodynamic equation that relates state variables (temperature, pressure, volume, internal energy or specific heat) and allows calculating fluid properties. Brown et al. [214] first estimated the thermodynamic properties with the Peng– Robinson EOS for R1234ze(E) and other fluorinated olefins. Akasaka applied a new thermodynamic property model for R1234ze(E). Typical uncertainties of vapor pressure, liquid density and isobaric heat capacities (liquid and vapor) are 0.2%, 0.5% and 5%, respectively [215].

Then, he presented a new EOS valid for temperatures from 240 K to 420 K and for pressures up to 15 MPa in the case of R1234ze(E) [216] (and not recommendable for critical region). Average uncertainties are 0.1% in liquid density, 0.2% in vapor density, 3% in liquid heat capacities, 0.05% in the vapor-phase speed of sound, and 0.1% in vapor pressure. Developments in R1234ze(E) properties and properties calculations are included in fluid databases as REFPROP [217] that allow accurate property calculations.

Alavianmehr et al. [218] modified Tao–Mason EOS and the AAD (average absolute deviation) of 34 R1234ze(E) points was 0.36 (it was the lowest deviation obtained). Lai et al.

[219] used the molecular based BACKONE and PCSAFT EOS to describe the thermodynamic properties of R1234ze(E). Relative differences are mostly within 1%. R1234ze(E) is a medium pressure refrigerant proposed as an R134a alternative in new design systems.

It is not recommended to drop-in or retrofit in R134a due to the difference in their thermophysical properties, as can be seen in Fig 2.4

The vapor pressure of R1234ze(E) is between −28% and −24% compared with R134a (Fig 2.4 a), so the compressors can work with R1234ze(E) at lower pressures.

The liquid density of R1234ze(E) is between −4.7% and −1% compared with R134a (Fig 2.4 b), and the refrigerant charge needed for the alternative is also lower. In the case of vapor density, this is approximately 20% lower for R1234ze(E)).

Finally, the R1234ze(E) liquid viscosity is slightly lower at low temperatures, but 7.37% at 343 K. This will imply lower pressure losses in pipes and components for the HFO. A summary of different properties is also shown in Table 2.2.

Additionally to that discussed before, it highlights the great GWP reduction, 1300 versus 4 and low flammability of R1234ze(E).

R1234yf was intended to replace R134a in MAC (Mobile Air Conditioning) systems. However, it has met with opposition because is flammable. In the same way, flammability could difficult the use of R1234ze(E), as happened for R1234yf. R1234ze(E) is classified as low-flammable refrigerant (A2L) by ASHRAE 34 [220] even though it is slightly less flammable than R1234yf. R1234ze(E) LFT becomes quite lowwhen the humidity condition increases [221] and it is non-flammable if the air humidity is equal to or less than 10% corrected for 296.15 K [222].

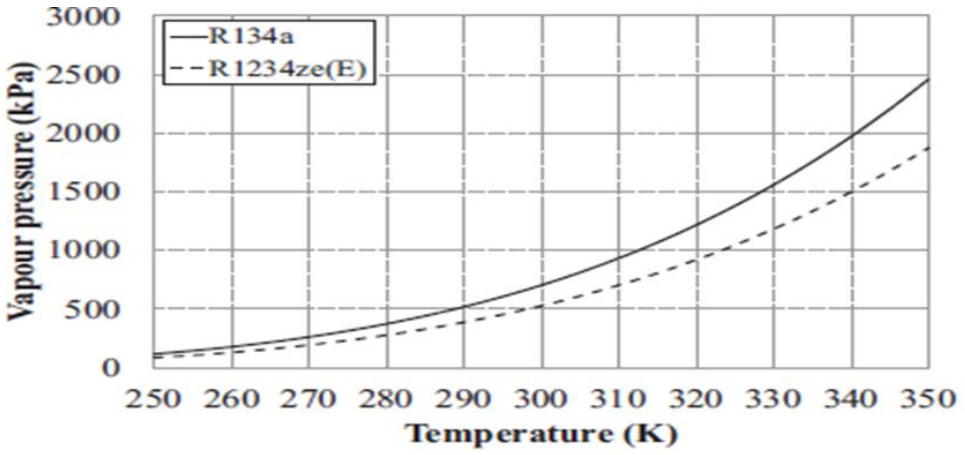
For heat pump systems, it is demonstrated that refrigerants will not pose an ignition risk during normal operation [223].

In the case of release in the outdoor unit, risks involving R1234ze(E) are equal to that calculated for R1234yf and four times lower than R32 (and well below the overall risk of house fires from any cause).

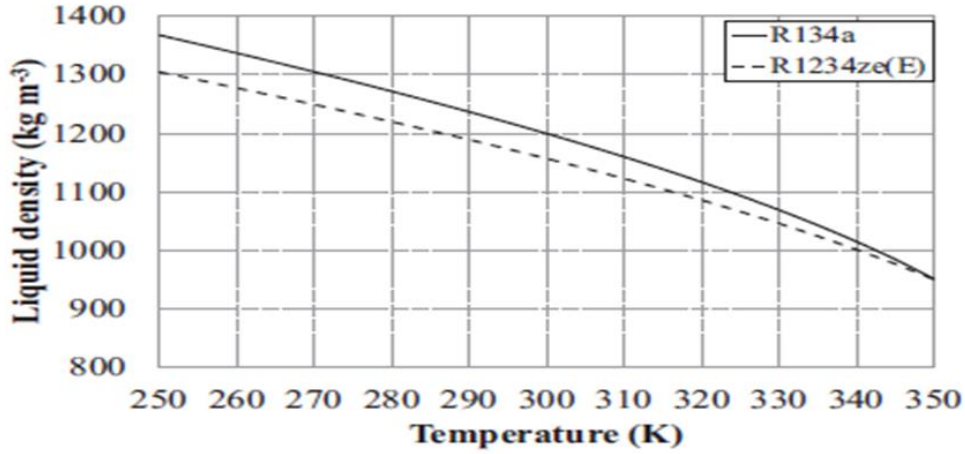
Besides, R1234ze(E) is compatible with that materials and oil lubricants used with HFC. Majurin et al. [224] studied the material compatibility of R1234ze(E) and blend of R1234yf, R1234ze(E), and R32, with nine different elastomers, three gaskets, five polymers, and tenmotor materials and considering lubricant effect.

Higher risk was found with a few materials, which will require more investigation.

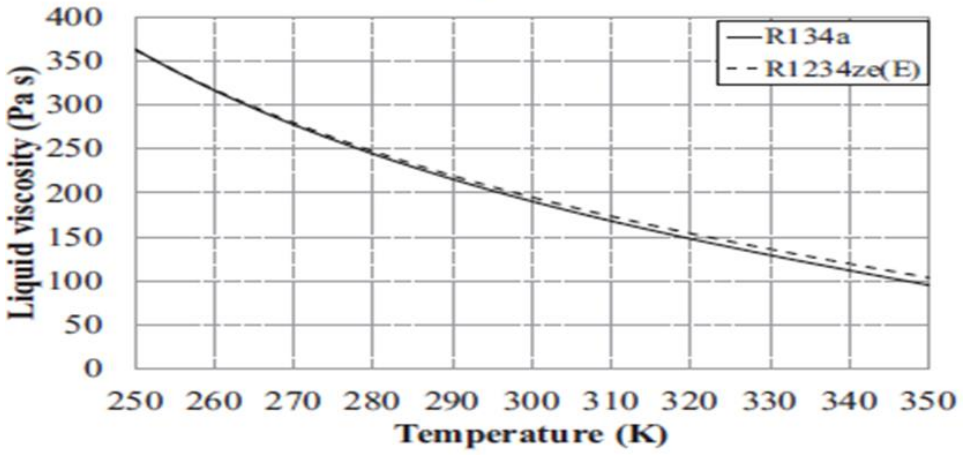
Sun et al. [225] proved that R1234ze(E) is highly soluble in two lubricants precursors of POE (PEC7 and PEC9) at temperatures from 283.15 to 353.15 K.



a)



b)



c)

Figure 2.4 : Comparison between R1234ze(E) and R134a at different temperatures [217]: a) vapor pressure, b) liquid density and c) liquid viscosity

Table 2.2: Main refrigerant properties of R1234ze(E) and R134a [217]

Main refrigerant properties of R1234ze(E) and R134a

	R134a	R1234ze(E)	Sign/influence on vapor compression system
ASHRAE safety classification	A1	A2L	
ODP	0	0	
100-year GWP	1300	4	
Critical temperature (K)	374.21	382.51	2% higher/lower volumetric capacity and higher COP
Critical pressure (kPa)	4059.28	3634.90	10% lower
NBP (K)	247.08	253.88	3% higher/lower evaporation range
Liquid density[a] ($kg\ m^{-3}$)	1295.27	1240.56	4% lower/lower pressure drop
Vapor density[a] ($kg\ m^{-3}$)	14.35	11.65	19% lower/lower mass flow rate per unit volume of compression
Liquid c_p[a] ($kJ\ kg^{-1}\ K^{-1}$)	1.34	1.32	2% lower/higher liquid subcooling at the exit of condenser
Vapor c_p[a] ($kJ\ kg^{-1}\ K^{-1}$)	0.90	0.88	Similar[b]
Latent heat of vaporization ($kJ\ kg^{-1}$)	198.72	184.28	7% lower/lower refrigerating effect
Liquid therm. cond.[a] ($W\ m^{-1}\ K^{-1}$)	$92.08 \cdot 10^{-3}$	$83.11 \cdot 10^{-3}$	10% lower/lower heat transfer
Vapor therm. cond.[a] ($W\ m^{-1}\ K^{-1}$)	$11.50 \cdot 10^{-3}$	$11.57 \cdot 10^{-3}$	Similar[b]
Liquid viscosity[a] ($Pa\ s^{-1}$)	$267.04 \cdot 10^{-6}$	$269.44 \cdot 10^{-6}$	Similar[b]
Vapor viscosity[a] ($Pa\ s^{-1}$)	$10.72 \cdot 10^{-6}$	$11.19 \cdot 10^{-6}$	4% higher/higher pressure drop

[a] At 273 K.
[b] Relative difference less than 1.5%.

Table 2.3: Basic properties of the R1234ze(E) refrigerant [217,226]

Property	Value
Group	HFO
Chemical formula	trans-$CF_3CH = CHF$
Molar mass, kg/kmol	114
Critical temperature, °C	109.36
Critical pressure, bar	36.4
Critical density, kg/m^3	489.2
Normal boiling point, °C	−19.3
Triple point, °C	−104.53
ODP (ozone depletion potential)	0
GWP_{20} (global warming potential) 20 years	4
GWP_{100} (global warming potential) 100 years	1
Atmospheric lifetime of individual components, days	16.4

2.4.3 Properties and state equations for the refrigerant R1234ze [227]

Saturated liquid region

$$T = \sum_{n=1}^{6} a_n . lnp^n + a_0 \quad (1)$$

$$h' = \sum_{n=1}^{8} a_n . lnp^n + a_0 \quad (2)$$

$$s' = \sum_{n=1}^{8} a_n . lnp^n + a_0 \quad (3)$$

$$C_p' = \sum_{n=0}^{8} a_n . P^n \quad (4)$$

$$\rho' = \sum_{n=1}^{8} a_n . lnp^n + a_0 \quad (5)$$

$$V' = \sum_{n=0}^{8} a_n . P^n \quad (6)$$

$$\lambda' = \sum_{n=1}^{8} a_n . lnp^n + a_0 \quad (7)$$

$$\mu' = \sum_{n=1}^{8} a_n . lnp^n + a_0 \quad (8)$$

$$P_r' = \sum_{n=1}^{9} a_n . lnp^n + a_0 \quad (9)$$

$$\sigma = \sum_{n=1}^{8} a_n . lnp^n + a_0 \quad (10)$$

Table 2.4: Coefficients of polynomials describing the temperature, specific enthalpy, specific entropy, and specific heat of the R1234ze(E) refrigerant in the saturated liquid state

Coef	Equation			
	T = f(p) (1)	h′ = f(p) (2)	s′ = f(p) (3)	c_p' = f(p) (4)
a_0	$2.53879921713140 \times 10^{2}$	$1.74968285360988 \times 10^{2}$	$9.05279244602078 \times 10^{-1}$	1.24083270657197
a_1	$2.28770347319237 \times 10^{1}$	$2.93484680604720 \times 10^{1}$	$1.15356542959209 \times 10^{-1}$	$4.51902938229883 \times 10^{-2}$
a_2	2.45670755735841	3.00047504671966	$7.24618471191152 \times 10^{-3}$	$-5.63723496516354 \times 10^{-3}$
a_3	$3.14117394078267 \times 10^{-1}$	1.19253718641735	$2.73012551482764 \times 10^{-3}$	$6.42959196900272 \times 10^{-4}$
a_4	$-6.76941445013617 \times 10^{-2}$	$6.99952705225739 \times 10^{-1}$	$1.71764538194706 \times 10^{-3}$	$-3.54112766926212 \times 10^{-5}$
a_5	$4.07277016474858 \times 10^{-2}$	−1.51604024263818	$-3.86378154015459 \times 10^{-3}$	$5.37559165828602 \times 10^{-7}$
a_6	$-5.95404205600932 \times 10^{-3}$	$9.67067796211943 \times 10^{-1}$	$2.45968598111626 \times 10^{-3}$	$3.84386880084408 \times 10^{-8}$
a_7	-	$-2.62092375289440 \times 10^{-1}$	$-6.67334247116959 \times 10^{-4}$	$-1.88423766967265 \times 10^{-9}$
a_8	-	$2.66563442687942 \times 10^{-2}$	$6.78181882644024 \times 10^{-5}$	$2.54741811878324 \times 10^{-11}$

Table 2.5: Coefficients of polynomials describing the density, specific volume, and heat transfer coefficient of the R1234ze(E) refrigerant in the saturated liquid state

Coef	Equation		
	ϱ' = f(p) (5)	ν' = f(p) (6)	λ' = f(p) (7)
a_0	$1.29396343579499 \times 10^{3}$	$7.29710663744474 \times 10^{-4}$	$9.03143423982640 \times 10^{-2}$
a_1	$-6.20669713392757 \times 10^{1}$	$5.01608980784443 \times 10^{-5}$	$-8.80066599536261 \times 10^{-3}$
a_2	−2.53752547194416	$-9.30886654653688 \times 10^{-6}$	$-9.99542811098308 \times 10^{-4}$
a_3	−9.31562506661149	$1.37045258345160 \times 10^{-6}$	$2.92095921761060 \times 10^{-4}$
a_4	−7.20333951838005	$-1.23148305617849 \times 10^{-7}$	$3.50549588319595 \times 10^{-4}$
a_5	$1.64294878085487 \times 10^{1}$	$6.76679411090488 \times 10^{-9}$	$-7.30082138730070 \times 10^{-4}$
a_6	$-1.04093686983023 \times 10^{1}$	$-2.20602504790423 \times 10^{-10}$	$4.40360054711903 \times 10^{-4}$
a_7	2.81591566729637	$3.91341788788786 \times 10^{-12}$	$-1.14689158182047 \times 10^{-4}$
a_8	$-2.86461830242391 \times 10^{-1}$	$-2.90062006624196 \times 10^{-14}$	$1.10956525980123 \times 10^{-5}$

Table 2.6: Coefficients of polynomials describing the dynamic viscosity coefficient, Prandtl number, and surface tension of the R1234ze(E) refrigerant in the saturated liquid state

Coef	Equation		
	μ' = f(p) (8)	Pr′ = f(p) (9)	σ = f(p) (10)
a_0	$3.30126989957222 \times 10^{-4}$	4.67836170077957	$1.59343062468816 \times 10^{-2}$
a_1	$-1.03228385472871 \times 10^{-4}$	$-8.07941153808255 \times 10^{-1}$	$-4.27582523407763 \times 10^{-3}$
a_2	$1.09405636740428 \times 10^{-5}$	$1.78574619681131 \times 10^{-1}$	$1.08824350295615 \times 10^{-5}$
a_3	$-1.54688847220722 \times 10^{-6}$	$-4.54256602128744 \times 10^{-1}$	$-2.88012392508621 \times 10^{-5}$
a_4	$-2.44961988256085 \times 10^{-7}$	$1.75299143854024 \times 10^{-1}$	$1.02007105181399 \times 10^{-5}$
a_5	$9.19517023370312 \times 10^{-7}$	$5.54715409594885 \times 10^{-1}$	$-3.46263550356762 \times 10^{-5}$
a_6	$-6.03952237218337 \times 10^{-7}$	$-6.97630428910946 \times 10^{-1}$	$2.31347786949313 \times 10^{-5}$
a_7	$1.66816987767627 \times 10^{-7}$	$3.38689978995674 \times 10^{-1}$	$-6.30855999198157 \times 10^{-6}$
a_8	$-1.71375788331681 \times 10^{-8}$	$-7.62417081213265 \times 10^{-2}$	$6.68652044821767 \times 10^{-7}$
a_9	-	$6.62560394142489 \times 10^{-3}$	-

Saturated vapour region

$$h'' = \sum_{n=1}^{8} a_n \,.\, lnp^n + a_0 \quad (11)$$

$$s'' = \sum_{n=1}^{8} a_n \,.\, lnp^n + a_0 \quad (12)$$

$$C_p'' = \sum_{n=0}^{8} a_n \,.\, P^n \quad (13)$$

$$\rho'' = \sum_{n=0}^{9} a_n \,.\, P^n \quad (14)$$

$$V'' = \sum_{n=1}^{8} a_n \,.\, lnp^n + a_0 \quad (15)$$

$$\lambda'' = \sum_{n=1}^{9} a_n \,.\, lnp^n + a_0 \quad (16)$$

$$\mu'' = \sum_{n=1}^{8} a_n \,.\, lnp^n + a_0 \quad (17)$$

$$Pr'' = \sum_{n=0}^{8} a_n \,.\, P^n \quad (18)$$

Table 2.7: Coefficients of polynomials describing the specific enthalpy, specific entropy, specific heat, and density of the R1234ze(E) refrigerant in the saturated vapour state

Coef	Equation			
	$h'' = f(p)$ (11)	$s'' = f(p)$ (12)	$c_p'' = f(p)$ (13)	$\varrho'' = f(p)$ (14)
a_0	$3.70657366815286 \times 10^{2}$	1.67622654205859	$7.63398360227738 \times 10^{-1}$	$2.27768588078390 \times 10^{-1}$
a_1	$1.62926056610703 \times 10^{1}$	$-5.81493952118715 \times 10^{-3}$	$7.32627000545461 \times 10^{-2}$	5.54068367754339
a_2	2.46905883267318	$6.61688503765656 \times 10^{-3}$	$-1.06783110270413 \times 10^{-2}$	$-1.70610755621257 \times 10^{-1}$
a_3	−1.13621954845305	$-2.94796323909036 \times 10^{-3}$	$1.22686997407115 \times 10^{-3}$	$3.58297189467255 \times 10^{-2}$
a_4	−1.08070437166134	$-2.75644193419488 \times 10^{-3}$	$-7.15472829720056 \times 10^{-5}$	$-3.97722125575951 \times 10^{-3}$
a_5	2.49195790709675	$6.33081705594435 \times 10^{-3}$	$1.61584178260620 \times 10^{-6}$	$2.97586911550852 \times 10^{-4}$
a_6	−1.57431720780436	$-3.99095180784525 \times 10^{-3}$	$3.78799626428319 \times 10^{-8}$	$-1.42888359942333 \times 10^{-5}$
a_7	$4.25121219497403 \times 10^{-1}$	$1.07579556459832 \times 10^{-3}$	$-2.62846106511664 \times 10^{-9}$	$4.26062135708768 \times 10^{-7}$
a_8	$-4.32428413533420 \times 10^{-2}$	$-1.09130621835064 \times 10^{-4}$	$3.84463040954545 \times 10^{-11}$	$-7.16416594446346 \times 10^{-9}$
a_9	-	-	-	$5.23362423501008 \times 10^{-11}$

Table 2.8: Coefficients of polynomials describing the specific volume, heat transfer coefficient, dynamic viscosity coefficient, and Prandtl number of the R1234ze(E) refrigerant in the saturated vapour state

Coef	Equation			
	$\nu'' = f(p)$ (15)	$\lambda'' = f(p)$ (16)	$\mu'' = f(p)$ (17)	$Pr'' = f(p)$ (18)
a_0	$1.77433953172014 \times 10^{-1}$	$1.00685420897056 \times 10^{-2}$	$1.05062529128478 \times 10^{-5}$	$8.74440749215016 \times 10^{-1}$
a_1	$-1.66936428639188 \times 10^{-1}$	$2.01521099378549 \times 10^{-3}$	$9.52821100098587 \times 10^{-7}$	$-2.39936282800067 \times 10^{-2}$
a_2	$7.75579038246079 \times 10^{-2}$	$4.91117080105326 \times 10^{-4}$	$-3.00951147568936 \times 10^{-7}$	$1.25205016486864 \times 10^{-2}$
a_3	$-2.41489018240415 \times 10^{-2}$	$-1.75824023764422 \times 10^{-3}$	$5.32152051905147 \times 10^{-7}$	$-2.27389415072141 \times 10^{-3}$
a_4	$5.61391538794325 \times 10^{-3}$	$7.60350748872995 \times 10^{-4}$	$4.70502421614829 \times 10^{-7}$	$2.36745600186706 \times 10^{-4}$
a_5	$-9.65998396886106 \times 10^{-4}$	$2.19935489007404 \times 10^{-3}$	$-1.09002347169414 \times 10^{-6}$	$-1.45822262459754 \times 10^{-5}$
a_6	$9.87363959178734 \times 10^{-5}$	$-2.83720578521593 \times 10^{-3}$	$6.84901655972941 \times 10^{-7}$	$5.30654276070867 \times 10^{-7}$
a_7	$-7.48240927743627 \times 10^{-7}$	$1.40136740639282 \times 10^{-3}$	$-1.84631268281049 \times 10^{-7}$	$-1.05453244596624 \times 10^{-8}$
a_8	$-7.07631682979349 \times 10^{-7}$	$-3.20515361896471 \times 10^{-4}$	$1.86385265681204 \times 10^{-8}$	$8.89411840080677 \times 10^{-11}$
a_9	-	$2.83753380724076 \times 10^{-5}$	-	-

Superheated vapour region

$$h = \sum_{n=1}^{5}(a_n.P + b_n.t + c_n)^n \quad (19)$$

$$h = \sum_{n=1}^{4}(a_n.lnp + b_n.lns + c_n)^n \quad (20)$$

$$s = \sum_{n=1}^{5}(a_n.lnp + b_n.t + c_n)^n \quad (21)$$

$$T = \sum_{n=1}^{3}(a_n.P + b_n.h + c_n)^n \quad (22)$$

$$\sigma = \sum_{n=1}^{6}(a_n.lnp + b_n.lnh + c_n)^n \quad (23)$$

Table 2.9: Coefficients of polynomials describing the properties of the R1234ze(E) refrigerant in the superheated vapour state (h = f(p,t), h = f(p,s), s = f(p,t))

Coef	Equation		
	h = f(p,t) (19)	h = f(p,s) (20)	s = f(p,t) (21)
a_1	$-1.22538219116946 \times 10^{1}$	9.70737789929653	$1.02201325065485 \times 10^{3}$
a_2	$-1.19684176263820 \times 10^{-1}$	$2.61874436156932 \times 10^{-1}$	2.11930425863317
a_3	$2.56418987553419 \times 10^{-2}$	$7.03198731354432 \times 10^{-2}$	$-2.25093762714879 \times 10^{-1}$
a_4	$1.12370072751876 \times 10^{-1}$	$2.04713651916276 \times 10^{-1}$	$-4.13156661967710 \times 10^{-1}$
a_5	$-7.84589730210466 \times 10^{-2}$	-	$-2.66667859197166 \times 10^{-1}$
b_1	$1.07613121977651 \times 10^{1}$	$2.14480351606632 \times 10^{2}$	-7.38442317160207
b_2	$1.27909162098184 \times 10^{-1}$	8.78348541751969	$-1.54691107365295 \times 10^{-2}$
b_3	$-2.17557771059542 \times 10^{-2}$	2.33196204712552	$1.61160247230101 \times 10^{-3}$
b_4	$-1.33475632720526 \times 10^{-2}$	6.31343053191083	$4.11509116217012 \times 10^{-3}$
b_5	$1.30152145421200 \times 10^{-2}$	-	$2.68867618687700 \times 10^{-3}$
c_1	$9.20939997738017 \times 10^{2}$	$1.30915602277249 \times 10^{2}$	$1.00415786839940 \times 10^{4}$
c_2	$-1.70804798986579 \times 10^{1}$	6.23649470729840	$-1.12883262503797 \times 10^{2}$
c_3	-9.36024775369566	1.07200578512649	$-2.83482394816380 \times 10^{1}$
c_4	$6.34415745181292 \times 10^{-1}$	-2.26086399298466	$-9.09256164033981 \times 10^{-1}$
c_5	-1.25745577415437	-	-1.13294272169830

Table 2.10: Coefficients of polynomials describing the properties of the R1234ze(E) refrigerant in the superheated vapour state (T = f(p,h), σ = f(p,h))

Coef	Equation	
	T = f(p,h) (22)	ϱ = f(p,h) (23)
a_1	$1.80123820111647 \times 10^{1}$	$2.81203869542640 \times 10^{1}$
a_2	$8.24003323530265 \times 10^{-2}$	$1.15184541343782 \times 10^{-1}$
a_3	$2.51686613531001 \times 10^{-2}$	2.45938820598331
a_4	-	$8.43110685237400 \times 10^{-1}$
a_5	-	$-2.05663545341847 \times 10^{-3}$
a_6	-	1.15342507562934
b_1	−9.57478728374795	$-2.27670387576552 \times 10^{1}$
b_2	$-4.92373151059871 \times 10^{-2}$	3.83041059824037
b_3	$1.88344691904411 \times 10^{-2}$	−4.86420752353526
b_4	-	$-1.09064973382657 \times 10^{1}$
b_5	-	$-1.20058186844573 \times 10^{-1}$
b_6	-	−4.74405743126640
c_1	$-6.16759701982095 \times 10^{3}$	$2.65873399640243 \times 10^{2}$
c_2	$-8.19380014241848 \times 10^{1}$	$-2.22556557307299 \times 10^{1}$
c_3	$-1.11076735383728 \times 10^{1}$	$2.57855441990927 \times 10^{1}$
c_4	-	$6.47202322127270 \times 10^{1}$
c_5	-	−1.99964641247140
c_6	-	$2.66402045824145 \times 10^{1}$

Subcooled liquid region

$$h = \sum_{n=1}^{6}(a_n.P + b_n.t + c_n)^n \quad (24)$$

$$s = \sum_{n=1}^{5}(a_n.P + b_n.t + c_n)^n \quad (25)$$

$$T = \sum_{n=1}^{4}(a_n.P + b_n.h + c_n)^n \quad (26)$$

Table 2.11: Coefficients of polynomials describing the properties of the R1234ze(E) refrigerant in the subcooled liquid state (h = f(p,t), s = f(p,t), T = f(p,h))

Coef	Equation		
	h = f(p,t) (24)	s = f(p,t) (25)	T = f(p,h) (26)
a_1	$-1.24632495027227 \times 10^{2}$	1.53492509731654	−2.54401494933800
a_2	$-8.93767310439441 \times 10^{-2}$	$1.14188030931082 \times 10^{-2}$	$1.41981737305051 \times 10^{-2}$
a_3	$-5.13970645120413 \times 10^{-3}$	$-2.27977637362198 \times 10^{-3}$	$4.17004268014005 \times 10^{-3}$
a_4	$-7.81419045658094 \times 10^{-4}$	$-9.09151613042750 \times 10^{-4}$	$-4.57959473157251 \times 10^{-3}$
a_5	$4.22545925349730 \times 10^{-4}$	$-4.02681309084223 \times 10^{-4}$	-
a_6	$3.59229939083742 \times 10^{-4}$	-	-
b_1	$-8.14460833381591 \times 10^{3}$	−8.64303643796513	8.02627024648105
b_2	−6.05289428492502	$-6.37870935254633 \times 10^{-2}$	$-4.09757320861048 \times 10^{-2}$
b_3	$-3.94885910243123 \times 10^{-1}$	$1.30109052596914 \times 10^{-2}$	$-1.18576883918572 \times 10^{-2}$
b_4	$-7.25230146369704 \times 10^{-2}$	$5.37778256355485 \times 10^{-3}$	$1.08815116545496 \times 10^{-3}$
b_5	$2.69851262120827 \times 10^{-2}$	$4.62322186390055 \times 10^{-3}$	-
b_6	$1.40090835277157 \times 10^{-2}$	-	-
c_1	$5.51597947695862 \times 10^{5}$	$1.05287623121195 \times 10^{3}$	$-7.10087317464252 \times 10^{3}$
c_2	$-3.62158965210490 \times 10^{2}$	$-2.75983526288628 \times 10^{1}$	$8.50746165042646 \times 10^{1}$
c_3	$-5.21112983842346 \times 10^{1}$	$-1.25845749595145 \times 10^{1}$	−2.84134460440402
c_4	$-1.64400591142357 \times 10^{1}$	−3.66028024779350	$-6.47159328560425 \times 10^{-1}$
c_5	$-1.44044662909068 \times 10^{1}$	$-3.23703650445058 \times 10^{-1}$	-
c_6	−4.26763585954523	-	-

Table 2.12: The scope of equations describing the properties of the R1234ze(E) refrigerant and the amount of data used for analysis

State	Scope	Amount of Data
Saturated liquid	p: 0.5–30.0 bar	591
Saturated vapour	p: 0.5–30.0 bar	591
Superheated vapour	p: 0.5–30.0 bar; t: t″ – 120 °C	18,186 [1]
Subcooled liquid	p: 0.5–30.0 bar; t: −80 °C–t′	41,901

[1] for ϱ from 25 kg/m^3 and up to 470 kJ/kg; 9608 pieces of data.

2.4.4 Properties and state equations for the refrigerant R134a [228]

$$X = 1 - (\frac{T_{sat}}{T_c})^{\frac{1}{3}} \quad (27)$$

$$\Delta T = T_{vap} - T_{sat} \quad (28)$$

Table 2.13: Field of use of the proposed mathematical models

	Saturation (°C)	Superheating (°C)		Subcooling (Tliq ≤ Tsat) (°C)	
	Tsat	Tsat	ΔT	Tsat	Tliq
R12	[-60,60]	[-60,60]	]0,60]	[-60,60]	[-70,60]
R22	[-60,60]	[-60,60]	]0,60]	[-60,60]	[-80,60]
R134a	[-40,70]	[-40,70]	]0,60]	[-60,70]	[-60,70]
R717	[-60,60]	[-60,60]	]0,80]	[-40,60]	[-40,60]
R718	[0.1,60]	[0.1,60]	]0,60]	[0.1,60]	[0.1,60]
R744	[-50,25]	[-50,23]	]0,60]	[-50,25]	[-50,25]

Saturation presure and temperature

$$T_{sat} = -273.15 + \frac{1}{a_1 + a_2.ln(P_{sat}) + a_3.(ln(P_{sat}))^2} \quad (29)$$

$$P_{sat} = \exp\left(\frac{1}{(2.a_3)}.\left(-a_2 - \sqrt{{a_2}^2 - 4.a_3.\left(a_1 - \frac{1}{T_{sat}+273.15}\right)}\right)\right) \quad (30)$$

Liquid enthalpie

$$h_{liq} = h_0 + a_4.T_{liq} + a_5.{T_{liq}}^2 + a_6.{T_{liq}}^3 \quad (31)$$

Enthalpie of saturated vapor

$$h_{vsat} = a_7 + a_8.T_{sat} + a_9.{T_{sat}}^2 + a_{10}.{T_{sat}}^3 \quad (32)$$

Enthalpie of superheated vapor

$$h_{vap} = h_{vsat}.(1 + a_{11}.\Delta T + a_{12}.\Delta T^2 + a_{13}.\Delta T.X + a_{14}.\Delta T^2.X + a_{15}.\Delta T.X^2 + a_{16}.\Delta T^2.X^2) \quad (33)$$

Liquid density

$$d_{liq} = a_{17} + a_{18}.T_{liq} + a_{19}.T_{liq}^{2} + a_{20}.T_{liq}^{3} \quad (34)$$

Density of saturated vapor

$$d_{vsat} = \left(\exp\left(a_{21} + \left(\frac{a_{22}}{(Tsat+273.15)}\right).\left(a_{23} + a_{24}.T_{sat} + a_{25}.T_{sat}^{2} + a_{26}.T_{sat}^{3}\right)\right)^{-1}\right) \quad (35)$$

Density of superheated vapor

$$d_{vap} = d_{vsat}.(1 + a_{27}.\Delta T + a_{28}.\Delta T^{2} + a_{29}.\Delta T.X + a_{30}.\Delta T^{2}.X + a_{31}.\Delta T.X^{2} + a_{32}.\Delta T^{2}.X^{2}) \quad (36)$$

Liquid entropy

$$S_{liq} = S_0 + a_{33}.T_{liq} + a_{34}.T_{liq}^{2} + a_{35}.T_{liq}^{3} \quad (37)$$

Entropy of saturated vapor

$$S_{vsat} = a_{36} + a_{37}.T_{sat} + a_{38}.T_{sat}^{2} + a_{39}.T_{sat}^{3} \quad (38)$$

Entropy of superheated vapor

$$S_{vap} = S_{vsat}.(1 + a_{40}.\Delta T_{vap} + a_{41}.(\Delta T_{vap})^{2} + a_{42}.(\Delta T_{vap}).X + a_{43}.(\Delta T_{vap})^{2}.X + a_{44}.(\Delta T_{vap}).X^{2} + a_{45}.(\Delta T_{vap})^{2}.X^{2}) \quad (39)$$

Enthalpy isentropic compression

$$h_{is} = a_{46} + a_{47}.T_{sat} + a_{48}.T_{sat}^{2} + a_{49}.S_{vap}. + a_{50}.S_{vap}^{2} + a_{51}.T_{sat}.S_{vap} \quad (40)$$

Table 2.14: Coefficients ai of equations

a_i	R12	R22	R134a	R717	R718	R744
$a_1\ 10^{-3}$	5.843232	6.037869	5.609168	5.686016	3.569924	7.715324
$a_2\ 10^{-4}$	-3.548510	-3.548078	-3.170755	-3.100500	-1.854387	-4.888100
$a_3\ 10^{-6}$	-4.524289	-4.487872	-4.580596	-3.957699	-1.463356	-1.001128
a_4	933.4904	1168.0925	1338.0622	4624.7203	4209.7740	2447.3508
a_5	1.026399	1.489095	1.507776	3.044944	-0.839768	9.194688
$a_6\ 10^{-3}$	4.032561	7.677558	7.292187	18.891608	7.618166	56.566465
a_7	352834.51	405126.62	398609.67	1462322.86	2500901.18	431238.61
a_8	445.8697	371.0977	590.5335	1075.8725	1833.1707	-660.8484
a_9	-0.81203	-1.89686	-1.13969	-8.49466	-0.20638	-22.59507
$a_{10}\ 10^{-3}$	-7.00607	-12.58487	-15.73327	-31.05215	-6.05559	-208.30322
$a_{11}\ 10^{-3}$	5.47703	8.13689	8.23046	11.71932	5.16547	19.15273
$a_{12}\ 10^{-5}$	-2.64216	-4.92947	-4.75759	-3.79892	-1.30210	-17.90999
$a_{13}\ 10^{-3}$	-5.90694	-10.28964	-9.86889	-17.35459	-9.13672	-23.50476
$a_{14}\ 10^{-5}$	4.48780	8.49809	8.47381	6.30905	2.45292	26.46450
$a_{15}\ 10^{-3}$	2.20215	3.94769	3.84411	7.36310	4.72034	8.14065
$a_{16}\ 10^{-5}$	-1.78156	-3.57420	-3.63399	-2.60099	-1.15144	-9.89948
a_{17}	1398.3424	1284.8722	1298.0506	639.2159	999.8288	938.4298
$a_{18}\ 10^{-2}$	-320.96166	-338.91768	-325.94519	-136.25921	5.1650729	-609.54639
$a_{19}\ 10^{-3}$	-7.160636	-9.283395	-8.625745	-2.466172	-7.345471	-58.901389
$a_{20}\ 10^{-5}$	-3.739924	-4.569758	-6.440877	-1.287854	3.153641	-52.22636
$a_{21}\ 10^{-2}$	-1159.2719	-1182.5136	-1245.3638	-1109.5956	0.4878488	-1303.3016
$a_{22}\ 10^{-3}$	2375567.464	2390467.218	2668925.495	2692540.743	0.31965885	2311018.538
$a_{23}\ 10^{-4}$	10118.860	10182.751	10135.428	9978.461	0.1199948	9911.821
$a_{24}\ 10^{-6}$	619.5416	552.6469	863.4947	654.5539	0.0889521	-1162.4296
$a_{25}\ 10^{-6}$	-6.342958	-15.14413	-6.773819	1.848153	0.00338858	-160.4710
$a_{26}\ 10^{-7}$	-2.285547	-2.654354	-3.158333	-2.224413	0	-13.364015
$a_{27}\ 10^{-2}$	3.586143	4.390244	4.434543	3.912153	-6.646023	6.542875
$a_{28}\ 10^{-5}$	-9.026194	-19.617300	-18.888209	-7.343152	52.884405	-49.193233
$a_{29}\ 10^{-2}$	-5.770439	-6.921101	-7.065903	-6.441045	14.007886	-8.122005
$a_{30}\ 10^{-5}$	13.3453111	31.7316578	29.3996329	9.8164049	-111.506424	66.8106846
$a_{31}\ 10^{-2}$	2.666274	3.066596	3.143090	3.009273	-7.724722	2.767173
$a_{32}\ 10^{-5}$	-4.7668247	-12.8406310	-11.1825841	-2.9501863	59.669058	-22.7956237
a_{33}	3.409982	4.251773	4.890121	16.831278	15.402714	8.836752
$a_{34}\ 10^{-3}$	-3.542555	-4.104185	-4.855040	-23.486942	-30.495175	5.493089
$a_{35}\ 10^{-5}$	1.245397	2.503762	2.707040	10.046954	7.914522	-34915.457
a_{36}	1559.30177	1750.62329	1727.04011	5619.89937	9155.57210	1846.39540
a_{37}	-0.440998	-1.435285	-0.548617	-13.059478	-26.732618	-5.826816
$a_{38}\ 10^{-3}$	5.122753	6.392713	6.678329	50.081790	119.460729	-49.035416
$a_{39}\ 10^{-5}$	-5.102562	-7.812310	-7.364528	-33.787714	-34.140701	-72.076271
$a_{40}\ 10^{-3}$	3.979782	5.682377	5.723118	9.005031	2.993367	14.741853
$a_{41}\ 10^{-5}$	-2.297127	-3.972229	-3.770371	-3.811660	-2.482249	-14.527905
$a_{42}\ 10^{-3}$	-4.865303	-7.197635	-6.964950	-12.689854	-4.791869	-17.668023
$a_{43}\ 10^{-5}$	3.798349	6.575172	6.359620	6.241957	5.032120	20.751189
$a_{44}\ 10^{-3}$	2.347955	3.028382	3.099797	5.297648	2.543805	6.121913
$a_{45}\ 10^{-5}$	-1.681490	-2.840202	-2.818940	-2.709667	-2.664690	-7.689485
a_{46}	501932.4012	581913.2066	302254.7477	2927425.0656	10781059.2464	419552.5512
a_{47}	-1125.1198	-1626.2465	-1069.5344	-9624.9662	-45139.5048	-2662.9979
a_{48}	-1.400607	-1.554612	-1.969477	-3.648675	29.17398	0.2855097
a_{49}	-464.900043	-476.457408	-165.976191	-774.873742	-2074.07989	-247.823559
a_{50}	0.236855	0.214460	0.128489	0.091446	0.127596	0.137949
a_{51}	1.080774	1.365268	1.036463	2.577302	6.022026	1.939631

2.5 Development of the numerical model

2.5.1 Software used (MATLAB)

MATLAB (an abbreviation of "MATrix LABoratory") is a proprietary multi-paradigm programming language and numeric computing environment developed by MathWorks. MATLAB allows matrix manipulations, plotting of functions and data, implementation of algorithms, creation of user interfaces, and interfacing with programs written in other languages.

Although MATLAB is intended primarily for numeric computing, an optional toolbox uses the MuPAD symbolic engine allowing access to symbolic computing abilities. An additional package, Simulink, adds graphical multi-domain simulation and model-based design for dynamic and embedded systems.

As of 2020, MATLAB has more than four million users worldwide.They come from various backgrounds of engineering, science, and economics. As of 2017, more than 5000 global colleges and universities use MATLAB to support instruction and research.

MATLAB was first released as a commercial product in 1984 at the Automatic Control Conference in Las Vegas MathWorks, Inc. was founded to develop the software and the MATLAB programming language was released The first MATLAB sale was the following year, when Nick Trefethen from the Massachusetts Institute of Technology bought ten copies.

By the end of the 1980s, several hundred copies of MATLAB had been sold to universities for student use.The software was popularized largely thanks to toolboxes created by experts in various fields for performing specialized mathematical tasks.Many of the toolboxes were developed as a result of Stanford students that used MATLAB in academia, then brought the software with them to the private sector.

Over time, MATLAB was re-written for early operating systems created by Digital Equipment Corporation, VAX, Sun Microsystems, and for Unix PCs. Version 3 was released in 1987. The first MATLAB compiler was developed by Stephen C. Johnson in the 1990s.

In 2000, MathWorks added a Fortran-based library for linear algebra in MATLAB 6, replacing the software's original LINPACK and EISPACK subroutines that were in C. MATLAB's Parallel Computing Toolbox was released at the 2004 Supercomputing Conference and support for graphics processing units (GPUs) was added to it in 2010.

Some especially large changes to the software were made with version 8 in 2012.The user interface was reworked[citation needed] and Simulink's functionality was expanded.By 2016, MATLAB had introduced several technical and user interface improvements, including the MATLAB Live Editor notebook, and other features.

The MATLAB application is built around the MATLAB programming language. Common usage of the MATLAB application involves using the "Command Window" as an interactive mathematical shell or executing text files containing MATLAB code.

2.5.2 Heat and mass transfer equations

When considering a control volume encompassing the refrigerant side of the evaporator, the refrigerant's mass flow rate ($\dot{m}$) is defined as follows [229]:

$$\dot{m} = \frac{Q_e}{(h_1 - h_4)} \tag{2.1}$$

Where: h1 and h4 are the specific enthalpies at states (1) and (4), respectively (kJ/kg). Qe is the heat transfer rate, which is referred to as the cooling capacity (kW).

The compressor power consumption is defined as follows [230]:

$$W = \frac{\dot{m}(h_2 - h_1)}{\eta_e . \eta_b . \eta_m} \tag{2.2}$$

Where: h_2 is the specific enthalpy at state (2) (kJ/kg). ηe, ηb, and ηm are respectively called as electric motor efficiency, belt transmission efficiency and compressor mechanic efficiency. Knowing the compressor exit temperature, the specific enthalpy (h2) at the exit of the compressor can be determinated.

The discharge temperature based on the polytropic is calculated as follows [231]:

$$T_2 = T_1 \left(\frac{P_c}{P_e}\right)^{\gamma - 1/\gamma} \tag{2.3}$$

Where: Pc and Pe are the condenser and evaporator pressures, respectively (bar).

γ is the polytropic exponent (defined as the ratio between the specific heat at constant pressure and constant volume, Cp/Cv.

For a control volume enclosing the refrigerant side of the condenser, the rate of heat transfer (Qc) from the refrigerant per unit mass of refrigerant is as follows:

$$Q_c = \dot{m}(h_2 - h_3) \tag{2.4}$$

The process in expansion valve is usually modeled as a throttling process for which:

$$h_3 = h_4 \tag{2.5}$$

Where h3 is the specific enthalpy at state (3) (kJ/kg).

2.6 Definition of different operating conditions

To model the solar vapor compression refrigeration system,the principles of mass conservation and the first law of thermodynamics are utilized for every cycle component, considering the following assumptions:

• Steady-state operation
• Reversible heat transfer
• Polytropic compression
• Negligible variations in kinetic and potential energy
• Insignificant pressure drops
• Consistent cooling capacity

The fundamental operational parameters, derived from previous studies, which determine the performance of the cycle, are provided in Table 2..15

Table 2.15: Operating parameters

Parameter	Value
Nominal cooling capacity	2 kW
Evaporating Temperature	0°C
Condenser temperature approach	15 K
Superheat	5 K
Subcooling	5 K
Electric motor efficiency	95%
Belt transmission efficiency	100% (direct transmission)
Compressor mechanic efficiency	80%
PV panel efficiency	20%

The fundamental solar PV module parameters used in our study, are provided in Table 2.16

.

Table 2.16: Solar PV module (Vertex 580 W+ Trina Solar, TSM-580 DE19R) parameters

Parameter	Value
PV panel efficiency	21.5 %
Peak power of the unit photovoltaic field	580 W
NOCT	43 °C
Emissivity of the panel	0.9
Voc	46.3 V
Isc	15.94 A
Number of photovoltaic cells	132
Vmpp	39 V
Impp	14.86 A
Dimensions	2384 x 1134 x 35 mm
Weight	29,1 kg
Module surface	2.703456 m^2
PMAX temperature coefficient	-0.34 %/°K
VOC temperature coefficient	-0.25 %/°K
ISC temperature coefficient	0.04 %/°K
Fill Factor	0.7859
Stefan Boltzmann constant (σ)	5.67×10^{-8} W/m^2. K
Sun temperature	5780 K

CHAPTER 3

THERMODYNAMIC PERFORMANCE ANALYSIS

CHAPTER 3

Thermodynamic performance analysis

3.1 Coefficient of performance (COP)

Coefficient of the performance (COP) is defined as the cooling power, Qe divided by the work input, W :

$$COP = \frac{Qe}{W} \tag{3.1}$$

3.2 Thermodynamic efficiency

Heat losses are a common occurrence in cooling systems, leading to a deviation between actual coefficient of performance (COP) and its theoretical maximum COP.

The thermodynamic efficiency refers to the ratio between the COP of the actual refrigeration system and the COP of a reversible refrigeration system operating within the same temperature range:

$$\eta_{th} = \frac{COP}{COP_{max}} \tag{3.2}$$

Where: COPmax is the maximum coefficient of performance of the refrigeration system which depends mainly on its operating temperatures.

$$COP\ max = \frac{Te}{Tc-Te} \tag{3.3}$$

Equations for calculations of the thermodynamic properties of R134a and R1234ze refrigerants are presented in [227] and [228], respectively. The developed correlations are a function of one variable for the state of saturation and two variables for the subcooled liquid and superheated vapor regions.

3.3 Solar PV panel

The calculation of PV power production involves the utilization of the solar electric panel's efficiency, denoted as ηPV, and the solar radiation input, represented as Qs [232].

$$W_{PV} = \eta_{PV}.Q_s \tag{3.4}$$

The generation of solar radiation from the surface area of the panel and the overall efficiency of a cooling system assisted by solar PV are defined as follows:

$$Q_s = A.I \tag{3.5}$$

$$\eta_s = \eta_{PV}.COP = \frac{Q_e}{Q_s} \tag{3.6}$$

Where: A is the solar cell or panel surface area (m^2) and I is solar radiation (kW/m^2). In the solar vapor compression refrigeration system, the objective is to fulfill the compressor's power requirements through electricity generated by solar PV panels. Consequently, it is necessary to ensure an adequate number of PV panels with appropriate characteristics to meet the system's energy demand entirely. The daily cumulative power consumption of the compressor and the daily cumulative power production of the PV panels can be calculated using the following expressions:

$$W_T = \sum_{i=1}^{k} W_i \quad (k = 1, 2, \dots, 24) \tag{3.7}$$

$$(W_{PV})_T = \sum_{i=1}^{k} (W_{PV})_i \quad (k = 1, 2, \dots, 24) \tag{3.8}$$

Where: k is the hour of the day.

The required PV panel area can be determined by using the following equation:

$$A = \frac{W_T}{\eta_{PV} . I_T} \tag{3.9}$$

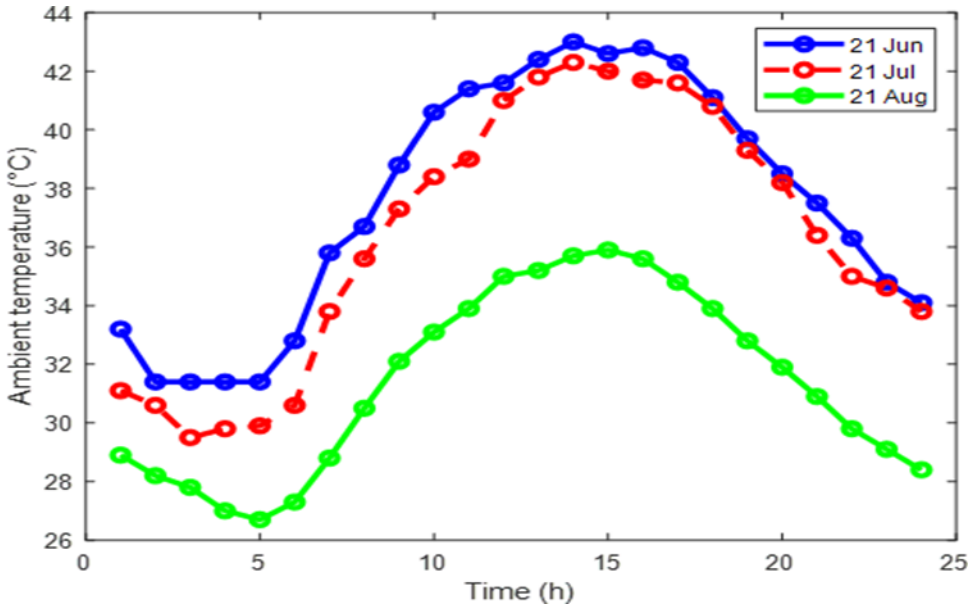
Here: IT is the daily total solar radiation ($kWh/m^2/day$).

3.4 Results and discussion

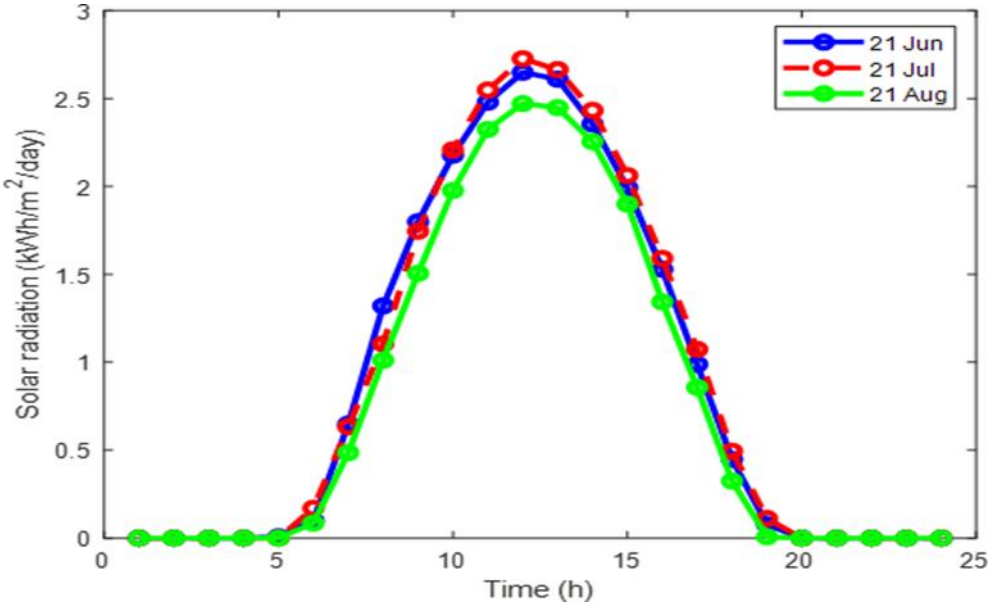
Figure 3.1 illustrates the measured hourly average variations of solar radiation and ambient temperature for the Ghardaia region during the 21st day of June, July, and August. As depicted in Figure 3.1 (a), the hourly ambient temperature experiences a significant range of variation throughout the day, with the highest average temperature occurring in June and July, and the lowest in August. Figure 3.1 (b) demonstrates that solar irradiation increases with sunlight, reaching its peak values at noon. Subsequently, it gradually decreases during the evening hours when the solar energy's influence diminishes, and there is no solar energy effect between 8:00 PM and 4:00 AM. Moreover, the hourly solar radiation values in July surpass those of other months. The maximum solar radiation value, with a magnitude of 2.726 kWh/m^2, is recorded at 12:00 PM on July 21.

Comparing the maximum values of ambient air temperature and solar radiation, it is observed that the maximum atmospheric temperature occurs between 1:00 PM and 2:00 PM, whereas the maximum solar radiation is registered between 12:00 PM and 1:00 PM. Figure 3.2 presents a comparison of the hourly mass flow rates for both refrigerants on July 21.

The calculation results indicate that the mass flow rate of R1234ze is noticeably higher than that of R134a. This difference is primarily due to R134a having a higher boiling point and heat of vaporization compared to R1234ze at a given temperature.



(a) Ambient temperature



(b) Solar radiation

Figure 3.1: Hourly mean variation of solar radiation and ambient temperature (Ghardaïa site) [194]

Consequently, R134a exhibits a greater cooling capacity, as depicted in Figure 3.3, meaning that a lower mass flow rate of R134a is typically required to achieve the same cooling effect as R1234ze. The lower cooling capacity for R1234ze refrigerant compared to R134a, with an average reduction equal to 10% is comparable with the findings of other experimental works present in the literature [233 – 235].

Furthermore, R134a has a lower specific volume and higher density in comparison to R1234ze. This implies that a smaller mass of R134a can occupy the same volume as a larger mass of R1234ze, resulting in a reduced mass flow rate requirement for R134a. Additionally, the mass flow rate experiences variations throughout the day. As the ambient temperature rises, the heat load on the system increases, necessitating a higher mass flow rate of refrigerant to maintain the desired cooling capacity.

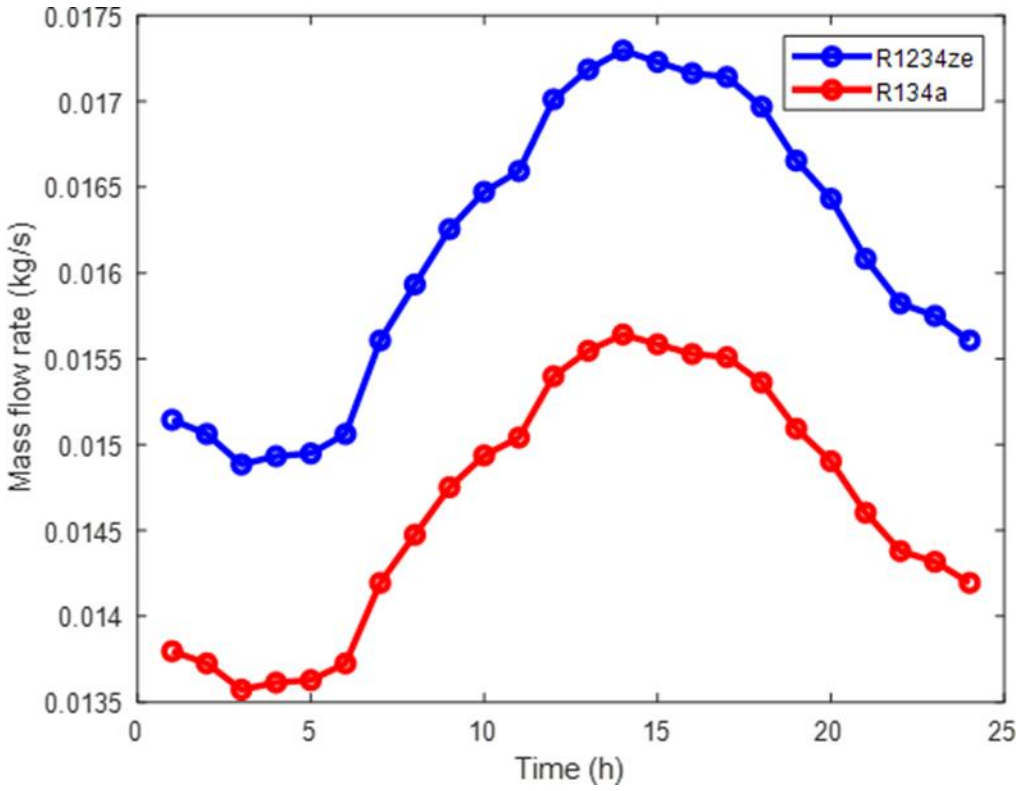


Figure 3.2: Hourly variation of mass flow rate (Ghardaïa site) [194]

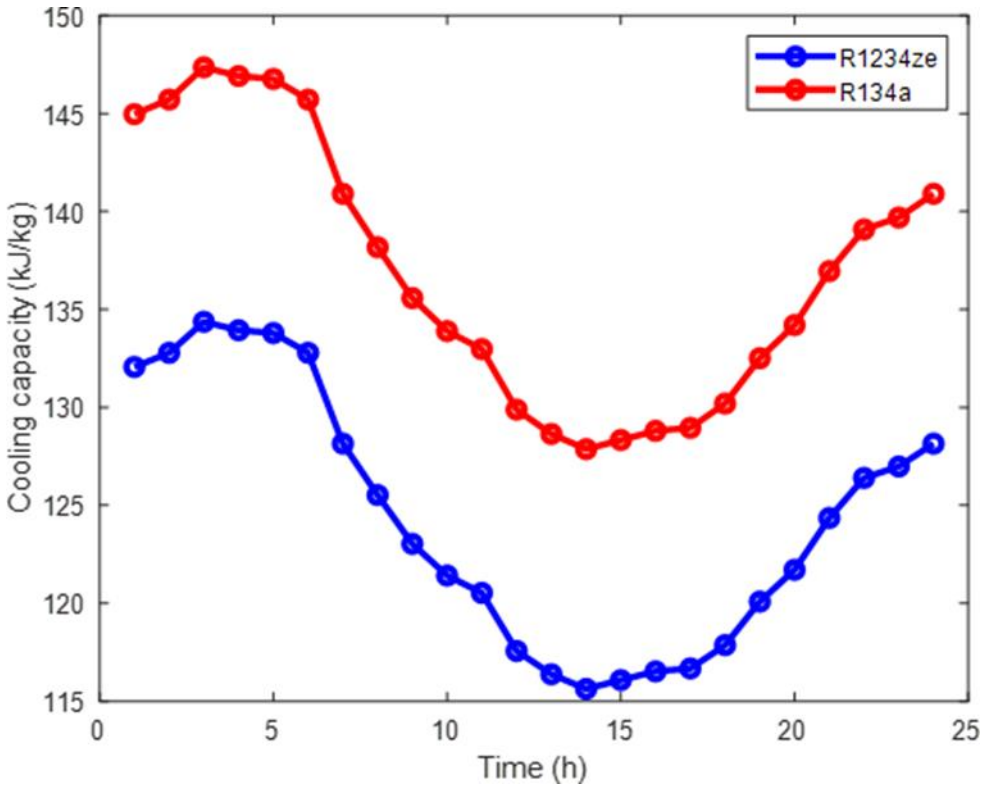


Figure 3.3: Hourly variation of cooling capacity (Ghardaïa site) [194]

Figure 3.4 illustrates the variation of the coefficient of performance (COP) for both refrigerants throughout the 21st day of July. The graph indicates that the COP of the R1234ze refrigerant surpasses that of R134a, given the specific evaporating and condensing temperatures. Moreover, the COP of R1234ze remains consistently above 4 throughout the entire 24-hour simulation period, demonstrating its superior performance within a broad operational range. For R1234ze, the COP of the VCR system fluctuates between 4.37 and 5.77, while for R134a, it ranges from 2.56 to 3.17. Therefore, the use of the refrigerant R1234ze(E) leads to an average increase of the COP value to 43.5%. The experimental works conducted by Leighton et al. [236] and Kabeel et al.
[237] also shown the same trends as in the presented work. They concluded that R1234ze has high COP by about 37.5% and 33%, respectively compared to R134a.
During the period from midnight to sunrise, the COP exhibits an increase due to the decrease in outside temperature, resulting in enhanced system performance.
Conversely, as the atmospheric temperature rises, leading to higher condenser temperatures, the system's performance diminishes.

Subsequently, from sunrise until around 14:00 PM, the COP experiences a decrease as the outside temperature gradually rises during this daytime period. However, the COP begins to rise again as the outside temperature decreases during the nighttime. It is worth noting that the COP values for R1234ze remain close to and exceed 90% of the maximum COP value, as depicted in Figure 3.5.

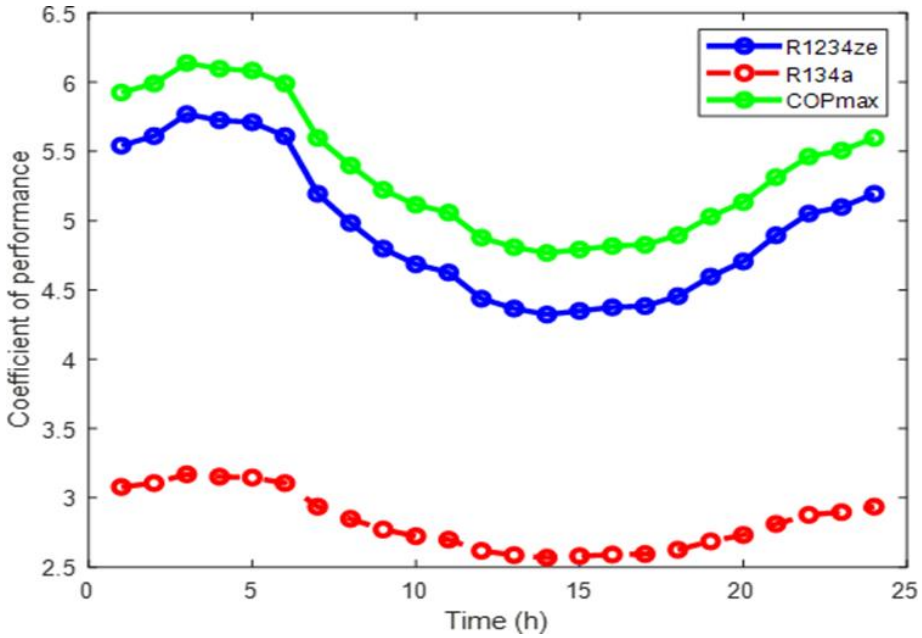


Figure 3.4: Hourly variation of coefficient of performance (Ghardaia region) [194]

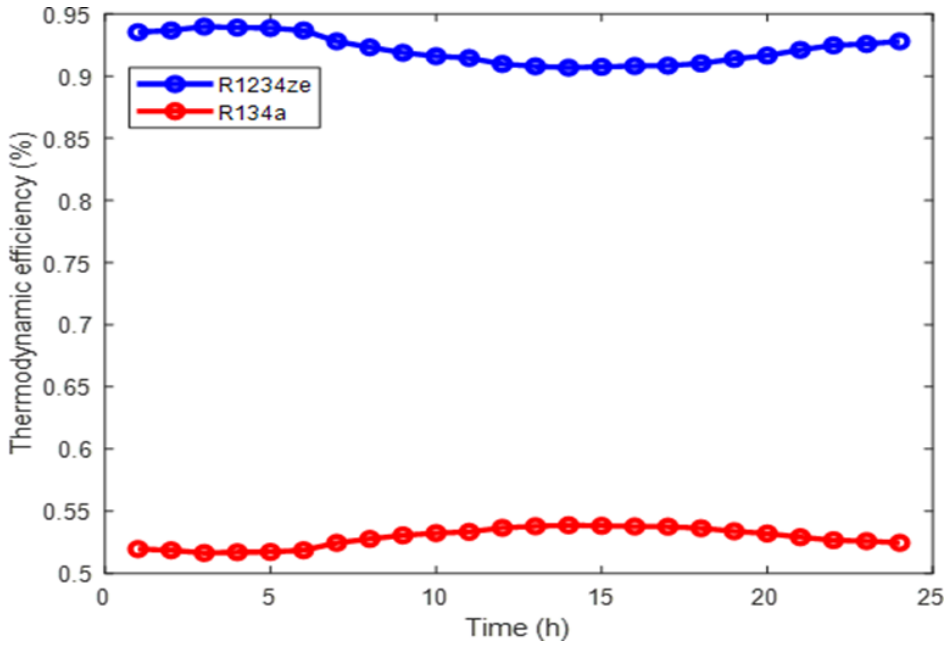


Figure 3.5: Hourly variation of thermodynamic efficiency (Ghardaia region) [194]

The results in Figure 3.5 are mainly due to the different hourly variation of the thermodynamic properties of the two refrigerants R1234ze and R134a.

Figure 3.6 depicts the comparison of solar-to-cooling COP values for both refrigerants on the 21st day of July. It is evident that the solar-to-cooling efficiency of the VCR system tends to decrease as the ambient temperature rises. This decrease can be attributed to the decline in solar collector efficiency at higher temperatures, resulting in reduced conversion of solar energy into cooling output. The overall solar efficiency reaches its peak value around 03:00. Additionally, the VCR system's COP shows a downward trend at higher temperatures due to increased power consumption of the compressor and reduced refrigerant performance. The R1234ze refrigerant exhibits relatively favorable solar COP compared to R134a fluid. Between 10:00 and 19:00, the solar-to-cooling COP values range from 0.92 to 0.94.

It is worth mentioning that currently available refrigeration systems typically have COP values ranging from 3 to 6 across standard operating temperature ranges, resulting in total solar-to-cooling COPs in the range of 0.3 to 0.6. However, the solar-to-cooling COP values for VCR systems can vary significantly depending on various factors, including solar collector efficiency, efficiency of electrical components (such as the compressor and fan), choice of refrigerant, and operating conditions.

Figure 3.7 presents the hourly variation of PV power production in terms of amount. Based on the results obtained for the 21st day of July, the highest PV power production for R134a and R1234ze refrigerants is observed at midday (12:00 PM) with values of 2.8 kWh and 1.6 kWh, respectively. The daily total power consumption of the compressor aligns with the daily total PV power production, as depicted in Figure 3.8. The compressor power consumption reaches its peak values between 14:00 PM and 18:00 PM when the atmospheric temperature and cooling load are at their maximum levels.

Conversely, the compressor power consumption gradually decreases during the morning and evening hours, corresponding to the decrease in atmospheric temperature.

For the 21st day of July, the compressor power consumption ranges from 0.46 kW to 0.61 kW for R1234ze and from 0.83 kW to 1.02 kW for R134a. Thus, the compressor power consumption of R1234ze is 42.2 % lower than R134a. The obtained results are in accordance with the experimental data presented in [238 – 241].

The maximum compressor power consumption is observed at 14:00 PM.

Consequently, the compressor power consumption increases in direct proportion to the atmospheric temperature and cooling load. Under these conditions, the compressor requires a higher driving power and may struggle to operate efficiently.

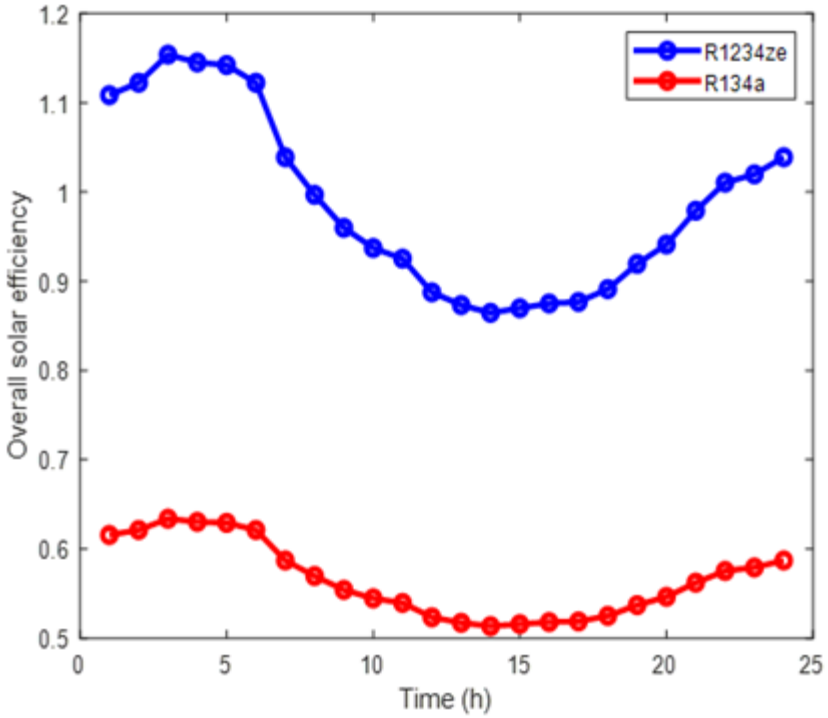


Figure 3.6: Hourly variation of overall solar efficiency (Ghardaia region) [194]

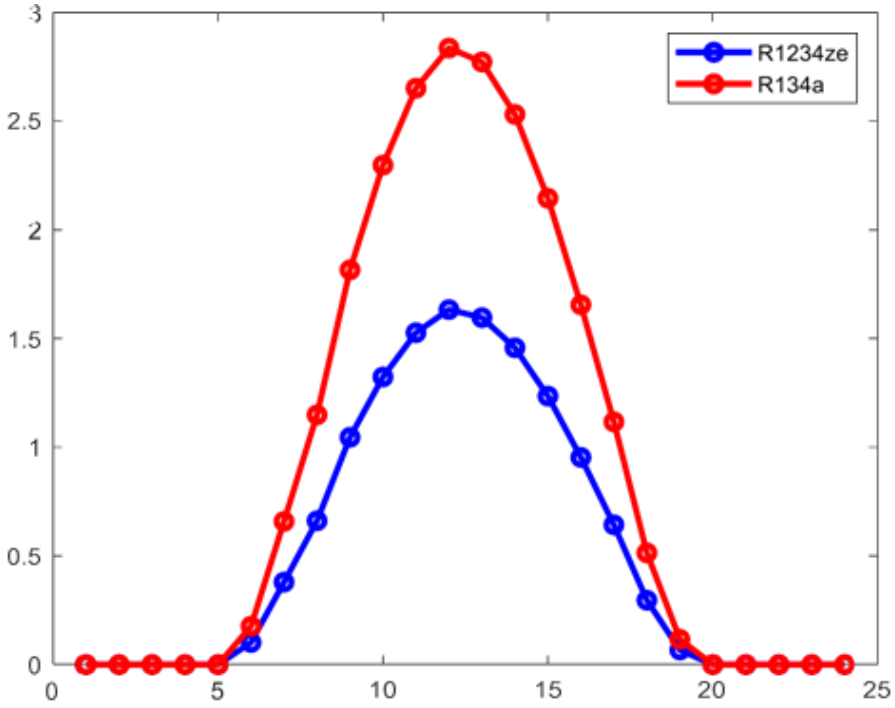


Figure 3.7: Hourly variation of PV power production (Ghardaia region) [194]

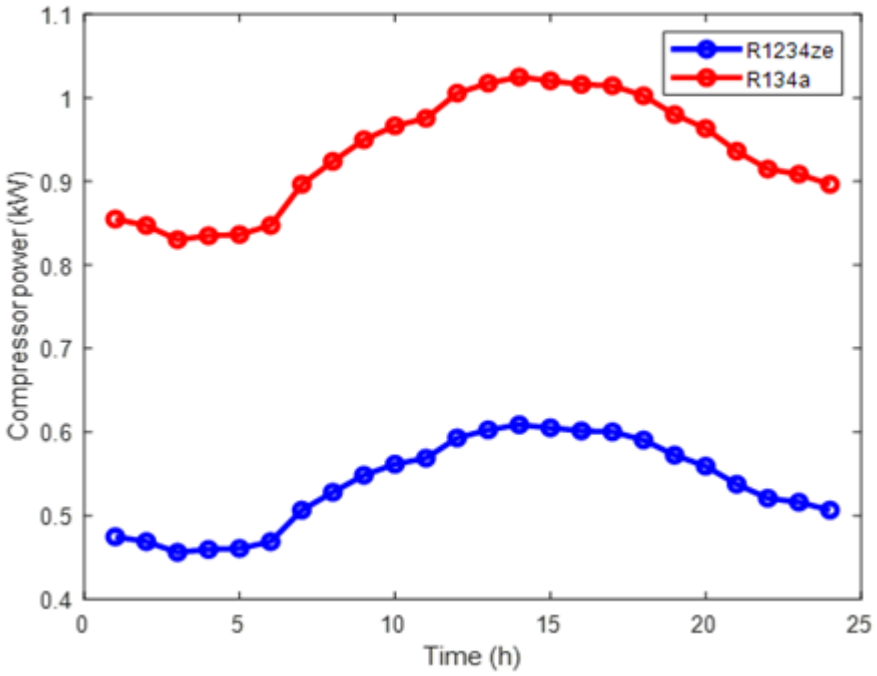


Figure 3.8: Hourly variation of compressor power (Ghardaia region) [194]

Figure 3.9 illustrates the hourly variation of the required PV panel area on July 21. It is evident that the PV surface area for both refrigerants exhibit an inverse relationship with ambient temperature, which is to be expected. Solar panels have a temperature coefficient, indicating the rate at which their efficiency decreases as temperature rises.

As the temperature of the solar panels increases, their efficiency declines, resulting in reduced power generation for the same amount of sunlight. In hotter environments, the solar panels produce less power, necessitating an increase in the required panel area to compensate for this efficiency decrease.

Additionally, the required solar PV area for R134a refrigerant is higher compared to R1234ze fluid. This can be attributed to the larger quantity of R134a refrigerant needed to generate the same cooling effect as R1234ze.

Consequently, a larger solar PV system is required to power the compressor responsible for circulating the refrigerant in the system. The larger system necessitates more solar panels and, therefore, a larger surface area for capturing sunlight and generating electricity.

However, it is worth noting that the PV panel surface area does not vary significantly with ambient temperature between 08:00 AM and 16:00 PM. This is because the power output of a PV panel primarily depends on the amount of solar radiation it receives rather than the ambient temperature. While temperature can impact panel efficiency, it does not directly influence the surface area required to generate a specific amount of power.

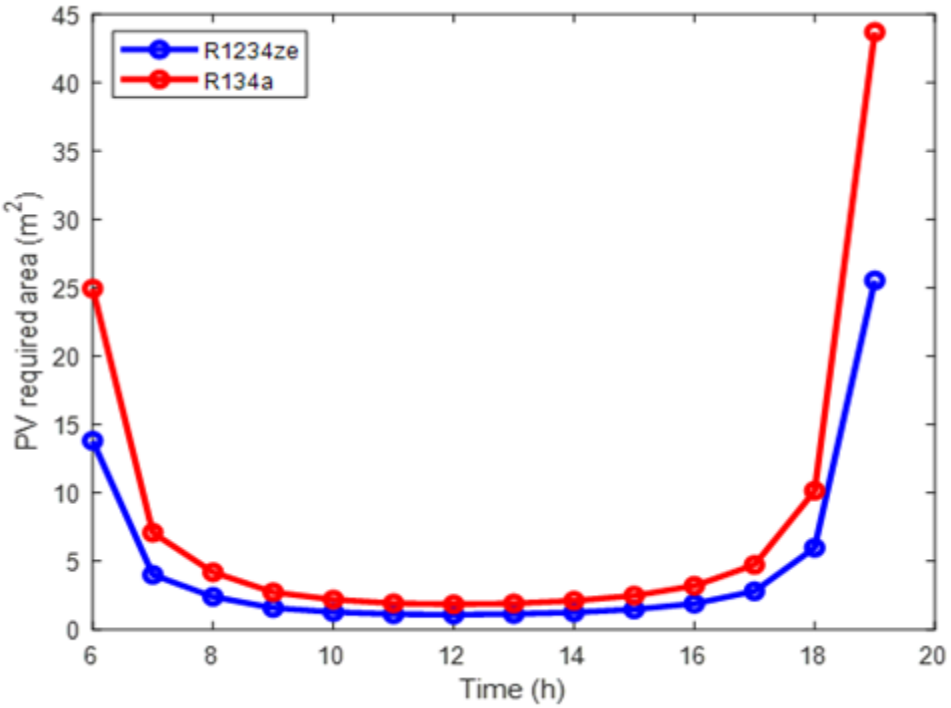


Figure 3.9: Hourly variation of PV required area (Ghardaia region) [194]

Figure 3.10 presents a comparison between the power consumed by the compressor and the power generated by PV panels on July 21st, utilizing R1234ze refrigerant at an evaporating temperature of 0°C.

During the period of 7:00 PM to 6:00 AM, the PV panels generate a relatively low amount of power due to limited solar energy availability.

Consequently, the energy demand cannot be fully met during this timeframe.

However, from 8:00 AM to 16:00 PM, the PV panels produce more electricity than what the compressor motor requires.

Any excess energy generated during this period is stored in an accumulator and utilized later to partially or entirely fulfill the compressor power demand between 19:00 PM and 6:00 AM.

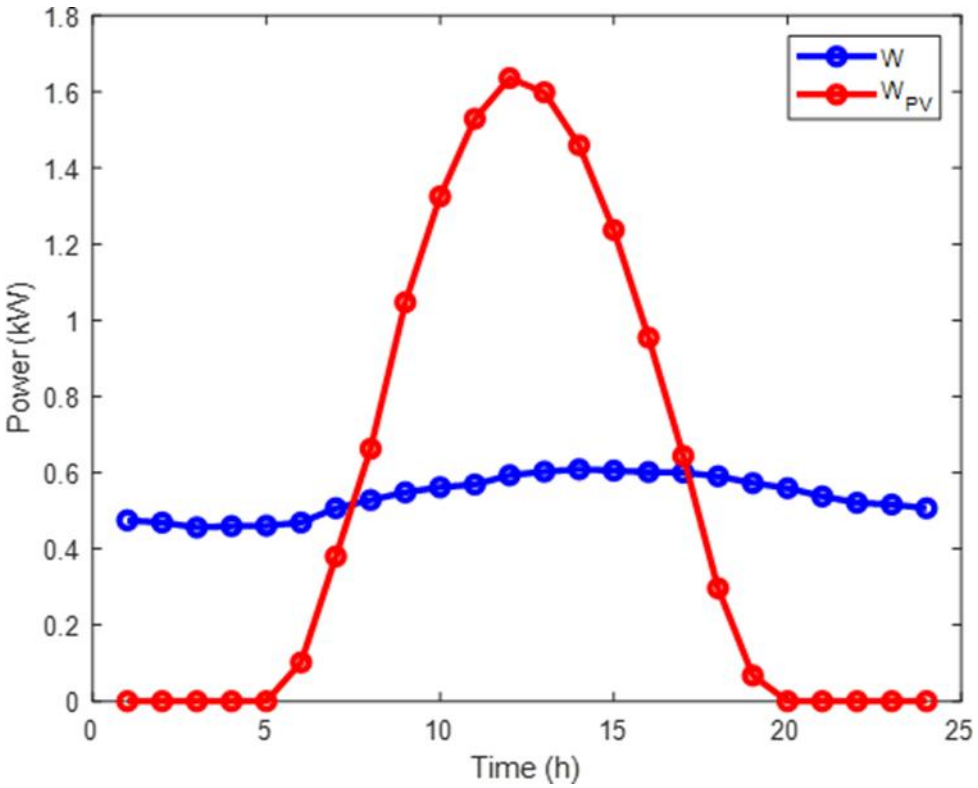


Figure 3.10: Comparison of the compressor power consumption and PV power production for R1234ze (Ghardaia region) [194]

According to Figure 3.11, the cumulative PV power production until 10:00 AM falls short of meeting the cumulative compressor power consumption. At 11:00 AM, the cumulative energy production and consumption become equal, and from that point onwards, the cumulative energy production surpasses the consumption resulting in surplus solar-electricity being stored in the accumulators.

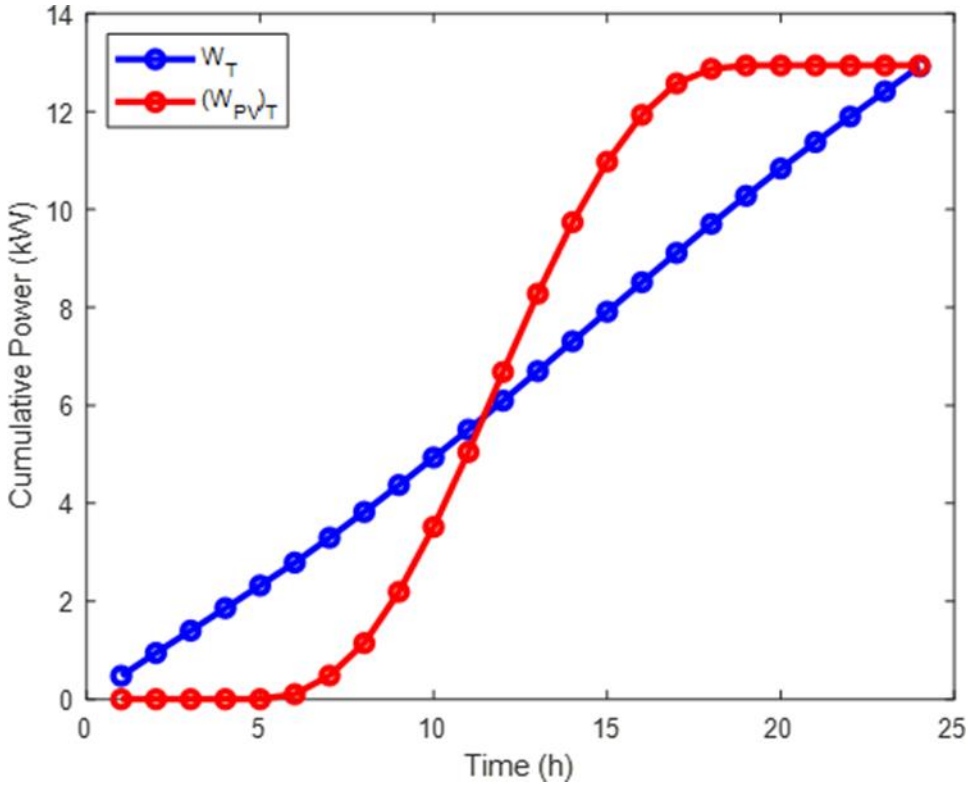


Figure 3.11: Comparison of the cumulative compressor power consumption and cumulative PV power production for R1234ze (Ghardaia region) [194]

3.5 Conclusion

The growing demand for cooling applications and environmental concerns have spurred the development of solar-driven vapor compression refrigeration (VCR) systems with low GWP refrigerants. This study focuses on analyzing a solar-driven VCR system for cooling purposes in the Ghardaïa region of Southern Algeria. The study compares the performance of R134a and its potential replacement, R1234ze, as working fluids. Key findings are as follows:

In Ghardaïa, the peak solar radiation occurs at 12:00 PM on July 21, reaching 2.726 kWh/m^2, with July generally experiencing higher radiation level.

-At a given temperature, R134a requires a lower mass flow rate due to its higher enthalpy of vaporization. However, density becomes the dominant factor favoring a higher mass flow rate for R1234ze.

-R1234ze demonstrates a higher COP compared to R134a, thanks to its lower compressor power requirement and improved thermodynamic efficiency for the same cooling capacity.

-The solar-to-cooling COP declines as temperatures rise, primarily due to increased compressor power consumption and diminished refrigerant performance. Consequently, cooling capacity and efficiency are reduced.

-Although the required surface area of solar PV panels shows minimal variation with ambient temperature, panel temperature directly influences performance and, conse-quently, affects the required area.

-Cumulative PV power production exceeds compressor power consumption, indicating excess energy generation that can be stored for future use.

In conclusion, employing a solar PV-driven VCR system with low GWP refrigerants offers an energy-efficient and environmentally friendly cooling solution for the Ghardaïa region.

Utilizing R1234ze as the refrigerant significantly enhances system performance, resulting in noteworthy energy savings and cost reductions. Further research is necessary to assess the feasibility and scalability of implementing this system for commercial applications.

CHAPTER 4

EXERGETIC PERFORMANCE ANALYSIS

Chapter 4

Exergetic performance analysis

4.1 Introduction

Exergy analysis proves valuable in identifying actual thermodynamic losses and enhancing the environmental and economic efficiency of systems, particularly in vapor compression refrigeration (VCR) systems. In this chapter, exergy analyses was performed for the previous PVsolar VCR system using R1234ze(E) as an ecological alternative of R134a refrigerant in the region of Ghardaïa (Southern Algeria). A numerical model was developed in MATLAB software to calculate losses in different system components and determine the exergy efficiency of the solar refrigeration system. In addition, a parametric study was carried out to examine the influence of evaporating and ambient temperatures on the system's exergy destruction and efficiency.

4.2 Definition of exergy

In its simplest terms, exergy is the measure of the maximum work a system can perform when it is brought into equilibrium with a reference environment.

Example: imagine having a full battery in a mobile phone. The exergy of that battery would be its potential to perform tasks such as taking photos or making calls.

In a nutshell, exergy is the 'useful' energy within a system that can be utilised to do work. Despite its importance, exergy's concept isn't always clear-cut. It's worth deep-diving a little:

Exergy takes into account both the system and its environment. Unlike energy, which is always conserved (according to the first law of thermodynamics), Exergy isn't always conserved and can be destroyed (in line with the second law of thermodynamics). This 'destruction' is often due to irreversibility in a system, such as friction.

a- Difference between Exergy and Energy

While both exergy and energy play vital roles in engineering thermodynamics, they are not the same.

Energy is the ability to do work, while Exergy is the maximum useful work possible from an energy source when it reaches equilibrium with a dead state.

This might sound a little tricky, so let's break it down with a suitable analogy:

Picture a waterfall: the total amount of water flowing is the energy. The part of the water that can be captured and used to rotate a turbine is the exergy.

Table 4.1: Differences between exergy and energy

Exergy	Energy
Can be destroyed	Always conserved
Depends on the environment	Independent of the environment
Non-conservative property	Conservative property

b- Exergy transfer equation

To fully grasp the exergy transfer equation, we must first understand how exergy transfer occurs. Exergy transfer can happen via heat transfer, work, and mass flow. Now, let's examine these transfer methods:

Heat transfer: although it might seem counter-intuitive, not all heat transferred can be converted into work. It depends on the temperature at which the heat transfer occurs. The amount of exergy during heat transfer can be defined as: $Q.\left(1 - \left(\frac{T0}{T}\right)\right)$

with **T0**: being the environmental temperature, **T** the temperature at which the heat transfer occurs, and **Q** the quantity of heat transferred.

Work: in an ideal scenario, all work potential can be converted into useful work, meaning there's no exergy loss.

Mass flow: the exergy transfer due to mass flow occurs when mass enters or leaves the system. It is calculated from the flow exergy per unit mass **(Ψ),** multiplied by the mass flow rate **(ṁ).**

After familiarizing with the concepts above, we can understand the exergy transfer equation, which is formulated as:

$$Extransfer = \dot{m}(\Psi in - \Psi out) + Q\left(1 - \left(\frac{T0}{T}\right)\right)$$

This equation essentially highlights each path through which exergy can enter or exit a system and the quantification thereof.

c- Understanding exergy through real world examples

Often, the best way to grasp complex engineering concepts like exergy is through real life examples. These examples can provide a tangible understanding and vivid illustration of the principles in an easily relatable and comprehendible manner. Let's explore some. Various examples illustrating exergy in everyday life

-Heating a room: consider the usage of a heater to warm a room. As the heater operates, it converts electrical energy into thermal energy to increase the room's temperature. If the outside temperature is lower than the room's temperature, heat will naturally flow outside, until an equilibrium is reached. The exergy in this case is the potential of the heater to warm up the room until it reaches the desired temperature.

-Charging a phone: when charging a phone, the electrical energy from the grid is transferred into the phone's battery, storing potential energy. This stored energy, or the battery's ability to do work, for instance, lighting up the screen or running applications, can be referred to as the exergy.

-Driving a car: a running car engine demonstrates exergy at work. The fuel (often petrol or diesel) contains chemical potential energy, which, when burnt in the engine, creates heat. Some of this heat is useful and is converted into mechanical work to move the car (this is the exergy), while the rest is expelled as exhaust, representing exergy loss as that could not be converted into useful work. These examples offer a glimpse into how exergy plays a part in everyday experiences, and how it's always tied to the efficient use of energy.

d- Examples of exergy applications in engineering

Exergy analysis has emerged as an essential tool in the engineering sector, enabling the design and optimisation of energy systems. Here are key areas where the concept of exergy is applied:

-Energy production: power plants, whether it's a coal-fired one, a nuclear one, or a renewable energy station like solar or wind, are grounded in the conversion of one form of energy into electrical energy. An efficient plant maximises its exergy, meaning it converts as much input energy as possible into useful work, i.e., electricity.

-Transportation: areas like the design of vehicles or the devising of fuel efficient travel routes use exergy analysis for optimisation.

For instance, in designing a car engine, engineers strive to maximise the exergy, i.e., convert as much chemical energy from the fuel into mechanical work to drive the car.

-Heating, Ventilation, and Air Conditioning (HVAC): the design of efficient HVAC systems is another practical application of exergy analysis. With the goal being to heat, cool, or ventilate a space using minimal energy, an understanding of exergy helps to design systems that limit energy waste.

-Industrial processes: many industrial processes involve the conversion of energy. For instance, a steel manufacturing plant involves heating processes where exergy losses need to be minimised. Exergy analysis can help identify where losses occur and suggest appropriate remedial measures.

e- The role of exergy in engineering thermodynamics

In engineering thermodynamics, exergy is employed as a powerful analytical tool, providing insight into the efficiency of energy utilisation within a system. Instead of merely focusing on energy conservation, exergy analysis allows examination of the quality of energy and its ability to do work.

Exergy is the maximum useful work that can be extracted from a system in a specific environment. The analysis of exergy helps identify where and why performance loss occurs, leading to opportunities for system improvement. Two primary exergy destruction points tend to be heat loss and friction. By identifying these inefficiencies, engineers can find ways to optimise system performance and reduce energy wastage. Taking a steam power plant as an example, traditional thermodynamic analysis may not contemplate the quality or usability of the energy. Whereas, exergy analysis can highlight performance losses, such as wasted heat potential, and provide a deeper understanding of where useful work can be maximised. Exergy is used in the calculation of various thermodynamic principles including:

-First law efficiency: this is the ratio of actual work output to the maximum possible work output, best described with the formula: n I = W actual/W ideal

-Second law efficiency: this is the ratio of actual heat transfer to reversible heat transfer, given by the formula: n II = Q actual/Q reversible

-Exergetic efficiency: this is the ratio of useful exergy output to the exergy input, generally given by: n Ex = Ex useful/ Ex input

4.3 Exergy analisys

4.3.1 Exergy analisys of photovoltaic panels

The equations used for the exergy analysis of photovoltaic panels based on previous research work are as follows:

Using the first law of thermodynamics:

$$Exin - Exout = Exloss \quad (4.1)$$

The energy conversion efficiency of the solar PV (**ηpc**) is calculated from the following equation (Sahin et al [242] ; Joshi et al [243]):

$$\eta pc = \frac{Voc \times Isc \times FF}{A \times G} \quad (4.2)$$

The electric power output of PV is:

$$Pel = I \times V \quad (4.3)$$

The maximum output power is given by:

$$Pmax = VOC \times ISC \times FF = Vmp \times Imp \quad (4.4)$$

$$Exergy\ Input = Exergy\ Output + Exergy\ Loss \quad (4.5)$$

The exergy efficiency of the solar PV can be defined as the ratio of the exergy gained by the solar PV (exergy output) to the exergy of the solar radiation (exergy input) (Petela [244]):

$$\eta ex = \frac{Exoutput}{Exinput} \quad (4.6)$$

Inlet exergy of a PV system includes only solar radiation intensity exergy (Petela [244] ; [245]):

$$Exin = (A.G).\left(1 - \left(\frac{4}{3}\right).\left(\frac{Ta}{Ts}\right) + \left(\frac{1}{3}\right).\left(\frac{Ta}{Ts}\right)^4\right) \quad (4.7)$$

The exergy output of the PV system can be calculated as outlet exergy for a PV system, including thermal exergy and electrical exergies (Sarhaddi et al. [246]):

$$Exout = Exthermal + Exelectrical \quad (4.8)$$

Exergy of the thermal energy:

$$Exthermal = Q.(1 - \left(\frac{Ta}{Tm}\right) \quad (4.9)$$

where:

$$Q = U.A.(Tm - Ta) \quad (4.10)$$

The overall heat loss coefficient of a PV module includes convection and radiation losses:

$$U = hconv + hrad \quad (4.11)$$

Convective heat transfer coefficient (Boyle [247]):

$$hconv = 2.8 + 3Vw \quad (4.12)$$

Radiative heat transfer coefficient between PV array and surroundings (Watmuff et al [248]):

$$hrad = \varepsilon\sigma(Tsky + Tm).(Tsky^2 + Tm^2) \quad (4.13)$$

Effective temperature of the sky (Watmuff et al [248]):

$$Tsky = Ta - 6 \quad (4.14)$$

Temperature of the module can be calculated on the basis of the NOCT value:

$$Tm = Ta + ((NOCT - 20) \cdot \left(\frac{G}{800}\right)) \quad (4.15)$$

Electrical exergy in the output electrical power of the PV module (Joshi et al [243])

$$Exelectrical = Voc \times Isc \times FF \quad (4.16)$$

$$Pmax = Ppvu.\left(1 - \left(\left(-\frac{CoeffTPmax}{100}\right).(Tm - (25 + 273.15))\right)\right) \quad (4.17)$$

$$\eta energy = \left(\frac{Pmax}{1000*A}\right).100 \quad (4.18)$$

4.3.2 Exergy analysis of vapor compression refrigeration system VCR

The equations used for the exergy analysis of vapor compression refrigeration system based on previous research work are as follows:

The specific exergy in any state is (Bejan et al [249]) :

$$\dot{E}x = \dot{m}r.((h - h0) - T0(S - S0) \quad (4.19)$$

where $h0$ and S0 are the specific enthalpy and entropy of the fluid, respectively at the environmental conditions $T0$ and $P0$.

The total exergy balance, presented in a rate form, is described as [250]:

$$\sum_{in}\left(1 - \frac{T0}{Ti}\right).\dot{Q}\imath + \dot{W}in + \sum_{in}\dot{m}\imath.exi = \sum_{out}\left(1 - \frac{T0}{Ti}\right).\dot{Q}\imath + \dot{W}out +$$

$$\sum_{out}\dot{m}\imath.exi + E\dot{X}D \quad (4.20)$$

Exergy efficiency serves as a critical metric for assessing the thermodynamic effectiveness of a system or its components. Generally, exergetic efficiency is defined as [251]:

$$\eta ex = \frac{\sum E\dot{X}\imath n}{\sum EX\dot{o}ut} = 1 - \frac{\sum E\dot{X}D}{\sum E\dot{X}\imath n} \quad (4.21)$$

Exergy destruction (ĖD) or internal exergy destruction losses which are caused by irreversibilites of the system is the algebric sum of total exergy at the inlet and outlet of the system. General exergy balance is given by (Dincer and Kanoglu [252]):

$$\dot{E}D = \dot{E}in - \dot{E}out \tag{4.22}$$

The exergy destruction and exergetic efficiency in each component of vapor compression cycle is given by the following equations [253]):

Evaporator:

$$\left(\dot{E}\dot{D}\right)evp = \dot{E}\dot{X}4 + \dot{Q}e\left(1 - \left(\frac{T0}{Tb}\right)\right) - \dot{E}\dot{X}1 \tag{4.23}$$

Compressor:

$$\left(\dot{E}\dot{D}\right)comp = \dot{E}\dot{X}1 + \dot{W}comp - \dot{E}\dot{X}2 \tag{4.24}$$

Condenser:

$$\left(\dot{E}\dot{D}\right)cond = \dot{E}\dot{X}2 - \dot{E}\dot{X}3 \tag{4.25}$$

Expansion valve:

$$\left(\dot{E}\dot{D}\right)exp = \dot{E}\dot{X}3 - \dot{E}\dot{X}4 \tag{4.26}$$

Total exergy destruction of the system is the sum of exergy destruction in each component of the system.

The total exergy destruction in vapor compression cycle is given by:

$$\Sigma\left(\dot{E}\dot{D}\right) = \left(\dot{E}\dot{D}\right)evp + \left(\dot{E}\dot{D}\right)comp + \left(\dot{E}\dot{D}\right)cond + \left(\dot{E}\dot{D}\right)exp \tag{4.27}$$

Exergetic efficiency is an important parameter for evaluating thermodynamic performance of a system or a system component. In general, exergetic efficiency is defined as (Dincer and Kanoglu [252]):

$$\eta ex = \frac{\Sigma E\dot{o}ut}{\Sigma\dot{E}in} = 1 - \frac{\Sigma\dot{\dot{E}}D}{\Sigma(\dot{E}in)} \tag{4.28}$$

For a VCR system, the exergy efficiency is determined by the ratio of the exergy absorbed in the evaporator from the cooled space at the temperature *T*b to the actual compressor work input (Ẇcomp) (Arora and Kaushik [254]):

$$\eta ex = \frac{\left|\dot{Q}e\left(1-\left(\frac{T0}{Tb}\right)\right)\right|}{\dot{W}comp} \tag{4.29}$$

4.3.3 Exergy analysis of global system (PV+ vapor compression refrigeration cycle VCR)

The exergetic efficiency of global system (PV+ vapor compression refrigeration cycle VCR) is the ratio of exergy in products to the exergy input, it is given by Dalya Amjed Omer et al [255]):

$$\eta ex = \frac{\left|\dot{Q}e \left(1-\left(\frac{T0}{Tb}\right)\right)\right|}{Exin} \quad (4.30)$$

Total exergy destruction of the global system (PV+ vapor compression refrigeration cycle) is the sum of exergy destruction in each component of the system PV and vapor compression refrigeration cycle it is expressed as:

$$\Sigma\left(\dot{E}D\right)_{sys} = \left(\dot{E}D\right)evp + \left(\dot{E}D\right)comp + \left(\dot{E}D\right)cond + \left(\dot{E}D\right)exp + Exloss \quad (4.31)$$

4.4 Results and discussion

4.4.1 Exergy analysis of the PV system

The climatic data used in this study (ambient temperature and solar radiation) were measured at the meteorological station situated in the Renewable Energy Applied Research Unit (URAER), Ghardaia.Figure 4.1 depicts the input exergy and electrical exergy of the PV module on July 21. It is obvious from this figure that the electrical exergy generated by the PV module is significantly lower than what could potentially be obtained, primarily due to substantial exergy loss resulting from the irreversibility of the PV system, such as thermal losses, optical losses, and non-ideal behavior of PV materials. The input exergy pattern closely tracks the global irradiance, with larger differences observed at higher irradiance levels. This signifies that the solar exergy, driven by the sun's high temperature, holds significant potential for performing useful work. it can be also observed that solar irradiation and exergy input rise as sunlight intensifies, peaking around noon. Following this peak, they gradually decline as evening approaches, with minimal to no solar energy influence between 8:00 PM and 4:00 AM.

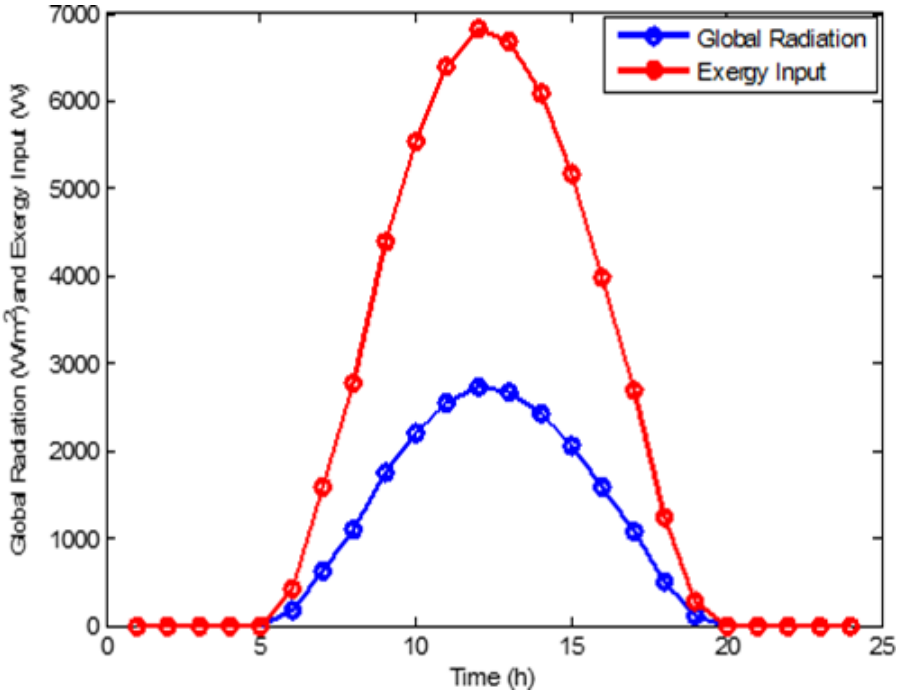


Figure 4.1: Hourly variation of solar radiation intensity and input exergy

Figure 4.2 shows the input exergy and electrical exergy of the PV module on July 21. It is clearly understood from the figure that electrical exergy from the PV module is much less than could be extracted, because of major loss of exergy as a result of irreversibility.

It should be noted that the maximum exergy input is 6835,44 W at 12:00 PM, and that the maximum electrical exergy extracted is 1073,75 W also at 12:00 PM.

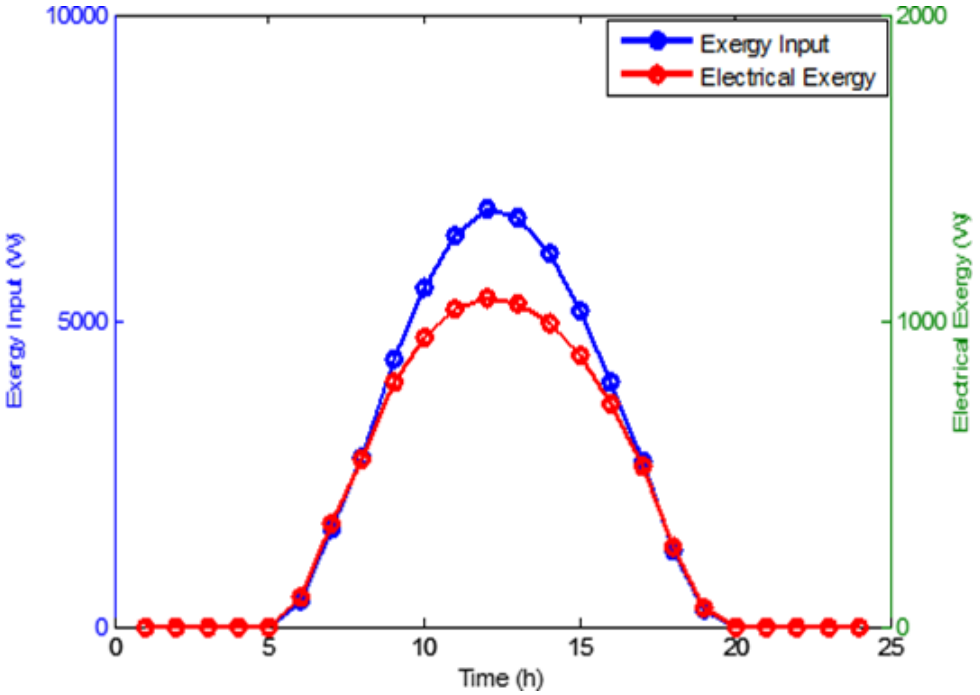


Figure 4.2: Hourly variation of input solar exergy and electrical exergy

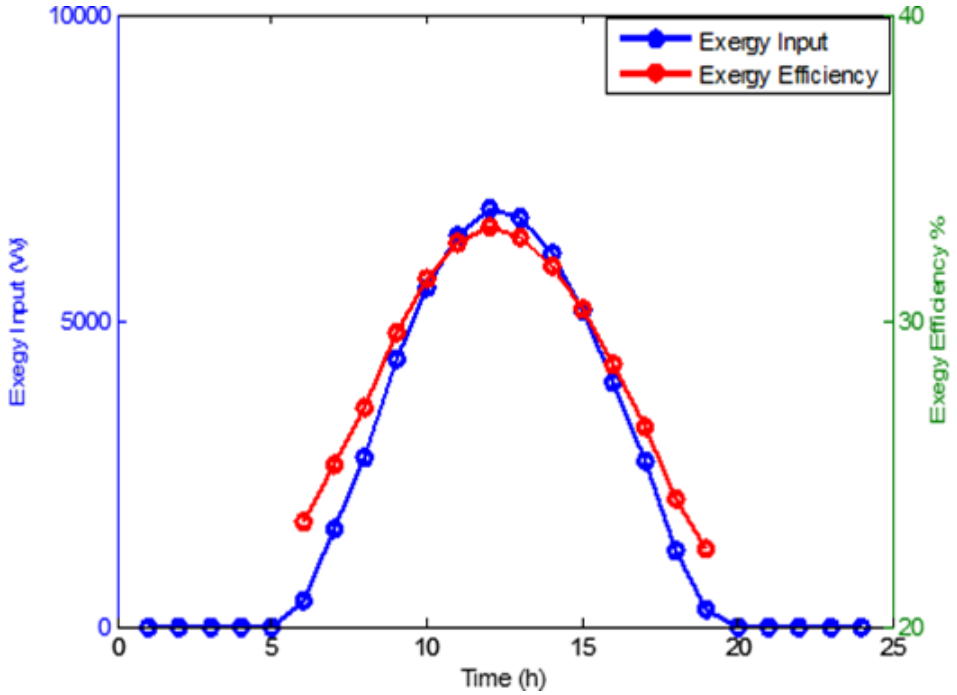


Figure 4.3: Hourly variation of input solar exergy and exergy efficiency

Figure 4.3 illustrates the fluctuation of exergy efficiency and input exergy on the PV module. The exergy efficiency of the PV system remains relatively modest, reaching its highest point at noon with a value of 33.05%, considerably lower than the theoretically ideal 100% reversible process. This inefficiency is attributed to the irreversible nature of the PV conversion process, leading to a notable dissipation of incident solar exergy on the module. Despite the widespread use and advantages of conventionally available silicon modules, like mono-crystalline silicon, they still incur substantial exergy losses. Notably, mono-crystalline silicon cells, employed in this study, offer the highest efficiency among the three most common crystalline silicon cell technologies, reaching up to 20%. Additionally, it's observed that the exergy efficiency of the PV module rises as solar intensity increases.

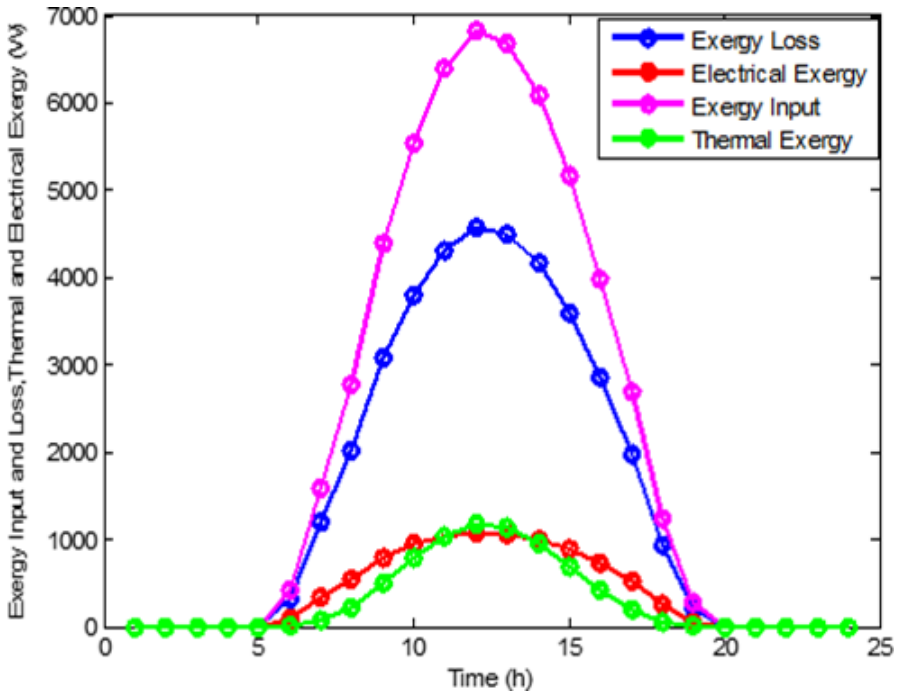


Figure 4.4: Hourly variation of destroyed exergy, solar input exergy, electrical exergy and thermal exergy

Figure 4.4 displays the distribution of exergy loss, electrical exergy, exergy input, and thermal exergy on July 21. As shown in this figure, the trend of the loss exergy variation follows that of the input exergy, and the relative loss of exergy exceeds 66% at noon. This substantial loss highlights the inefficiency in harnessing the high exergy content of sunlight by current silicon modules. The exergy efficiency of conventional silicon solar PV panels is notably low due to the low quality of the output energy, leading to significant exergy losses within the panels.

The electric efficiency is higher than thermal efficiency, which means that most of the heat has been wasted and absorbed by the solar panel.

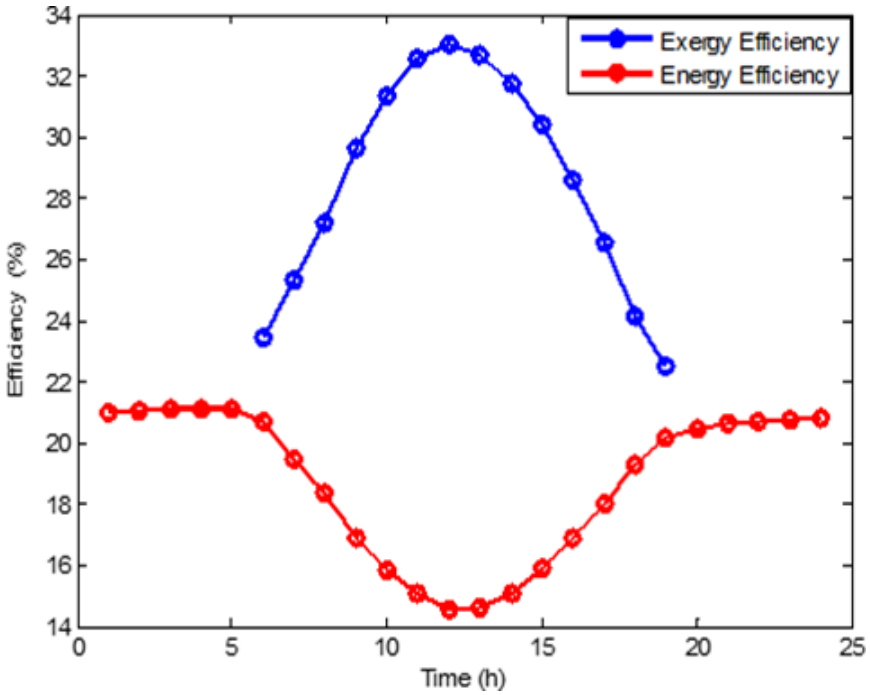


Figure 4.5: Hourly variation of energy and exergy efficiencies

Figure 4.5 shows the hourly changes in energy and exergy efficiencies of the PV system. It can be seen that the maximum energy and exergy efficiency values at noon are 21.12 % and 33.05 %, respectively.

As temperature increases, the exergy efficiency increases while the energy efficiency drops due to heat losses from the system. The results agree with the findings of Oruc et al. [256]. It can also be seen that the exergy efficiency is much higher than the energy efficiency because of the substantial degradation of energy quality imposed by the second law of thermodynamics.

To achieve optimal energy and exergy efficiencies, it is imperative to maintain the temperature of the PV module close to its operating temperature, which essentially means controlling the PV module temperature through surface cooling using either water or air.

4.4.2 Exergy analysis of the VCR system

Figure 4.6 illustrates how the exergy efficiency of the VCR system is influenced by ambient temperature for both refrigerants R134a and R1234ze(E).

The exergy efficiency increases as ambient temperature rises due to the increased compressor work, but the increase of $\left|\dot{Q}e\left(1-\left(\frac{T0}{Tb}\right)\right)\right|$ is greater, so the result $\frac{\left|\dot{Q}e\left(1-\left(\frac{T0}{Tb}\right)\right)\right|}{\dot{W}\,comp}$ increases.

However, R1234ze(E) exhibits higher exergy efficiency compared to R134a with maximum values of 28.06% and 14.95%, respectively. The lower irreversibility observed when using R1234ze(E) compared to R134a can be attributed to several factors. First, R1234ze(E) exhibits more favorable thermodynamic properties such as lower pressure ratios and higher volumetric efficiencies, which result in reduced thermodynamic losses during compression and expansion processes. In addition, R1234ze(E) demonstrates superior heat transfer performance, particularly at higher temperatures, leading to more efficient heat exchange in the evaporator and condenser and minimizing irreversibility associated with heat transfer processes. These results are in agreement with previous findings from other studies [257,258].

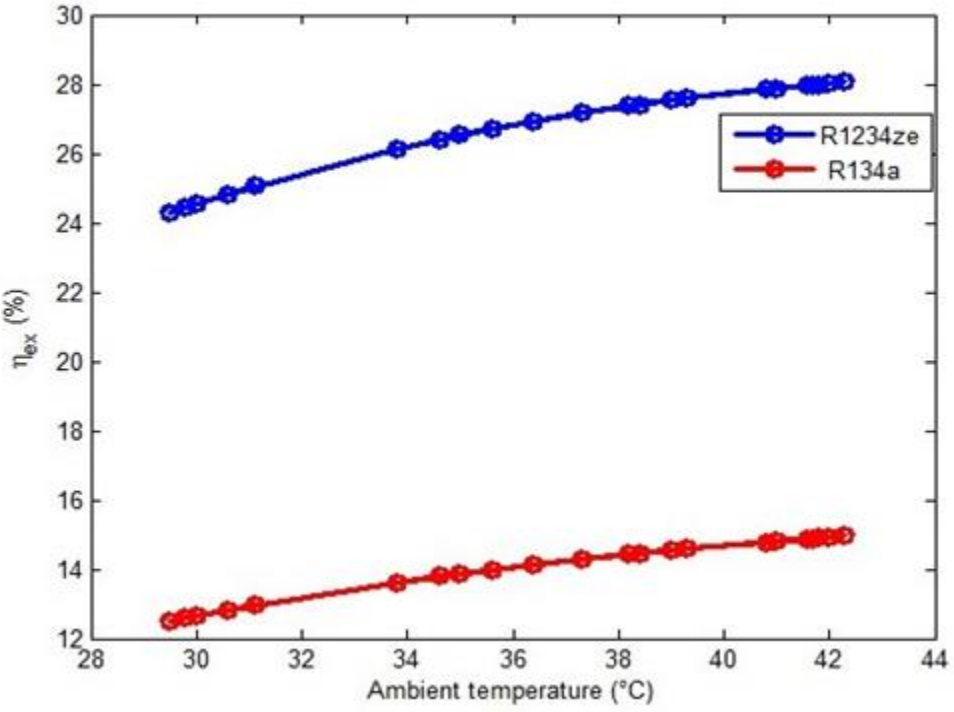


Figure 4.6: Variation of exergy efficiency of the VCR cycle with ambient temperature ($Tev = 0°C$)

The hourly variations of exergy efficiency of the vapor compression refrigeration system for both refrigerants R1234ze and R134a are plotted in Figure 4.7. The exergy efficiency of the system is maximum at 14:00 PM with a value of 28,06 % and 14,95 %, and minimum at 3:00 AM with a value of 24,29 % and 12,51 % for R1234ze and R134a respectively.

It is observed that the shape of the variation of exergy efficiency follows that of the ambient temperature for the same reasons explained for Figure 4.6. The exergy efficiency of R1234ze is higher than that of R134a throughout the day.

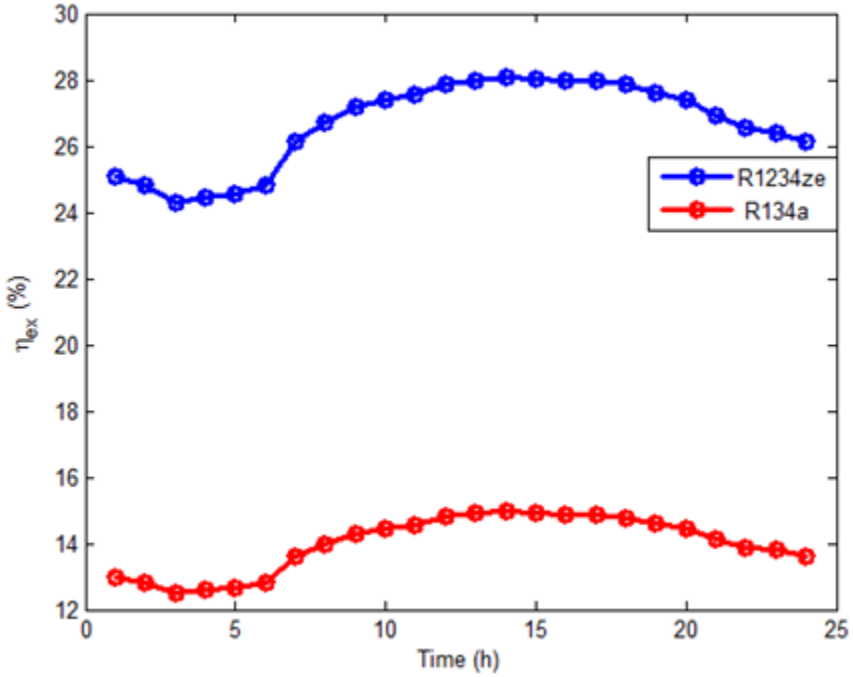


Figure 4.7: Hourly variation of exergy efficiency of the vapor compression refrigeration cycle (Tev = 0°C)

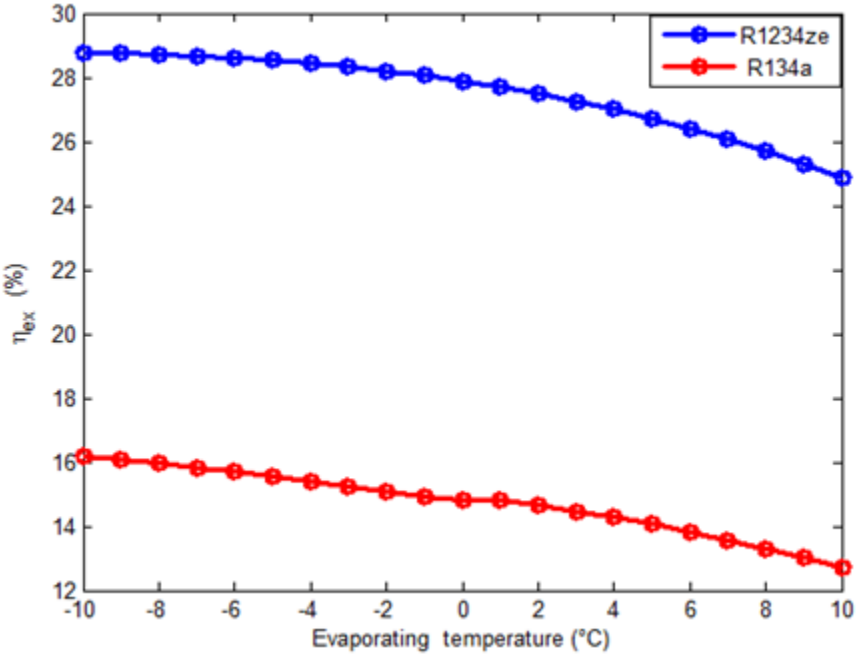


Figure 4.8: Variation of exergy efficiency of the VCR cycle with evaporating temperature

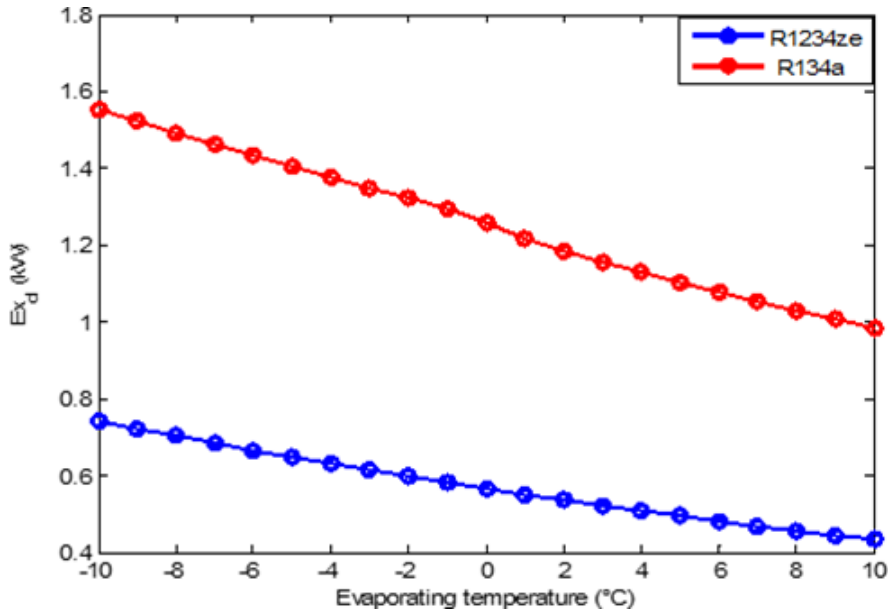


Figure 4.9: Variation of total exergy destruction of the VCR cycle with evaporating temperature

Figure 4.8 illustrates the changes in exergy efficiency with evaporating temperature for both R134a and R1234ze(E) refrigerants in the VCR cycle. As the evaporating temperature increases, the exergy efficiency decreases due to the decrease of the compressor work and the increase of heat transfer in the evaporator. The trend is the same for both refrigerants. However, the irreversibilities within the R1234ze(E) cycle are notably lower compared to that of R134a. as shown in Figure 4.9. The average second-law efficiency increase is about 45% when using R1234ze(E) in the VCR cycle. The average exergy destruction for R1234ze(E) is around 55% smaller than R134a.

Figure 4.10 depicts the hourly variation of total exergy destruction of the vapor compression refrigeration cycle for both refrigerants R1234ze and R134a. The total exergy destruction increase with the ambient temperature and their shape follows him.

For the various ambient temperatures, and throughout the day the irreversibility when using R1234ze are lower than that of R134a. With a total exergy destruction of 0,58 kW for R1234ze, and 1,30 kW for R134a we have a difference of 55,38 % at 14:00 PM.

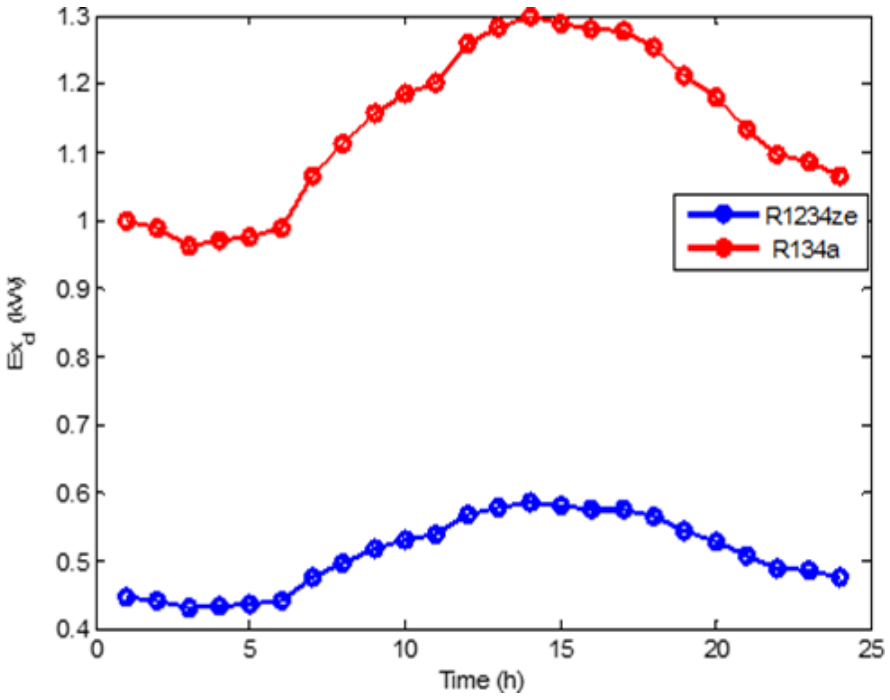


Figure 4.10: Hourly variation of total exergy destruction of the vapor compression refrigeration cycle (Tev = 0°C)

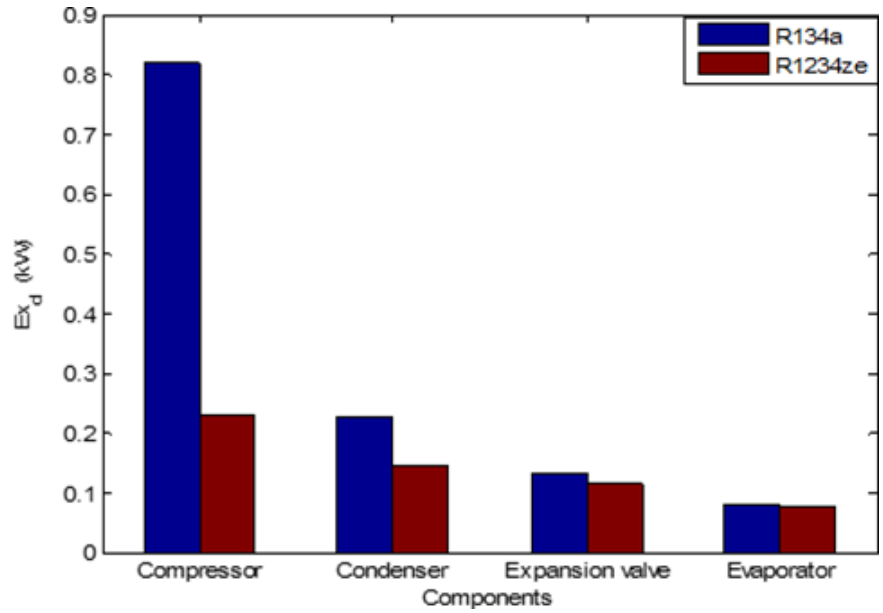


Figure 4.11: Exergy destruction in each component of the VCR cycle

The exergy destructions of the main components of the VCR system are compared in Figure 4.11 for $Tev = 0°C$ at noon on July 21 using both studied refrigerants.

It can be seen that the compressor exhibits the highest exergy destruction, followed by the condenser, expansion valve, and evaporator. For R1234ze(E) fluid, the total irreversibility is 0.57 kW, distributed as follows: compressor 40.71%, condenser 25.77%, expansion valve 20.07%, and evaporator 13.45%. On the other hand, the total irreversibility for R134a refrigerant is 0.82 kW, with 65.09% occurring in the compressor, 18.04% in the condenser, 10.50% in the expansion valve, and 6.37%. in the evaporator.

Therefore, improving the compressor's efficiency will have the most significant impact on reducing overall system irreversibility and enhancing exergy efficiency. This can be achieved by implementing advanced designs like variable-speed or multi-stage compressors, using materials with superior thermal properties and durability, optimizing lubrication systems to reduce friction losses, maintaining a rigorous maintenance schedule to ensure peak performance, and integrating heat recovery systems to utilize waste heat. These measures will collectively reduce energy losses and improve the compressor's efficiency, leading to a more efficient and effective overall system.

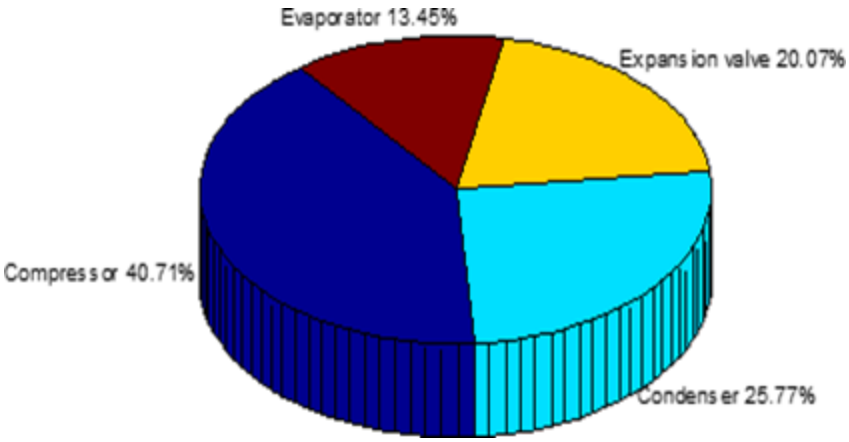


Figure 4.12: The ration of exergy destruction in each component of the vapor compression refrigeration cycle at Tev = 0°C and t = 12:00 PM (refrigerant R1234ze)

The Figures 4.12 and 4.13 present the relative irreversibility of each component using R1234ze and R134a, respectively. The compressor is responsible for the highest exergy destruction, followed by the condenser, the expansion valve and the evaporator. The irreversibility of the cycle using R1234ze is 0.57 kW. The contributions of the different components are 0,23 kW (40.71 %) for the compressor, 0,14 kW (25.77 %) for the condenser, 0,11 kW (20.07 %) for the expansion valve and 0,076 kW (13.45 %) for the evaporator.

The irreversibility corresponding to the R134a is 0,82 kW (65.09 %) for the compressor, 0,23 kW (18.04 %) for the condenser, 0,13 kW (10.50 %) for the expansion valve and 0,08 kW (6.37 %) for the evaporator. The total exergy destruction is 1,26 kW. The irreversibility of all components and the whole R1234ze vapor compression refrigeration system is lower than that of R134a. The improvements are 71.95 % for the compressor, 39.13 % for the condenser, 15.38 % for the expansion valve, 5 % for the evaporator and 54.76 % for the entire system.

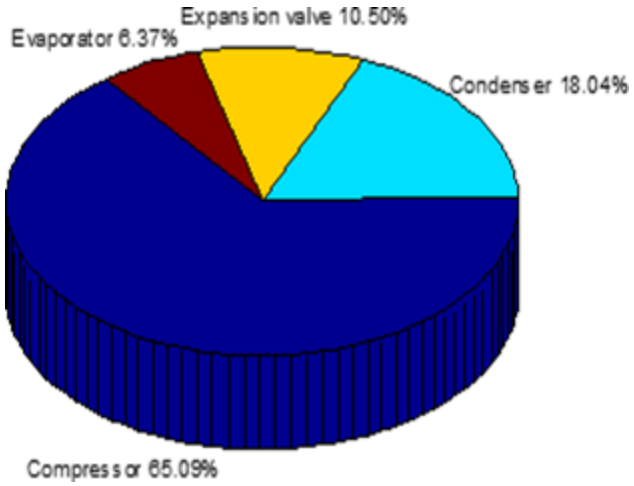


Figure 4.13: The ration of exergy destruction in each component of the vapor compression refrigeration cycle at Tev = 0°C and t = 12:00 PM (refrigerant R134a)

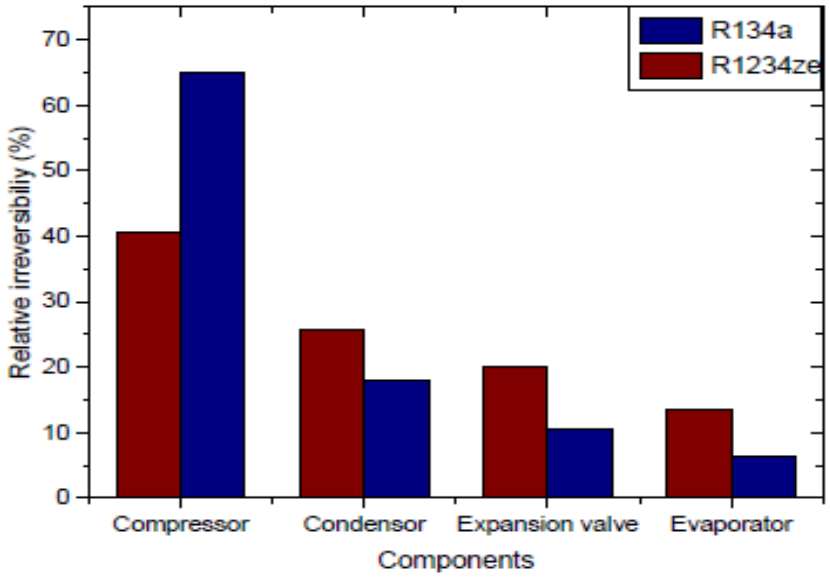


Figure 4.14: Relatives irreversibilities for different components

Figures 4.14 depict the comparative irreversibility of individual components when utilizing R134a and R1234ze(E), respectively. Across all components and the whole system, R1234ze(E) exhibits lower irreversibility compared to R134a. Specifically, the improvements made with R1234ze(E) are 71.95% for the compressor, 39.13% for the condenser, 15.38% for the expansion valve, 5% for the evaporator, and 54.76% for the overall system.

4.4.3 Exergy analysis of the global solar refrigeration system (PV + VCR)

If we talk about the global solar refrigeration system composed of the solar system of photovoltaic panels necessary for the operation of the global system, and the vapor compression refrigeration system ,the variations of exergy efficiency of the global solar refrigeration system and of the solar system of photovoltaic panels depending on the evaporating temperature, for both refrigerants R1234ze and R134a from -10 °C to 10 °C, at t = 12:00 PM on July 21 are illustrated in Figure 4.15. The exergy efficiency of solar system of photovoltaic panels, remains constant and it has the same value for the both refrigerants studied, because in this case the exergy efficiency does notdepend on the evaporating temperature, characteristics of the refrigerants, or the surface of thesolar panels used. it has a value of 33,05 %.

On the other hand, for the entire interval of evaporating temperature studied, the exergy efficiency of the global solar refrigeration system operating with R1234ze is higher than that of R134a for the reason of the large surface area required of solar panels in the case of R134a compared to that in the case of R1234ze with a value of 1,46 % and 0,88 % at -10 °C with a difference of 39,73 %, and a value of 1,05 % and 0,70 % at 10 °C with a difference of 33.33 %, for R1234ze and R134a respectively.

The variation of exergy efficiency of the global solar refrigeration system is lower than that of vapor compression refrigeration system for both refrigerants R1234ze and R134a.due to the high solar exergy at the entrance in the global system.

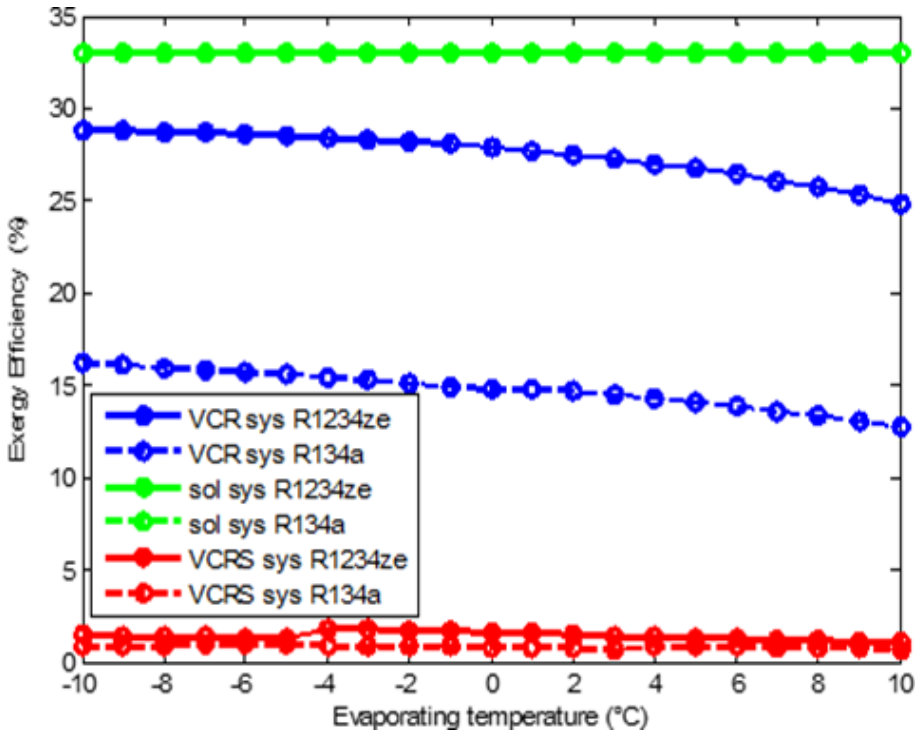


Figure 4.15: Variation of exergy efficiency of VCR sys, Sol sys, and VCRS sys depending on the evaporating temperature, at t = 12:00 PM

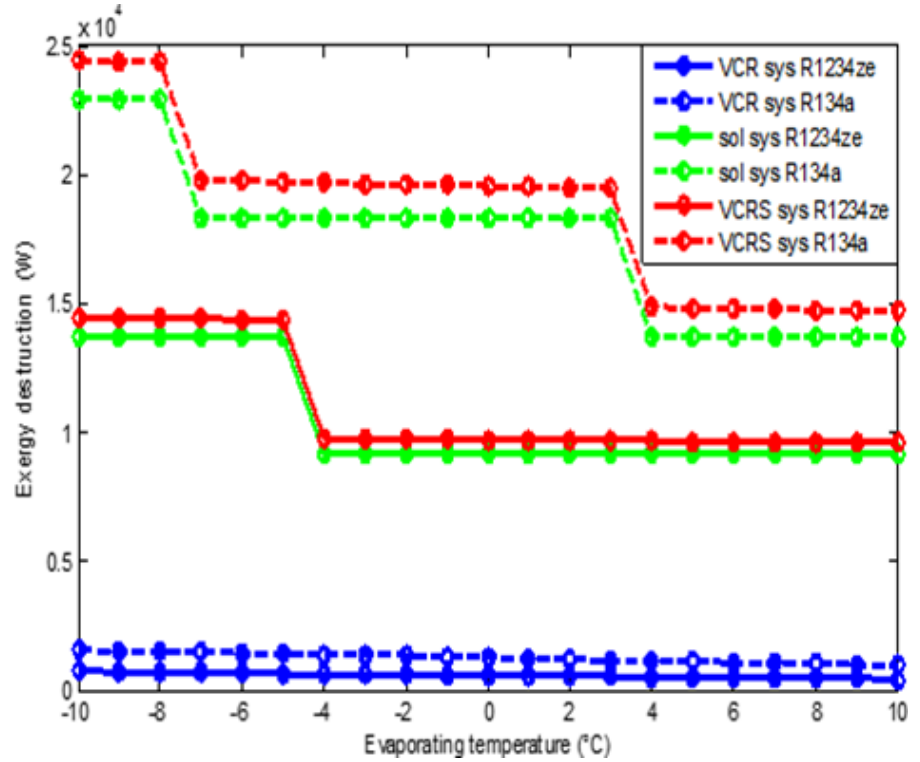


Figure 4.16: Variation of total exergy destruction of VCR sys, Sol sys,and VCRS sys depending on the evaporating temperature, at t = 12:00 PM

The variations of total exergy destruction of the global solar refrigeration system and of the solar system of photovoltaic panels depending on the evaporating temperature for both refrigerants R1234ze and R134a from -10 °C to 10 °C, at t = 12:00 PM on July 21 are presented in Figure 4.16. The total exergy destruction of solar system of photovoltaic panels, de-creases with increasing in evaporating temperature and that of R1234ze is lower than that of R134a because it depends mainly on the surface of the solar photovoltaic panels of which it is greater in the case of R134a and decreases in stages along the evaporating temperature interval studied. It is maximum at -10°C with a value of 22880,99 W and 13728,59 W with a difference of 40 %, and minimum at 10°C with a value of 13728,59 W and 9152,40 W with a difference of 33.33 % for R134a and R1234ze respectively.

For the same reason given above, the total exergy destruction of the global solar refrigeration system for both refrigerants studied decreases with increasing in evaporating temperature and that of R1234ze is lower than that of R134a.

It is maximum at -10 °C with a value of 24433,75 W and 14471,21 W with a difference of 40,77 %, and minimum at 10 °C with a value of 14712,61 W and 9585,25 W with a difference of 34,85 %, for R134a and R1234ze respectively.

Once again the total exergy destruction of the global solar refrigeration system is higher than that of vapor compression refrigeration system for both refrigerants R1234ze and R134a, mainly for the reason of the large exergy lost in solar photovoltaic panels.

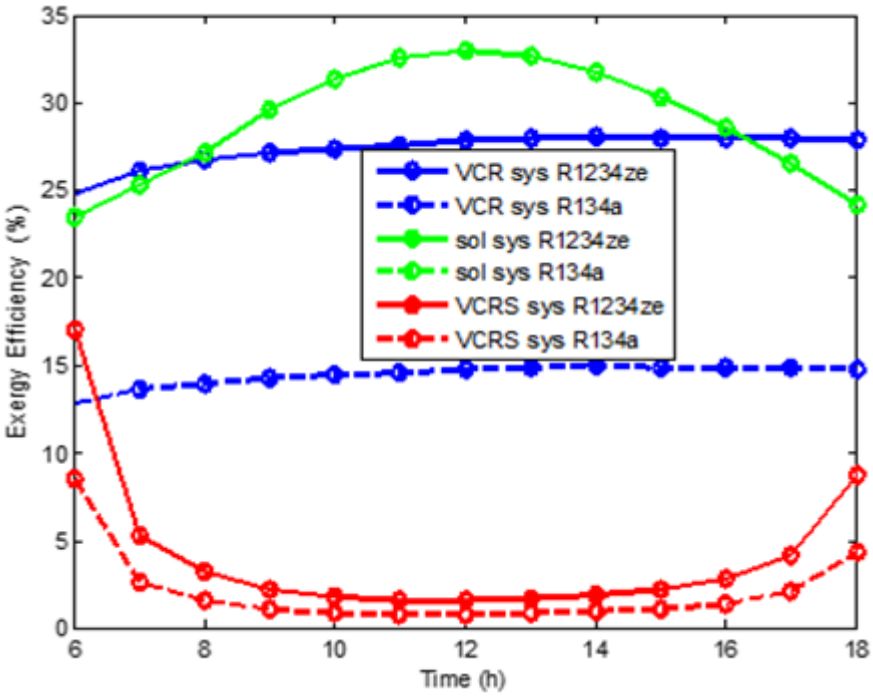


Figure 4.17: Hourly variation of exergy efficiency of VCR sys, Sol sys and VCRS sys, at Tev = 0°C

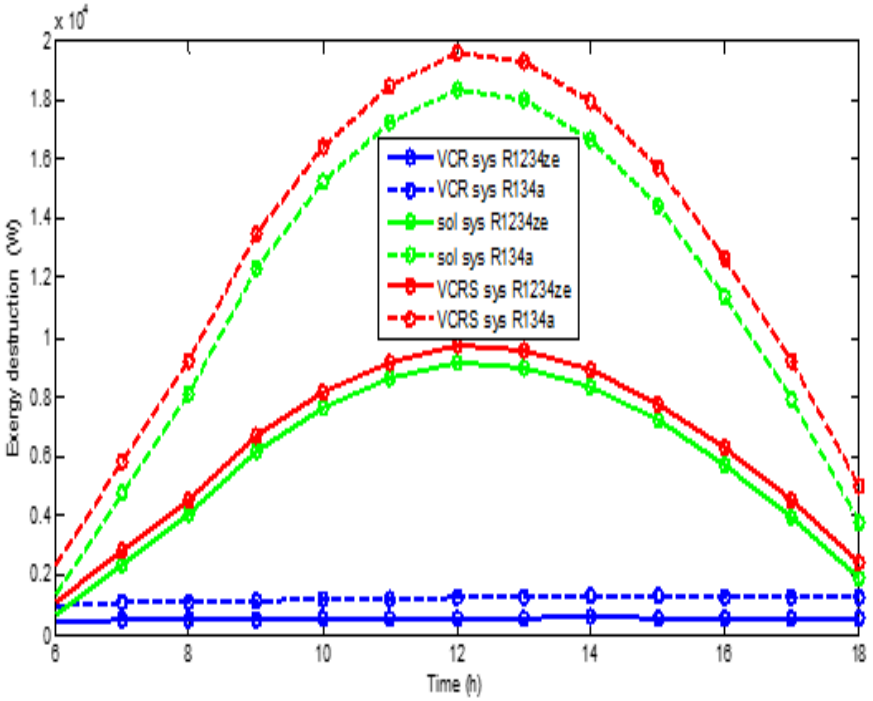


Figure 4.18: Hourly variation of total exergy destruction of VCR sys, Sol sys, and VCRS sys, at Tev = 0°C

The hourly variations of the exergy efficiency of the overall solar refrigeration system and the solar photovoltaic panel system, for the two refrigerants R1234ze and R134a from 6:00 A.M. to 18:00 P.M. at Tevap = 0°C on July 21 are plotted in Figure 4.17.

From 6:00 A.M. to 12:00 P.M the exergy efficiency of the solar system of photovoltaic panels increases with time and it is the same for the two refrigerants studied, because in this case the exergy efficiency follows and depends mainly on the intensity of solar radiation which increases in this interval time, and also depends on the characteristics of the photovoltaic solar panels but not on those of the refrigerants or the surface area of the solar panels used. It is maximum at 12:00 P.M. with a value of 33.05 % and minimum at 6:00 A.M. with a value of 23.44 %.

On the other hand, the exergy efficiency of the overall solar refrigeration system for the two refrigerants studied decreases with time, because in this case it is equal to: $\frac{\left|\dot{Q}e\left(1-\left(\frac{T0}{Tb}\right)\right)\right|}{Exin}$, the Exin term increases in this time interval, so the result decreases. For this entire time interval studied, the exergy efficiency of R1234ze is higher than that of R134a due to the large required surface area of the solar panels in the case of R134a compared to that of R1234ze with a minimum value at 12:00 PM of 1.60 % and 0.80 % with a difference of 50 %, and a maximum value at 6:00 A.M. of 17.03 % and 8.52 % with a difference of 49.97 %, for R1234ze and R134a respectively.

From 12:00 P.M. to 18:00 P.M the exergy efficiency of solar system of photovoltaic panels, decreases over time and it is the same for the both refrigerants studied, because in this case the exergy efficiency follows and depends mainly on the intensity of solar radiation which decreases in this time interval, and also depends on the characteristics of the solar photovoltaic panels but not on those of the refrigerants or of the surface of the solar panels used. It is maximum at 12:00 PM with a value of 33,05 % and minimum at 18:00 PM with a value of 24,15 %. On the other hand, the exergy efficiency of the global solar refrigeration system for both refrigerants studied increases over time, because in this case it is equal to: $\frac{\left|\dot{Q}e\left(1-\left(\frac{T0}{Tb}\right)\right)\right|}{Exin}$, the term Exin decreases in this time interval, so the result increases. For this entire time interval studied, the exergy efficiency of R1234ze is higher than that of R134a for the reason of the large surface area required of solar panels in the case of R134a compared to that in the case of R1234ze with a minimum value at 12:00 PM of 1,60 % and 0,80 % with a difference of 50 %, and a maximum value at 18:00 PM of 8,78 % and 4,39 % with a difference of 50 %, for R1234ze and R134a respectively.

It should be noted that the variation of exergy efficiency of the global solar refrigeration system is lower than that of vapor compression refrigeration system for both refrigerants R1234ze and R134a, due to the high solar exergy at the entrance in the global system.

The hourly variations of total exergy destruction of the global solar refrigeration system and the solar photovoltaic panel system for the two refrigerants R1234ze and R134a from 6:00 A.M. to 12:00 P.M. at Tevap = 0°C on July 21 are presented in Figure 4.18 . The total exergy destruction of the solar system of photovoltaic panels increases with time and that of R1234ze is lower than that of R134a because it follows and depends mainly on the intensity of solar radiation which increases in this time interval, and also depends on the surface of the photovoltaic solar panels of which it is greater in the case of R134a.

It is maximum at 12:00 P.M. with a value of 18304.79 W and 9152.40 W with a difference of 50 %, and minimum at 6:00 A.M. with a value of 1307,99 W and 654 W with a difference of 50 % for R134a and R1234ze respectively.

For the same reasons, the total exergy destruction of the global solar refrigeration system for the two refrigerants studied increases with time and that of R1234ze is lower than that of R134a. It is maximum at 12:00 P.M. with a value of 19564.07 W and 9718.64 W with a difference of 50.32 %, and minimum at 6:00 A.M. with a value of 2296.3W and 1094.4W with a difference of 52.34 %, for R134a. and R1234ze respectively

From 12:00 P.M. to 18:00 P.M the total exergy destruction of solar system of photovoltaic panels, decreases over time and that of R1234ze is lower than that of R134a because it follows and depends mainly on the intensity of solar radiation which decreases in this time interval, and also depends on the surface of the solar photovoltaic panels of which it is greater in the case of R134a.

It is maximum at 12:00 PM with a value of 18304,79 W and 9152,40 W with a difference of 50 %, and minimum at 18:00 AM with a value of 3760,04 W and 1880,02 W with a difference of 50 % for R134a and R1234ze respectively.

For the same reasons, the total exergy destruction of the global solar refrigeration system for both refrigerants studied decrease over time and that of R1234ze is lower than that of R134a.

It is maximum at 12:00 PM with a value of 19564,07 W and 9718,64 W with a difference of 50,32 %, and minimum at 18:00 AM with a value of 5013,49 W and 2443,45 W with a difference of 51,26 %, for R134a and R1234ze respectively.

We also observe that the total exergy destruction of the global solar refrigeration system is higher than that of vapor compression refrigeration system for both refrigerants R1234ze and R134a, mainly due to the large exergy lost in solar photovoltaic panels.

4.5 Industrial implication, recommendations for improvement

The findings of this study have significant industrial implications, particularly for sectors reliant on refrigeration systems, such as food storage, pharmaceuticals, and chemical processing. The demonstrated exergy efficiency improvements with R1234ze(E) as a replacement for R134a highlight several key advantages for industrial applications. Firstly, the substantial improvements in exergy efficiency, especially the 71.95% enhancement in compressor performance, indicate a considerable reduction in energy consumption. This can lead to lower operational costs for industries, which is crucial given the high energy demand for refrigeration systems. Reduced energy consumption translates directly into cost savings, making operations more economically viable.

Moreover, the adoption of R1234ze(E) aligns with global efforts to reduce greenhouse gas emissions and combat climate change. By demonstrating lower irreversibility and improved overall system efficiency, this study supports the transition to eco-friendly refrigerants. This shift can help industries meet environmental regulations and sustainability goals, thus reducing their carbon footprint and contributing to global environmental conservation efforts.

Additionally, the enhanced efficiency and reduced exergy destruction across system components (compressor, condenser, expansion valve, and evaporator) suggest that systems using R1234ze(E) may experience less wear and tear. This can lead to extended equipment lifespan, reduced maintenance needs, and lower replacement costs, which are significant considerations for industrial operations. Longer-lasting equipment and less frequent maintenance can improve operational reliability and reduce downtime.

Furthermore, with increasing regulatory pressures to phase out high-GWP (Global Warming Potential) refrigerants like R134a, the industrial adoption of R1234ze(E) can facilitate compliance with environmental standards and avoid potential penalties. The demonstrated performance benefits provide a strong case for industries to invest in retrofitting or upgrading their existing systems, ensuring they stay ahead of regulatory changes and avoid costly fines.

Also, industries that adopt advanced, eco-friendly refrigeration technologies can enhance their market competitiveness by promoting their commitment to sustainability and energy efficiency. This can be a significant differentiator in markets where consumers and stakeholders increasingly value environmental responsibility. Companies can leverage their green credentials to attract environmentally conscious customers and investors.

Finally, the study's methodology and findings can spur further research and innovation in the development of next-generation refrigeration systems. Industries can leverage these insights to explore new designs, materials, and technologies that further enhance efficiency and sustainability. Continuous innovation can lead to the development of even more advanced refrigeration systems, driving progress in industrial cooling applications.

Finally as we have seen above to reduce the energy destroyed and improve the performance of the system we can improving compressor efficiency which will have the most significant impact on reducing overall system irreversibility and improving exergy efficiency. by implementing advanced designs such as variable speed or variable speed compressors. multiple stages, using materials with superior thermal properties and durability, optimizing lubrication systems to reduce friction losses, maintaining a rigorous maintenance program to ensure optimal performance, and integrating heat recovery systems to use waste heat. These measures will collectively reduce energy losses and improve compressor efficiency, leading to a more efficient and effective overall system.

4.6 Conclusion

A complete exergy study of a solar PV vapor compression refrigeration system located in Ghardaïa region in the south of Algeria is proposed based on a Matlab program, the study compares the exergy performance of R134a and its potential replacement R1234ze, as working fluids.

The study reached the following results :

Environmental conditions have significant effects on exergy loss, electrical exergy, exergy input, and thermal exergy of the SP-VCR system.

• The exergy efficiency of the PV modules is very low (33.05%) indicating that current silicon modules use only a small portion of the considerable exergy content present in solar radiation.

• The maximum energy and exergy efficiency values at noon are 21.12 % and 33.05 %, respectively.

• The exergy efficiency of the SP-VCR system increases with rising ambient temperature and is notably higher with R1234ze(E) compared to R134a.

• The exergy efficiency of the refrigeration system decreases as the evaporating temperature rises, with R1234ze(E) displaying superior performance over R134a.

• Exergy destruction is primarily attributed to the compressor, followed by the condenser, expansion valve, and evaporator.

• R1234ze(E) refrigerant exhibits higher exergy efficiency compared to R134a with maximum values of 28.06% and 14.95%, respectively.

• For the entire interval of evaporating temperature studied, the exergy efficiency of the global solar refrigeration system operating with R1234ze is higher than that with R134a due also to the large surface area required of solar panels in the case of R134a, with a difference from 33.33 %, at 10°C to 39,73 %, at -10 °C .

• The total exergy destruction of the global solar refrigeration system for both refrigerants studied decreases with increasing in evaporating temperature, and that of R1234ze is lower than that of R134a, with a difference from 34.85 %, to 40.77 %, because it mainly depends on the surface area of the photovoltaic solar panels, which it is greater in the case of R134a, and which decreases in stages throughout the evaporating temperature interval studied.

• The exergy efficiency of the global solar refrigeration system for both refrigerants studied decreases over time, (6:00 AM to 12:00 PM), and the exergy efficiency of R1234ze is higher than that of R134a due to the large surface area required of solar panels in the case of R134a compared to that in the case of R1234ze with a difference from 49.97 % to 50 %.

• The total exergy destruction of the global solar refrigeration system for both refrigerants studied increase over time, (6:00 AM to 12:00 PM), and that of R1234ze is lower than that of R134a. with a difference from 50,32 %, to 50.34 %, for the same reason given above.

• The exergy efficiency of the global solar refrigeration system for both refrigerants studied increases over time, (12:00 PM to 18:00 PM), and the exergy efficiency of R1234ze is higher than that of R134a due to the large surface area required of solar panels in the case of R134a compared to that in the case of R1234ze with a difference of 50 %.

• The total exergy destruction of the global solar refrigeration system for both refrigerants studied decrease over time, (12:00 PM to 18:00 PM), and that of R1234ze is lower than that of R134a. with a difference from 50,32 %, to 51,26 %, for the same reason given above.

Finally, despite its modest exergy efficiency and notable exergy destruction, a SP-VCR system using low GWP refrigerants remains a promising environmentally friendly solution, especially for remote locations with ample solar radiation. Furthermore, Enhancements in system design and component characteristics are pivotal for minimizing irreversibilities, particularly within the solar PV panels, which contribute significantly to overall system irreversibilities.

Therefore, it's crucial to maintain the PV module temperature close to its operational level to optimize the exergy efficiency of the entire system.

CONCLUSIONS AND RECOMMENDATIONS

CONCLUSIONS AND RECOMMENDATIONS

This research work has highlighted the energy and environmental interest, and also the solution to the problem of isolated sites by the use on the one hand of the energy produced by photovoltaic solar panels for the power supply of the vapor compression refrigeration systems in the region of Ghardaia in the south of Algeria, and on the other hand to operate its systems with the new generation HFO refrigerant with low GWP as well as low impact on the environment R1234ze as a replacement for HFC R134a fluid with better performance and energy saving. There is a fairly significant potential for solar radiation emitted in this region that can be exploited to provide a sustainable source of electrical energy from solar photovoltaic panel units.

The results of the modeling and performance study of the solar refrigeration system can be summarized as follows:

-R1234ze demonstrates a higher COP compared to R134a, thanks to its lower compressor power requirement and improved thermodynamic efficiency for the same cooling capacity.

-The solar-to-cooling COP declines as temperatures rise, primarily due to increased compressor power consumption and diminished refrigerant performance.

-Although the required surface area of solar PV panels shows minimal variation with ambient temperature, panel temperature directly influences performance and, consequently, affects the required area.

-Cumulative PV power production exceeds compressor power consumption, indicating excess energy generation that can be stored for future use.

Furthermore, the following conclusions can be drawn from the exergy analysis of the system studied:

-In order to have maximum exergy efficiency, PV module temperature should be kept near the cell operating.

-The exergy efficiency of the vapor compression refrigeration system increases with increasing in ambient temperature and it is higher for R1234ze than that of R134a.

-The exergy efficiency of the vapor compression refrigeration system decreases with increasing in evaporating temperature (-10 °C to 10 °C) and it is higher for R1234ze than that of R134a.

-The total exergy destruction of the vapor compression refrigeration system increase with the ambient temperature throughout the day, the irreversibility using R1234ze is lower than that of the R134a.

-The total exergy destruction of the vapor compression refrigeration system decrease with the evaporating temperature, the irreversibility using R1234ze is lower than that of the R134a.

-The compressor is responsible for the highest exergy destruction, followed by the condenser, the expansion valve and the evaporator for both fluids, and if we use R1234ze, the improvements are 71.95 % for the compressor, 39.13 % for the condenser,15.38 % for the expansion valve, 5 % for the evaporator and 54.76 % for the entire system.

-The exergy efficiency of the global solar refrigeration system for both refrigerants studied decreases over time, (6:00 AM to 12:00 PM), and the exergy efficiency of R1234ze is higher than that of R134a due to the large surface area required of solar panels in the case of R134a compared to that in the case of R1234ze with a difference of 50 %.

-The total exergy destruction of the global solar refrigeration system for both refrigerants studied increase over time, (6:00 AM to 12:00 PM), and that of R1234ze is lower than that of R134a, for the same reason given above.

-The exergy efficiency of the global solar refrigeration system for both refrigerants studied increases over time, (12:00 PM to 18:00 PM), and the exergy efficiency of R1234ze is higher than that of R134a due to the large surface area required of solar panels in the case of R134a compared to that in the case of R1234ze with a difference of 50 %.

-The total exergy destruction of the global solar refrigeration system for both refrigerants studied decrease over time, (12:00 PM to 18:00 PM), and that of R1234ze is lower than that of R134a, for the same reason given above.

-For the entire interval of evaporating temperature studied, the exergy efficiency of the global solar refrigeration system operating with R1234ze is higher than that with R134a due also to the large surface area required of solar panels in the case of R134a.

-The total exergy destruction of the global solar refrigeration system for both refrigerants studied decreases with increasing in evaporating temperature, and that of R1234ze is lower than that of R134a, because it mainly depends on the surface area of the photovoltaic solar panels, which it is greater in the case of R134a, and which decreases in stages throughout the evaporating temperature interval studied.

Thus, a more representative validation of the system will only be possible after experimental tests of prototypes which will provide a better understanding of the system, taking into account in particular the fluctuations present in a system powered by an extremely variable and unpredictable intermittent source, such as solar energy.

Finally and to conclude, it is recommended to:

- Carrying out this vapor compression refrigeration system powered by solar photovoltaic panels, and studying :

Its performance in the Ghardaia area, with real thermal loads.

The influence of other factors such as superheating, sub-cooling, the integration of an internal heat exchanger… etc.

The storage batteries (capacity, number, …etc).

- The analysis and simulation was based on the change in one day (July 21) which constitutes the sunniest day of the year with the best solar irradiation conditions.

However, for photovoltaic refrigeration systems, the inherent intermittency and instability of solar radiation is a more concerning issue.

It is therefore recommended to study the system during all months of the year as well as on the least sunny day of the year.

- It is suggested to complete the performance analysis of the solar-powered vapor compression refrigeration system with R1234ze as a refrigerant applied to different specific application scenarios, such as air conditioning, fruit and vegetable preservation, etc., to improve the direction of this study for practical applications.

To finally finish with a techno-economic study of the system.

BIBLIOGRAPHICAL REFERENCES

BIBLIOGRAPHICAL REFERENCES

[1] Cooling for All, "An inquiry into sustainable, affordable and efficient cooling pathways." 2017.

[2] Ecofys, "Savings and benefits of global regulations for energy efficient products." 2015.

[3] J. Henley, "World set to use more energy for cooling than heating." 2015.

[4] International Energy Agency," The Future of Cooling: Opportunities for energy efficient air-conditioning." 2018.

[5] International Energy Agency, " Energy Technology Perspectives." 2017.

[6] G.I.Z., Green Cooling Technologies, " Market trends in selected refrigeration and air conditioning subsectors." 2015.

[7] F. Bouffard and D. S. Kirschen, "Centralised and distributed electricity systems," Energy Policy 2008, vol. 36, pp. 4504–4508.

[8] C. Christofides, "Autonomous photovoltaic power system or connection with .electrical grid. A preliminary feasibility study for small and isolated communities Solar Cells"., vol 26, pp. 165–175, 1989.

[9] G. Venkatarathnam and S. Srinivasa Murthy, "Refrigerants for vapour compression refrigeration systems," Resonance, vol. 17, no. 2, pp. 139–162, 2012, doi: 10.1007/s12045-012-0015-x.

[10] T. Blaschke, M. Biberacher, S. Gadocha, and I. Schardinger, "Energy landscapes: meeting energy demands and human aspirations," Biomass- Bioenergy, vol. 55, pp. 3–16, 2013.

[11] World Energy Outlook, " International Energy Agency; 2012," http://www. worldenergyoutlook .org/weo2012/, Mar. 2016.

[12] International Energy Agency. "2DS-hiRen Scenario," Energy Technology Perspectives, 2012.

[13] M. S. Arif, "Residential solar panels and their impact on the reduction of carbon emissions. reduction of carbon emissions using residential solar panels." [Online]. Available: https:// www.nature.berkeley.edu/classes/es196/projects/2013final/ArifM_2013.pdf ;2013.

[14] Renewable Energy Policy Network for the 21st Century (Ren21). "Renewables 2016 Global Status Report." [Online]. Available: http://www.ren21.net/status-of-renewables/global statusreport/.

[15] J. Holm-Nielsen and E. A. Ehimen, "Biomass supply chains for bioenergy and. biorefining."Woodhead Publishing, 2016.

[16] P. G. V. Sampaio and M. O. A. González, "Photovoltaic solar energy: conceptual framework," Renew Sustain Energy Rev, vol. 2017, no. 74, pp. 590–601, 2017.

[17] M. A. Al-Tameemi and V. Chukin, "Global water cycle and solar activity variations," J Atmos Sol Terr Phys, no 142, pp. 55–9, 2016.

[18] M. Hart, "Hubris: the troubling science, economics, and politics of climate change". Compleat Desktops Publisher; 2015.

[19] M. Luqman, K. Ahmad SR, A. S, R. U, A. A, and F., "Estimation of solar energy potential from rooftop of Punjab government servants cooperative housing society Lahore using GIS," article ID:56795]. Smart Grid andRenewable Energy, vol. 6, no. 05, 2015, doi: 10.4236/sgre.2015.65012.

[20] National Aeronautics and Space Administration.” Plotted from satellite data supplied by NASA Clouds and the Earth’s Radiant Energy System.” CERES, 2014.

[21] International Renewable Energy Agency.“Estimating the Renewable Energy Potential in Africa A GIS-based approach.” 2014.

[22] M. Adaramola, “Solar energy: application, economics, and public perception.” CRC Press, Technology & Engineering, 2014.

[23] Q. Hang, Z. Jun, Y. Xiao, and C. Junkui, “Prospect of concentrating solar power in China-the sustainable future,” Renew Sustain Energy Rev, vol. 12, no. 9, pp. 2505–14, 2007.

[24] National Renewable Energy Laboratory. “Solar Has The Most Potential of Any Renewable Energy Source.” 〈http://thinkprogress.org/climate/2012/07/30/606271/national-renewable energy - laboratory-solar-has-the-most-potential-of-anyrenewable-energy-source/.

[25] Environmental Protection Agency,” EPA State Generation,” 2015.

[26] Bertelsmann Stiftung’s Transformation Index,” Morocco Country Report”, 2016.

[27] W. Tang, J. Qin, K. Yang, S. Liu, N. Lu, and X. Ni, “Retrieving high-resolution surface solar radiation with cloud parameters derived by combining MODIS and MTSAT data,” Atmos Chem Phys, vol. 16, pp. 2543–57, 2016.

[28] Australian Renewable Energy. “Integrated Solar Radiation Data Sources over Australia Final report: project results and lessons learnt.” 2016. [Online]. Available: http://arena. gov.au/files/2016/02/Integrated_Solar_Radiation_Data_SourcesFinal_Report.pdf.

[29] S. M. Besarati, R. V. Padilla, D. Y. Goswami, and E. Stefanakos, “The potential of harnessing solar radiation in Iran: generating solar maps and viability study of PV power plants,” Renew Energy, vol. 53, pp. 193–9, 2013.

[30] D. Sun and L. Wang, "Research on heat transfer performance of passive solar collectorstorage wall system with phase change materials," Energy Build, vol. 119, no. [183–18]., 2016.

[31] M. Herrando and C. N. Markides, "Hybrid PV and solar-thermal systems for domestic heat and power provision in the UK: techno-economic considerations," Appl Energy, vol. 161, pp. 512–32, 2016.

[32] P. Mohanty, T. Muneer, E. J. Gago, and Y. Yash Kotak," Solar radiation fundamentals and PV system components". Springe Int Publ, 2015. doi: 10.1007/978-3-319-.

[33] N. J. Jeon, J. Lee, J. H. Noh, M. K. Nazeeruddin, M. Gratzel, and S. I. Seok, "Efficient inorganic– organic hybrid perovskite solar cells based on pyrenearylamine derivatives as hole-transporting materials," J Am Chem Soc, vol. 135, no. 51, pp. 19087–90, 2013.

[34] M. A. Green, A. Ho-Baillie, and H. J. Snaith, "The emergence of perovskite solar cells," Nat Photonics, vol. 8, no. 7, pp. 506–14, 2014.

[35] F. H. Alharbi and S. Kais, "Theoretical limits of photovoltaics efficiency and possible improvements by intuitive approaches learned from photosynthesis and quantum coherence," Renew Sustain Energy Rev, vol. 43, pp. 1073–89, 2015.

[36] S. Seddegh, X. Wang, A. D. Henderson, and Z. Xing, "Solar domestic hot water systems using latent heat energy storage medium: a review," Renew Sustain Energy Rev, vol. 49, pp. 517–33, 2015.

[37] M. R. Islam, K. Sumathy, and S. U. Khan, "Solar thermal systems and their market trends," Renew Sustain Energy Rev, vol. 17, pp. 1–25, 2013.

[38] International Energy Agency ."Renewable energy technologies: Solar energy. perspectives."Paris: OECD/IEA Publications, 2011.

[39] M. Romero and J. González-Aguilar, “Solar thermal CSP technology,” WIREs Energy Environ, vol. 3, pp. 42–59, 2014.

[40] PBL Netherlands Environmental Assessment Agency. “Trends in global CO2 emissions: 2015 Repor,” 2015., http://edgar.jrc.ec.europa.eu/news_docs/jrc-2015- trends-in-global-co2- emissions-2015-report-98184.pdf.

[41] C. Jones, P. Gilbert, M. Raugei, E. Leccisi, and S. Mander, “An approach to prospective consequential LCA and net energy analysis of distributed electricity generation”,Energy Policy ,pp. 350–8, 2017. doi: 10.1016/j.enpol.2016.08.030.

[42] European Renewable Energy Research Centres Agency. “The photovoltaic sector Report; 2015.” ⟨http:// www .knowres - jobs.eu /en /upload /Documents /Know RES -%2 D1.4.1 %20 Photovoltaics %20 sectoral %20 report.pdf).

[43] Renewable Energy Policy Network. “Renewable Energy’s Record Year Helps Uncouple Growth of Global Economy and CO2 Emissions.” 2015. [Online]. Available: ⟨http://www. ren21.net/wp content/uploads/2015/06/REN21_press-release-GSR-2015_ENGLISH.pdf⟩.

[44] Mercom Capital Group.“Global Solar Installations To Reach 64.7 GW In 2016.” [Online]. Available:http://mercomcapital.com/global-solar-installations - forecast – to reachapproximately 64.7-gw -in-2016-reports-mercom-capital-group.

[45] E. Meza, Solar Power Europe: “2015 was a very good year for solar.” 2016.

[46] Solar Energy Industries Association. “Solar Market Insight Q4. 2016.” 2015. [Online]. Available: http:// www.seia.org/research-resources/solar-market-insight-2015-q4.

[47] S. Server, “Australian solar PV Installations hit the 5 GW mark; 913 MW added in 2015; 2015.”.[Online].Available:www.solarserver.com/solar - magazine/solarnews/current/2016/kw06/ australian - solar-pv-installations-hit-the-5-gw-mark-913 mw-added-in-2015.

[48] Ministry of New and Renewable Energy,." State wise installed solar power capacity".Govt, of India, 2016.

[49] F. Macdonald, "France will install 1,000 km of solar-panelled roads in the next 5 years." .⟨http://www.sciencealert.com/france-is-planning-to-install-1,000- km - ofsolar- panelled- roads-in-the-next-5-years⟩.

[50] D. M. Chapin, C. S. Fuller, and G. L. Pearson, "Affiliation," Appled . Phys, vol. 25, p. 676, 1954.

[51] Irena working paper, 'Renewable Energy technologies: cost analysis series," IRENA, vol. 1, issue 4/5., 2012.

[52] M. A. Green, " Clean Energy from Photovoltaics ". Hackensack, NJ: World Scientific Publishing Co, 2001.

[53] S. solar, "Solar Crystalline Silicon Technology",internet:http. [Online]. Available: //www.us.schott.com/ photovoltaic/english/About_pv/technologies/crystalline.

[54] B.Mills, Internet :http://commons.wikimedia.org/wiki/File: Silicon-unit-cell-3D-balls.png. Sep. 2007.

[55] D. G. E. Agency, "Information about German renewable energy, industries, companies and product (Federal Ministry of Economics and Technology)". ISIN: B002MNZE4U, p. 41, 2013-2014.

[56] Energy Market Authority," Handbook for solar photovoltaic (PV) systems", p. 8.

[57] E. Sachs and J. Cryst, "String Ribbon Growth Technique",(Evergreen Solar, Sovello) Growth, vol 82, p.117, 1987.

[58] K. L. Chopra, P . D. Paulson, and V. Dutta, “Thin - film solar cell overview", Prog. Photovoltaic: Res.,vol. 12, pp. 69–92, 2004.

[59] Mehta S., Technology, “ PV Production and Cost". Outlook: 2010-2015, Greentech Media Research, 2010.

[61] A. Smets, K. Jäger, O. Isabella, R. Swaaij, and M. Zeman, “Solar Energy, Fundamentals, Technolgy, and systems (UIT Cambridge)", p. 109, 2014.

[60]] A. A. Hossam El –din, C. F. Gabra and Ahmed H. H. Ali ," A Comparative Analysis Between the Performances of Monocrystalline, Polycrystalline and Amorphous Thin Film in Different Temperatures at Different Locations in Egypt", Solar Energy Conference, March 2014.

[62] NREL, “Best research-cell efficiency".[Online]. Available: http://www.nrel.gov/.

[63] M. A. Green, “Solar Cell E£ciency Tables progress in Photovoltaics: Research and Applications", vol. 19. pp. 84–92, 2011.

[64] J. L. Bernard Augstin, G. Zubi and G. V. Fracastoro, “High concentration photovoltaic systems applying III-V cells,” Renewable & Sustainable Energy Reviews, vol. 13, no. 9, pp. 2645–2652, 2009.

[65] K.Ryu, J.G.Rhee,K.M.Park, and J.Kim,”Conceptand design of modular Fresnel lenses for concentration solar PV system”, Solar Energy, vol. 80, no. 12, pp. 1580–1587, 2006.

[66] V. Garboushian, D. Roubideaux, and S. W. Yoon, “Integrated high-concentration PV alternative for large-scale solar electric power,”Solar Energy Materials & Solar Cells, no. 1–4, pp. 315–323, 1997.

[67] V. M. Andreev, V. A. Grilikhes, and V. P. Khvostikov, “Concentrator PV modules and solar cells for TPV systems,” Solar Energy Materials & Solar Cells, vol. 84, no. 1–4, pp. 3–17, 2004.

[68] J. I. Rosell, X. Vallverd´ u, M. A. Lech´ on, and M. Ib´ a˜ nez, “Design and simulation of a low concentrating photovoltaic/thermal system”, Energy Conversion & Management, no. 18-19, pp. 3034–3046, 2005.

[69] Y.P.Wu, P.Eames, T.Mallick,and M.Sabry,” Experimental characterisation of a Fresnel lens photovoltaic concentrating system,” Solar Energy, vol. 86, no. 1, pp. 430–440, 2012.

[70] M. Li, X. Ji, G. L. Li, Z. M. Yang, S. X. Wei, and L. L. Wang, “Performance investigation and optimization of the Trough Concentrating Photovoltaic/Thermal system,”Solar Energy, vol. 85, no. 5, pp. 1028–1034, 2011.

[71] Z.L.Xu, J.D.Liu, P.F.Feng, D.P.Hou, J.Y.Zhang, and Y.M. Zhang, “Research on a butterfly concentrator for photovoltaic generation,”Acta Energiae Solaris Sinica,vol.28, no. 2. pp. 174–177, 2007.

[72] L. Zhu, R. F. Boehm, Y. P. Wang, C. Halford, and Y. Sun, “Water immersion cooling of PV cells in a high concentration system,”Solar Energy Materials & Solar Cells, vol. 95, no. 5, pp. 538–545, 2011.

[73] J. Fern´ andez-Reche, I. Ca˜ nadas, M. S´ anchez et al., “PSA Solar furnace: a facility for testing PV cells under concentrated solar radiation,”Solar Energy Materials & Solar Cells, no. 15, pp. 2480–2488, 2006.

[74] C. S. Solanki, C. S. Sangani, D. Gunashekar, and G. Antony,”Enhanced heat dissipation of V-trough PV modules for better performance,”Solar Energy Materials & Solar Cells, no. 12, pp. 1634–1638, 2008.

[75] L. Zhang and D. Jing, Liang Zhao at el,” Review Article Concentrating PV/T Hybrid System for Simultaneous Electricity and Usable Heat Generation, “photoenengy, p. 8, 2012.

[76] T. T. Chow, “A Review on photovoltaic / thermal hybrid solar technology,”Applied Energy, vol. 87, no. 2, pp. 365–379, 2010.

[77] J. Wennerberg, J. Kessler, J. Hedstr¨ om, L. Stolt, B. Karlsson, and M. R¨ onnelid, “Thin film PV modules for lowconcentrating systems,”Solar Energy, vol. 69, supplement 6, pp. 243–255, 2001.

[78] M. Hein, F. Dimroth, G. Siefer, and A. W. Bett, “Characterisation of a 300×photovoltaic concentrator system with one-axis tracking,”Solar Energy Materials & Solar Cells, vol. 75, no. 1-2, pp. 277–283, 2003.

[79] Orga PV net,"Technology Roadmap Towards Stable & Low-cost Organic Based Solar Cells,” in Orga PV net, 2009.

[80] European Photovoltaic Industry Association (EPIA) , Solar Generation 6 : Solar Photovoltaic Energy Empowering the World. Brussels: EPIA, 2011.

[81] A. Nozik, “Multiple Exciton Generation in Colloidal Quantum Dots, Singlet Fission in Molecules, Quantum Dot Arrays, Quantum Dot Solar Cells, and Effects of Solar Concentration,” in Presentation to the symposium “Third-Generation and Emerging Solar-Cell Technologies”, April 26–29, 2011.

[82] S. Leung, “Third-Generation and Emerging Solar - Cell Technologies,” in Engineered Optical Absorption of Nano/Micro-pillar Arrays for Efficient Photovoltaics, presentation to the symposium, April 26–29, 2011.

[83] BASF company, " layer of organic materal.” [Online]. Available: http: http: // www .solarserver .com/solarmagazin/solar-report_0807_e.html.

[84] EcoFriend ,"the last update in renewable energy and organic PV".[Online]. Available: http ://www. ecofriend.com/category/latest.

[85] M. Grätzel and B. O'Regan, "A Low-Cost, High - E£ciency Solar Cell Based on Dyesensitized Colloidal TiO2 Films," Nature, vol. 353, pp. 737-740, 1991.

[86] H. Savin, Päivikki Repo at el," Black silicon solar cells with interdigitated back- contacts," Nature nano technology, vol. 10, pp. 624–628, 2015.

[87] T. Esram, I. E. E. E. Student Member, P. L. Chapman, and I. E. E. E. Senior Member, "Comparison of Photovoltaic Array Maximum Power Point Tracking Techniques," IEEE Transactions on energy conversion, vol. 22, no. 2, Jun. 2007.

[88] R. E. Campos, E.Y. Sako, M. V. Gomes dos Reis, and M. G. Villalva, "A Review of the Main Methods to trace the I-V Characteristic Curve of PV Sources", 13th IEEE International Conference on Industry Applications, 2018.

[89] Cours Energie Solaire Photovoltaïque, Dr. BELAID LALOUNI Sofia, 2014.

[90] S. Ajib and A. Alahmer, "Solar Cooling Technologies," in Energy Conversion - Current Technologies and Future Trends, 2018.

[91] S. Ajib, "Acetone/zinc bromide (C3H6O/ZnBr2) as an alternative working solution in low temperature driven absorption refrigeration machines; some investigation results and perspectives," International Symposium on Energy 7, 13–17, Aug. 2017.

[92] H. I. Mohammed, D. Giddings, and G. S. Walker, "CFD simulation of a concentrated salt nanofluid flow boiling in a rectangular tube," Int J Heat Mass Transfer, vol. 125, pp. 218–28, 2018.

[93] A. Fasfous, J. Asfar, A. Al-Salaymeh, A. Sakhrieh, Z. Al hamamre, A. Al-Bawwab, and M. Hamdan, "Potential of utilizing solar cooling in The University of Jordan," Energy Convers Manage, vol. 65, pp. 729–35, 2013.

[94] A. Alahmer, S. Ajib, and X. Wang, “Comprehensive strategies for performance improvement of adsorption air conditioning systems: a review,” Renew Sustain Energy Rev, vol. 99, pp. 138–58, 2019.

[95] D. Mugnier and U. Jakob, “Status of solar cooling in the World: markets and available products,” Wiley Interdisc Rev Energy Environ, vol. 4, no. 3, pp. 229–34, 2015.

[96] Y. Fan, L. Luo, and B. Souyri, “Review of solar sorption refrigeration technologies: development and applications,” Renew Sustain Energy Rev, vol. 11, no. 8, pp. 1758–75, 2007.

[97] S. Phansopkar, “Refrigeration world: solar mechanical refrigeration.”.2018. [Online]. Available: http://refrigerationworld.blogspot.com/2013/01/solar-mechanical-refrigeration.html.

[98] S. Ajib and W. Günther, “Solar thermally driven cooling systems: some investigation results and perspectives,” Energy Convers Manage, vol. 65, pp. 663–9, 2013.

[99] A. Alazazmeh and E. Mokheimer, “Review of solar cooling technologies,” J Appl Mech Eng, vol. 4, no.5,pp.1–15 , 2015.

[100] X. Wang and H. T. Chua, “Absorption cooling: a review of lithium bromide-water chiller technologies,” Recent Patents Mech Eng, vol. 2, no. 3, pp. 193–213, 2009.

[101] VHasse, “Natural Refrigerants,” 2008. [Online]. Available: http: //www.r 718 .com /news/ viewprintable/3432.

[102] “The basics of R718: the adsorption cycle,” Shecco, 2012. Available: http: //www.r 718 .com/articles/3432/the_basics_of_ r718_the_adsorption_cycle_br.

[103] ”Bry-air adsorption coolers.” Jul-2018, Accessed. [Online]. Available: http:// simplycooler .co.uk/bry-air-adsorption- coolers /.

[104] S. Patil and S. G. Dambhare, “Review on Study of Solar Powered Adsorption Refrigeration System,” International Journal of Innovative and Emerging Research in Engineering, vol. 2, pp. 2394–5494, 2015.

[105] B. M. Tashtoush, MdA. Al-Nimr, and M. A. Khasawneh, “A comprehensive review of ejector design, performance, and applications,” Applied Energy, vol. 240, pp. 138–72, 2019.

[106] B. J. Huang, J. M. Chang, C. P. Wang, and V. A. Petrenko, “A 1-D analysis of ejector performance,” International Journal of Refrigeration, vol. 22, pp. 354–64, 1999.

[107] J. H. Keenan, “An investigation of ejector design by analysis and experiment,” Journal of Applied Mechanics, p.117, 1950.

[108] J. T. Munday and D. F. Bagster, “A New Ejector Theory Applied to Steam Jet Refrigeration. Industrial & Engineering Chemistry Process Design and Development.,” vol. 16. pp. 442–9, 1977.

[109] K. Braimakis, “Solar ejector cooling systems: A review,” Renewable Energy, RENE, vol. 14228, 2020.

[110] R. Al-Rbaihat, A. Sakhrieh, J. Al-Asfar, A. Alahmer, O. Ayadi, and A. Al-Salaymeh, “Performance assessment and theoretical simulation of adsorption refrigeration system driven by flat plate solar collector,” Jord J Mech Ind Eng, vol. 11, no. 1, pp. 1–11, 2017.

[111] Y. Hwang, R. Radermacher, A. A. Alili, and I. Kubo, “Review of solar cooling technologies,” Hvac&R Res, vol. 14, no. 3, pp. 507–28, 2008.

[112] N. Enteria and K. Mizutani, “The role of the thermally activated desiccant cooling technologies in the issue of energy and environment,” Renew Sustain Energy Rev, vol. 15, no 4 , pp. 2095–122, 2011.

[113] A. Zendehboudi and H. Esmaeili, “Effect of supply/regeneration section area ratio on the performance of desiccant wheels in hot and humid climates: an experimental investigation,” Heat Mass Transfer, vol. 52, no. 6, pp. 1175–81, 2016.

[114] A. Alahmer, “Thermal analysis of a direct evaporative cooling system enhancement with desiccant dehumidification for vehicular air conditioning,” Appl Therm Eng, vol. 98, pp. 1273–85, 2016.

[115] R. K. Collier, R. S. Barlow, and F. H. Arnold, “An overview of open-cycle desiccant-cooling systems and materials,” J Sol Energy Eng, vol. 104, no. 1, pp. 28–34, 1982.

[116] C. H. Liang, L. Z. Zhang, and L. X. Pei, “Performance analysis of a direct expansion air dehumidification system combined with membrane-based total heat recovery,” Energy, vol. 35, no 9, pp. 3891–901, 2010.

[117] S. Muthu, P. Talukdar, and S. Jain, “Modelling and parametric simulation of coupled heat and mass transfer phenomena in a rotary desiccant wheel,” in Proceedings of the 22th National and 11th International ISHMT-ASME Heat and Mass Transfer Conference, Dec. 2013, 28–31.

[118] M. Kuroda, K. Kimura, and M. Komori, “Improvement of dehumidification performance of desiccant rotors regenerated at a low temperature,” Heat Transfer Eng, vol. 37, no. 7–8, pp. 650–8, 2016.

[119] S. Sabek, K. B. Nasr, R. Chouikh, and A. Guizani, “Analytical study of a heat recovery/ desiccant cooling system under Tunisian climatic conditions,” J Clean Energy Technol, vol. 3, no 3, pp. 159–64, 2015.

[120] J. L. Niu, L. Z. Zhang, and H. G. Zuo, “Energy savings potential of chilled-ceiling combined with desiccant cooling in hot and humid climates,” Energy Build, vol. 34, no. 5, pp. 487–95, 2002.

[121] C. Baldwin and C. A. Cruickshank, “A review of solar cooling technologies for residential applications in Canada,” Energy Procedia, vol. 30, pp. 495–504, 2012.

[122] A. Alahmer, S. Alsaqoor, and G. Borowski, “Effect of parameters on moisture removal capacity in the desiccant cooling systems,” Case Stud Therm Eng, vol. 13, no. 100364, 2019.

[123] G. Lychnos and P. A. Davies, “Modeling and experimental verification of a solar- powered liquid desiccant cooling system for greenhouse food production in hot climates,” Energy, vol. 40, no. 1, pp. 116–130, 2012.

[124] N. Audah, N. Ghaddar ⇑, and K. Ghali., “Optimized solar-powered liquid desiccant system to supply building fresh water and cooling needs,” Applied Energy, vol. 88, pp. 3726–3736, 2011.

[125] G. P. Narayan, M. H. Sharqawy, E. K. Summers, J. H. Lienhard, S. M. Zubair, and M. A. Antar, “The potential of solar-driven humidification–dehumidification desalination for small-scale decentralized water production,” Renew Sust Energy Rev, vol. 14, pp. 1187–201, 2010.

[126] A. M. Radhwan, H. N. Gari, and M. M. El-Sayed, “Parametric study of a packed bed dehumidifier /regenerator using CaCl2 liquid desiccant,” Renew Energy, vol. 3, no. 1, pp. 49–60, 1993.

[127] K. Saikia, M. Vall`es, A. Fabregat, R. Saez, and D. Boer, “A bibliometric analysis of trends in solar cooling technology,” Sol Energy, vol. 199, pp. 100–14, 2020.

[128] N. I. Ibrahim, F. A. Al-Sulaiman, and F. N. Ani, “Solar absorption systems with integrated absorption energy storage–a review,” Renew Sustain Energy Rev, vol. 82, pp. 1602–10, 2018, doi: 10.1016/j.rser.2017.07.005.

[129] M. Alobaid, B. Hughes, J. K. Calautit, D. O’Connor, and A. Heyes, “A review of solar driven absorption cooling with photovoltaic thermal systems,” Renew Sustain Energy Rev, vol. 76, pp. 728–42, 2017, doi: 10.1016/j.rser.2017.03.081.

[130] K. R. Ullah, R. Saidur, H. W. Ping, R. K. Akikur, and N. H. Shuvo, "A review of solar thermal refrigeration and cooling methods," Renew Sustain Energy Rev, vol. 24, pp. 499–513, 2013.

[131] H. Sheikhani, R. Barzegarian, A. Heydari, A. Kianifar, A. Kasaeian, et al ,"A review of solar absorption cooling systems combined with various auxiliary energy devices," J Therm Anal Calorim, vol. 134, pp. 2197–212, 2018, doi: 10.1007/s10973-018-7423-4.

[132] A. Shirazi, R. A. Taylor, G. L. Morrison, and S. D. White, "Solar-powered absorption chillers: a comprehensive and critical review," Energy Convers Manag, vol. 171, pp. 59–81, 2018, doi: 10.1016/j.enconman.2018.05.091.

[133] A. Ghafoor and A. Munir, "Worldwide overview of solar thermal cooling technologies," Renew Sustain Energy Rev, vol. 43, pp. 763–74, 2015, doi: 10.1016/j.rser.2014.11.073.

[134] A. Kasaeian, E. Bellos, A. Shamaeizadeh, and C. Tzivanidis, "Solar-driven polygeneration systems: recent progress and outlook," Appl Energy, vol. 264, 2020, [Online]. Available: https://doi.org/ 10.1016/ j.apenergy.2020.114764.

[135] S. Suman, M. K. Khan, and M. Pathak, "Performance enhancement of solar collectors – a review," Renew Sustain Energy Rev, vol. 49, pp. 192–210, 2015, doi: 10.1016/j.rser.2015.04.087.

[136] D. R. Rajendran, E. Ganapathy Sundaram, P. Jawahar, V. Sivakumar, O. Mahian, and E. Bellos, "Review on influencing parameters in the performance of concentrated solar power collector based on materials, heat transfer fluids and design," J Therm Anal Calorim, vol. 140, pp. 33–51, 2020, doi: 10.1007/s10973-019-08759-8.

[137] K. Khanafer and K. Vafai, "A review on the applications of nanofluids in solar energy field,"Renew Energy, vol. 123, pp. 398–406, 2018, doi: 10.1016/j.renene.2018.01.097.

[138] X. Zhao, E. J, G. Wu, Y. Deng, D. Han, and B. Zhang, “A review of studies using graphenes in energy conversion energy storage and heat transfer development,”Energy Convers Manag, vol. 184, pp. 581–99, 2019 . doi: 10.1016/j.enconman.2019.01.092.

[139] X. Zhao, E. J, Z. Zhang, J. Chen, G. Liao, and F. Zhang, “A review on heat enhancement in thermal energy conversion and management using Field Synergy Principle,” Appl Energy, vol. 257, no. 113995, 2020, doi: 10.1016/j. apenergy.2019.113995.

[140] J. Jiaqiang, X. Zhao, H. Liu, J. Chen, W. Zuo, and Q. Peng, “Field synergy analysis for enhancing heat transfer capability of a novel narrow-tube closed oscillating heat pipe,” Appl Energy, vol. 175, pp. 218–28, 2016, doi: 10.1016/j.apenergy.2016.05.028.

[141] A. S. Alsagri, A. A. Alrobaian, and S. A. Almohaimeed,” Concentrating solar collectors in absorption and adsorption cooling cycles: An overview,” Energy Conversion and Management, vol. 223, p. 113420, 2020.

[142] V. K. Jebasingh and G. M. J. Herbert, “A review of solar parabolic trough collector,” Renew Sustain Energy Rev, vol. 54, pp. 1085–91, 2016, doi: 10.1016/j.rser.2015.10.043.

[143] FJ.Cabrera, A .Fern´andez-García, RMP. Silva, M .P´erez-García,“Use of parabolic trough solar collectors for solar refrigeration and air-conditioning applications,” Renew Sustain Energy Rev, vol. 20, pp. 103–18, 2013, doi: 10.1016/j.rser.2012.11.081.

[144] R. LR. Gonz´alez MI, “Solar powered adsorption refrigerator with CPC collection system: collector design and experimental test,” Energy Convers Manag, vol. 48, pp. 2587–94, 2007, doi: 10.1016/j.enconman.2007.03.016.

[145] M. Li, C. Xu, R. H. E. Hassanien, Y. Xu, and B. Zhuang, “Experimental investigation on the performance of a solar powered lithium bromide–water absorption cooling system,” Int J Refrig, vol. 71, pp. 46–59, 2016, doi: 10.1016/j.ijrefrig.2016.07.023.

[146] Y. Hang, M. Qu, R. Winston, L. Jiang, B. Widyolar, and H. Poiry, “Experimental based energy performance analysis and life cycle assessment for solar absorption cooling system at University of Californian, Merced,” Energy Build, vol. 82, pp. 746–57, 2014.

[147] A. Alahmer, X. Wang, R. Al-rbaihat, K. C. A. Alam, and B. B. Saha, “Performance evaluation of a solar adsorption chiller under different climatic conditions,” Appl Energy, vol. 175, pp. 293–304, 2016, doi: 10.1016/j.apenergy.2016.05.041.

[148] S. A. Kalogirou, “Solar thermal collectors and applications,” vol. 30. 2004. doi: 10.1016/j.pecs.2004.02.001.

[149] E. Jiaqiang, G. Liu, T. Liu, Z. Zhang, H. Zuo, and W. Hu, “Harmonic response analysis of a large dish solar thermal power generation system with wind-induced vibration,” Sol Energy, vol. 181, pp. 116–29, 2019, doi: 10.1016/j.solener.2019.01.089.

[150] H. Zuo, G. Liu, E. Jiaqiang, W. Zuo, K. Wei, and W. Hu, “Catastrophic analysis on the stability of a large dish solar thermal power generation system with wind-induced vibration,” Sol Energy, vol. 183, pp. 40–9, 2019, doi: 10.1016/j.solener.2019.03.003.

[151] A. Bianchini, A. Guzzini, M. Pellegrini, and C. Saccani, “Performance assessment of a solar parabolic dish for domestic use based on experimental measurements,” Renew Energy, vol. 133, pp. 382–92, 2019, doi: 10.1016/j.renene.2018.10.046.

[152] E. Bellos and C. Tzivanidis, “Assessment of linear solar concentrating technologies for Greek climate,” Energy Convers Manag, vol. 171, pp. 1502–13, 2018, doi: 10.1016/ j. enconman. 2018.06.076.

[153] J. Do, H. Bentaher, and A. Morgenstern, “First results of a pilot installation of a solar thermally driven cold store,” International Journal of Refrigeration, vol. 9, pp. 2–10, 2013, doi: 10.1016/j.ijrefrig.2013.11.010.

[154] K. R. Ullah, R. Saidur, H. W. Ping, R. K. Akikur, and N. H. Shuvo, "A review of solar thermal refrigeration and cooling methods," Renewable and Sustainable Energy Reviews, vol. 24, pp. 499–513, 2013.

[155] M. Alobaid, B. Hughes, J. Calautit, D. O'Connor, and A. Heyes, "A review of solar-driven absorption cooling with photovoltaic thermal systems," Renewable and Sustainable Energy Reviews, vol. 76, pp. 728–742, 2017.

[156] T. A. Kattakayam and K. Srinivasan, "Thermal performance characterization of a photovoltaic driven domestic refrigerator," International Journal of Refrigeration, vol. 23 (2000), pp. 190–196, 2000.

[157] R. Opoku, S. Anane, I. A. Edwin, M. S. Adaramola, and R. Seidu, "Comparative techno-economic assessment of a converted DC refrigerator and a conventional AC refrigerator both powered by solar PV," International Journal of Refrigeration, 2016.

[158] M. Bilgili, "Hourly simulation and performance of solar electric-vapor compression refrigeration system," Solar Energy, vol. 85, pp. 2720–2731, 2011.

[159] Y. Gao, J. Ji, K. Han, and F. Zhang, "Comparative analysis on performance of PV direct-driven refrigeration system under two control methods," International Journal of Refrigeration, vol. 127, pp. 21–33, 2021.

[160] A. Mota-Babiloni, P. Makhnatch, and R. Khodabandeh, "Recent investigations in HFCs substitution with lower GWP synthetic alternatives: Focus on energetic performance and environ-mental impact," Int. J. Refrig, vol. 82, pp. 288–301, 2017.

[161] R. Ben Jemaa, R. Mansouri, I. Boukholda, and A. Bellagi, "Energy and Exergy Investigation of R1234ze as R134a Replacement in Vapor Compression Chillers," Int.Energ y, pp. 1–11, 2016.

[162] P. Rajendran, S. Sidney, I. Ramakrishnan, and M. L. Dhasan, “Experimental studies on the per-formance of mobile air conditioning system using environmental friendly HFO 1234yf as a refrigerant,” Proc Inst Mech Eng Part E J Process Mech Eng, 2019.

[163] R. Touaibi and H. Koten, “Energy Analysis of Vapor Compression Refrigeration Cycle Using a New Generation Refrigerants with Low Global Warming Potential,” Journal of Advanced Research in Fluid Mechanics and Thermal Sciences, vol. 87, no. 2, pp. 106–117, 2021.

[164] U. S. Prasad, R. S. Mishra, R. K. Das, and H. Soni, “Experimental and Simulation Study of the Latest HFC/HFO and Blend of Refrigerants in Vapour Compression Refrigeration System as an Alternative of R134a,” Processes, vol. 11, p. 814, 2023.

[165] E. M. Salilih and Y. T. Birhaneb, “Modelling and performance analysis of directly coupled vapor compression solar refrigeration system,” Solar Energy, vol. 190, pp. 228–238, 2019.

[166] S. Pattarapanitchai, S. Janjai1, S. Sirikaew, B. K. Bala,” Performance and ARX Modelling of a Solar Vapour Compression Refrigeration System,” Journal of Renewable Energy and Smart Grid Technology, vol. 17, no. 1, Jan. 2022.

[167] V. Palomba, E. Varvagiannis, S. Karellas and A. Frazzica.,” Hybrid Adsorption-Compression Systems for Air Conditioning in Efficient Buildings: Design through Validated Dynamic Models,” Energies, vol. 12, p. 1161, 2019, doi: 10.3390/en12061161.

[168] S. Barghash, A. Bahman, and O. Ibrahim, “Solar-Powered Mechanical Subcooling Refrigeration System for Hot Climates.” 2021. [Online]. Available: https://docs.lib.purdue.edu/iracc/2129.

[169] B. Narváez-Romo, E. H. Suzuki, and J. R. Simões-Moreira, “A comparative study of solar cooling technologies,” REHVA, 14 th HVAC World Congress 22 nd – 25 th May,Rotterdam, The Therlands, Clima 2022.

[170] C. L. Hana and T. Ooa, “Design and Analysis of Solar Powered Vapour Compression Refrigeration System,” International Journal of Research Publications, 2018.

[171] G. W. M. Musifu, T. Ngonda, and C. Magoda, “The solar powered refrigerator and heat pump for urban street vendors,” in MATEC Web of Conferences ICARAE2022.

[172] I. D. M. C. Santosa, I. G. N. S. Waisnawa, I. G. A. B. Wirajati, and I. M. Arta, “Analysis Key Performance of Refrigerator Prototype With Photovoltaic,” Proceedings of the International Conference on Innovation in Science and Technology (ICIST 2020), vol. 208.

[173] S.V. Ganorkar, K. Y. Yuvraj, K. G. Babasaheb, and S. K. Subhash,“Solar assisted refrigeration system,”.Journal of information, Knoledge and research in mechanical, engineering, ISSN 0975, in 668XI NOV 16 TO OCT 17, vol. 04, no issue. 2, 2017.

[174] O. Ekren, A. Yilanci, E. Cetin, and H. K. Ozturk, “Experimental Performance Evaluation of a PV-Powered Refrigeration System,” Electronics and electrical ISSN 1392 – 1215, no. 8(114)., 2011.

[175] C. Amaris, F. Barbosa, and M. Balbis-Morejon, “Energy Performance Analysis of a Solar Refrigerator Using Ecological Refrigerants,” Journal of Sustainable Development of Energy. Water and Environment Systems, vol. 11, no issue. 2, p. 1110446, 2023.

[176] K. S. Al Qdah, “Performance of Solar-Powered Air Conditioning System under AlMadinah Al-Munawwarah Climatic Conditions,” Smart Grid and Renewable Energy, vol. 6, pp. 209-219 2015.

[177] I. Daut, M. Adzrie, M. Irwanto, P. Ibrahim, and M. Fitra, “Solar Powered Air Conditioning System,” Energy Procedia, vol. 36, pp. 444-453, 2013.

[178] R. Yvon, M. K. Nematchoua, and R. Chrysostome. “Performance modelling of an electric vapor compression solar refrigeration system (SE-VCR), case for Madagascar,” International Journal of Frontiers in Life Science Research, vol. 01, no.02, pp. 028–051, 2021.

[179] K. K. Samar, S. Kothari, and S. Jindal, “Solar Refrigeration Model. energética india.” Jul. 2015.

[180] L. Haiyan, G. Wei, and D. Chuanshan, “Experimental study of a micro-refrigeration system driven by photovoltaic power generation,” Energy Procedia, vol. 158, pp. 516–521, 2019.

[181] M. S. Jamaluddin, M. M. Rahman, M. F. Hasan, A. Saat, and M. Abd Wahid, “Performance evaluation of a small-scale solar driven refrigeration system,” Journal of Advanced Research in Fluid Mechanics and Thermal Sciences, vol. 36, no issue. 1, pp. 10–20, 2017.

[182] M. A. Eltawil and D. V. K. Samuel, “Vapour Compression Cooling System Powered By Solar PV Array for Potato Storage,” Agricultural Engineering International: the CIGR Ejournal, Manuscript EE 06 003, vol. IX, June 2007.

[183] M. Aktacir, “Experimental study of a multi-purpose PV-refrigerator system,” International Journal of Physical Sciences, vol. 6, pp. 746–757, 2011.

[184] S. A. Atrooshi, “Experimental Investigation and Exergy Analysis of Solar Powered D.C. Vapor Compression Refrigeration,” Zanco, Journal of Pure and Applied Sciences / Salahaddin University – Hawler, vol. 24, no. 3, 2012.

[185] A. Meneghetti, C. Pagnin, and P. Simeoni, “Decarbonizing the cold chain: long-haul refrigerated deliveries with on-board photovoltaic energy integration,” Sustainability, vol. 13, no. 15, p. 8506, 2021.

[186] A. Meneghetti, F. Dal Magro, and A. Romagnoli, “Renewable energy penetration in food delivery: coupling photovoltaicswith transport refrigerated units,” Energy, vol. 232, p. 120994, 2021.

[187] B. L. Gupta, M. Bhatnagar, and J. Mathur, “Optimum sizing of PV panel, battery capacity and insulation thickness for a photovoltaic operated domestic refrigerator,” Sustainable Energy Technologies and Assessments, vol. 7, pp. 55–67, 2014.

[188] K. Daffallah, “Experimental study of 12V and 24V photovoltaic DC refrigerator at different operating conditions,” Phys. B, vol. 545, pp. 237–244, 2018.

[189] A. Zarei, M. Liravi, M. B. Rabiee, and M. Ghodrat, “A Novel, ecofriendly combined solar cooling and heating system, powered by hybrid Photovoltaic thermal (PVT) collector for domestic application,” Energy Conv. Manage, vol. 222, p. 113198, 2020.

[190] A. J. Dhondge and S. R. Kalbande, “Energy and exergy analysis of SPV powered vapor compression refrigeration system,” Multilogic in science, VOL. VIII, Special issue A, NAHEP, in ICAR Sponsored international conference on eares, 2019.

[191] D. A. Omer, M. M. Mahdi, and A. L. Shuraiji, “An experimental study optimization of a solar assisted D.C refiergerter under Iraqi climate,” Journal of Physics, IICESAT Conference, College of Material Engineering, University of Babylon, Iraq Conf. Ser. 1973 012082 , (2021).

[192] A. Hossain, S. Saha, M. A. Rahman, and M. A. Himel, “Low Power Consuming Solar Assisted Vapor Compression Refrigerator To Preserve Emergency Medicines And Vaccines In Rural Areas,” in 1st International Conference on Advances in Science, Engineering and Robotics Technology (2019), ICASERT, 2019, 978-1-7281-3445- 1/19/$31.00 ©2019 IEEE.

[193] H. Ikram, A. Javed, M. Mehmood, M. Shah, and M. Ali, “Adeel Waqas. Techno-economic evaluation of a solar PV integrated refrigeration system for a cold storage facility,” Sustainable Energy Technologies and Assessments, vol. 44, p. 101063, 2021.

[194] A. Selloum, Z. Trıkı, and Y. Chıba, “Thermodynamic analysis of a solar-driven vapor compression refrigeration system using R1234ze for cooling applications in Ghardaïa region (Southern Algeria,” Journal of Thermal Engineering, vol.10, no., pp. 130-141, January 2024, doi: 10.18186/thermal.1429427.

[195] L. Zaghba, M. Khennane, A. Fezzani, A. Borni, I. Hadj Mahammed, “Experimental performance assessment of a 2.25 kWp Rooftop PV system installed in the desert environment: a case study of Ghardaia, Algeria,” International Journal of Sustainable Engineering, 2020.

[196] T. Sivasakthivel and K. K. S. K. Reddy, “Ozone Layer Depletion and Its Effects : A Review,” Int. J. Environ. Sci. Dev, vol. 2, pp. 30–37, 2011.

[197] A. Kilicarslan and N. Muller, “A comparative study of water as a refrigerant with some current refrigerants,” Int. J. Energy Res, vol. 29, pp. 947–959, 2005.

[198] R. Ciconkov, “Refrigerants: There is still no vision for sustainable solutions,” Int. J. Refrig, vol. 86, pp. 441–448, 2018.

[199] P. Giménez-Prades, J. Navarro-Esbrí, C. Arpagaus, A. Fernández-Moreno, A. Mota-Babiloni, “Novel molecules as working fluids for refrigeration, heat pump and organic Rankine cycle systems,” Renew. Sustain. Energy Rev, vol. 167, p. 112549, 2022.

[200] K. Uddin, S. Arakaki, and B. B. Saha, “Thermodynamic analysis of low-GWP blends to replace R410A for residential building air conditioning applications,” Environ. Sci. Pollut. Res, vol. 28, pp. 2934–2947, 2021.

[201] I. H. Bell, P. A. Domanski, M. O. McLinden, and G. T. Linteris, “The hunt for nonflammable refrigerant blends to replace R-134a,” Int. J.Refrig, vol. 104, pp. 484–495, 2019.

[202] B. Yu, H. Ouyang, J. Shi, W. Liu, and J. Chen, “Evaluation of low-GWP and mildly flammable mixtures as new alternatives for R410A in air-conditioning and heat pump system,” Int. J. Refrig, vol. 121, pp. 95–104, 2021.

[203] A. Hamza and T. A. Khan, “Comparative Performance of Low-GWP Refrigerants as Substitutes for R134a in a Vapor Compression Refrigeration System,” Arab. J. Sci. Eng, vol. 45, pp. 5697–5712, 2020.

[204] K. Harby, “Hydrocarbons and their mixtures as alternatives to environmental unfriendly halogenated refrigerants: An updated overview,” Renew. Sustain. Energy Rev, vol. 73, pp. 1247-1264, 2017.

[205] I. Ikem, P. AUbi, M. IIbeh, S. EOfem, and A. TAssam, “Review of refrigerants for steam compression refrigeration machines,” Int. J.Eng. Technol, vol. 10, pp. 1172–1180, 2018.

[206] A. V. Antunes and E. P. B. Filho, “Experimental investigation on the performance and global environmental impact of a refrigeration system retrofitted with alternative refrigerants,” Int. J. Refrig.-Rev. Int, vol. 70, pp. 119–127, 2016.

[207] P. Saengsikhiao, J. Taweekun, K. Maliwan, S. Sae-ung, and T. Theppaya, “Development of Environmentally Friendly and Energy Efficient Refrigerants for Refrigeration Systems,” Energy Eng, vol. 118, pp. 411–413, 2021.

[208] M. Beshr, V. Aute, V. Sharma, O. Abdelaziz, B. Fricke, and R. Radermacher, “A comparative study on the environmental impact of supermarket refrigeration systems using low GWP refrigerants,” Int. J. Refrig, vol. 56, pp. 154–164, 2015.

[209] M. O. McLinden, J. S. Brown, R. Brignoli, A. F. Kazakov, and P. A. Domanski, “Limited options for low-global-warming-potential refrigerants,” Nat. Commun, vol. 8, p. 14476, 2017.

[210]] F. Alsouda , N. Bennett , S. C. Saha , F. Salehi and M. S. Islam, “Vapor Compression Cycle: A State-of-the-Art Review on Cycle Improvements, Water and Other Natural Refrigerants,” Clean technologies, vol. 5, pp. 584–608, 2023, doi: 10.3390/cleantechnol.

[211] G. Qiu, X. Meng, and J. Wu, “Density measurements for 2,3,3,3-tetrafluoroprop -1 -ene (R1234yf) and trans-1,3,3,3-tetrafluoropropene (R1234ze(E)),” J. Chem.Thermodyn, vol. 60, pp. 150–158, 2013.

[212] X. Meng, G. Qiu, J. Wu, and I. M. Abdulagatov, “Viscosity measurements for, vol. 2,3,3,3 tetrafluoroprop-1-ene (R1234yf) and trans-1,3,3,3-tetrafluoropropene (R1234ze(E),” J. Chem. Thermodyn,vol. 63, pp. 24–30, 2013.

[213] G. Di Nicola, C. Brandoni, C. Di Nicola, and G. Giuliani, “Triple point measurements for alternative refrigerants,” J. Therm. Anal. Calorim, vol. 108, pp. 627–631, 2012.

[214] J. S. Brown, C. Zilio, and A. Cavallini, “Thermodynamic properties of eight fluorinated olefins,” Int. J. Refrig, vol. 33, pp. 235–241, 2010.

[215] R. Akasaka, “An application of the extended corresponding states model to thermodynamic property calculations for trans-1,3,3,3-tetrafluoropropene (HFO-1234ze(E)),” Int. J. Refrig, vol. 33, pp. 907–914, 2010.

[216] R. Akasaka, “New fundamental equations of state with a common functional form for 2,3,3,3-tetrafluoropropene (R-1234yf) and trans-1,3,3,3-tetrafluoropropene (R-1234ze(E)),” Int. J. Thermophys, vol. 32, pp. 1125–1147, 2011.

[217] E. W. Lemmon, M. L. Huber, and M. O. McLinden, “R.E.F.P.R.O.P., NIST Standard Reference Database 23,” vol. 9, no. 1, 2014.

[218] M. M. Alavianmehr, F. Pahlavan, J. Moghadasi, and S. M. Hosseini, "Modeling thermodynamic properties of refrigerants from new version of Tao-Mason equation of state," Int. J. Refrig, vol. 45, pp. 100–106, 2014.

[219] N. A. Lai, "Equations of state for HFO-1234ze(E) and their application in the study on refrigeration cycle," Int. J. Refrig, vol. 43, pp. 194–202, 2014.

[220] American Society of Heating, Refrigerating and Air-Conditioning Engineers, Standard 34 Designation and Safety Classification of Refrigerants. ASHRAE, 2013.

[221] S. Kondo, K. Takizawa, and K. Tokuhashi, "Effect of high humidity on flammability property of a few non-flammable refrigerants," J. Fluor. Chem, vol. 161, pp. 29–33, 2014.

[222] S. Kondo, K. Takizawa, and K. Tokuhashi, "Effects of temperature and humidity on the flammability limits of several 2L refrigerants," J. Fluor. Chem, vol. 144, pp. 130–136, 2012.

[223] T. A. Lewandowski, "Risk assessment of residential heat pump systems using 2L flammable refrigerants," AHRI Project 8004 Final Report, 2012.

[224] J. Majurin, S. J. Staats, E. Sorenson, and W. Gilles, "Material compatibility of HVAC&R system materials with low GWP refrigerants, Sci," Technol. Built Environ, vol. 21, pp. 491–501, 2015.

[225] Y. Sun, X. Wang, N. Gong, and Z. Liu, "Solubility of trans-1,3,3,3-tetrafluoropropene (R1234ze(E)) in pentaerythritol ester heptanoic acid (PEC7) and in pentaerythritol tetranonanoate (PEC9) between 283.15 K and 353.15 K," Fluid Phase Equilib, vol. 387, pp.154–159, 2015.

[226] G. Myhre, D. Shindell, F.M. Bréon, W. Collins, J. Fuglestvedt, J. Huang, D. Koch, J.F. Lamarque, D. Lee, and B. Mendoza, "Anthropogenic and Natural Radiative Forcing. In Climate Change 2013," The Physical Science Basis. Contribution of Working Group I to the Fifth Assessment Report of the Intergovernmental Panel on Climate Change. Cambridge, UK; New York, NY, USA: Cambridge University Press, 2013.

[227] P. Życzkowski, M. Borowski, R. Łuczak, Z. Kuczera, and B. Ptaszyński, "Functional Equations for Calculating the Properties of Low-GWP R1234ze(E)," Refrigerant Energies, vol. 13, p.3052, 2020.

[228] M. Kourchi and A. Rachdy, "Calcul Rapide des Propriétés Thermodynamiques des Frigorigènes [Fast Calculation of Thermodynamic Properties of Refrigerants," Int J Innov Appl Stud, vol. 14, 2016.

[229] M. J. Moran and H. N. Shapiro," Fundamentals of Engineering Thermodynamics," Fifth ed. John Wiley and Sons Inc, 2006.

[230] R. Yamankaradeniz, I. Horuz, O. Kaynakli, S. Coskun, and N. Yamankaradeniz, "Refrigeration Techniques and Heat Pump Applications," Dora Company, ISBN: 978-605-4118-14–4, 2009.

[231] A. Bahadori, "Chapter 5 - Gas Compressors in Natural Gas Processing," Gulf Professional Publishing, p.p 223 −273, 2014.

[232] D. S. Kim and C. A. Infante-Ferreira, "Solar refrigeration options - state-of-the-art review," Int J Refrig, vol. 31, pp. 3−15, 2008.

[233] D. Sánchez, R. Cabello, R. Llopis, I. Arauzo, J. Catalán-Gil, E. Torrella , "Energy performance evaluation of R1234yf, R1234ze(E), R600a, R290 and R152a as low-GWP R134a alternatives," Int J Refrig, vol. 74, pp. 267-280, 2017.

[234] L. P. M. Colombo and A. Lucchini, “Molinaroli L.Experimental analysis of the use of R1234yf and R1234ze(E) as drop-in alternatives of R134a in a water-to-water heat pump,” Int J Refrig, vol. 115, pp.18−27, 2020.

[235] A. Mota-Babiloni, J. Navarro-Esbrí, A. Barragán, F. Molés, and B. Peris, “Drop-in energy performance evaluation of R1234yf and R1234ze(E) in a vapor compression system as R134a replacements,” Appl Therm Eng, vol. 71, pp. 259−265, 2014.

[236] D. Leighton, Y. Hwang, and R. Radermacher, “Modeling of household refrigerator performance with low global warming potential alternative refrigerants,” ASHRAE Trans, vol. 118, pp. 658−665, 2012.

[237] A. E. Kabeel, A. Khalil, M. M. Bassuoni, and M. S. Raslan, “Comparative experimental study of low GWP alternative for R134a in a walk-in cold room,” Int J Refrig, vol. 69, pp. 303−312, 2016.

[238] J. M. Mendoza-Miranda, A. Mota-Babiloni, and J. Navarro- Esbrí, “Evaluation of R448A and R450A as low-GWP alternatives for R404A and R134a using a micro-fin tube evaporator model,” Appl Therm Eng, vol. 98, pp. 330−339, 2016.

[239] R. Conte, M. Azzolin, S. Bernardinello, and D. Del Col, “Experimental investigation of large scroll compressors working with six low-GWP refrigerants,” Therm Sci Eng Prog, vol. 44, p. 102043, 2023.

[240] L. Molinaroli, A. Lucchini, and L. P. M. Colombo, “Experimental comparison of the use of R134a and R1234ze(E,” in in a semi-hermetic reciprocating compressor. Proceedings of the 25th IIR International Congress of Refrigeration: Montréal, Canada, Aug 24-30, 2019.

[241] HG. Ramírez - Hernández, A. Morales - Fuentes, FA. Sanchez - Cruz, S. Méndez - Díaz, HD. García-Lara, S. Martínez-Martínez, "Experimental study on the operating characteristics of a display refrigerator phasing out R134a to R1234ze(E) and its binary blends," Int J Refrig, vol. 138, pp. 1-12, 2022.

[242] A. D. Sahin, I. Dincer, and M. A. Rosen, "analysis of solar photovoltaic cell systems," Solar Energy Materials & Solar Cells, vol. 91, pp. 153–159, 2007.

[243] A. S. Joshi, I. Dincer, and B. V. Reddy, "Thermodynamic Assessment of Photovoltaic Systems," Solar Energy, vol. 83, no. 8, pp. 1139–1149, 2009.

[244] R. Petela, "Exergy of Undiluted Thermal Radiation," Solar Energy, vol. 74, pp. 469–488, 2003.

[245] R. Petela, "An Approach to the Exergy Analysis of Photosynthesis," Solar Energy, vol. 82 no. 3, pp. 11–328, 2008.

[246] F. Sarhaddi, S. Farahat, H. Ajam, and A. Behzadmehr, "Performance Evaluation of a Solar Photovoltaic (PV) Array," Australian Journal of Basic and Applied Sciences, vol. 4, no. 3, pp. 502–519, 2010.

[247] G. Boyle, "Renewable Energy Power for a Sustainable Future," 2nd ed. Oxford: Ox-ford University Press, 2004.

[248] J. H. Watmuff, W. W. S. Charters, and D. Proctor, "Solar and wind induced external coefficients for solar collectors," Cooperation Mediterraneenne pour l'Energie Solaire, Revue Internationale d'Heliotechnique, 2nd Quarter, vol. 2, p. 56, 1977.

[249] A. Bejan AB, G. Tsatsaroni, and M. Moran, "Thermal Design & Optimization." 1996.

[250] N. Bouaziz and D. Lounissi, “Energy and exergy investigation of a novel double effect hybrid absorption refrigeration system for solar cooling,” Int J Hydrogen Energy, vol. 40, no. 39, p. 13849e56, 2015.

[251] R. Terzi, I. Tu¨ Kenmez, E. Kurt, “Energy and exergy analyses of a _VVER type nuclear power plant,” Int J Hydrogen Energy, vol. 41, no. 29, 2016.

[252] I. Dincer and M. Kanoglu, Refrigeration systems and applications. New York: Wiley, 2010.

[253] S. Agarwal, A. Arora, B.B. Arora, “Energy and exergy investigations of R1234yf and R1234ze as R134a replacements in mechanically subcooled vapour compression refrigera-tion cycle,” Journal of Thermal Engineering, vol. 7, no. 1, pp. 109-132, Jan. 2021.

[254] A. Arora and S. C. Kaushik, “Theoretical analysis of a vapour compression refrigeration system with R502, R404A and R507A,” International journal of refrigeration, vol. 31, no. 6, pp. 998-1005, Sep 1. 2008.

[255] D. A. Omer, M. M. Mahdi, and A. L. Shuraiji, “An experimental study optimization of a solar assisted D.C refiergerter under Iraqi climate,” Journal of Physics.2021.

[256] M. E. Oruc, A. V. Desai, P. J. A. Kenis, and R. G. Nuzzo, “Comprehensive Energy Analysis of a Photovoltaic Thermal Water Electrolyzer,” Applied Energy, vol. 164, pp. 294–302, 2016.

[257] R. B. Jemaa, R. Mansouri, I. Boukholda, and A. Bellagi, “Energy and Exergy Investigation of R1234ze(E) as R134a Replacement in Vapor Compression Chillers,” International Journal of Hydrogen Energy, vol. 42, pp. 12877–12887, 2017.

[258] S. Agarwal, A. Arora, and B. B. Arora, “Energy and exergy investigations of R1234yf and R1234ze as R134a replacements in mechanically subcooled vapour compression refrigeration cycle,” Journal of Thermal Engineering, vol. 7, no. 1, pp. 109–32, 2021.

APPENDICES

APPENDIX A

Hourly variation of ambient temperature (°C)

(Ghardaia region)

Hour	June 21	July 21	August 21
1	33,2	31,1	28,9
2	31,4	30,6	28,2
3	31,4	29,5	27,8
4	31,4	29,8	27
5	31,4	30	26,7
6	32,8	30,6	27,3
7	35,8	33,8	28,8
8	36,7	35,6	30,5
9	38,8	37,3	32,1
10	40,6	38,4	33,1
11	41,4	39	33,9
12	41,6	41	35
13	42,4	41,8	35,2
14	43	42,3	35,7
15	42,6	42	35,9
16	42,8	41,7	35,6
17	42,3	41,6	34,8
18	41,1	40,8	33,9
19	39,7	39,3	32,8
20	38,5	38,2	31,9
21	37,5	36,4	30,9
22	36,3	35	29,8
23	34,8	34,6	29,1
24	34,1	33,8	28,4

APPENDIX B
Hourly variation of solar radiation (KWh/m^2)
(Ghardaia region)

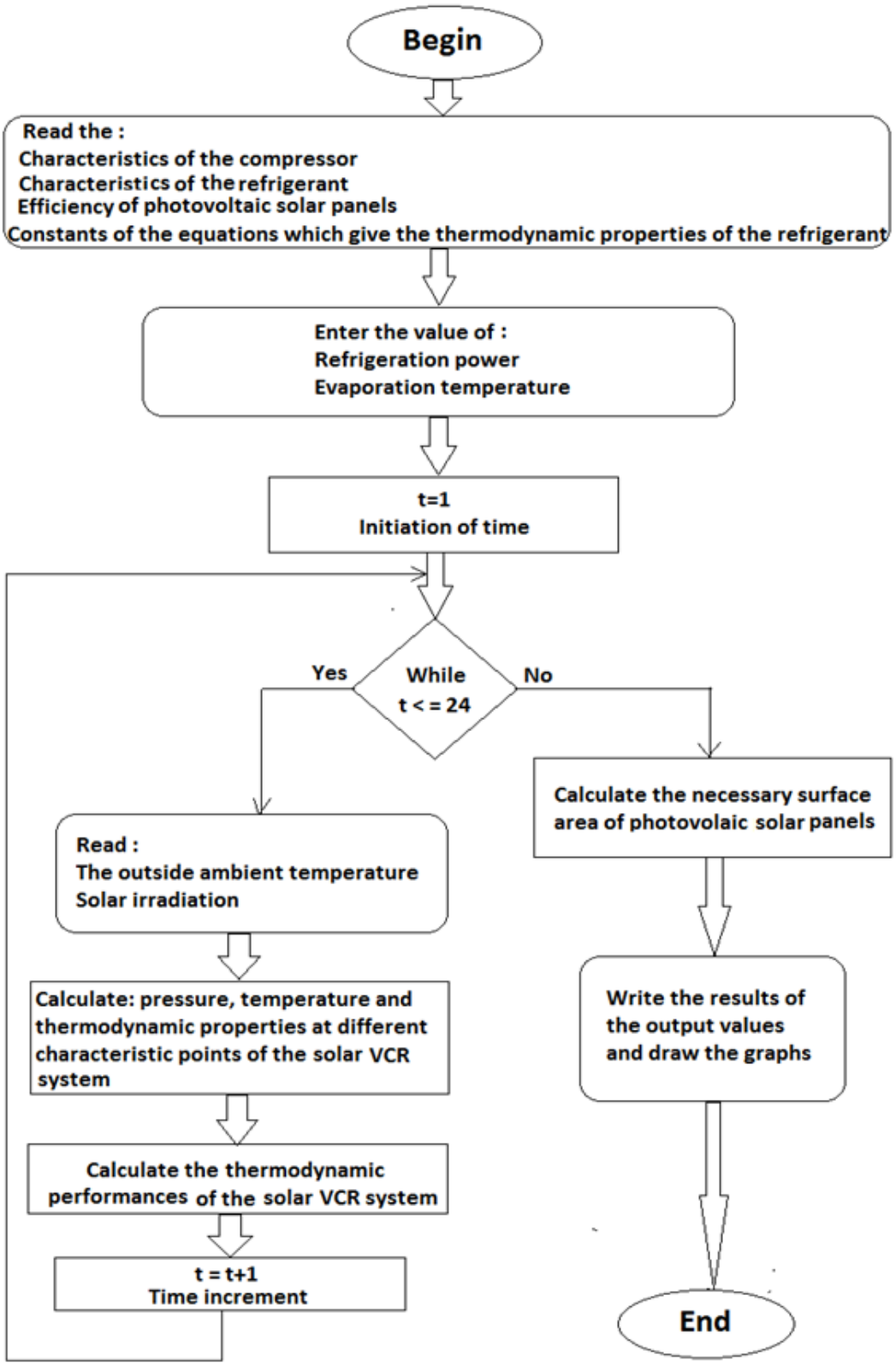
Hour	June 21	July 21	August 21
1	0	0	0
2	0	0	0
3	0	0	0
4	0	0	0
5	0,00772223	0	0
6	0,10038889	0,16988889	0,08494446
7	0,64866666	0,63322223	0,4865
8	1,3205	1,10427777	1,01161111
9	1,79927777	1,74522223	1,50583334
10	2,17766666	2,20855554	1,97688889
11	2,47883334	2,54833334	2,32438889
12	2,64872223	2,72594446	2,47111111
13	2,61011111	2,66416666	2,44794446
14	2,35527777	2,4325	2,25488889
15	1,99233334	2,06183334	1,89966666
16	1,529	1,59077777	1,34366666
17	0,98844446	1,07338889	0,85716666
18	0,44788889	0,49422223	0,32433334
19	0,07722223	0,11212769	0,00772223
20	0	0	0
21	0	0	0
22	0	0	0
23	0	0	0
24	0	0	0

APPENDIX C

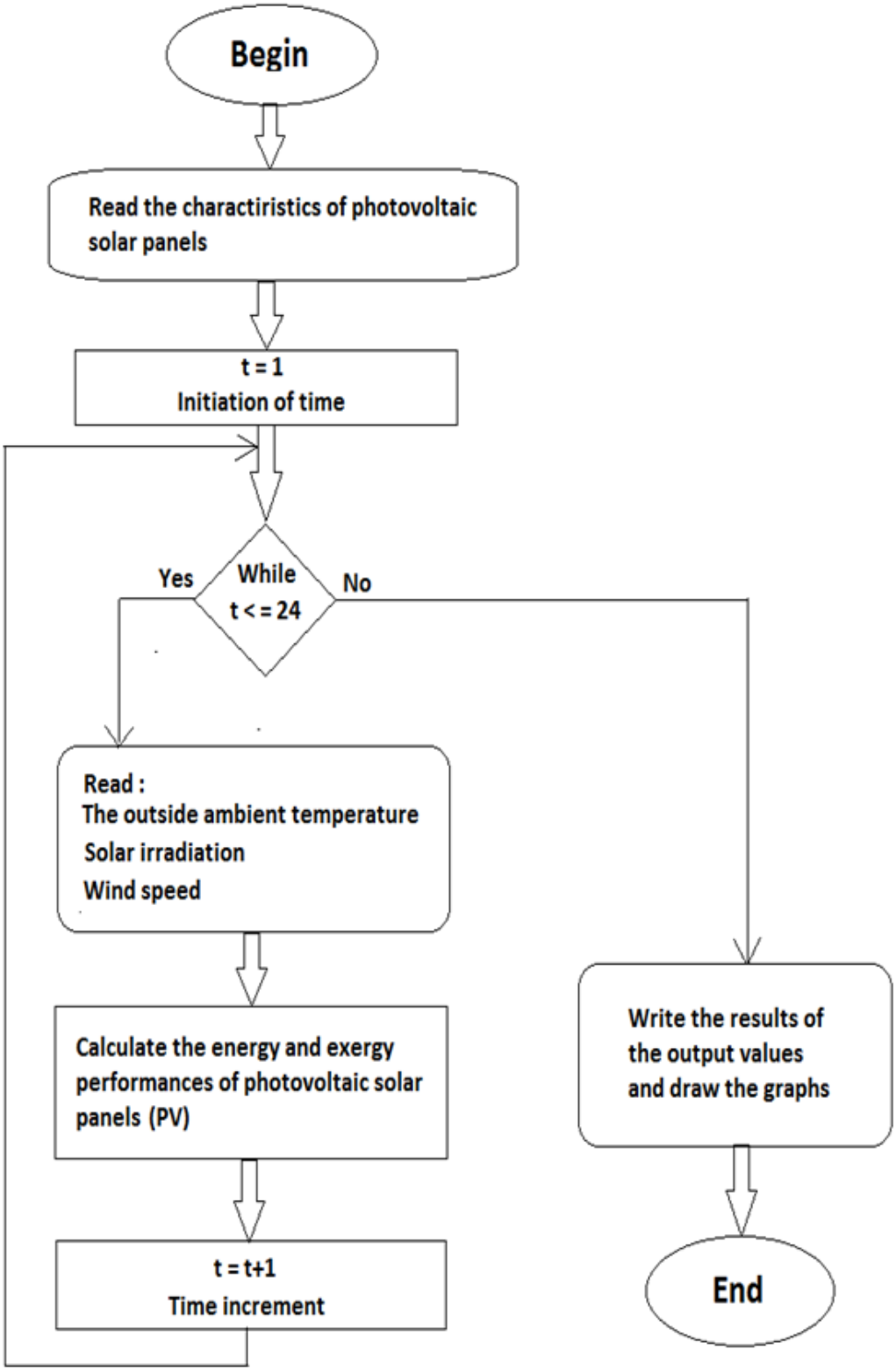
Hourly variation of wind speed (m/s) (Ghardaia region)

Hour	June 21	July 21	August 21
1	5,24	5,24	5,24
2	5,24	5,24	5,24
3	5,24	5,24	5,24
4	5,24	5,24	5,24
5	5,24	5,24	5,24
6	5,24	5,28	5,28
7	5,32	5,32	5,32
8	5,36	5,36	5,4
9	5,36	5,4	5,48
10	5,4	5,44	5,52
11	5,4	5,44	5,52
12	5,36	5,44	5,48
13	5,36	5,4	5,44
14	5,32	5,36	5,4
15	5,32	5,32	5,4
16	5,28	5,28	5,36
17	5,28	5,28	5,32
18	5,28	5,28	5,32
19	5,24	5,24	5,28
20	5,24	5,24	5,28
21	5,24	5,24	5,28
22	5,24	5,24	5,28
23	5,24	5,24	5,28
24	5,24	5,24	5,28

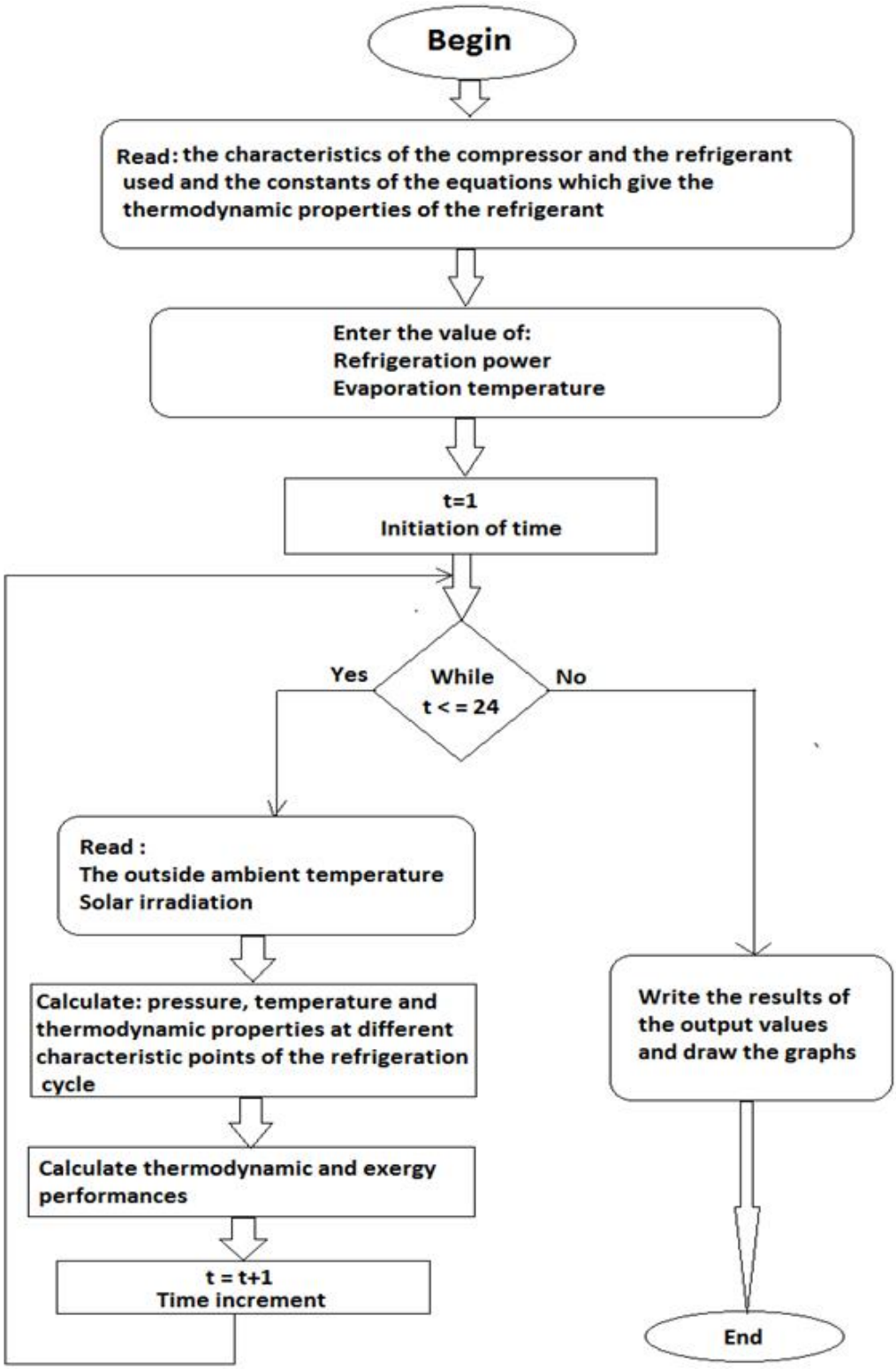
APPENDIX D : Algorithm used for thermodynamic analysis of solar PV vapor compression refrigeration system



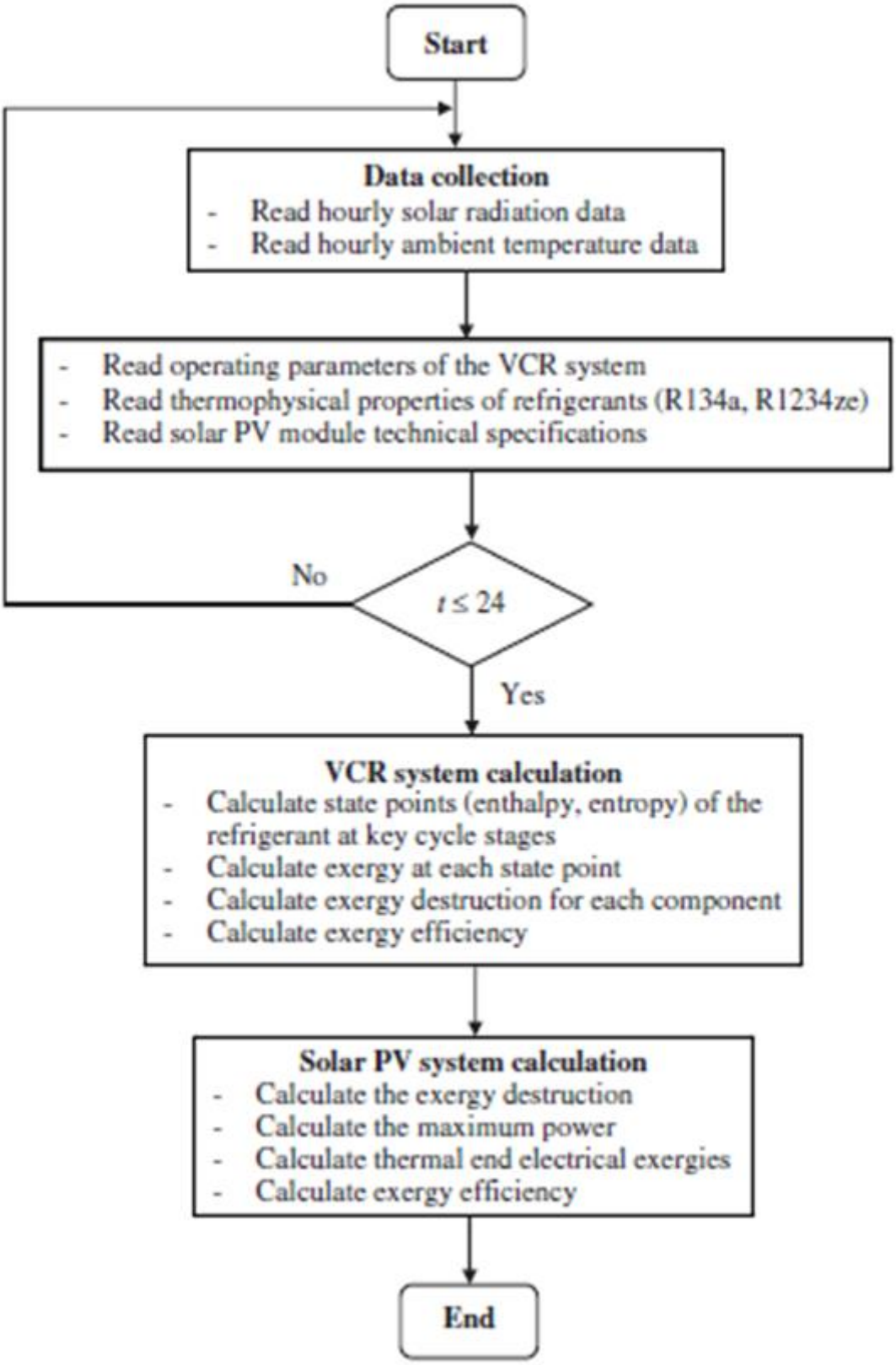
APPENDIX E: Algorithm used for exergy analysis of photovoltaic PV solar panels



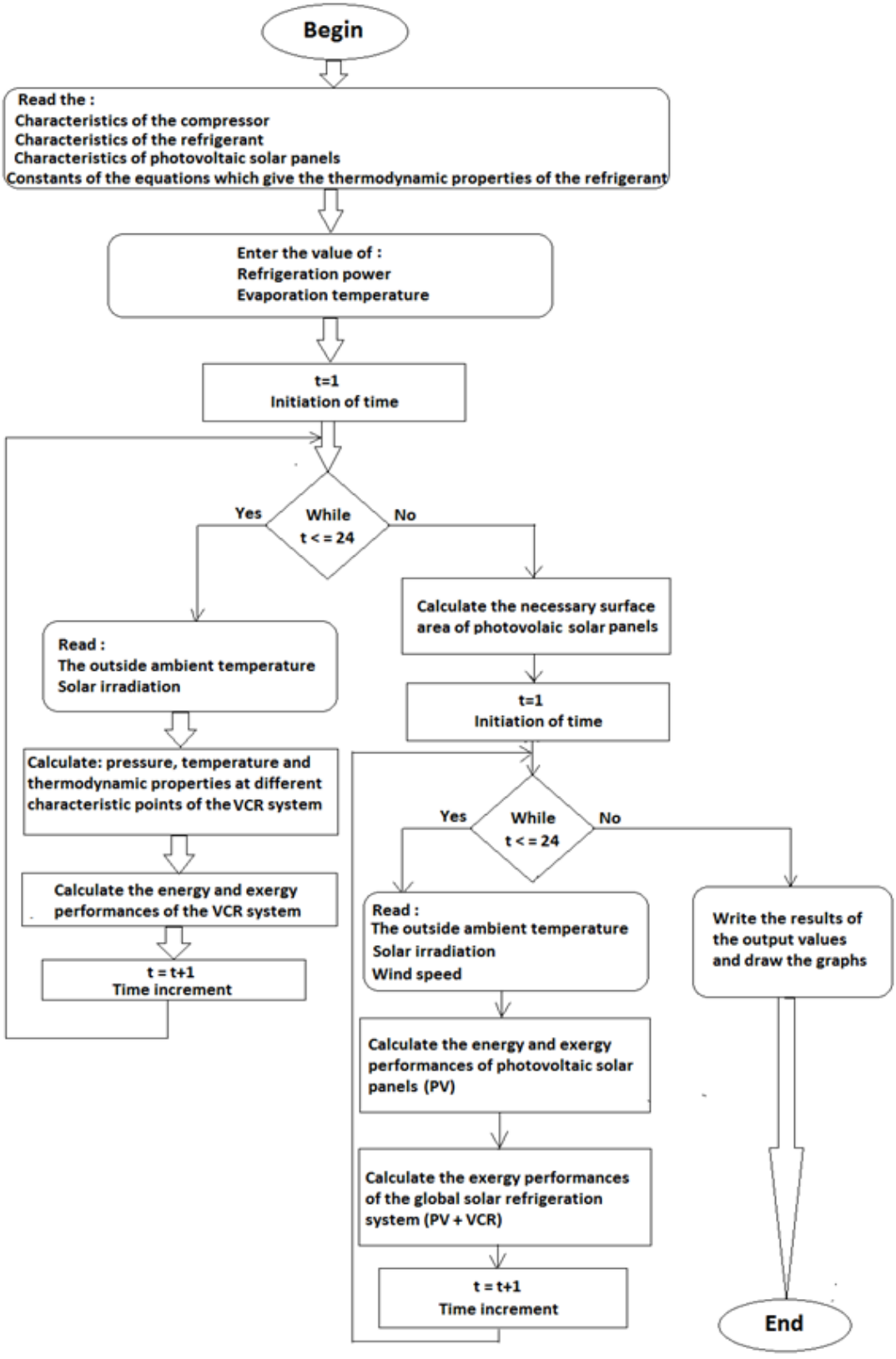
APPENDIX F : Algorithm used for exergy analysis of vapor compression refrigeration system



APPENDIX G : Algorithm used for the SP-VCR system calculation



APPENDIX H : Algorithm used for exergy analysis of the global solar refrigeration system (PV + VCR)



PUBLICATIONS AND CONFERENCES

Algerian Symposium on Renewable Energy and Materials
ASREM2020, December 16-17, 2020 Médéa- Algeria
http://www.asrem2020.cf/

December 17th, 2020

CERTIFICATE

We hereby certify that

Ahmed SELLOUM

Yahia FARES -Médéa University, Médéa – Algeria

Has presented the paper referenced below in Algerian Symposium on Renewable Energy and Materials (ASREM2020), which took place in Médéa, Algeria from 16th to 17 th, December 2020

Title : **A review on the recent solar energy applications in hybrid refrigeration and air conditioning systems**

Co-author(s) : Z. TRIKI, Y. CHIBA

Signature ASREM2020 Chair

ASREM 2020
General Chair
Dr. Younes Chiba

1er Séminaire national sur le Génie climatique, Énergie renouvelables & Efficacité énergétique (GÉCLEREE2021)

04-05 Décembre 2021, Médéa, Algérie

ATTESTATION DE PARTICIPATION

Le comité scientifique du premier séminaire national sur le Génie climatique, Energies renouvelables et Efficacité énergétique «GéCLEREE2021 » tenu les 04 et 05 Décembre 2021 à l'Université de Médéa, atteste que :

SELLOUM Ahmed

a participé à cette manifestation par une communication « **Poster** » intitulée :

Systèmes de réfrigération et de conditionnement d'air hybrides (à adsorption et à compression de vapeur) fonctionnant à l'énergie solaire

Selloum A., Triki Z., Chiba Y.

Président du séminaire

Président du Séminaire GéCLEREE

Dr. TRIKI Zakaria

Séminaire national sur le Génie climatique, Energies renouvelables & Efficacité énergétique GéCLEREE

Laboratoire de Biomatériaux et Phénomènes de Transport

AIR LAB

sonelgaz

Sinal

Second International Refrigeration Energy and Environment Colloquium
IREEC2 2023

Hammamet 17-20 March 2023

CERTIFICATE OF PARTICIPATION

Ahmed Selloum

has attended the Second International Refrigeration Energy and Environment Colloquium (IREEC2), which has been held on 17-20 March 2023 at Hammamet, Tunisia, with an oral communication entitled:

Study, simulation, and performance analysis of a vapor compression refrigeration system, operating with R1234Ze low GWP refrigerant, and powered by electrical energy produced by photovoltaic solar panels, located in the Ghardaïa region

Co-authors: Zakaria Triki, Younes Chiba

Professor Lakdar Kairouani
IREEC2 Chairman
ATRC President

Association Tunisienne
De Réfrigération et de Climatisation
Président
GSM: 58.212.772

J Ther Eng, Vol. 10, No. 1, pp. 130−141, January, 2024

Journal of Thermal Engineering
Web page info: https://jten.yildiz.edu.tr
DOI: 10.18186/thermal.1429427

Research Article

Thermodynamic analysis of a solar-driven vapor compression refrigeration system using R1234ze for cooling applications in Ghardaïa region (Southern Algeria)

Ahmed SELLOUM[1], Zakaria TRIKI[1,*], Younes CHIBA[1]

[1]*Laboratory of Biomaterials and Transport Phenomena, University of Medea, Medea 26000, Algeria*

ARTICLE INFO

Article history
Received: 21 June 2023
Accepted: 04 October 2023

Keywords:
Solar Energy; Vapor Compression Refrigeration; Low GWP Refrigerant; Cooling Applications; Performance; Comparison

ABSTRACT

This study presents a thermodynamic analysis of a solar-driven vapor compression refrigeration (VCR) system designed for use in the region of Ghardaïa (Southern Algeria) which is located in a desert with a semi-arid climate where the demand for cooling is high, and the solar radiation is abundant. Two working fluids are tested and compared, the HFC high GWP going to phased out, R134a and the low GWP, HFO refrigerant recently introduced R1234ze. The performance of the solar VCR system was evaluated using a numerical model developed in MATLAB software, based on thermodynamic properties of R1234ze and R134a refrigerants. The results showed that coefficient of performance (COP) and thermodynamic efficiency of the solar VCR system increased with decreasing ambient temperature due to the increase in the compressor power consumption. The COP during the 21st day of July month is obtained in the range of 4.37–5.77 for R1234ze refrigerant which are close and more than 90% of the maximum COP value, while it is in the range of 2.56–3.17 for R134a fluid. The lowest COP values are found around noon hours during 12:00 AM and 15:00 PM. In addition, the greatest amount of the PV power production for R134a and R1234ze refrigerants occurs in the middle of the day (12:00 PM) as 2.8 and 1.6 kWh, respectively.

Cite this article as: Selloum A, Triki Z, Chiba Y. Thermodynamic analysis of a solar-driven vapor compression re-frigeration system using R1234ze for cooling applications in Ghardaïa region (Southern Algeria). J Ther Eng 2024;10(1):130−141.

INTRODUCTION

Solar-based cooling is an indispensable domain within the realm of renewable energy and has garnered noteworthy accomplishments. Its significance arises from the heightened requirement for cooling during periods of intensified solar radiation, which often aligns with hotter climates. Furthermore, solar cooling stands out for its environmentally conscious nature, given its absence of greenhouse gas emissions and its contribution to curbing reliance on fossil fuels. Notably, it offers cost-effective advantages by lowering energy expenditures and entailing minimal maintenance costs. Another notable advantage lies in its applicability to

***Corresponding author.**
*E-mail address: triki.zakaria@univ-medea.dz

This paper was recommended for publication in revised form by Ahmet Selim Dalkılıç

Published by Yıldız Technical University Press, İstanbul, Turkey
Copyright 2021, Yıldız Technical University. This is an open access article under the CC BY-NC license (http://creativecommons.org/licenses/by-nc/4.0/).

Frontiers in Heat and Mass Transfer

Tech Science Press

DOI: 10.32604/fhmt.2024.052223

Published Online: 08 July 2024

ARTICLE

Exergy Analysis of a Solar Vapor Compression Refrigeration System Using R1234ze(E) as an Environmentally Friendly Replacement of R134a

Zakaria Triki[1], Ahmed Selloum[1], Younes Chiba[1], Hichem Tahraoui[1,2], Dorsaf Mansour[3], Abdeltif Amrane[4,*], Meriem Zamouche[5], Mohammed Kebir[6] and Jie Zhang[7]

[1]Laboratory of Biomaterials and Transport Phenomena, University of Medea, Medea, 26000, Algeria

[2]Laboratoire de Génie des Procédés Chimiques, Department of Process Engineering, University of Ferhat Abbas, Setif, 19000, Algeria

[3]Chemistry Department, College of Sciences, University of Hail, Hail, 55223, Saudi Arabia

[4]Univ Rennes, Ecole Nationale Supérieure de Chimie de Rennes, CNRS, ISCR–UMR6226, Rennes, F-35000, France

[5]Laboratoire de Recherche sur le Médicament et le Développement Durable (ReMeDD), Faculty of Process Engineering, University of Salah Boubnider Constantine 3, Constantine, 25000, Algeria

[6]Research Unit on Analysis and Technological Development in Environment (UR-ADTE/CRAPC), Bou-Ismail, Tipaza, 42004, Algeria

[7]School of Engineering, Merz Court, Newcastle University, Newcastle upon Tyne, NE1 7RU, UK

*Corresponding Author: Abdeltif Amrane. Email: abdeltif.amrane@univ-rennes1.fr

Received: 27 March 2024 Accepted: 13 June 2024

ABSTRACT

Refrigeration plays a significant role across various aspects of human life and consumes substantial amounts of electrical energy. The rapid advancement of green cooling technology presents numerous solar-powered refrigeration systems as viable alternatives to traditional refrigeration equipment. Exergy analysis is a key in identifying actual thermodynamic losses and improving the environmental and economic efficiency of refrigeration systems. In this study exergy analyze has been conducted for a solar-powered vapor compression refrigeration (SP-VCR) system in the region of Ghardaïa (Southern Algeria) utilizing R1234ze(E) fluid as an eco-friendly substitute for R134a refrigerant. A MATLAB-based numerical model was developed to evaluate losses in different system components and the exergy efficiency of the SP-VCR system. Furthermore, a parametric study was carried-out to analyze the impact of various operating conditions on the system's exergy destruction and efficiency. The obtained results revealed that, for both refrigerants, the compressor exhibited the highest exergy destruction, followed by the condenser, expansion valve, and evaporator. However, the system using R1234ze(E) demonstrated lower irreversibility compared to that using R134a refrigerant. The improvements made with R1234ze are 71.95% for the compressor, 39.13% for the condenser, 15.38% for the expansion valve, 5% for the evaporator, and 54.76% for the overall system, which confirm the potential of R1234ze(E) as a promising alternative to R134a for cooling applications.

KEYWORDS

Solar cooling; vapor compression refrigeration; eco-friendly refrigerant; thermodynamic losses; exergy analysis

This work is licensed under a Creative Commons Attribution 4.0 International License, which permits unrestricted use, distribution, and reproduction in any medium, provided the original work is properly cited.